i

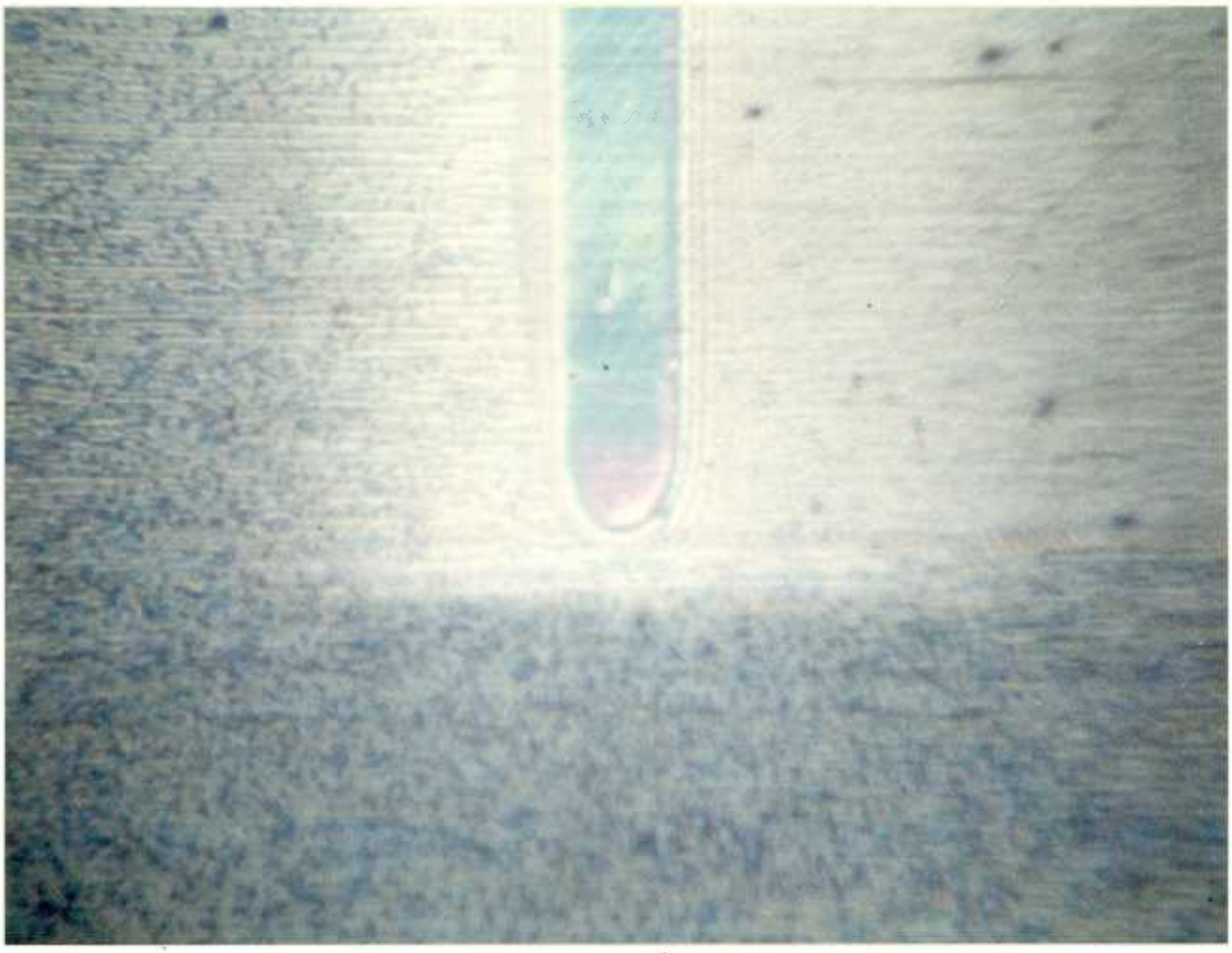

AN OPTICAL INVESTIGATION INTO THE LUBRICATION OF CYLINDRICAL ROLLER BEARINGS

by

JONATHAN CLOWES PEMBERTON

A thesis submitted for the degree of

DOCTOR OF PHILOSOPHY

of the University of London

and also for the

DIPLOMA OF IMPERIAL COLLEGE

January 1976

Lubrication Laboratory
Department of Mechanical Engineering
Imperial College of Science and Technology
London S.W.7.

ABSTRACT

A test rig has been designed to enable stroboscopic observation of the inner and outer contacts of rolling element bearings, in a journal configurations. Sapphire windows have been inserted into the inner and outer raceways of commercially available roller bearings. The technique of optical interferometry has been applied to measure the film thickness at the outer race contacts, and the distribution of oil around these contacts in the loaded and unloaded regions of the bearing, has also been studied.

At low speeds film thickness measurements, made at the centre and exit regions of the contacts, are consistent with theoretical isothermal solutions. However at speeds above about 1000 R.P.M., accurate theoretical predictions could only be made if the effects of viscous heating in the inlet zone were considered. During these tests, the position of the inlet boundary was observed, and and at all speeds the contacts were effectively fully flooded. The inlet boundary distance was found to be proportional to viscosity and inversely proportional to speed. Rolling element spacing had no effect on the boundary shape or position.

A study of the oil flow around a point contact has revealed the mechanism whereby oil can be entrained

into the inlet regions from the track edges.

A brief examination of oil globules, that are suspended in between contacts, reveals that oil can pass through the bearing without wetting the surfaces.

Operation of the bearing under conditions of acute lubricant starvation has shown that the contacts can be supported on substantial oil films, when there are only minute quantities of oil in the inlet regions. This results in the removal of all film constrictions.

ACKNOWLEDGEMENTS

The author gratefully acknowledges the following in support of this work:

Prof. A. Cameron for the opportunity to undertake this work, and his guidance and supervision.

The Science Research Council for a studentship and an equipment grant.

Westland Helicopters Ltd., Yeovil, for loan of the video equipment, financing many of the costs of producing the rig, and for providing financial assistance that has enabled this work to be completed.

Dr. P.B. Macpherson for the interest he has consistently shown in this work, and for valuable discussions and advice.

Mr. R. Dobson for his valuable assistance and advice in the laboratory.

Mr. Rutherford, Dr. Poon, and Dr. Thorpe, of the R.H.P. bearing company for so generously supplying all the bearings and rollers required for this study.

Mr. D. Long of Ealing-Beck Ltd. for assistance with the design of the optical system.

Messrs M. Benson and J. Leather for assistance with the design of the electronics for flash synchronisation.

Dr. D. Wymer, Dr. G. Paul, and Dr. A. Jackson, for their valuable discussions and advice.

Mr. G.D. Galvin of the Thornton Research Centre, Chester, for the supply of lubricant 1.

My wife Gail for her encouragement and patience during the course of this work, also for drawing and labelling some of the figures and proof reading.

Miss S. Hutchinson for typing the script.

Mr. A. Justice for his help, and use of his equipment for printing the photographs.

TABLE OF CONTENTS

Page

Page

Page

LIST OF FIGURES

Page

Page

NOMENCATURE

Symbols used infrequently are defined in the text.

a : Hertzian circular point contact radius

b : Hertzian line contact half-width

c : capacitance

d : optical path difference

E_1, E_2 : elastic moduli of solids in contact

E' : reduced elastic modulus

G^* : materials parameter = $\alpha E'$

H^* : film thickness parameter = h/R

h_0^* : central film thickness parameter = h_0/R

$\bar{H}$: film thickness parameter = $\pi h_0 LE'/4W$

H_1^* : minimum exit constriction film thickness parameter = h_1/R

$H_1^{*\prime}$: minimum exit constriction film thickness parameter, calculated accounting for the effect of viscous heating

h : film thickness

$\bar{h}$: film thickness at point of maximum pressure

h_0 : central film thickness

h_1 : minimum film thickness

h_∞ : central film thickness under flooded inlet conditions

I : light intensity

k : thermal conductivity

L : length of line contact

$\bar{L}$: thermal loading parameter = $U^2 \eta_0 \gamma / k$

N : fringe order (integer)

n : refractive index

n_o : refractive index at ambient pressure

p : pressure

p_{max} : maximum Hertz pressure

q : reduced pressure = $(1 - e^{\alpha p})/\alpha$

R_i : Inner race radius

R_o : outer race radius

R : effective radius of solids in contact = $R_o r/(R_o - r)$ for outer race contacts, and = $R_i r/(R_i + r)$ for inner race contacts

R : reflectivity

R : electrical resistance

r : radius of the rollers

r : angle of refraction

$\bar{S}$: speed parameter = $.75 U \eta_0 \alpha b L^2 \pi^2 E'^2 / W^2$

T : temperature

Ts : Sapphire surface temperature

T_j : Oil Jet temperature

U : mean surface velocity of solids in contact

U* : speed parameter = $U\eta_0/E'R$

V : fringe visibility

V : voltage

W : total load on solids in contact

W* : load parameter = $W/LE'R$

x,y,z : cartezian co-ordinates

X_i : inlet distance measured from edge of Hertzian region

α : pressure-viscosity coefficient

β : starvation film thickness parameter = h/h_∞

γ : temperature coefficient of viscosity

Δ : clearance between the rollers and the outer race for an unloaded bearing

δ : optical phase differences

δ : approach between two bodies under load

η : lubricant dynamic viscosity

η_o : lubricant dynamic viscosity at inlet temperature and ambient pressure

η_o' : effective dynamic viscosity at the inlet

Θ : angle of incident light rays

λ : optical wavelength

ν : lubricant kinematic viscosity

ρ : lubricant density

ρ_o : lubricant density at ambient pressure

σ_1, σ_2 : Poisson's ratios of solids in contact

ϕ : optical phase change

Ψ_i : inlet distance parameter = $X_i \, b^{1/3} / (2Rh_\infty)^{2/3}$

ω_c : angular velocity of the inner race

ω_i : angular velocity of the cage

Abbreviations

Å : angstrom (1 Å = 10^{-10} metres)

c.l.a. : centre line average

E.H.D. : elastohydrodynamic

E.H.L. : elastohydrodynamic lubrication

p.s.i. : pounds per square inch

R.P.M. : revolutions per minute

μ : micro (unit is multiplied by 10^{-6})

CHAPTER I

INTRODUCTION

It is somewhat suprising that gears and bearings and other such systems, where contact stresses are very large, operated for so long without an understanding of the mechanism of their lubrication. The need for oil was realised, but not until recently was its function fully understood. Since 1949 developments have shown, both theoretically and experimentally, that it is possible to form substantial oil films at pressures for which classical hydrodynamic theory would have predicted practically zero film thickness.

Elastohydrodynamic lubrication takes place when the pressure occurring at the lubricated contact is high enough to cause elastic deformation. In gears or bearings, where conformity is low, small loads cause pressures high enough to deform the steel surfaces. When oil enters this type of contact its viscosity is dramatically increased. It is for this reason that oil is capable of forming a film at the pressures encountered in normal elasto-hydrodynamic situations. Before accurate predictions of film thickness could be made, classical hydrodynamic theory had to be extended to include the effects of surface deformation, and the influence of the viscosity-pressure characteristic of the lubricant. This was not successfully

achieved until 1949. Progress since then has been rapid, and theoretical solutions have been verified experimentally.

The most decisive of all measurements have been provided by using optical interferometry to measure film thickness. The technique has proved to be extremely versatile, for as well as providing an exact contour map of the surfaces actually within the contact, it also immediately shows if there is sufficient oil,within the contact entry region,to ensure adequate distance for the pressure build up essential for maintaining the oil film.

The demands placed on bearings are becoming increasingly severe,and failure can have disasterous consequences. Rolling element bearings run in gas turbines at speeds up to 40,000 RPM, and transient loads can be very high. At these speeds it is likely that starvation is dropping the film thickness substantially, even though large quantities of oil may be flowing through the bearings. It has been shown that the viscosity-pressure characteristic is time dependent (1),and thus at the very short transit times involved,this could also cause a drop in film thickness. These are just two of the factors that emphasise the need for the study of the mechanism of lubrication of real bearings.

Film thickness measurements have previously

been made in actual bearings, but these have nearly all been of an electrical nature, and the majority have only given an average value of film thickness for the whole bearing. Optical interferometry has successfully been used to obtain equations for film thickness in point and line contact, and to investigate the starvation phenomena. These investigations have been carried out in a counter-rotating mode. That is the ball or roller remains stationary in the field of view while the races revolve in opposite directions.

The object of this project is to investigate, using the optical technique, the lubrication of a cylindrical roller bearing operating at speeds up to 2,500 RPM, under elastohydrodynamic conditions. The cage is free to rotate and the fringe patterns are studied stroboscopically. The techniques developed in this project, in which a pulsed laser is used for higher speed tests, could be applied to bearings running at speeds up to 100,000 RPM.

CHAPTER II

A REVIEW OF THE LITERATURE

2.1 Early Work Leading to the Recognition of E.H.L.

The absence of substantial wear in gear teeth contacts led to the belief that the surfaces may be separated by a hydrodynamic oil film, and attempts were made to verify this theoretically. In 1916 Martin (2) represented the contact geometry of gear teeth as equivalent to a cylinder near a plane. (This is common practice in the analysis of E.H.D. contacts and the theory is well explained in (31)). By solving Reynold's equation, assuming rigid solids and an incompressible isoviscous fluid, he obtained the following equation for film thickness:

$$\frac{h_0}{R} = 4.896 \quad \frac{un_0}{W/L} \qquad \ldots\ldots 2.1$$

For typical values encountered in a lubricated, highly loaded contact, Martin's equation gives film thickness predictions of the order of 1μin. This is clearly insufficient to separate all but the most highly polished of surfaces. Martin's equation demonstrated the inadequacy of conventional hydrodynamics to explain this type of lubrication, and led to statements such as made in 1919 by Lanchester (3): "There exists an entire world of lubrication outside that which Reynold's conditions obtain".

In 1926 Schering and R. Vieweg (4) demonstrated the existance of an oil film in a ball bearing by an electrical capacity method. It was suggested in 1927 (5), that in roller bearings, an oil wedge formation creates a hydrodynamic pressure build up under the leading edge of the rollers. This becomes great enough to lift them off the races as the speed increases. An analysis undertaken by Way (6) in 1935, investigating pitting occurring at roller line contacts came extremely close to a theoretical prediction of the E.H.D. effect. To begin with he calculated the load capacity of a 200 μin. oil film, which was just thick enough to separate the two discs used in his experimental apparatus. Undeformed surfaces were assumed, but the effect of pressure on viscosity was considered, based on tables given by Hyde (7). By this analysis he calculated that the maximum pressure generated in the contact was 2150 p.s.i. Ignoring the pressure-viscosity effect, a pressure of 2030 p.s.i. was calculated. He concluded that the pressure distribution was insufficient to separate the surfaces, and confirmed by electrical resistance measurements that the film was indeed broken. By next assuming that the bulk of the load was carried by metallic contact, and that there was elastic deformation in accordance with Hertz's law (8), he calculated the pressure distribution due to the oil carried in between asperity contacts.

However in this analysis he ignored the pressure-viscosity effect, previously shown to be small. Had he combined the two types of analysis, and extended it to include faster surface speeds and smoother surfaces, he may have predicted the E.H.D. situation, in which the load capacity of oil films is extremely large.

Peppler (1935 (9), 1938(10)) and Meldahl (1941 (11)) examined the lubrication of gear teeth, considering elastic distortion, but assuming an isoviscous fluid. Their solutions showed that taking into account elastic deformation produced a benefical effect on film thickness predictions.

In 1940 Needs (12) produced interesting experimental evidence concerning the behaviour of oil films between two cylinders, loaded and rotated end on. The film effectively showed infinite viscosity in the radial direction under normal approach, but only small increases in the circumferential direction, under rotating load. Film thickness measurements were made by a technique utilising optical interferometry, and resistance measurements were also made. He concluded that the film rigidity builds up, as the close proximity of the metal surfaces influences the molecular structure of the fluid. He explained the phenomena of directional rigidity in terms of a critical shear rate, above which rigidity could not increase. This critical value was exceeded in the

circumferential direction, but not in the radial direction. In the light of today's knowledge, it seems likely that in fact he had produced a lubricant entrapment between the surfaces. However this paper produced some lively discussion, which typifies the argument prevalant at that time.

Rosenfeld (1944 (13)) recognised the role of lubrication in preventing metal to metal contact in bearings, and referring to work by Larson (1941 (14)) suggested that: "An oil pressure of more than 100,000 p.s.i. as occurring in roller bearings, can easily result in a ten fold viscosity build up. This may explain the great resistance of the oil film".

A theoretical approach to the problem considering the influence of the pressure-viscosity characteristic, was made by Gatcombe (1945 (15)). Although he assumed rigid cylinders, some of his results indicated a film thickness of the same order as surface irregularities. Brix (1947 (16)) showed evidence of film formation in a thrust type of bearing. He applied a variable voltage across the bearing, and measured the current flowing through the film. As he obtained a smooth relation that decreased with increasing load, he concluded that the film was thick enough to prevent metallic contact, which would have resulted in random current surges.

The following references are relevant to theoretical treatments of the problem considering rigid cylinders, and a pressure-viscosity characteristic: Hersey and Lowdenslager (1950 (17)), Blok (1950 (18)), Cameron (1952 (19)) and McEwen (1952 (20)).

These analyses showed an improvement in load carrying capacity by a factor of about 2.5 above the Martin prediction. At about the same time an important step forward was made by Lane and Hughes (1952 (21)), when they applied electrical resistance techniques to gears in motion. An oscilloscope was used to record the potential difference across the insulated gears, and this indicated the existence of separating oil films.

The first successful solution of the problem, considering the combined effects of elastic distortion and pressure dependent viscosity, was made by Ertel, and subsequently published in 1949 by Grubin (22). He assumed an exponential pressure-viscosity law, and that the surfaces were deformed, in accordance with the theory of Hertz (8) for dry static contact.

With the incorporation of the pressure-viscosity law:

$$\eta = \eta_0 e^{\alpha p}$$

Reynolds equation in line contact, with no side leakage reduces to:

$$e^{-\alpha p} \frac{dp}{dx} = 12 U\eta_0 \left[\frac{h - \bar{h}}{h^3}\right] \qquad \ldots\ldots (2.2)$$

The pressure distribution in the entry zone was then obtained by defining a 'reduced pressure' q such that:

$$\frac{dq}{dx} = e^{-\alpha p} \frac{dp}{dx} \qquad \ldots\ldots (2.3)$$

which upon integration yields:

$$q = \frac{1}{\alpha} (1 - e^{-\alpha p}) \qquad \ldots\ldots (2.4)$$

Equation 2.2 now becomes:

$$\frac{dq}{dx} = 12 U\eta_0 \left[\frac{h - \bar{h}}{h^3}\right] \qquad \ldots\ldots (2.5)$$

The assumption was made that at the edge of the contact the pressure was high enough to put:

$$e^{-\alpha p} \simeq 0$$

ie. $$q \simeq \frac{1}{\alpha} \qquad \ldots\ldots (2.6)$$

Thus the film shape was assumed to be constant throughout the Hertzian region and:

$$\bar{h} = h_0$$

Solving equation (2.5) for the reduced pressure at the edge of the contact zone, substituting equation (2.6) and rearranging gives the following expression for the film thickness h_0:

$$h_0 = 1.95 \left(\frac{\alpha\eta_0 U}{R}\right)^{0.727} \left(\frac{W}{LE'R}\right)^{-0.091} \quad \ldots\ldots \quad (2.7)$$

Although this analysis only rigidly satisfies the equations in the contact entry region, it predicts the required separation of the bodies within the actual contact. This equation gives good estimates of film thickness in line contact, which were subsequently confirmed experimentally. Ertel also qualitatively discussed the pressure distribution throughout the contact zone and predicted the existence of a pressure spike near the Hertzian zone outlet.

Theoretical work by Petrousevich, (1951 (23)) confirmed the existence of the pressure spike, and predicted an almost parallel oil film within the contact zone, followed by a film constriction near the exit.

Further resistance measurements, carried out using discs to simulate gear tooth contact, confirmed that hydrodynamic films were produced (24, 25, 26). However it was not possible to relate film thickness to electrical measurements, until Lewicki (1955 (25)) demonstrated the feasibility of using capacitance movements. He recorded

film thickness of the order of 40 μin. in between lubricated cylindrical rollers.

The most convincing of electrical resistance measurements was made by Crook (1957 (27)). Using a disc machine he showed that hydrodynamic lubrication was possible, even at loads large enough to cause plastic deformation. His measurements also illustrated the process of 'running in', during which the resistance of the oil film gradually increased until a state of complete hydrodynamic lubrication was reached. This paper was responsible for the removal of the last doubts concerning the feasibility of elastohydrodynamic lubrication.

2.2 Development of the Theory

2.2.1 Line Contact.

Ertel's analysis of the inlet region had developed the basic approach to the E.H.D. problem, but a complete solution was not produced until ten years later, when Dowson and Higginson used numerical techniques to solve the 'inverse' hydrodynamic lubrication problem. This involved assuming a pressure distribution and using it to calculate a film shape. Elastic theory was then used to predict surface deformations, and the shape so obtained compared with the first solution. Iteration proceeded by successively modifying the pressure profile until satisfactory agreement was reached. Initial results (1959 (28)), obtained at a single speed over a range of loads, failed to predict the secondry pressure spike. Subsequent solutions (1960 (29)), covering a range of speeds, loads and material properties, clearly showed the presence of the spike. Dowson and Higginson (1961 (30)) facilitated the calculation of minimum film thickness by using the following non-dimensional parameters:

$$H^* = \frac{h}{R} \qquad \text{Film thickness parameter.}$$

$$U^* = \frac{U\eta_0}{E'R} \qquad \text{Speed parameter.}$$

$$W^* = \frac{W}{LE'R} \qquad \text{Load parameter.}$$

$$G^* = E'\alpha \qquad \text{Materials parameter.}$$

Their formula for the minimum film thickness occurring at the exit constriction, then became:

$$H_1 = 1.6\ U^{*0.7}\ W^{*-0.13}\ G^{*0.6} \qquad \ldots\ldots\ (2.8)$$

An extensive review of their solutions, and of the whole subject of E.H.D. lubrication up to that time, is given by Dowson and Higginson in (1966 (31)).

The effect of lubricant compressibility was considered by Dowson, Higginson and Whitaker (1962 (32)). Although this appreciably modified the pressure distribution, the effect on film thickness was small. Film shapes and corresponding pressure distributions, obtained considering an incompressible lubricant at constant load and various speeds, are shown in figure 2.1 and figure 2.2.

The introduction of the energy and heat transfer equations led to solutions of the problem that incorporated thermal effects. Cheng and Sternlight (1965 (33)) considered heat conduction by the surfaces, as well as convection in the oil. They also included the effect of various degrees of sliding, and found that the appreciable temperatures generated under sliding, had only a small effect upon film thickness. This had already been confirmed experimentally by Crook (1961 (34)), who also found that it was the inlet viscosity of the oil, that effected film thickness. Cheng (1965 (35, 36)) showed that

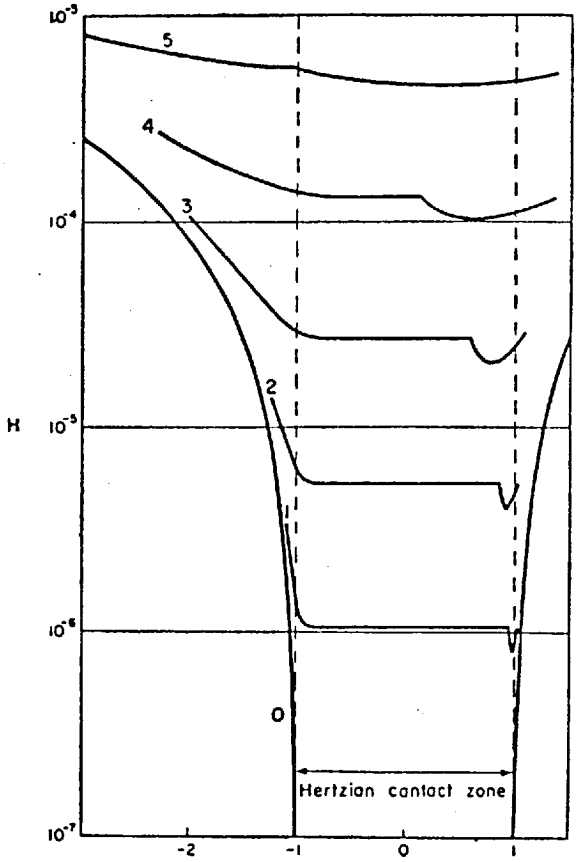

Figure 2.1 Theoretical film shapes for an incompressible lubricant in E.H.D. line contact.

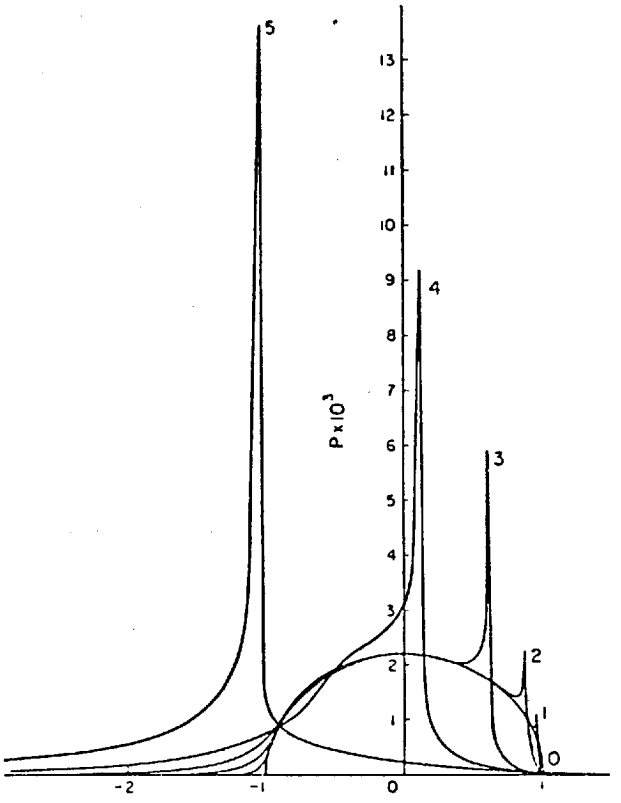

Figure 2.2 Theoretical pressure distributions for an incompressible lubricant in E.H.D. line contact. $W^*=3\times10^{-5}$, $G^*=5000$. U=(0)(dry contact),(1)10^{-13},(2)10^{-12}, (3)10^{-11}, (4)10^{-10}, (5)10^{-9}.

(after Dowson, Higginson, and Whitaker (32))

viscous heating in the inlet zone could produce a substantial reduction in film thickness. However the lubricant properties considered in this investigation, were such that the effect was only manifested at very high surface speeds. Greenwood and Kauzlarich (1973 (171)) derived an approximate method for correcting for thermal effects in the inlet zone, assuming that the inlet pressure distribution was unaffected by viscous heating. Their analysis predicted significant film thickness reduction at all but the lowest speeds and viscosities. In a recent paper, Murch and Wilson (1975 (172)) applied a thermal form of Reynold's equation, previously derived by Wilson and Wong (1974 (173)), to a 'Grubin' type analysis of the inlet zone. Their results were in good agreement with those of Cheng, and with the experimental results of Dyson, Naylor and Wilson (1966 (64)). They found that viscous heating decreased the pressure gradient in the inlet zone, which explained the discrepancy between their results and those of Greenwood and Kauzlarich. They concluded that the increased length of the inlet zone could accentuate the effects of lubricant starvation, under conditions of high 'thermal loading'.

Surveys and refinements of solutions for the line contact E.H.L. problem can be found in the following: (37, 38, 39, 40).

2.2.2 Point Contact.

Point contact theory was understandingly slower to develop than that for line contact, because it introduced a third dimension into the analysis. First attempts at a solution, again assuming rigid surfaces and an isoviscous lubricant,(1946 (41)), (1955 (42)), (1958 (43)), predicted film thicknesses in the region of 10^{-8}in.

However in 1961 Archard and Kirk (44) demonstrated that E.H.D. films of up to 100μin. thickness could be generated in the nominal point contact, created between two crossed steel cylinders. It had been difficult for people to accept the concept of E.H.L. in line contact, and it was widely believed that point contact could only operate under boundary lubrication conditions. This was indeed a remarkable demonstration that hydrodynamic lubrication existed under geometrically unfavourable conditions.

A more realistic approach to solve the theoretical problem, including the effect of surface deformation, was adopted by Archard and Cowking (1965 (45)). They made assumptions similar to those used by Ertel in the line contact analysis, and applied the two dimensional form of Reynold's equation to a number of elemental strips in the inlet region. Pressure reduction due to side leakage, was taken into account with the use of an ellipticity factor.

They also obtained a solution using the Reynold's equation in three dimensions, together with the 'Grubin' assumptions of Hertzian shape and a reduced pressure equal to $1/\alpha$ at the edge of the Hertzian region. Cheng (1970 (46)) extended the analysis to elliptical contact, and Wedeven, Evans and Cameron (1970 (47)) produced a refined solution for circular point contact, which showed good agreement with their experimental work and Cheng's solution. Ranger (1974 (48)) has recently produced a complete solution for the point contact situation.

Petrousevich et al. (1972 (49)) investigated the effect that an oscillating load would have on film thickness. They found that normal approach velocity had a significant effect on the hydrodynamic load capacity of the contact zone, and an additional film constriction was formed at the contact inlet.

2.3 Experimental Method and Measurements in E.H.L.

2.3.1 Film Thickness and Profile.

The convincing demonstration by Crook (27) left no doubts as to the existance of E.H.L., and opened a whole new field for experimentation. Research was quick to follow.

The early resistance measurements, although clearly demonstrating the presence of the E.H.D. oil film, failed as a means of measuring film thickness. Some success was achieved by use of a 'voltage discharge method' (1958 (50)), (1958 (51)), (1960 (52)). However the results had considerable scatter, and the technique was later shown to be unreliable.

The use of capacitance techniques has proved a powerful technique in experimental E.H.L. The first application of capacitance methods was achieved by Crook (1957 (53)), using a disc machine. Pads were lightly loaded against the surface of each disc, and the capacitance between pad and disc measured. This enabled the film thickness of oil adhering to each disc, after contact, to be calculated. The volumetric flow rate through the contact, and hence the film thickness, was then a matter of simple calculation. The advantage of this method was that it avoided having to estimate the shape of the contact surfaces and effects of high pressure on the dielectric constant. Crook (1961 (54)) then went on to make direct capacitance measurements between the two discs, assuming Hertzian deformation. Fair agreement with theory was achieved, when it was assumed that the inlet viscosity was governed by the temperature of the disc surface.

The E.H.D. film shape predicted theoretically, was then experimentally verified by Crook (1961 (55)). A thin strip of chromium was vacuum deposited on the

surface of a glass disc. As this electrode passed through the contact, the rate of change of capacitance between it and the steel disc, was monitored on an oscilloscope. The classic shape of an E.H.D. contact, that is of a near parallel film followed by an exit constriction, was immediately apparent. Thus with this electrode, local film thicknesses within the actual contact could be measured. The use of vapour deposited strips was an important development in experimental technique and has subsequently been successfully employed for pressure and temperature measurements.

Archard and Kirk (1961 (44)) applied the capacitance technique to the point contact occurring between crossed steel cylinders. Additional assumptions regarding geometry had to be made, but they managed to produce an empirical relationship from their results. Archard and Cowking (1965 (45)) simulated ellipical contact with a crossed cylinders machine, and obtained good agreement with their theoretical predictions.

In 1960 a new technique of measuring film thickness had been developed by Sibley et al. (56). A collimated beam of X-rays was directed at the contact between lubricated discs, and a geiger counter used to measure the amount of radiation passing through the gap. This could then be related to film thickness. The beam was aimed in the direction of rolling, and thus their

measurements were for the case of minimum film thickness at the exit constriction. Although calibration proved to be a complex task, they obtained an empirical formula that,both fitted their results and exhibited good agreement with theoretical predictions for line contact.

The introduction of optical interferometry as a method of measuring film thickness in lubricated contacts, was first made by Kirk (57) in 1962 and again reported by Archard and Kirk (1963 (58)). This was to herald a new era in experimental technique,which has led to a considerable advance in the understanding of the mechanism of E.H.L. Kirk, using the crossed cylinders machine with perspex rollers, produced coloured interference fringes by using white light. However although these were very faint, because of the low reflectivity of perspex in oil, constrictions at each side of the point contact were seen. Despite low contact pressures in this experiment, it was demonstrated that optical interferometry could provide an extremely direct method of measuring film thickness, involving the minimum of calibration and assumptions.

Gohar and Cameron (1963 (59)), (1965 (60)), (1966 (61)), applied the technique to a steel ball sliding on a high refractive index glass plate. Fringe visibility was now sufficiently good to enable accurate measurement

of film thickness. A typical film shape mapped by interferometry is shown in fig. 2.3. The pressures generated in the glass/steel contact were sufficiently high, to ensure that the oil pressure-viscosity characteristic was significant. Higher pressures still, were generated by using sapphire or diamond as the transparent plate (1967 (62)). Their results showed that the constrictions occurring at the sides of the contact were of greater severity, and also far more sensitive to load, than that occurring at the rear edge. Line contact was also briefly investigated by replacing the ball with a roller, and here again the side constrictions were observed. Film thickness measurements in pure rolling, that were made by Gohar (1967 (63)), showed agreement with the theory of Archard and Cowking for point contact.

Meanwhile Dyson, Naylor and Wilson (1965 (64)) published results they had obtained from capacitance measurements, conducted in a disc machine. These results, although obtained in the same way, showed much closer agreement with theory, than the earlier measurements of Crook.

Foord et al. (1967 (65)), (1968 (66)), (1969 (67)), significantly improved the interferometry technique by depositing a thin semi-reflecting layer of chromium on the surface of the glass plate thatwas in contact with the ball. An anti-reflection coating of magnesium fluoride was

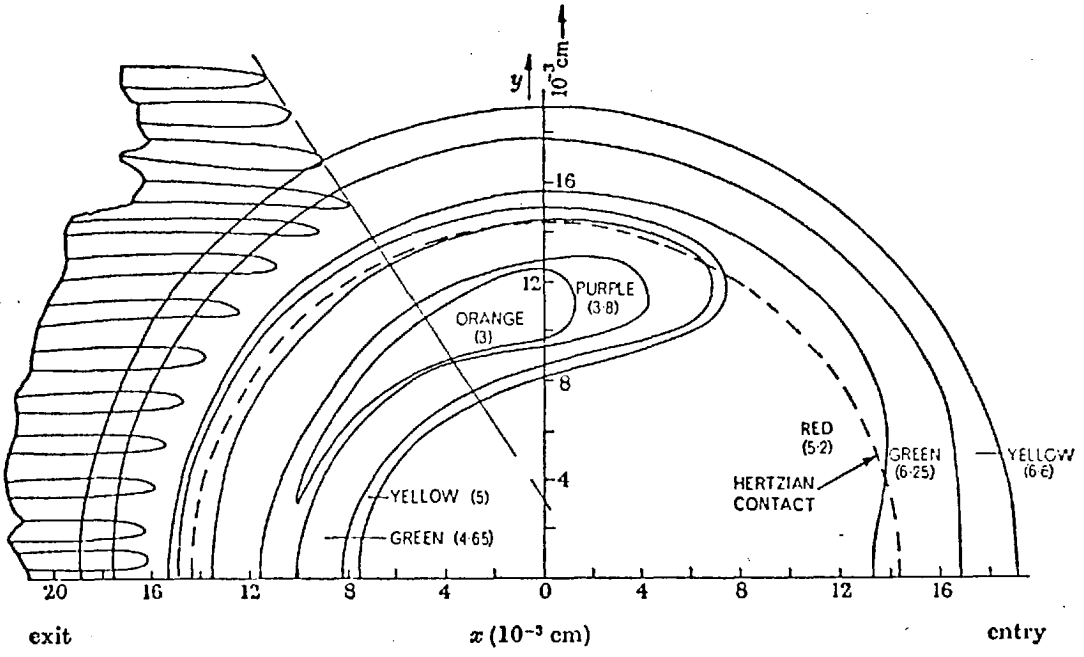

Figure 2.3 Film thickness contours in point contact.

(after Cameron and Gohar (61))

deposited on the other surface. The plate was made of crown glass, and the reflectivity of the chromium coating optimised to give fringes of the highest visibility, for two beam interference.

This type of system now formed the basis for many studies of E.H.L., using optical interferometry. One of the great advantages of the optical technique is that the distribution of oil in the contact is immediately apparent. In particular it shows whether there is sufficient oil, in the contact entry region, to prevent oil starvation, which can significantly drop the film thickness.

Optical studies of the effect of starvation were first made by Wedeven and Cameron (1968 (68)), (1970 (47, 69)), and an expression for film thickness was developed, including a starvation-parameter that could be calculated from the position of the lubricant inlet boundary.

An interesting phenomena that was revealed by optical interferometry was the formation of lubricant entrapments during normal approach of a steel ball and glass plate. Studies of this have been made by Dowson and Jones (1967 (70,71)) and by Westlake and Cameron (1967 (72, 73)), (1969 (74)).

One of the limitations of the early interferometric studies was that, for monochromatic light, the first

bright fringe did not occur until a thickness of about 1000 Å was reached. Westlake and Cameron very elegantly overcame this problem by interposing a spacer layer of silicon dioxide, between the ball and plate. As this layer has effectively the same refractive index as oil, the two are optically identical, and the spacer layer forms an artificial oil film, the thickness of which can be varied. Thus the oil film thickness, at which the first fringe occurs, can be chosen. In this way films as thin as 100 Å can be measured. They also took the technique of optical interferometry to its limits of precision, using multi-layer dielectric semi-reflecting coatings, and a laser as the light source. Extremely sharp multiple beam fringes were thus obtained. These techniques were then applied to a rolling contact rig (1970 (75)), (1971 (76)), and acute starvation investigated. The spacer layer technique has demonstrated the feasibility of using optical interferometry for study of the change from pure E.H.L. to boundary lubrication (1972 (77)).

Optical studies of lubricant entrapments led to the development by Paul and Cameron (1972 (78)) of an absolute high pressure viscometer. An entrapment is formed by dropping a ball onto a sapphire plate. The rate of oil leakage away from the entrapment is then measured by photographing interferograms of the contact at discreet intervals. Reynold's equation can then be used to deter-

mine the oil viscosity at extremely high pressures, such as occur in E.H.D. contacts.

The effect of elastic modulus on film thickness has been investigated by Gohar (1970 (182)). He showed that the empirical formulae for point contact, derived from previous optical work, could be applied for all material combinations investigated, except steel on perspex. Optical measurements in elliptical contacts, such as occur in a ball race, have been made by Thorp and Gohar (1971 (79)) using a ball sliding in a grooved glass plate.

Wymer (1972 (80)), and Wymer and Cameron (1974 (81)) have recently made an extensive study of the E.H.L. of a rolling line contact, using a taper roller and glass plate in a thrust bearing configuration. From optical measurements, Wymer obtained the following empirical formulae for film thickness at the contact centre and at the exit constriction:

$$H_0^* = .44\ U^{*0.64}\ W^{*-0.17}\ G^{*0.58} \quad \ldots\ldots (2.9)$$

$$H_1^* = 1.56\ U^{*0.71}\ W^{*-0.17}\ G^{*0.57} \quad \ldots\ldots (2.10)$$

Unblended rollers were seen to exhibit extremely severe side constrictions, which where far more sensitive to load than the exit constriction. Profiles measured through the side constriction are shown in figure 2.4.

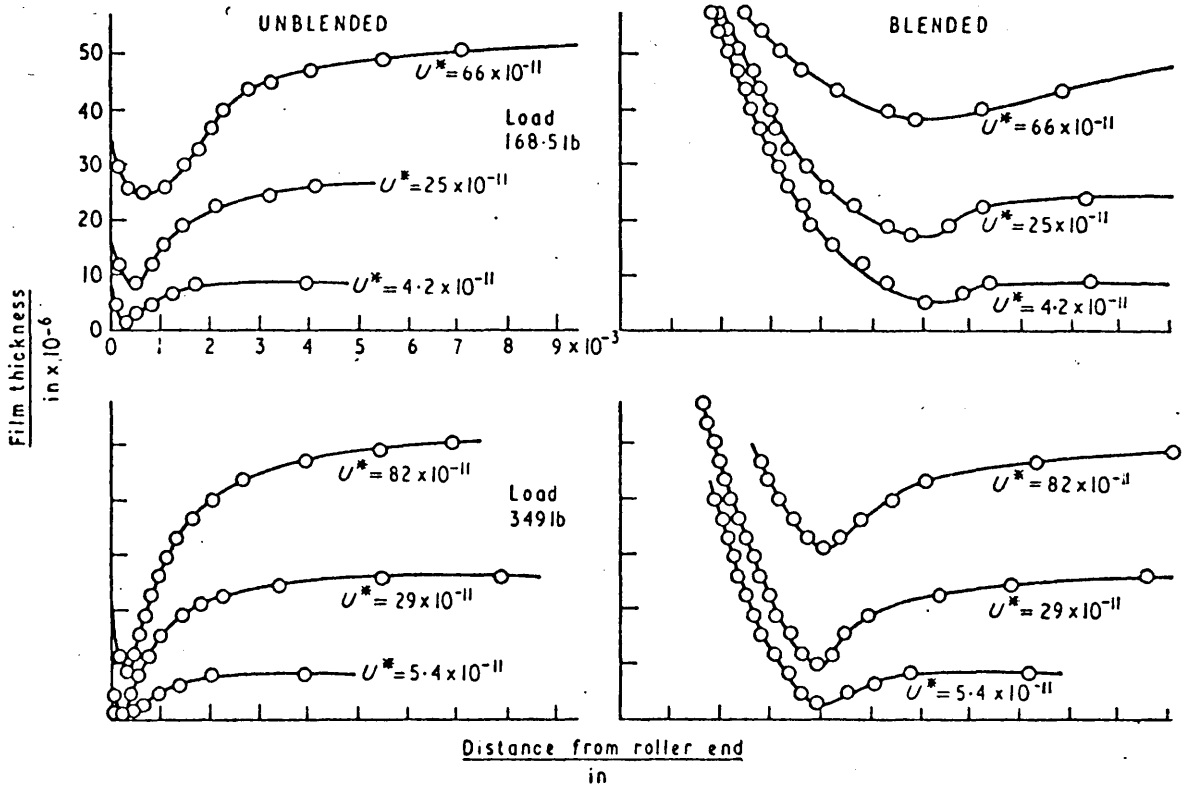

Figure 2.4 Shape profiles measured through the side constriction in a line contact.

(after Wymer and Cameron (81))

Central film thickness was measured under starvation conditions and the dependence upon inlet boundary distance determined. Simultaneous interferometric and electrical measurements were made by using the semi-reflecting metallic coating as an electrical conductor. Electrical resistance measurements enabled asperity contact to be monitored with an accurate knowledge of film thickness. Capacitance measurements were also used, and the technique refined by using a silica insulating spacer layer to prevent short circuits through the film. The results showed excellent agreement with those obtained optically.

Jackson (1973 (82)),and Cameron and Jackson (1974 (83)) have used optical interferometry to make a study of the lubrication of rough surfaces. A smooth glass plate was rotated over a static steel ball on which artificial, two dimensional roughnesses had been created. Placing the roughness lay parallel to the sliding direction resulted in a substantial drop in film thickness. With the lay transverse to the sliding direction, no appreciable drop in film thickness occurred. However in this orientation it was seen that cavitation, occurring behind a predominant asperity,could cause starvation of the following contact. This is shown in figure 2.5. Of great significance to the lubrication of real surfaces was the demonstration that micro-E.H.L. of asperities is feasible.

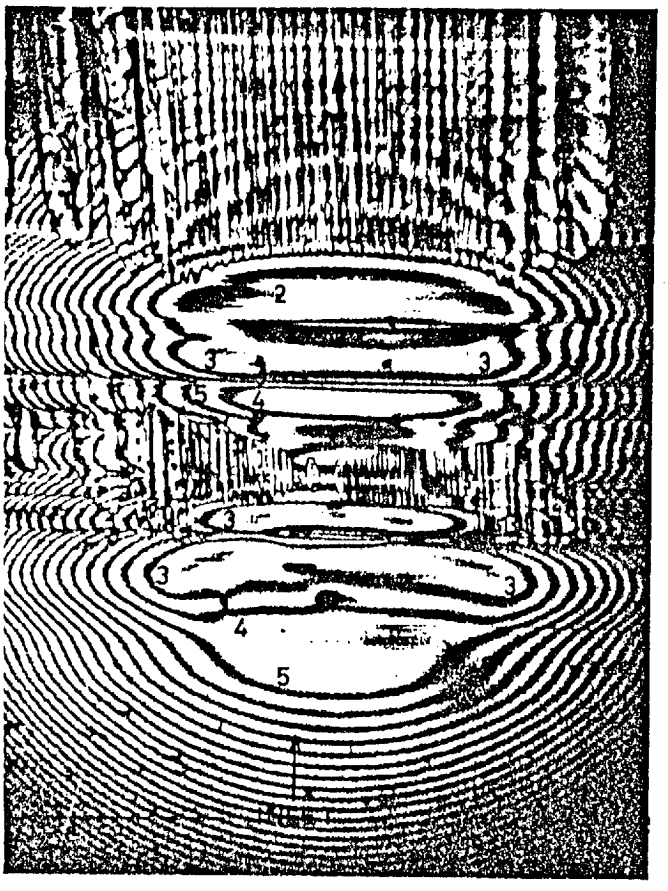

Figure 2.5 Cavitation behind a predominant asperity.

(after Jackson and Cameron (83))

2.3.2 Pressure and Temperature Measurement.

Conventional methods of measurement by the use of manometry and thermocouples, were hindered by the physical size of an E.H.D. contact. Early attempts overcame this by using large radius discs under very heavy loads (1963 (84, 85)), (1964 (86)). Results were in basic agreement with theory, but pressures were still not high enough to be typical of an actual E.H.D. contact. Longfield (1965 (87)) produced pressures as high as 30,000 p.s.i. and reported the existence of a small pressure peak near the exit. This was also found by Niemann and Gartner (1965 (88)).

Kannel, Bell and Allen (1965 (89)), who were unsuccessful in predicting pressure curves from X-ray film profile measurements, introduced a technique similar to that used by Crook for film thickness measurements. A thin strip of manganin was evaporated across the surface of one of the quartz discs. The resistance of manganin is sensitive to pressure, and only slightly to temperature. Monitoring the resistance of the strip as it passes through the contact, enables a pressure curve to be obtained. Initial results did not show the pressure peak, but this may have been obscured by the finite width of the transducer.

Cheng and Orcutt (1965 (90, 91)) used a strip of platinum, which is temperature sensitive, as well as a

manganin strip. In this way they obtained simultaneous profiles of pressure and temperature. In addition film thickness profiles were obtained from capacitance measurements, using one of the strips. Figure 2.6 shows typical oscilloscope traces.

The existence of the pressure peak was confirmed by Kannel (1965 (92)), (1966 (93)), and later by Hamilton and Moore (1967 (94)). This was as a result of using narrower transducers, and higher pressures. The peak was still considerably less than that predicted by theory. However the technique is still limited by the physical size of the transducer.

Photoelastic techniques have also been applied to measure pressure distribution by Klemz, Gohar and Cameron (1971 (95)), and Cope and Hains (1969 (96)). Under certain conditions Klemz et al. showed the existence of a truncated pressure spike. Wymer (1972 (80)) has computed pressure distributions, from optically measured film profiles, which show a marked pressure peak just before the exit constriction.

Turchina, Sanborn and Winer (1973 (97)) have recently made temperature measurements, by using an infra-red radiometric detector to measure the radiation emitted by a ball sliding on a sapphire plate. The spot size of 0.0014 in. enabled temperature to be determined

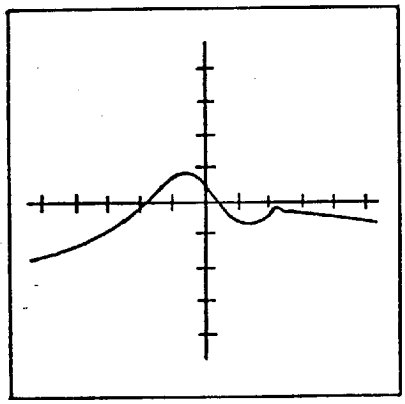

Surface temperature, no sliding, 135in/sec, 700lb/in, 1.45°F/div.

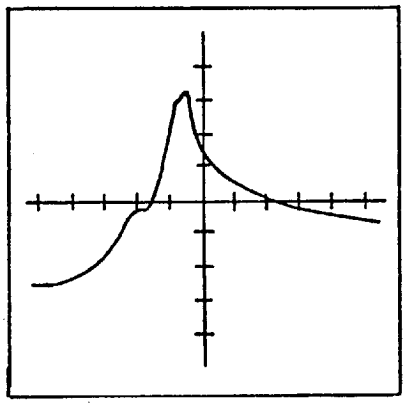

Surface temperature, U_1=141in/sec, U_2=125in/sec, 700lb/in, 1.45°F/div.

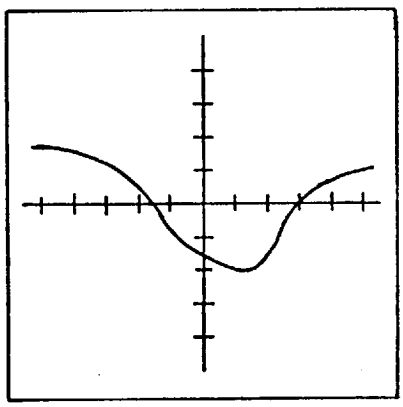

Deformation profile, 135in/sec, 1000lb/in, Hertz zone = 2.34 div.

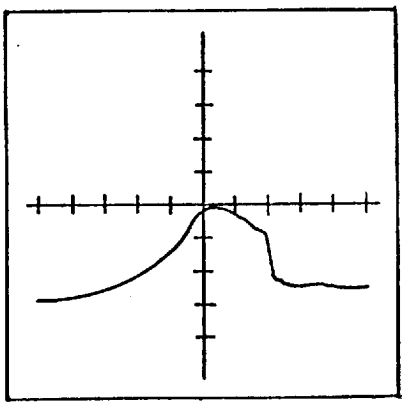

Pressure distribution, 135in/sec, 1000lb/in, 200μV/div.

Figure 2.6 Oscilloscope traces of temperature, film thickness, and pressure, obtained from evaporated transducers.

(after Orcutt (90))

at various points of the contact. Both the local steel ball surface temperature, and the local lubricant temperature, averaged through the film, could be measured. Ball temperatures as high as 115°C, and fluid temperatures of 360°C were reported. Wymer and Macpherson (1974 (98)) have applied the same technique to the measurement of gear tooth surface temperature, immediately after mesh. With the gears transmitting 275 hp., temperature rises of 50°C above bulk were measured. A scoring/healing cycle was also observed. The technique is not difficult to apply, is instanteous in response, and does not interfere with the surface under study. However the measured radiation is extremely difficult to interpret in terms of actual temperature.

Temperature measurements in lubricated E.H.D. contacts confirm the theoretical approach, that it is the contact inlet conditions that determine the film thickness within the actual contact.

2.3.3 Traction and Non-Newtonian Behaviour in E.H.L.

It has been shown that the film thickness in concentrated contacts can be accurately predicted by coupling the conventional Reynolds equation, and equations for elasticity of the bounding surfaces, with the pressure-viscosity characteristic of the fluid. However it is not

possible to predict traction behaviour, assuming a conventional Newtonian lubricant. This again reflects the fact that film thickness in E.H.D. contacts is dependent upon inlet conditions, whereas the traction forces that can be transmitted by the lubricant, depend upon conditions within the contact itself.

If traction force is plotted against sliding speed, a characteristic curve emerges. This is shown in figure 2.7. Typical examples of this have been obtained by Crook (1963 (99)), and Johnson and Cameron (1967 (100)). At low sliding speeds, and thus small values of shear rate, the curve is linear; as sliding is increased the curve becomes increasingly non-linear, until a maximum traction force is reached. Any further increase in sliding then results in a fall in traction.

The traction characteristic is of great significance to the lubrication of rolling element bearings, in particular to the case of lightly loaded high speed applications, where the bearing may be operating near the peak of the traction curve. Skidding of the rolling elements will occur if there is insufficient traction to drive the cage at epicyclic speed. High temperatures are then produced as a result of the large shear rates within the contacts, and the film thickness drops. In a rolling element bearing, slip is most likely to occur at the inner race contacts. The lower cage speed will reduce the

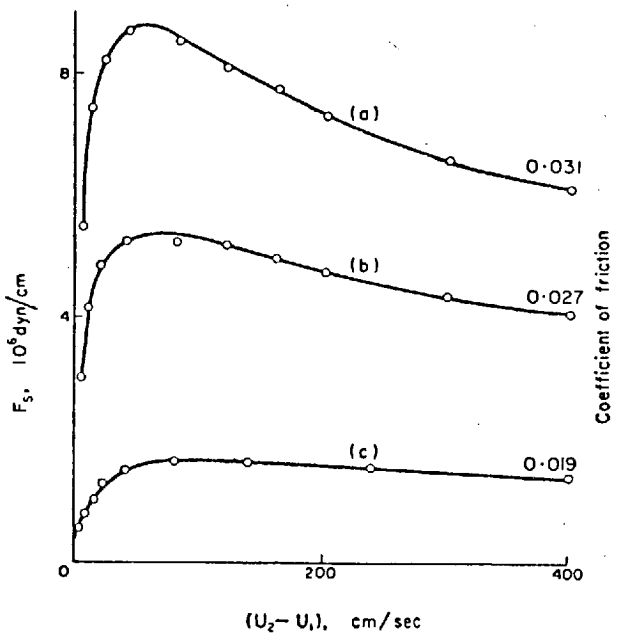

Rolling speed constant at 400 cm/sec. Load (10^7 dyn/cm):
(a) 20 (b) 15 (c) 7·5.

Figure 2.7 Variation of traction with sliding speed.

(after Crook (99))

amount of oil supplied to these contacts by the surfaces of the rolling elements, and starvation may occur. If the traction peak is exceeded, the cage speed may become unstable, resulting in excessive skidding and ultimate failure. Bearing tests demonstrating this have been recently carried out by Ford and Foord (1975 (101)).

Many theories have been put forward to try to explain the shape of the traction curve, and there has been much speculation as to the nature of the fluid itself, when subjected to extremely high pressures for a very short time duration. The thermal approach to the problem, assuming Newtonian lubricant (1961 (102)), (1965 (35, 37)), predicts the general shape of the traction curve. However Johnson and Cameron (100) have shown that, in addition to thermal effects, non-Newtonian viscoelastic behaviour of the lubricant must be considered.

In 1967 Fein (103) postulated that fluid in a rolling contact would not reach its equilibrium viscosity, owing to the very short duration of the application of high pressure. This has now been confirmed experimentally by Paul (1974 (1)). Harrison and Trachman (1972 (104)) used this approach, assuming Newtonian response to small shear rates, to obtain good correlation with measurements of effective viscosity by Johnson and Cameron (100). However Crook (1963 (105)), and Dyson (1970 (106)), have hypothesised that the oil was responding to small shear strains as an

elastic solid. In order to try to ascertain the type of fluid response to small strain rates, which is the region where the traction curve is linear, Johnson and Roberts (1974 (107)) divised a method of differentiating between viscous (liquid) and elastic (solid) response, when small amounts of sliding are imposed on a rolling contact. This was achieved by tilting the axis of one of the discs in their disc machine, and so introducing 'spin' at the contact. A Newtonian fluid will develop shear stresses in proportion to shear rate, whereas an elastic solid develops shear stresses in proportion to the total shear strain. During rolling with spin, a viscous liquid will give zero tractive force, while an elastic solid produces a force at right angles to the rolling direction. It was concluded that the lubricant showed a transition from predominantly viscous to predominantly elastic behaviour, with increasing pressure at constant temperature. This transition which also occurred with decreasing temperature, at constant pressure, shows general agreement with predictions of a simple viscoelastic model, based on Maxwell theory. The suggestion that time dependent viscosity significantly effects E.H.D. traction measurements was found to be inconsistent with their observations.

At high shear rates when the traction curve is non-linear, Smith (1965 (108)), Dyson (106), Johnson and Cameron (100), postulate the existence of a limiting shear

stress, independant of shear rate, that can be sustained by the film. This limiting value is dependent upon pressure and temperature. Trachman and Cheng (1972 (109)) have made good predictions of the whole of the traction curve by assuming a hyperbolic relation between shear stress and shear rate,based on a limiting shear stress. They also took into account the effects of a delayed response of viscosity to a pressure step.

2.4 Lubricant Starvation

The formation of an E.H.D. film in concentrated contacts is dependent upon there being sufficient oil, within the entry region, to provide a medium for pressure build up to occur. If the inlet region is adequately supplied with lubricant ,the resulting film thickness is unaffected by an increase of lubricant supply, and the contact is 'fully flooded'. If the inlet is inadequately filled, pressure build up is delayed, and the film thickness becomes dependent upon the available lubricant supply. This situation is defined as lubricant 'starvation'. Conventional solutions to the E.H.D. problem assume that the pressure build up starts at an effectively infinite distance from the edge of the contact zone. However there is now considerable experimental evidence to suggest that this is not always the case in practical situations.

Booser and Wilcock (1953 (110)) conducted experiments with ball bearings lubricated with minute quantities of oil. Their results showed that bearing life varied exponentially with the amount of oil present. They also found that life was related to the rate at which oil was lost from the bearing, this being dependent upon viscosity and surface tension. This was a clear indication that these bearings were running under starved conditions. Gyroscope bearings contain a minimum of lubricant to minimize both lubricant and rotor mass shifts. Horsch (1963 (111)) has shown that these bearings typically run on a film thickness of the order of 10 μin. Small quantities of oil added to the bearing resulted in large increases in film thickness, demonstrating that the bearing was running starved.

Wymer (1974 (81)),who found great difficulty in avoiding starvation while making optical measurements with a single roller thrust bearing,states: 'it is very likely that almost every commercial roller bearing must run heavily starved'.

The theoretical approach to the problem initially considered the effect of reduced inlet position (where $p = o$) on the load carrying capacity of rigid surfaces. Such a solution is given by Floberg (1961 (112)), Dowson and Whitaker (1965 (37)), Boness (1966 (113)), Dowson and Whomes (1966 (114)). These results show that the

inlet boundary position is not significant until it is very close to the line of centres. Fein and Kreutz (1967 (115)) considered starved E.H.D. lubrication of a hemispherical asperity model, and showed that the majority of pressure build up occurred within a distance of the Hertzian flat, equal to:

$$3\left(\frac{Rh_0}{a^{1/3}}\right)^{2/3}$$

Orcutt and Cheng (1966 (116) produced a solution for starved E.H.D. line contact. The effect of inlet boundary on film thickness, was deduced for a particular load and speed.

Lauder (1965 (117)) attempted to explain his low experimental film thickness results by proposing that $p = o$ where the fluid velocity and velocity gradient are zero ie. $u = \frac{du}{dz} = o$. This is represented by a point in mid-film, upstream of which fluid flows backwards relative to the Hertzian region. Wedeven (1970 (69)) calculates that in pure rolling this point occurs when $h/h_0 = 3$. His experimental results show that when the inlet boundary reaches this point, the film thickness has already been reduced by about 22%. Starvation was seen to occur for inlet boundary locations downstream of the point at which $h/h_0 \simeq 9$. Thus pressure build up, essential for establishment of flooded conditions, takes place over a region

where there is fluid backflow.

Tipei (1968 (118)) suggests that counter-flow in the inlet leads to formation of two bounded vortices (see figure 2.8), and that a line drawn through the centre of these defines the location where p = o. He calculates this to occur at $h/h_0 = 9$. Wedeven, on the basis of his experimental findings, chooses this as a criterion for the onset of starvation, but suggests that p = o at the point where the fluid film completely fills the gap between the bounding surfaces. The point at which $h/h_0 = 9$ was shown to occur at a distance from the edge of the Hertzian contact equal to:

$$\frac{3.52\ (Rh_0)^{2/3}}{a^{1/3}}$$

This is in very close agreement with the statement of Fein and Kreutz. Wedeven, Evans and Cameron (1970 (47)) have produced the following semi-empirical formula to represent their results for starved point contact:

$$H_0^* = 1.73 Ks \left(\frac{\alpha \eta_0 U}{R}\right)^{0.714} \left(\frac{W}{E^T R^2}\right)^{-0.048}$$

where

$$Ks = \left(\frac{S}{Sf}\left[2 - \frac{S}{Sf}\right]\right)^{\frac{1}{2}}$$

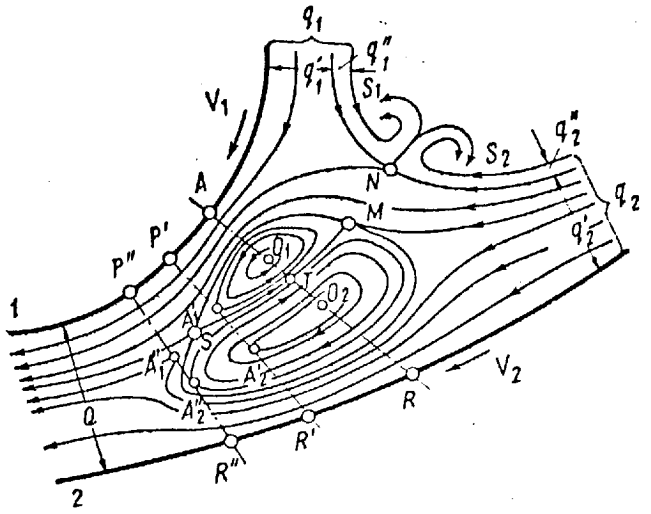

Figure 2.8 Flow spectrum in the inlet region

(after Tipei (118))

S is the inlet boundary distance, and S_f is the minimum inlet distance necessary to obtain flooded conditions. It was noted, from the optical experiments, that excess lubricant was frequently found at the sides of the track. Wedeven et al. proposed that these areas were acting as reservoirs, from which lubricant could flow into the inlet by the action of surface tension. They concluded that the consequences of starvation are not all detrimental, as it also has the effect of reducing rolling friction and increasing traction.

Wolveridge, Baglin and Archard (1970 (119)) have produced a semi-analytical solution for the starved lubrication of cylinders in line contact. Under E.H.D. conditions, 'Grubin' type assumptions were made. This solution enables β, the ratio of actual film thickness h to film thickness under fully flooded conditions h_∞, to be calculated from the value of Ψ_i, the inlet boundary parameter defined as:

$$\Psi_i = \frac{b^{1/3} X_i}{(2Rh_\infty)^{2/3}} \qquad \ldots\ldots (2.11)$$

Excellent agreement was found with the earlier result of Orcutt and Cheng.

Wymer (1974 (81)) has made optical measurements, similar to those of Wedeven, of the effect of inlet boundary position on film thickness in line contact. To

represent his results he derived the following empirical relation:

$$\beta = \frac{2}{\pi} \arctan \left[1.37 \left(\Psi_{i+\frac{1}{2}} \right)^2 \right] \qquad \ldots\ldots (2.12)$$

This relationship is shown by figure 2.9 together with the theory of Wolveridge et al. There is excellent agreement, except at low values of the inlet distance parameter. Wymer has shown that even at zero inlet distance, film formation is still possible.

A full solution to the problem of starved E.H.D. line contact has been presented by Castle and Dowson (1972 (120)). Figure 2.10 shows typical E.H.D. film shapes and pressure distributions for starved lubrication conditions. The variation of film thickness ratio β against starvation parameter Ψ_i, obtained for the full solution, were plotted for comparison with the results of Wolveridge et al. The exceptionally good agreement provided confirmation of the validity of the 'Grubin type' approach. An important observation made in this paper is that partial starvation of an E.H.D. contact can result in a significant decrease in rolling friction, with only a small reduction in film thickness. Archard and Baglin (1974 (121)) have presented a broad semi-analytic treatment of frictional tractions in starved E.H.D. lubrication. They too find that mild starvation can markedly reduce

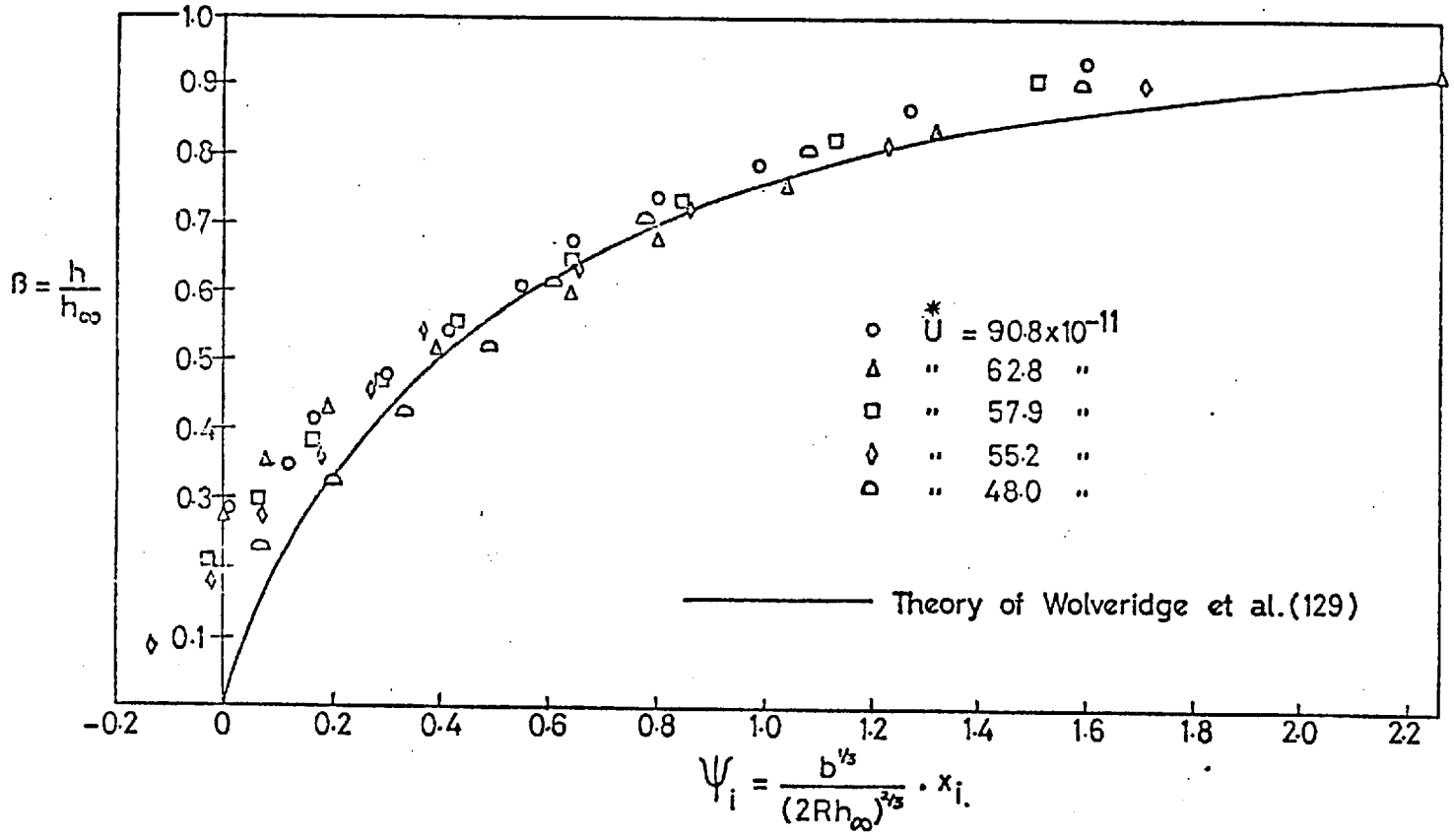

Figure 2.9 Variation of film thickness parameter β with inlet distance parameter Ψ_i.

(after Wymer and Cameron (81))

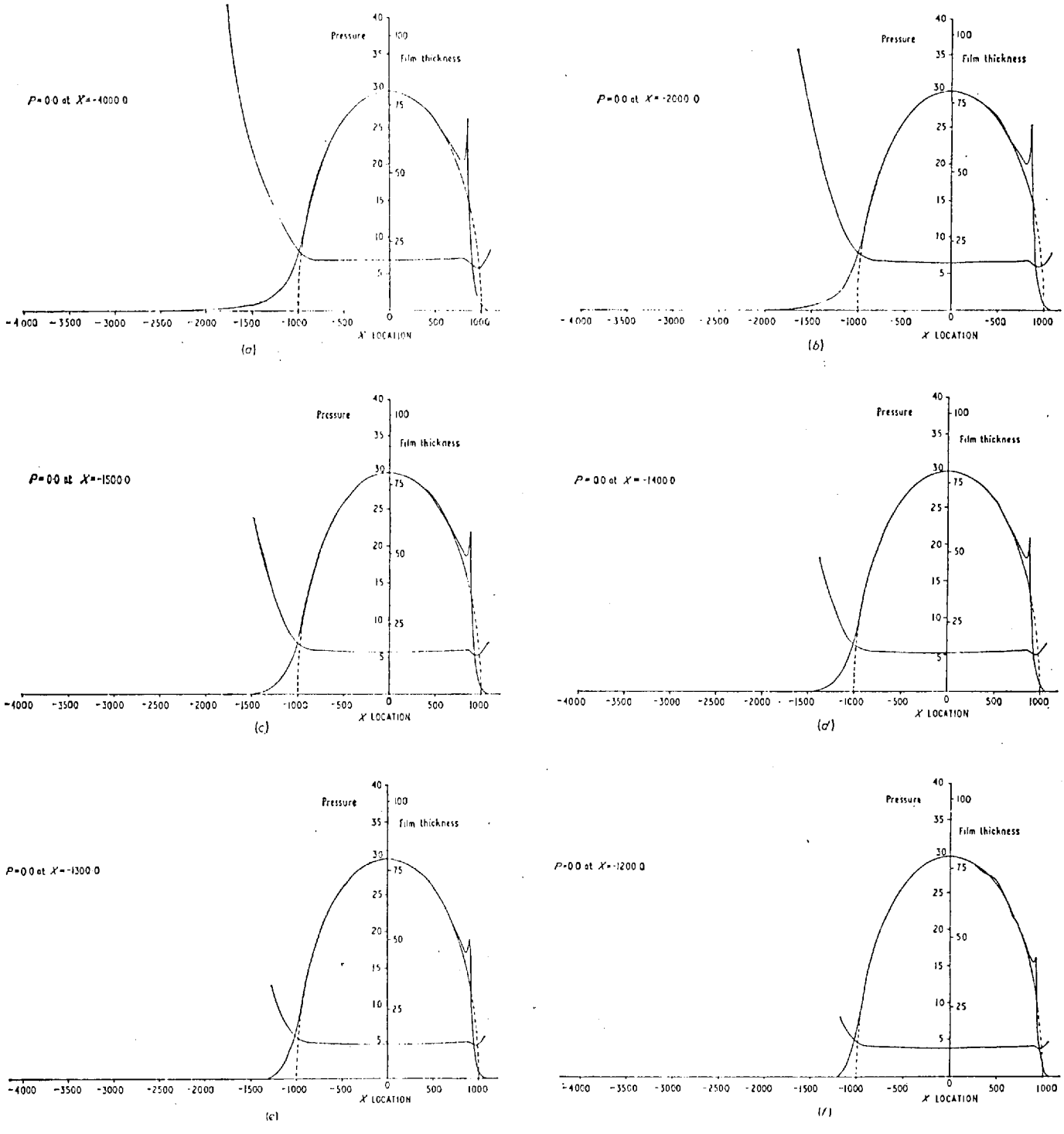

Figure 2.10 Theoretical film shapes and pressure distributions under starved conditions.

(after Castle and Dowson (120))

rolling friction, with negligible influence upon film thickness. However sliding friction, which is more dependent upon film thickness, is only markedly affected by severe starvation.

In order to explain the long term decay in film thickness that occurs in gyro bearings after an oil jog, Kingsbury (1972 (122)) has proposed a flow model in which the oil is gradually pumped out of the track, by cross flow occurring within the high pressure Hertzian region. Considering a particular gyro bearing running with no oil inflow, he calculates that it will take approximately 280 hours to pump all the oil out of a contact initially 20×10^{-6} in. thick and under a load of 100,000 lbs/in. He concludes that this type of calculation predicts bearing lifes of the same order as is experienced in retainerless bearings, which have no provision for oil recirculation.

Empirical and theoretical equations can accurately predict the film thickness in starved contacts, if the inlet boundary location is known. In a practical situation this is unlikely to be the case. Chiu (1974 (123)) has recently developed a theory to predict the occurrence, and effect of starvation in point contact. This theory does not rely on meniscus location as an input parameter, but on a knowledge of the oil/air surface tension and rolling element spacing. Chiu proposes that in a rolling element

bearing, the passage of a contact creates a depression in the fluid layer on the track surface. In between contacts oil is drawn in from the track edges, due to the surface tension gradient in the depression. The degree of oil replenishment, which controls the upstream fluid layer thickness and hence position of the inlet boundary, is dependent upon the time between successive contacts, the fluid viscosity and the surface tension of the liquid/air interface. The graph obtained by Chiu, shown in figure 2.11, illustrates the relation between plateau film thickness, speed, and a parameter dependent upon the oil/air surface tension and rolling element spacing. Also shown are experimental measurements of film thickness, made using a simple optical rig. Good correlation with theory was obtained. However the rig only allowed for operation with one ball. Two oils were tested, only one of which showed the drop in film thickness predicted by his theory. Kingsbury (124) has observed fringes in the oil film at the track edges of a ball bearing. Since these are seen to be unchanged by many ball passes he concluded that there is no oil rebound. Chiu's findings are not consistent with those of Ziegler (1972 (125)), who has made film thickness measurements in ball bearings, for various ball complements. Ziegler's measurements showed that for a given lubricant level, thicker films were generated with a six ball complement, than with a three ball complement, although power stability was not so good.

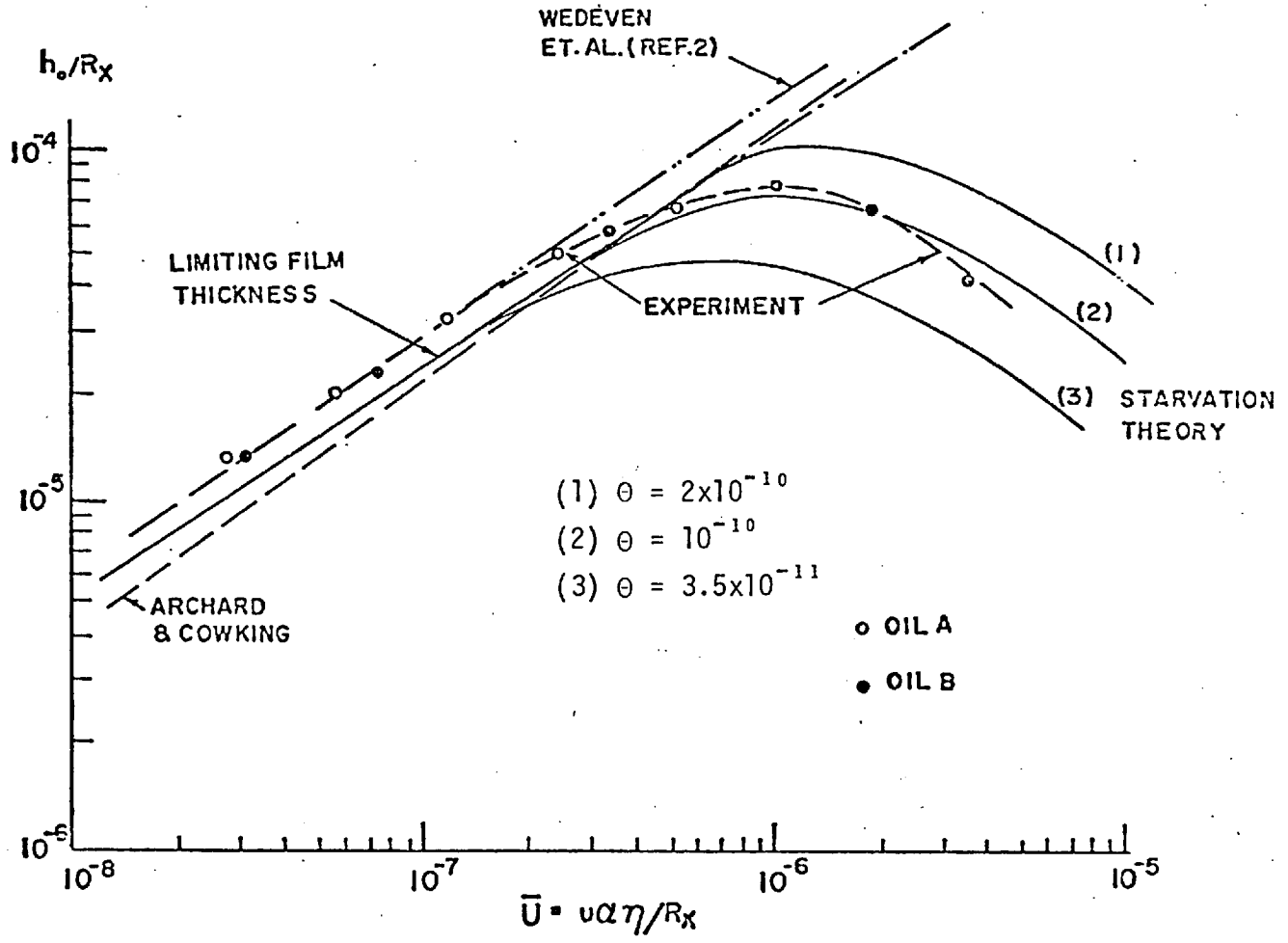

Figure 2.11 Relation between plateau film thickness, the parameter $U \propto \eta_o/Rx$, and a parameter θ, dependent upon the oil/air surface tension and rolling element spacing.

(after Chiu (123))

Of relevance to starvation is the quantity of oil that can be carried by the bearing surfaces. Smart and Ford (1974 (126)) have developed a fluorescence technique of measuring thin films adhering to the surfaces. A typical gas turbine lubricant applied to a race spinning at 10,000 R.P.M., resulted in a mean equilibrium thickness of 40 μin. This, they conclude, would barely supply enough lubricant to maintain a contact film thickness sufficient to separate the surface roughnesses.

Recently Dowson (1974 (127)) has made capacitance measurements of film thickness in a disc machine, running under starved conditions. He suggests that, in circumstances where the initial supply of lubricant is not supplemented during running, the inlet boundary adopts the position of the 'zero reverse flow condition'. This is the point where $u = \frac{du}{dz} = 0$, originally suggested by Lauder (117) as the start of the inlet pressure build up. Visual studies of the disposition and migration of the lubricant within the inlet region, were made using a photo-luminescence technique. This revealed that large side bands of lubricant were formed at the track edges. It was proposed that these bands provide lubricant for the conjunction, or accept excess fluid in order to conform with the 'zero reverse flow condition', under changing conditions of load and speed.

Wedeven (1975 (128)) has now made traction measurements for a point contact under starved E.H.D. conditions. In all cases a starved film was observed to produce greater traction, than the corresponding flooded film, for the same slide roll ratio. Under conditions of severe starvation and low shear rate, traction was lower than expected. It was suggested that the high shear stresses, produced by the large pressure gradient within the inlet region, may influence the traction developed in the Hertzian region.

2.5 The Lubrication of Rolling Element Bearings

2.5.1 Oil Film Measurements.

The majority of measurements, made in actual bearings, have been obtained using the electrical resistance technique. Although this does not allow actual film thickness measurement, it immediately shows whether the bearing is operating under conditions of hydrodynamic lubrication. Also the degree of metallic contact can be monitored.

Garnell and Higginson (1965 (129)) have made electrical resistance measurements in a roller bearing. Theoretical film thicknesses were calculated from E.H.L. theory and compared to resistance values obtained at various loads and speeds. This showed that as soon as

the theoretical film thickness exceeded the combined c.l.a. surface roughness values of roller and track, the resistance rose sharply, indicating the start of hydrodynamic lubrication. When the film thickness exceeds the peak-to-valley roughnesses there is virtually complete fluid film lubrication. Torque measurements were also made, and it was shown that viscous rolling friction makes a large contribution to the total torque. In a continuation of this work, Garnell (1966 (130)) makes the observation that zero resistance is never observed when the theoretical film thickness exceeds about three-quarters of the sum of the c.l.a. roughnesses. He concludes that there can be little actual metal-to-metal contact, and asperities are in general separated by thin films at least a few molecules thick.

Horsch (1963 (111)) made simultaneous measurements of capacitance and electrical resistance between the inner and outer races of a gyro bearing. He also measured the change in axial dimension between the loaded faces, using a linear variable differential transformer, as well as monitoring the torque. From these measurements Horsch demonstrated that it was possible to run gyro bearings on a full film, with less than 0.1 milligrams of lubricant. Positional instabilities such as jogs were seen to be caused by film thickness changes. Important observations concerning starvation were made (see section 2.4).

The feasibility of using evaporated transducers for film thickness measurements in an actual bearing, has been demonstrated by Kannel, Bell, Walowit and Allen (1968 (131)). Using a manganin transducer they made pressure measurements in an 85 mm. angular contact ball bearing. It was concluded that the pressure distribution does not depend significantly upon the lubricant type.

A direct displacement technique, using a distance transducer, was applied to a taper roller thrust bearing by Grafton (1968 (132)). However this was more successfully applied by Jones and Crease (1969 (133)), who obtained good correlation with the theory of Dowson and Higginson. Meyer and Wilson (1971 (134)) have developed a method, using a strain gauge, to measure film thickness in a preloaded bearing. The strain gauge was attached to the outer race of a three ball preloaded instrument bearing. The initial interference can be measured by noting the change in strain, as the balls roll around the raceway in the absence of lubricant. Lubricant is then added and strain readings taken, at the desired load and speed, to determine the new effective interference. The results showed good agreement with theory for diester lubricants, but at high speeds the film thickness produced by paraffinic lubricants was considerably lower than predicted.

Ziegler (1972 (125)) has made direct measurement of axial displacement in gyro bearings. Film thickness and torque stability were investigated for various ball configurations and lubricants, at minute flow rate. It was concluded that many instrument bearings must actually operate under starved conditions, with films a small fraction of that predicted by E.H.D. theory. Under these conditions the film thickness is merely dependent upon the amount of oil in the bearing track.

The resistance technique has been applied by O'Brien and Taylor (1973 (135)) to assess the contact conditions during a study of cage slip in roller bearings. An interesting observation was that, during a period of six hours after cut off of lubricant supply, cage slip decreased and percentage metallic contact also decreased. This was explained in terms of a reduction in heat generation, due to churning and shear, causing an increase in lubricant viscosity.

The application of the optical interferometry technique to measurement of oil film thickness in actual bearings is not easy. One of the races, or part of a race has to be optically transparent. Glass is usually used, but is not suitable for high loads. Sapphire, which can withstand very high pressures, is difficult to machine and polish. To simulate the kinematics of an actual bearing, it is necessary to allow the cage to rotate, therefore

the interference fringes must be observed stroboscopically.

Wedeven (1970 (69)) has observed interference fringes stroboscopically, for a thrust bearing assembly in which the upper race was made of glass. The effect of ball spin, caused by gyroscopic forces, was noted. Taper rollers were also used in the same rig, but loads were low for a line contact situation. Severe constrictions at the roller ends were noted.

Bahadoran and Gohar (1974 (136, 137)) have made optical film thickness measurements through the glass outer race of a cylindrical roller bearing, containing four rollers. However the bearing was operated in a counter-rotation mode (the cage is held stationary while inner and outer races rotate in opposite directions). Speeds and loads were low in comparison to typical values encountered in normal bearings. Starvation was seen to occur when only a light oil smear was applied to the outer race. Except at very small inlet distances the relation between film thickness and the inlet boundary position, was in extremely good agreement with the theory of Wolveridge, Baglin and Archard (119). It was noted that the inlet meniscus was often larger at the roller ends, than at the contact centre. This was attributed to an oil-replenishment action similar to that observed by Chiu (123). Bahadoran (136) has made film thickness measurements using crowned rollers to obtain elliptical

contacts, and also has investigated the effect of edge blending on the side constriction.

2.5.2 Effect of Film Thickness on Fatigue Life.

It has long been understood that lubricant films can prevent metallic contact in highly stressed components, such as gears and bearings; however it was not until the advent of E.H.D. theory that the actual film thickness could be accurately calculated, and related to such factors as fatigue life.

Dawson (1962 (138)) studied the effect of metallic contact on the pitting of lubricated rolling surfaces, using a disc machine. He plotted the number of revolutions to pit, against the total initial surface roughness, and obtained a straight line using log-log axes. This line was seen to be of the same slope as that obtained by plotting revolutions to pit, against oil film thickness, calculated from Crook's measurements. He concluded that increasing the oil film thickness had the same effect as reducing surface roughness. He therefore proposed the following dimensionless ratio to determine pitting behaviour:

$$D = \frac{\text{Total initial surface roughness of both discs}}{\text{oil film thickness}}$$

Dawson noted that when the calculated film thickness was several times greater than the total surface roughness, pitting still occurred at the extreme track edges. This, he suggested, was caused by side leakage from the contact area causing a drop in film thickness at the edges. By rounding the disc edges he was able to prevent pitting. He concludes that, in the complete absence of metallic contact, pitting does not occur at all.

Radio-isotope techniques have been used by Lawrence and Schmidt (1962 (139)) to investigate surface contact in rolling element bearings. They found that regions of maximum material transfer occurred at the roller ends. Under conditions of an uninterrupted film there appeared to be no material removal.

Tallian et al. have carried out extensive research concerning the failure of lubricated rolling contacts, (1964 (140)), (1965 (141, 142)), (1967 (143, 144)). A rolling four ball test configuration was used, and electrical conductivity measurements made. Predictions of contact time fractions and contact frequencies, based on ball surface profiles, agreed well with experimental results. Wear rate was monitored by a radio tracer technique and shown to be closely related to the amount of metallic contact. A dimensionless ratio, similar to that used by Dawson, is defined as:

$$\xi = \frac{\text{Mean film thickness}}{\text{Composite R.M.S. roughness of the surface}}$$

This parameter was found to have great influence on the wear rate and fatigue life of the balls. Figure 2.12 shows the relation obtained between ξ, and life to spalling (sub-surface) fatigue failure. Tallian (143) describes the transition from partial E.H.D. lubrication to boundary lubrication, as occurring when $\xi \approx 2$. In this region, substantial forces are transmitted through the asperities. When $\xi > 2$, the majority of the load is carried by the E.H.D. film, asperity contact is isolated, and wear is extremely small.

Harris (1966 (145)), Given (1966 (146)), and Danner (1970 (147)), have also published results relating fatigue life, with the ratio of film thickness to composite surface roughness. Endurance tests have been made on roller bearings by Skurka (1970 (148)). Surface finish, shaft speed, lubricant viscosity and lubricant temperature, were varied. The ratio of test life to calculated life, was plotted against the ratio of E.H.D. lubricant film thickness to the composite rolling contact surface finish. The graph he obtained showed a dramatic increase in life following the transition from minimum to full film lubrication conditions.

Popinceanu et al. (1972 (149)) have made fatigue tests, coupled with electrical resistance measurements, on

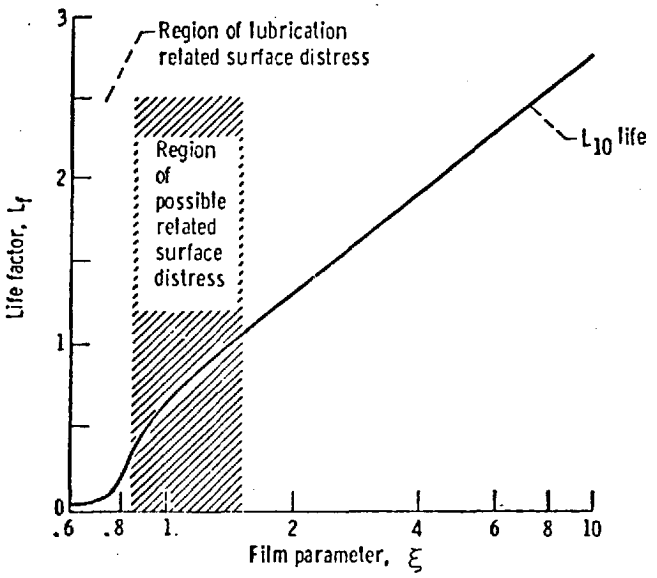

Figure 2.12 Relationship between the ratio of film thickness to surface roughness, ξ, and fatigue life.

(after Tallian (143))

mineral oil lubricated ball bearings. It appeared from these tests that there is an optimum viscosity that ensures maximum rolling contact fatigue life. This optimum viscosity increases with increasing load,and decreases with increasing speed. It is shown that the optimum viscosity is slightly higher than that required to produce a film, sufficient to just separate the total roughnesses of ball and raceway, as calculated from E.H.D. theory. Values of optimum viscosity obtained from the electrical resistance tests,were consistently higher than those obtained from the theoretical predictions, and life tests. This was attributed to a difference in temperature measurement technique,between the two tests. It was concluded that the reduction of fatigue life, when optimum viscosity is exceeded, could be caused by starvation effects, or by thermal effects, both of which can lead to a drop in film thickness below that necessary to separate the surface roughness. Similar behaviour had been observed earlier by Appeldoorn and Royle (1965 (150)), using a four ball tester to fatigue test Ceramic balls, and also by McCool (1971 (151)).

The effect of E.H.L. on pressure distribution and maximum sub-surface shear stress,has been extensively investigated by Kannel and co-workers. A review of this work is given in (1967 (152)). In pure rolling, the sub-surface stress level is shown to be not greatly different from that occurring in a static condition. However Diaconescu

(1975 (153)) has shown that, when sliding occurs, traction forces and asperity contact can have a significant effect on sub-surface stresses, which greatly alter fatigue life. He has made theoretical predictions of fatigue life which are in extremely good agreement with his experimental results.

Partial E.H.L., asperity contact and the possibilities of micro-E.H.L., are extremely complex subjects which, although relevant to some bearing situations, are considered to be beyond the scope of this review. The theory of partial E.H.L. has been extensively reviewed by Tallian (1972 (154)). Archard (1973 (155)) discusses the application of E.H.L. theory to real surfaces.

2.5.3 Cage and Roller Motion in High Speed Roller Bearings.

In general, temperatures of high speed rolling element bearings can be kept to a minimum by jet feed of large quantities of oil. Provided there is adequate scavenge arrangements on both sides of the bearing, the temperature can be reduced by increasing the oil flow rate. This has been observed by investigators in references (1952 (156, 157)), (1970 (158)). The number of oil jets and the necessary location to ensure optimum cooling, is discussed by Murteza (1958 (159)), and by Macks, Nemeth and Anderson (157).

Dowson and Higginson (1963 (160)) have shown that the cage motion in bearings operating in the E.H.D. regime, will be essentially epicyclic, whereas large amounts of slip can be expected in lightly loaded bearings. This has been confirmed experimentally by Garnell and Higginson (1965 (129)). However even with the cage turning at epicyclic speed, there may be considerable variation of roller speed around the track of a cylindrical roller bearing. This is shown to be the case by Iida and Igarashi (1959 (161)), particularily for large clearance bearings running at slow speeds. These rapid accelerations, that occur at the load zone inlet, can give rise to 'Skid mark damage' (143). Tests conducted by Smith (1962 (162)) with lightly loaded high speed roller bearings, such as those in an aircraft gas turbine, indicate that slip is often considerable. Although this may not be detrimental, slip can often result in unstable operation, and lead to excessive wear. Boness (1969 (163)), (1970 (164)), has made an extensive experimental and theoretical study of cage and roller motion. The theoretical work covers the regime of rigid bearing surfaces lubricated by a compressible fluid, having pressure-viscosity dependence. Predictions of cage slip based on the assumption of an infinite inlet boundary, were higher than experimental results. However by using the boundary condition of Lauder (see Section 2.4) he was able to accurately predict cage slip. Boness has shown that oil supply can have a significant effect upon cage

slip. He predicts theoretically that if the inlet boundary is reduced to the minimum distance required to maintain hydrodynamic conditions, an increase in cage speed of up to 75% will result. This is consistent with his experimental results using reduced oil supply, and with recent experimental work by O'Brien and Taylor (1975 (135)), and Hargreaves and Higginson (1975 (165)).

2.6 Implications

Lubricant film thickness has been shown to be an extremely important parameter regarding the life of bearings. Although there is still much to be learnt concerning the behaviour of oil within the actual contact area, film thickness can be accurately predicted from E.H.D. theory. That is provided the inlet is adequately filled with oil, or the position of the boundary is known. In practical situations the inlet boundary position is unknown, and there is evidence that many bearings may run starved,even when adequate lubricant is present.

The use of optical techniques for experimental measurements in E.H.L., not only produces a 'contour map' of film thickness at every point within the contact, but also shows the distribution and movement of oil outside the contact area. The purpose of this research is firstly to develop a means whereby the technique can be applied to an

actual bearing, running under realistic loads and speeds. Secondly it is to use the technique to gain a greater understanding of the state of lubrication within the bearing.

CHAPTER III

THE APPLICATION OF OPTICAL INTERFEROMETRY TO MEASUREMENTS IN A ROLLER BEARING

3.1 Introduction

The technique of optical interferometry has, for many years, been frequently used as a means of precise and sensitive measurement. In 1933 Derjaguin (166) used the principle to investigate the elastic properties of water films between optically smooth, plane and curved glass surfaces. The thickness of the film was determined by observing the Newtonian rings around the point of minimum distance between the two surfaces.

However it was not until 1962 that interferometry was used to examine E.H.D. films. Since then the technique has been considerably refined, and has provided a very significant contribution to lubrication research. Interferometric measurements are readily applicable to the E.H.D. situation, in which film thicknesses are of the same order as the wavelength of light. This chapter presents the basics of optical E.H.L., and shows how the technique has been applied to make measurements within a roller bearing.

3.2 The Principles of Interferometry

3.2.1 Interference by Division of Amplitude.

The energy emitted by a point light source can be considered to be propagated as a series of spherical expanding wavefronts, the centre of which is the source. Lines drawn normal to the wavefronts will pass through the centre, and can be considered as rays along which there is a periodic wave motion. However a light source does not emit a continuous train of waves, but a succession of finite length wave trains. There is no fixed phase relation between successive wave trains, the changes being completely random. The average length of a wave train is called the coherence length, and the time taken by light to travel this distance is the coherence time. The best monochromatic thermal sources have coherence times in the order of 10^{-8} seconds, whereas for a laser, it can be as great as 10^{-2} seconds.

If two beams from different sources are combined, interference may take place. However it will be completely random, and the intensity of the resulting beam will simply be the sum of the two initial intensities. Interference, that can be observed, will only occur if the two beams originate from the same source and are coherent. That is interference is always taking place between two sets of waves that have originated from the same wavetrain. The condition for this is that the path difference between

the two beams should be less than the coherence length of the source. Constructive interference will take place when the combining wavetrains are in phase, and the resulting intensity will be greater than that of the sum of the two separate beams. If the wavetrains are out of phase, destructive interference occurs, and the resulting intensity is less than that of the sum of the two separate beams.

Consider figure 3.1. A ray SA enters a transparent medium of thickness h, and refractive index n. At the points A, B, C, ... N, a proportion of the light is reflected and the rest is refracted. The rays which emerge at points A and C have only undergone one reflection, and are consequently of similar intensity. Rays 3, ... N, will at first be ignored. At point P, the rays 1 and 2 are superposed by the lens L. The optical path difference between the two is given by:

$$d = 2n\,h\,\mathrm{Cos}\,r \qquad \ldots\ldots (3.1)$$

If d is less than the coherence length of the source, interference can take place. For very small values of d the wave trains, meeting at P, will overlap almost over their entire length. For values of d close to the coherence length there will be only a small overlap. Thus the interference effects become less distinct as d increases.

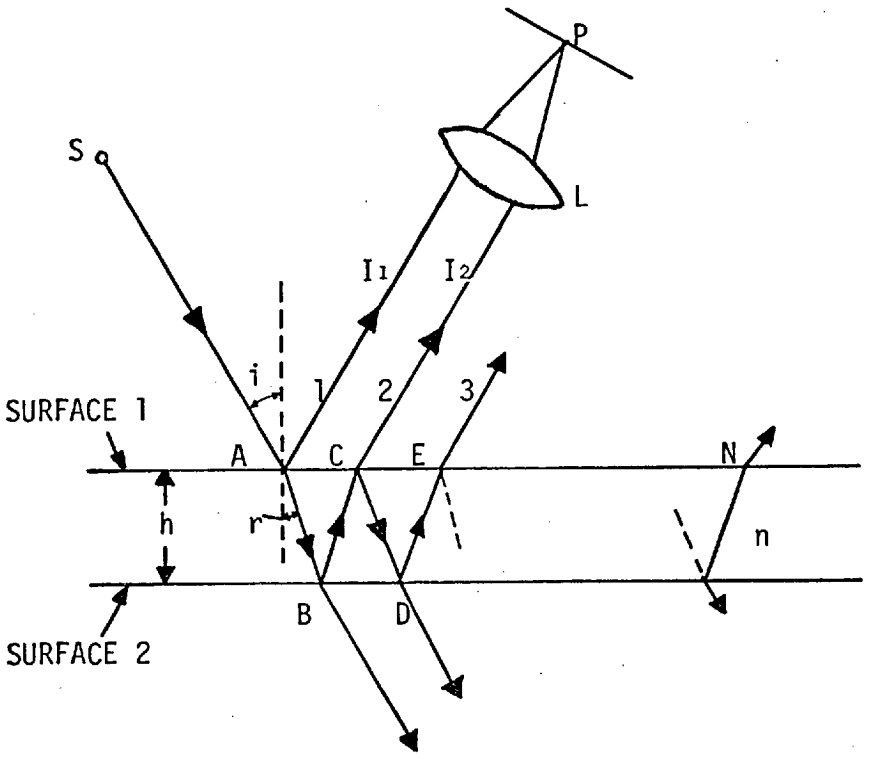

Figure 3.1 Interference by division of amplitude.

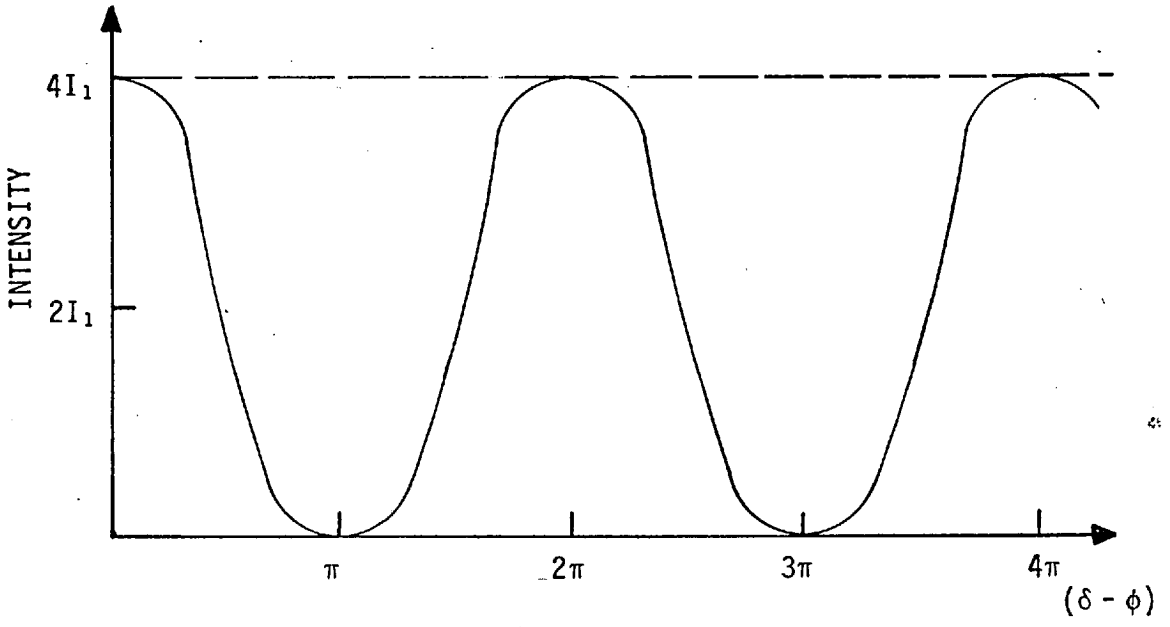

Figure 3.2 Intensity distribution in two beam interference.

The phase difference between the two beams, of wavelength λ, is given by:

$$\delta = \frac{2\pi d}{\lambda} + \phi \qquad \ldots\ldots (3.2)$$

where ϕ allows for any phase changes that may occur upon reflection. Substituting in equation 3.1, the phase difference is given by:

$$\delta = \frac{4\pi n\ h\ \mathrm{Cos}\ r}{\lambda} + \phi \qquad \ldots\ldots (3.3)$$

The combining waves will be in phase when $\delta = o, 2\pi, 4\pi, \ldots$. Thus bright fringes are produced when:

$$2N\pi = \frac{4\pi n\ h\ \mathrm{Cos}\ r}{\lambda} + \phi$$

where N = 0, 1,2 ..... The combining waves will be out of phase when $\delta = \pi, 3\pi, 5\pi \ldots$. Thus dark fringes are produced when:

$$2(N+\tfrac{1}{2})\pi = \frac{4\pi n\ h\ \mathrm{Cos}\ r}{\lambda} + \phi$$

where N = 0, 1,2 ....

If λ, Cos r, and ϕ are constant, the fringes will contour points of equal thickness. The thickness corresponding to the Nth bright fringe is therefore:

$$h = \frac{\lambda}{2n \cos r}\left(N - \frac{\phi}{2\pi}\right) \qquad \ldots\ldots (3.4)$$

Simularly, the Nth dark fringe will occur at a thickness of:

$$h = \frac{\lambda}{2n \cos r}\left((N + \tfrac{1}{2}) - \frac{\phi}{2\pi}\right) \qquad \ldots\ldots (3.5)$$

3.2.2 Two Beam Interference.

If the intensity of beams 3 ..... N, (see figure 3.1) is very small compared to that of beams 1 and 2, they will have a negligible effect upon the interference intensity distribution formed by beams 1 and 2. This is then the situation of two beam interference. The intensity distribution at point P is given by Fresnel's classical formula:

$$I = I_1 + I_2 + 2\sqrt{I_1}\sqrt{I_2}\cos(\delta - \phi) \qquad \ldots\ldots (3.6)$$

If beams 1 and 2 are of the same intensity then:

$$I = 4I_1 \cos^2\left(\frac{\delta - \phi}{2}\right) \qquad \ldots\ldots (3.7)$$

Fringe visibility is defined as:

$$V = \frac{Imax - Imin.}{Imax + Imin.} \qquad \ldots\ldots (3.8)$$

This is really a measure of fringe contrast, and it can be seen that by satisfying the condition of equal intensities ensures a maximum fringe visibility of 1. The resulting intensity distribution can take any value between zero and $4I_1$. This is illustrated by figure 3.2. The condition can be achieved by controlling the surface reflectivities.

3.2.2 Multiple Beam Interference.

If the surfaces 1 and 2 (see figure 3.1) both have high reflectivity and low absorption, the beams 3 .... N will make a significant contribution to the interference taking place at P. That is if the lens L is large enough to collect the multiple beams. (This is not the case in figure 3.1). The resulting fringe spacing is the same as for the two beam situation, but the dark fringes are considerably sharpened in a reflection system. (When viewed in transmission the bright fringes are sharpened). Suppose beams 1 and 2 are exactly out of phase. It follows that every beam will be exactly out of phase with its predecessor, and there will be a dark fringe at P. If there is now a very small variation of h, there will be a much larger change in the phase relation between beams 1 and N, than between beams 1 and 2. Hence the intensity at P will rise rapidly for a very small variation in h. For higher surface reflectivities there will be more interfering

beams, and the dark fringes will be correspondingly sharper.

The effect of reflectivity variation on intensity distribution is shown in figure 3.3. Absorption that occurs at the reflecting surfaces will not effect the sharpness of the fringes, but will prevent the minimum intensity from reaching zero, and seriously effect fringe visibility. To achieve multiple beam interference, the surfaces should be coated with a highly reflecting film of minimum absorption. Also to ensure that the spacing between beams 1 and N does not become too large, the angle of incidence should be near normal.

The use of multiple beam interferometry enables precise determination of the fringe position and is therefore desirable when high degrees of accuracy are required. The theory of multiple beam interferometry is extensively discussed by Tolansky (167).

3.2.4 White Light Interference.

A white light source can be considered as a large number of monochromatic sources, each of which contributes a system of fringes corresponding to its particular wavelength. For each of these systems, the change in thickness between successive maxima is given by equation 3.4:

$$\Delta h = \frac{\lambda}{2n \cos r} \qquad \ldots\ldots (3.9)$$

Thus if a thin wedge is observed, the red bands will be wider than the blue bands, and colour blending will occur. When a maximum from one set of fringes corresponds with a minimum from another, it is likely that one colour will predominate. The resulting fringe pattern is seen to consist of a series of coloured bands following a definite sequence. As the thickness is increased, the spacing of the sequence is reduced, until at an optical thickness of about 15,000 Å it varies so rapidly that only white light is seen. This places an upper limit of about 40 μin. for oil film thickness measurement, which is below that found in many E.H.D. situations. (White of higher order can be resolved by a spectroscope).

However there are several advantages to be gained from the use of white light. A small variation in thickness h may not be sufficient to produce a change from a dark fringe to a light fringe, or vice-versa, when monochromatic light is used. However, when using white light, this small variation can produce a marked colour change. Thus it is possible to detect smaller changes in thickness and hence film shape, with the white light system.

Another important consideration is that of fringe order. A monochromatic source will form a sequence of light and dark fringes. It is possible to calculate the optical film thickness corresponding to a particular fringe, only if the wavelength and the fringe order is known.

The sequence of coloured fringes, formed by a white light source, are not equally spaced for a constantly varying film thickness. Thus the various colours must be related to the optical film thickness, by calibration. However, once this has been performed, the optical film thickness corresponding to a particular colour is immediately known. Furthermore it is possible to determine whether the film thickness is increasing or decreasing; this cannot be easily resolved when a monochromatic source is used.

3.3 Technique of Optical Measurements in E.H.L.

Figure 3.4 illustrates the basic interferometric set up used for film thickness measurement in the E.H.D. contact, formed by loading together a transparent race and a steel ball or roller. The transparent race is usually made of glass, as this is inexpensive and easy to polish. However maximum pressures are limited to about 100,000 p.s.i. The use of synthetic sapphire, which has a very high Young's modulus, enables pressures of at least 250,000 p.s.i. to be generated. This is more typical of the pressures encountered in an E.H.D. situation. The disadvantage of sapphire is that it is far more expensive, and very much more difficult to polish, than glass.

The diameter or width of the Hertzian contact area, will typically be about .01 in. This necessitates the use of a microscope to view the interference fringes.

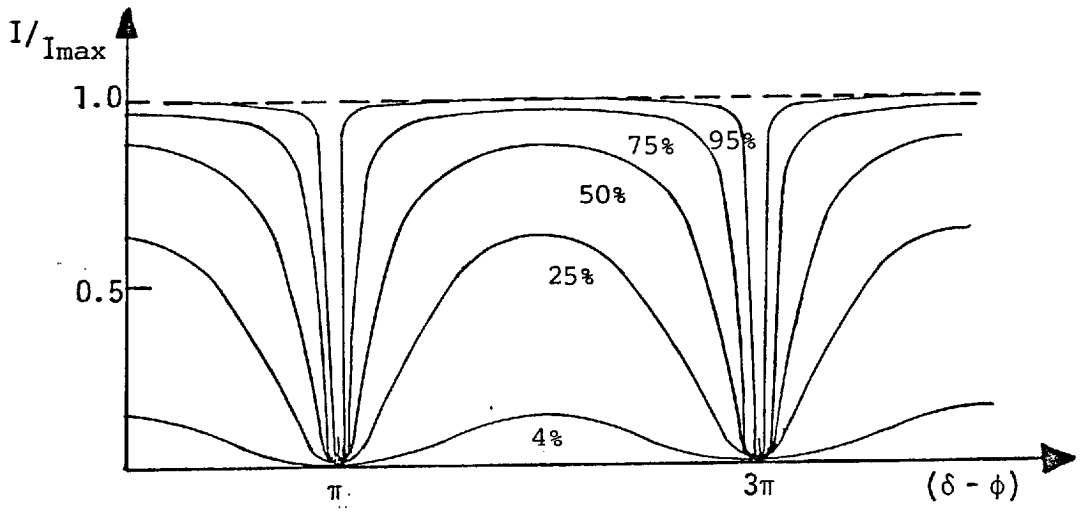

Figure 3.3 Variation of intensity with reflectivity for multiple beam interference.

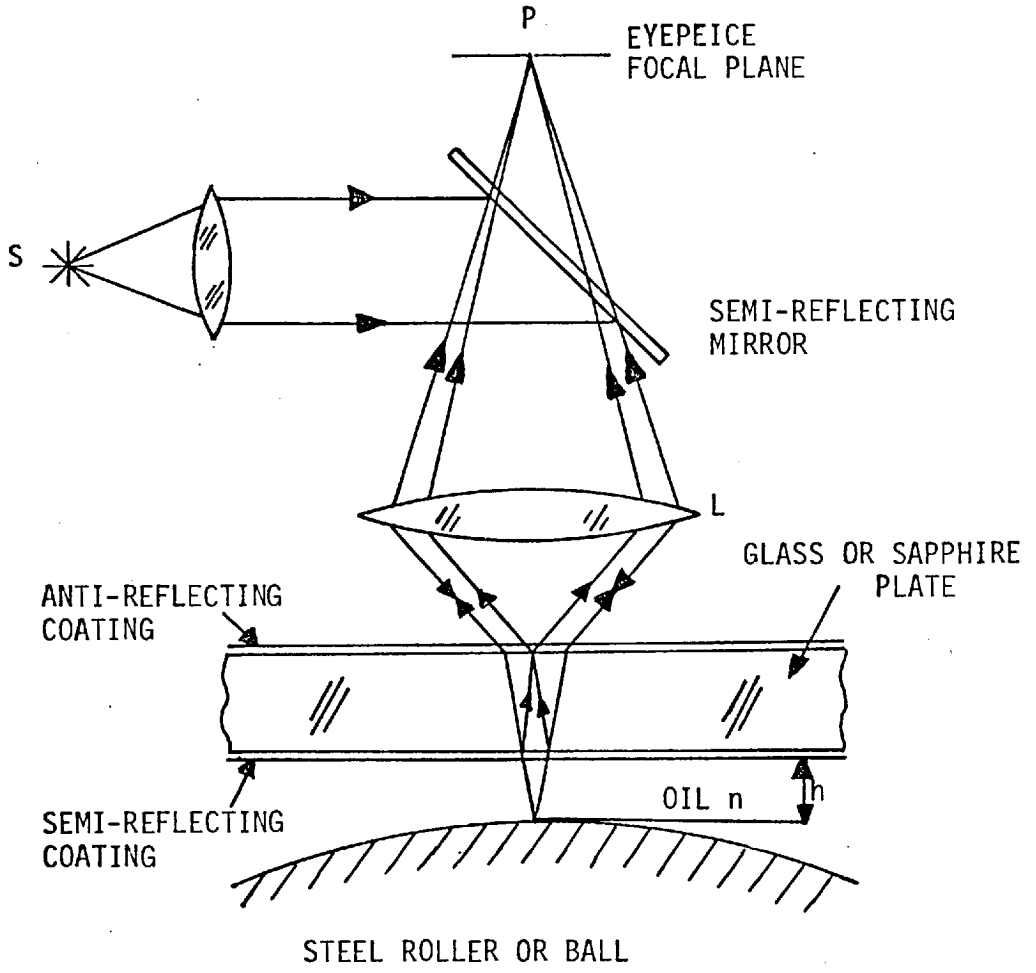

Figure 3.4 Basic interferometric system for measurements in E.H.D. contacts.

A magnification of about 50X will enable observation of both the Hertzian region, and the lubricant inlet boundary. In order to obtain near normal incidence, the axis of the illuminating cone is arranged to be coincident with the microscope axis. This is achieved by use of a semi-reflecting mirror. The mirror is usually positioned above the objective lens, to give maximum clearance between the microscope and the transparent raceway.

To investigate E.H.D. films generated in pure sliding, either the ball or raceway is held stationary, whilst the other is rotated. Pure rolling can be investigated by allowing the glass plate to revolve in one direction, whilst the race that supports the ball or roller, revolves in the opposite direction. In this way, the rolling element can be kept continuously under the field of view.

As the maximum angle of incidence is small, it follows that Cos r ≃ 1. Referring to equations 3.4 and 3.5, bright fringes will be formed when:

$$h = \frac{\lambda}{2n}\left(N - \frac{\phi}{2\pi}\right) \qquad \ldots\ldots (3.10)$$

and dark fringes when:

$$h = \frac{\lambda}{2n}\left((N + \tfrac{1}{2}) - \frac{\phi}{2\pi}\right) \qquad \ldots\ldots (3.11)$$

Since the film is illuminated by a cone of rays, the effect of non-normal incidence will be a slight broadening of the fringes either side of the fringe centre. For a fringe directly under the axis of illumination, the fringe centre will be unchanged. Fringes either side of the axis will be very slightly displaced to positions of greater film thickness. This increase in thickness, for varying angles of incidence, can be calculated from equation 3.4. An angle of incidence of 8^{o}, such as might occur at the edge of the field of view, will result in an increase of thickness of about .4%. This shift can therefore be neglected.

Figure 3.4 shows a ray diagram for a point source at S. Interference occurs at P, where the interfering beams have been superposed by the objective lens L. Therefore the fringes are not localized. However all sources have a finite size, and each point in the source produces its own fringe system. A point at the edge of the source will emit a cone of rays, the axis of which will now not be coincident with the axis of the microscope. The effect is that all the fringe systems will only coincide within the film itself, and it is in this plane that the aggregate fringe system is localized. The microscope must therefore be focused on this plane. The extended source will also lead to a greater range of incidence angle. The integrated effect of an extended source is a fringe broadening, and a slight reduction in fringe visibility. For thickness

measurements of a normal E.H.D. film, these effects are insignificant.

Far more important than the reduction of visibility and fringe broadening, caused by an extended source and non-normal incidence, is the consideration of intensity of illumination. A very small source will not be of sufficient intensity to provide adequate illumination. It is also desirable to use non-normal incidence to concentrate the light over the microscope field of view.

The first successful use of interferometry for measurement of film thickness in E.H.D. contacts, was reported by Gohar and Cameron (59, 60, 61). The system shown in figure 3.4 was used with a steel ball sliding on a high refractive index (1.93) glass disc. Since no surface coatings were used, the reflection coefficient at the boundary of two non-absorbing isotropic media, such as glass and oil, is given by:

$$R = \left(\frac{n_1 - n_2}{n_1 + n_2}\right)^2 \qquad \ldots\ldots (3.12)$$

The refractive index of oil under a pressure of 50,000 p.s.i. is approximately 1.6, and the reflectivity of the ball was probably about 50%. Thus the intensity of the first two interfering beams will be about .01 and .48 respectively. Fringe visibility was therefore very low.

Foord et al. (65, 66, 67) produced two beam fringes of very high visibility, by vapour depositing a semi-reflecting layer of chromium on the lower surface of the glass plate. The reflectivety of the coating is dependent upon the thickness, and it was found that a thickness of 150Å gave a reflectivity of about 15% at glass/chromium/oil interface. The steel ball had a reflectivity of about 58% in oil. Interference will only effectively occur between the first two beams, as the high absorption in the chromium film (30%) quickly suppresses multiple reflections. For these values, the intensities of the first two beams are .15 and .176 respectively. The intensities of these two beams are nearly equal and the resulting fringe visibility is .996. The system was further improved by the application of a magnesium flouride anti-reflection coating to the upper surface of the glass race. Thus uneccessary reflection, that lowers image intensity and fringe visibility, is reduced.

This is then the basis of the system as used by Wedeven et al. (68,69), and Wymer (80, 81), for point and line contact studies. A problem associated with the use of metallic coatings, such as chromium, is that the phase change upon reflection at the coating, is unknown. There are two metallic reflections in the interferometer, one from the coating, and the other from the opaque steel surface of the ball or roller. The phase change that occurs at an opaque metal surface is very close to π.

However in a semi-reflecting film, the phase change can be critically dependent upon the conditions under which the film was deposited. Thus set ups using a chromium coating must be independently calibrated.

Westlake and Cameron (72-76) used quarter wavelength dielectric coatings for the semi-reflecting layer. For dielectric materials, reflection from a rare to dense medium produces a phase change of π. From dense to rare dielectrics, there is no phase change. All the phase changes were known, and therefore calibration unneccessary. As there was no absorption in the dielectric coating, multiple beam interference took place. When the ball is in contact with the glass plate, all beams emerging from the coating after reflection at the steel surface, will be exactly out of phase by even multiples of π, with the beam initially reflected from the upper surface of the coating. Thus the contact area will be black, when dielectric coatings are used and there is no spacer layer. From equations 3.10 and 3.11, the film thickness is now given by the following simple relations:

For bright fringes, N = 1, 2, 3 ....

$$h = \frac{\lambda}{2n}\left(N - \tfrac{1}{2}\right) \qquad \ldots\ldots (3.12)$$

For dark fringes, N = 0, 1, 2, 3 ....

$$h = \frac{\lambda}{2n} N \qquad \ldots\ldots (3.13)$$

Westlake and Cameron produced coatings with reflectivities as high as 97%. This was achieved by using dielectric stacks of alternate high and low refractive indices. The two materials used, were titanium dioxide (refractive index = 2.9), and magnesium fluoride (refractive index = 1.38). The use of a laser gave an intense monochromatic source, and very fine multiple beam fringes were produced. An example of these is shown by figure 3.5.

3.4 The Insertion of Sapphire Windows into the Bearing Races

3.4.1 Preliminary Considerations.

The technique of optical interferometry cannot be directly applied to an actual bearing, without a means of optical access. Previous studies have either used a glass or a small sapphire plate, in a thrust bearing arrangement. A complete glass ring has also been used (137) as the outer race of a cylindrical roller bearing. Sapphire is preferable as it can withstand pressures that are typical of a relatively highly loaded E.H.D. system, and it is also extremely wear resistant. It is

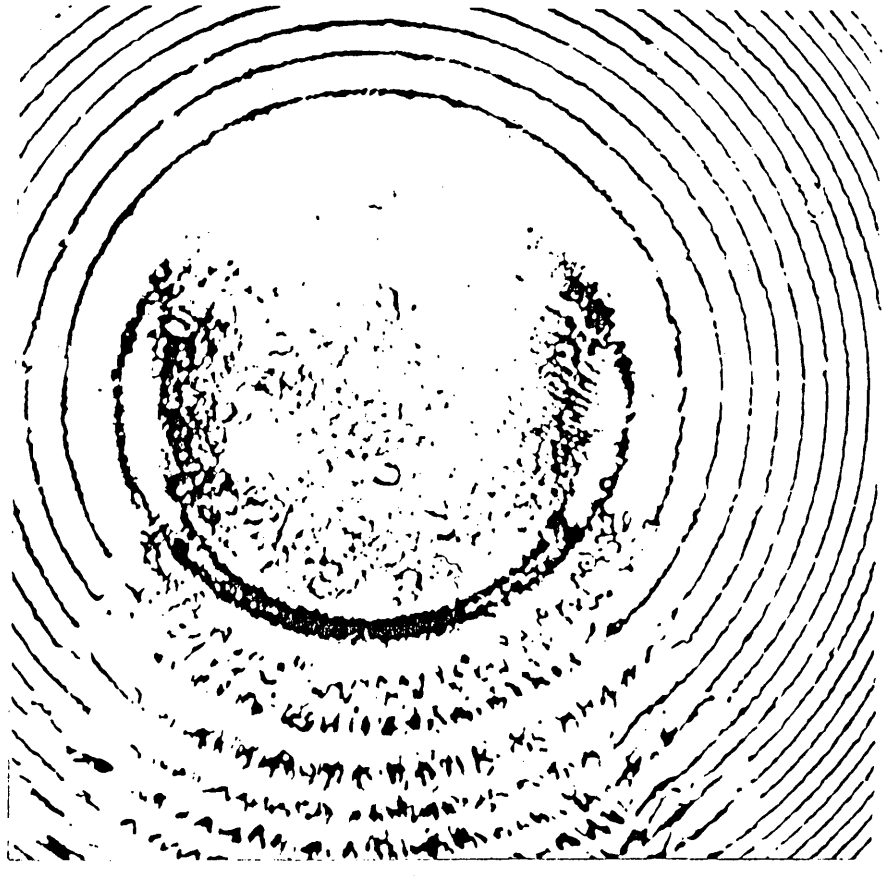

Figure 3.5 Multiple beam fringes in optical E.H.D.
(after Westlake and Cameron (77))

therefore far more suitable for use in a real bearing, where the frequency of rolling element passes over each point of the raceway, will be far greater than that encountered in the usual optical arrangement.

It is possible to manufacture a complete ring of sapphire, but this is extremely expensive. A 4.7 in. diameter ring of .9 in. width,would be required to make the outer race of the bearing used in this study. The cost of this would be prohibitive. It was therefore proposed to make interferometric measurements through sapphire windows,positioned in the bearing tracks. Once developed, this window technique will extend the application of optical E.H.L. to far more realistic situations, than have hitherto been examined.

3.4.2 The Bearings for Optical Study.

Two bearings were selected, both of the same external dimensions (bore = 65 mm.). These were standard bearings supplied by Ransome, Hoffmann and Pollard. The LRJ65 has a lipped inner race, a plane outer race, 16 rollers of $^{9}/_{16}$ in. diameter, and a brass cage which is located on the inner race. This bearing is shown in figure 3.6,which illustrates the sapphire window subsequently inserted in the outer race. The LLRJ65 has a lipped outer race, a plane inner race, 17 rollers of $\frac{1}{2}$in. diameter, and a brass cage which is located on the outer

Figue 3.6 Test bearing for optical study of the outer race.

Figure 3.7 Test bearing for optical study of the inner race.

race. A sapphire window was inserted in the inner race of this bearing. The bearing with the window in situ is illustrated in figure 3.7. Dimensions of the bearings are given in Appendix I.

Simultaneous measurements at the inner and outer race contacts are not possible unless two separate optical set ups are used. Since this was out of the question, different bearings were chosen for inner and outer race investigations, in order that each window could be inserted in a plane ring.

3.4.3 Design of the Window.

The design of the sapphire windows was based on the following criterion:

(a) They must be large enough to allow a field of view of at least ten Hertz widths.

(b) They must be capable of withstanding the applied load.

(c) There must be a smooth transition as the rollers roll onto the sapphire.

Sapphire has a high compressive strength (300,000 p.s.i.), and a relatively low tensile strength (modulus of rupture ≈ 60,000 p.s.i.). Therefore for maximum load carrying capacity, it is desirable to minimise tensile stresses. This could be achieved by using windows as shown in figure 3.8. The size of this type of window could also be kept to

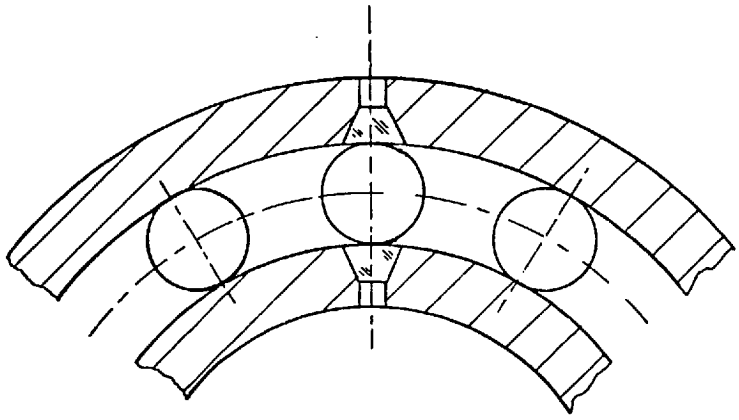

Figure 3.8 Small sapphire window to minimize tensile stress.

a minimum to just satisfy the first criterion, (about $^1/8$ inch). It can be argued that the smaller the wirdow, the more closely the system represents that of steel-to-steel contact. However, there is a large difference in modulus of elasticity between sapphire and steel (see Appendix 2), and the taper is in the wrong direction to satisfy criterion (c). There will be a very sharp transition from the steel to the sapphire, which will become increasingly severe with increasing load.

It was considered desirable to have a large window the whole way across the race, for several reasons. Firstly the load distribution will be uniform along the length of the roller, and the contact can be considered as one between sapphire and steel. With a small window, the load will be unevenly distributed between the sapphire and the steel. Also if it is slightly proud of the track surface, moderately low loads will produce excessive stresses in the sapphire/steel part of the contact, whilst stresses in the steel/steel part of the contact will be very low.

Secondly a large window will allow any disturbance created at the sapphire/steel interface, to 'die down' before measurements are made.

The third reason in favour of a large window, which covers the whole width of the track, is that it allows both ends of the rollers to be examined. This is an important consideration as it is at the ends that conditions of

lubrication are likely to be most severe. Also it is at the track sides that any lubricant replenishment effects are most likely to be observed.

The shock in the transition from the steel to sapphire can be minimized by placing the insert in a 'dove-tailed' slot. The load is then progressively taken by the sapphire as the roller rolls onto the window. This type of window demands that the sapphire is inserted from the side of the track and necessitates a separate viewing slot. The thickness of sapphire is therefore limited by the size of slot that can be machined in the bearing race, without affecting its overall rigidity. In this configuration tensile stresses are produced in the sapphire when the insert is loaded. As the insert will be thin, its failure load must be considered.

The windows designed in light of the above considerations, are shown in figures 3.9 and 3.10. Simple beam theory was used to calculate approximately the maximum permissible load. The window was assumed to be a beam built in at both ends, and the modulus of rupture for sapphire was taken to be 55×10^3 p.s.i. (This is the lowest value quoted by the manufacturer of synthetic sapphire). This type of analysis predicts failure at a roller load of 4000lbs. Using a safety factor of two, the maximum hertz width that can be permitted at the outer race contacts is .015 in. This corresponds to a peak Hertz pressure of about

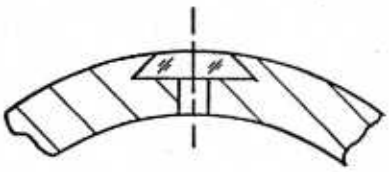

Section on AA

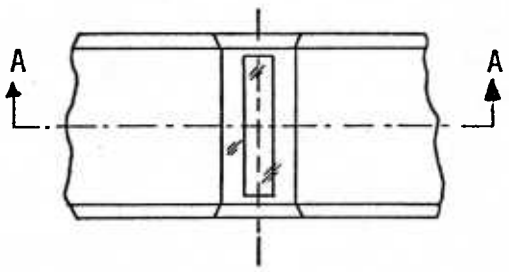

Figure 3.9 Sapphire window inserted in the inner race.

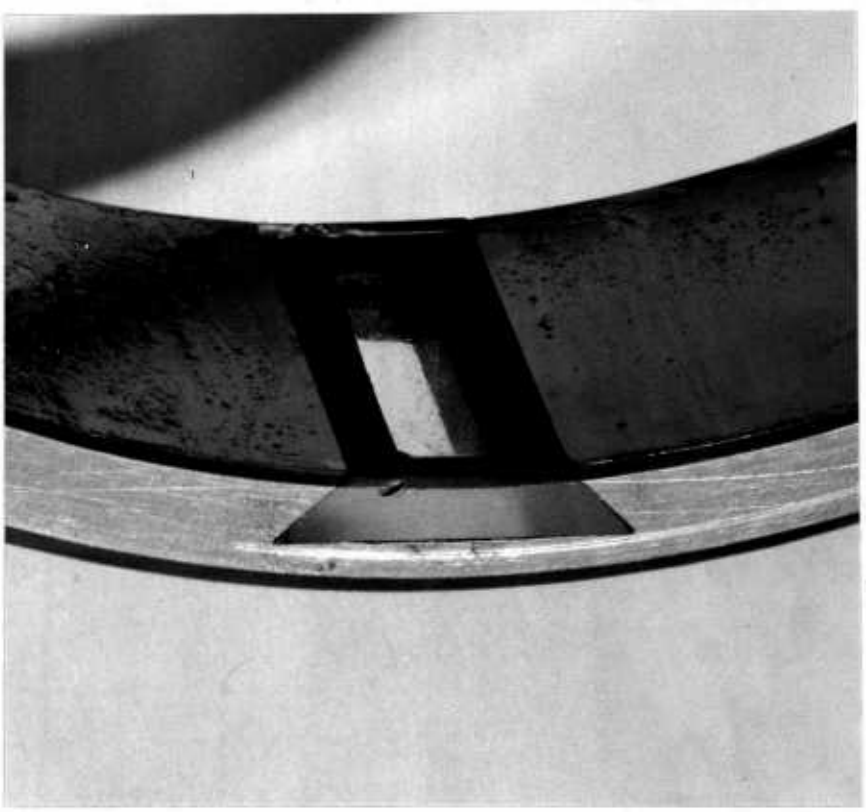

Figure 3.10 Sapphire window inserted in the outer race.

290,000 p.s.i. For the inner race, with the sapphire insert, the maximum Hertz width permitted is .013 in, corresponding to a peak Hertz pressure of 380,000 p.s.i. The Hertz width can be measured optically, through the sapphire windows. Thus it can be ensured that these limits are not exceeded. The windows are therefore capable of withstanding loads far greater than that required for operation within the E.H.D. regime.

3.4.4 Preparing the Races.

Several methods of surface treatment were considered as a means of matching the hardness, and modulus of elasticity of the surface, with the corresponding values for sapphire. (The physical properties of sapphire are given in Appendix 2). If the hardness can be matched, it is likely that the two materials will wear at an equal rate during polishing. If the moduli can be matched, there will be a smooth transition as the rollers roll onto the sapphire.

Materials such as aluminium oxide, chromic oxide, tungsten carbide, can be plasma sprayed to substantial thickness. However the physical properties of these coatings are very different to those of the pure material. None of these coatings have a modulus, or hardness as high as that of sapphire, and were not further investigated. Boronising and Spark hardening are both techniques in which it is claimed the surface is actually penetrated, as well as a layer

of material being built up on the surface. These techniques were actually applied to a bearing surface. Boronizing is analogous to carburising and nitriding, and is the diffusion of boron into the surface of a metal. Spark hardening is a technique by which tungsten carbide is transfered to the substrate, in a spark discharge from a tungsten carbide electrode. Micro-hardness tests, conducted on the specimens at several depths, revealed that these hardening techniques were not suitable for bearing steel.

It was therefore decided to attempt to fit the windows in standard untreated races. The bearing rings used had unground tracks, giving an adequate allowance of .01 in. for material removal during blending of the sapphire to the track. Slots were spark eroded in the bearing races using electrodes made of 'Elkonite'. This is a mixture of tungsten and copper, and has good wear characteristics when used for spark erosion. The electrodes were made very much longer than the length of the slots. Tapers produced by electrode wear, could then be minimized by moving the whole length of the electrode through the slot. The viewing slot was the minimum size necessary to view a width, approximately equal to ten Hertz widths, at a cone angle of 20 degrees.

3.4.5 Fitting of the Windows.

Before the windows were fitted into the slots, the lower surfaces were coated with an anti-reflection coating of magnesuim fluoride. Further details of this coating are given in section 3.5.2. A small section of the spark eroded surface, in line with the viewing slot, was very slightly relieved to allow the window to be positioned without scratching the coating.

In order that optical measurements can be made, the sapphire surface must be polished to a surface finish better than 1 μin. c.l.a. All the working of the sapphire, and the blending of the windows into the raceways, was conducted by an optical firm familiar with this type of problem. The inserts were bonded into the slots with cyanoacrylate cement. The raceways, with windows in situ, were then ground with a diamond wheel until about .003 in. was left for removal during lapping. Semi-circular solder laps were used in conjunction with 15, 3, and 1 micron diamond paste.

3.4.6 The Composite Races.

Satisfactory blending of the steel and sapphire was achieved in the outer race. As the inner race was unsatisfactory, the procedure was repeated using a race coated with hard chrome plate. Hard Chrome has a hardness of 1200 Vickers and a modulus of elasticity of 36×10^6 p.s.i.

This is a considerable increase above the corresponding values for bearing steel (see Appendix 2). Before plating the race, it was ground to a size such that there would be residual plating thickness of 0.015 in. However, during grinding and lapping, there was considerable chipping of the brittle chrome, at the edge of the sapphire. For this reason this race has not been run, although the sapphire is blended in well and it has good surface finish.

Figure 3.11 shows a 'Talyrond' trace made from the composite outer race. Although there appears to be a very sharp drop onto the sapphire, this is very much exaggerated by the magnification of X2000 in the radial direction. The sharp peaks shown on the trace are in fact only gradual slopes. For example the slope of BD is 4.2×10^{-5} in. per degree. The points I, G, H, J mark points on the sapphire, as illustrated by the figure. Consider a roller moving from right to left. Along AC the roller load will be progressively reduced (that is provided there is an adequate number of rollers in the bearing to carry the extra load). As the roller nears I, the sapphire will begin to carry a proportion of the now reduced roller load. At I the roller moves onto the sapphire surface, and along IE the load is progressively increased. The viewing slot is in the centre of EF where the load is effectively constant. Again as the roller moves off the sapphire, the load is substantially reduced, and then increased after the transition.

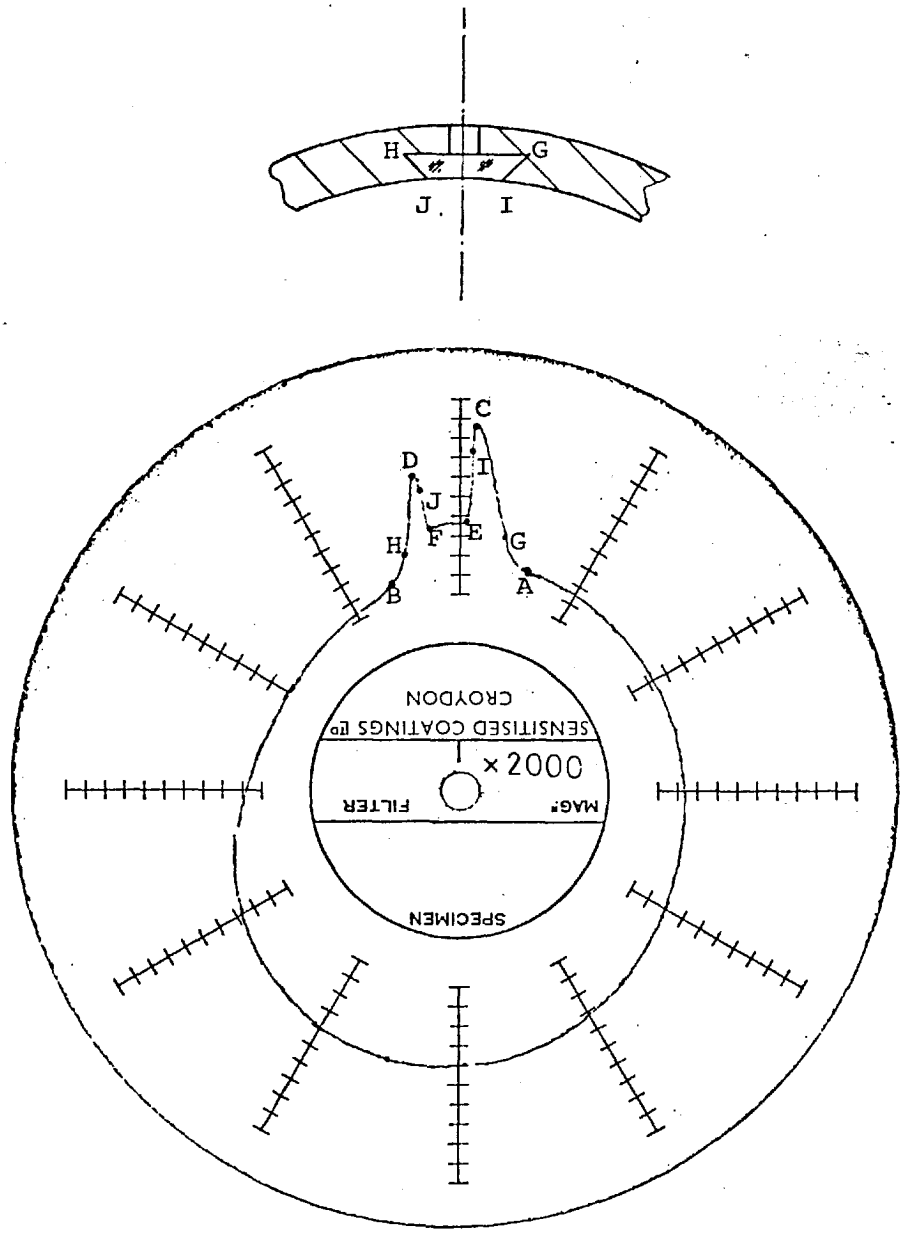

Figure 3.11 "Talyrond" trace of the outer race with sapphire window.

The effect that the presence of the outer race sapphire window has on the static load distribution within the bearing, has been calculated for a particular situation. That is when the sapphire is directly in the load line, and there is a roller loaded against it such that the Hertzian contact width is .008 in. This distribution was then compared to that produced in a normal bearing, where the top roller carries the same load as in the composite race. The results are shown in figure 3.12. The centre portion of the sapphire window is .0001 in. below the rest of the track, and the bearing has a diametrical clearance of .002 in.

The radial deflection at each angular position is the sum of the approaches between the rolling element and each raceway. Considering the composite race, the load carried by the roller over the sapphire can be calculated from Hertz theory. The deflection at this point can be calculated using an equation given by Allan (168). The radial deflection at other positions is given by:

$$\delta = (\delta_0 + .0001) \text{ Cosn } 22.5 - \Delta \quad \ldots\ldots \quad (3.14)$$

where n = 0, 1, 2 ...., and δ_0 is the deflection in the line of the load, after the roller has touched the sapphire. Δ is the clearance at the particular angular position, for the case of an unloaded bearing in which the top roller is just touching the surface of a perfectly round race. Roller

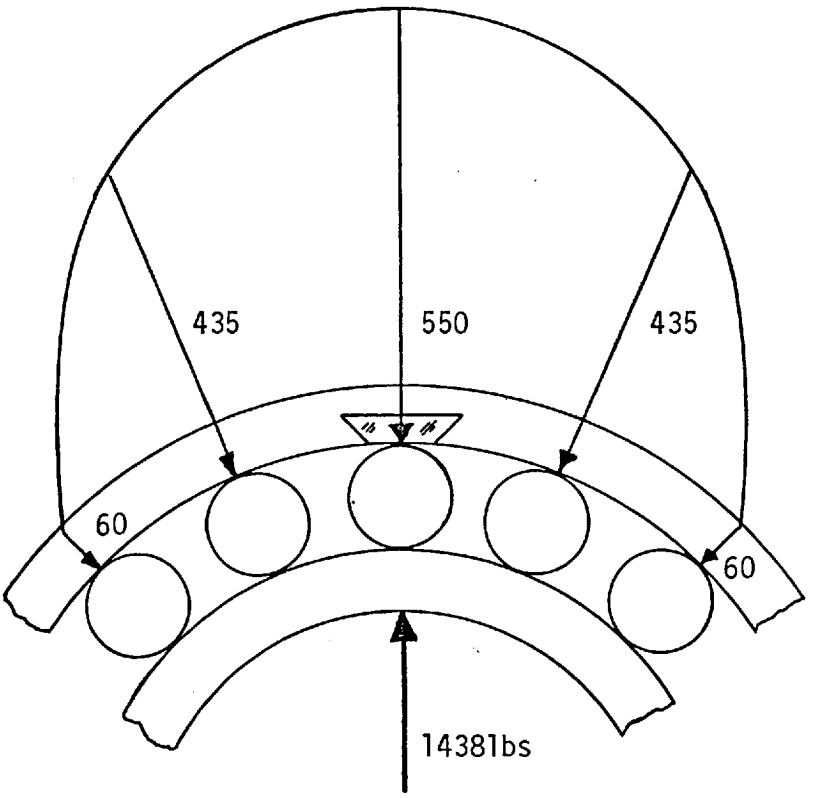

(a) with the sapphire window

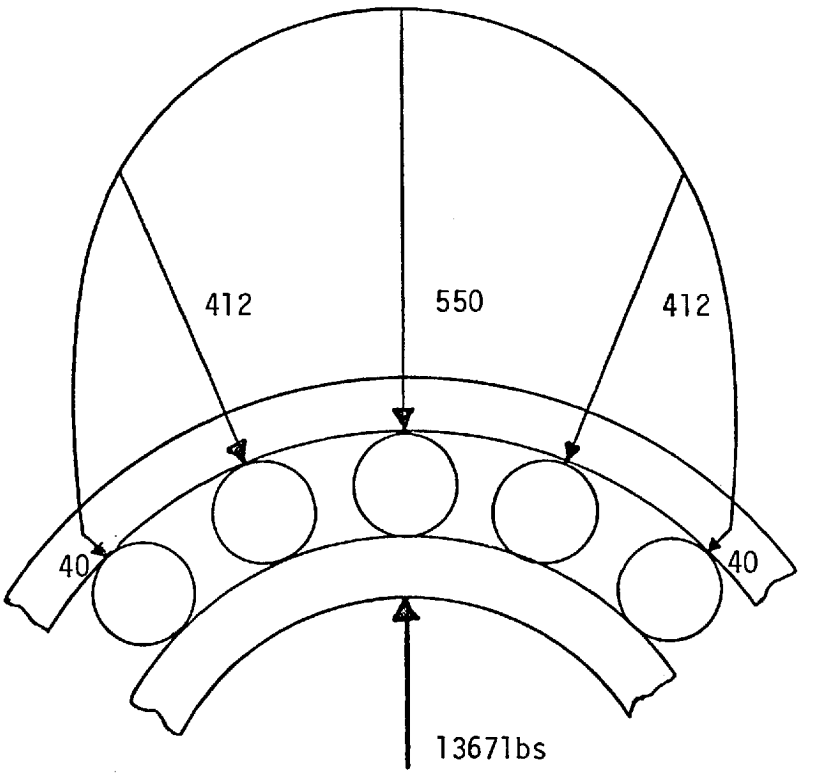

(b) without the sapphire window

Figure 3.12 Load distribution in the test bearing outer race.

load can be related to deflection by graphical solution of the equation given by Allan. The loads at each position are then found for values of δ given by equation 3.14. The procedure was then repeated for a normal bearing of the same dimensions and clearance. Equation 3.14 now simply becomes:

$$\delta = \delta_0 \text{ Cosn } 22.5 - \Delta$$

In both cases the load is carried by five rollers, and the load distributions are very similar. For the composite race, the load that must be applied to the bearing, to give a Hertz width of .008 in. at the sapphire window, is 1438 lbs. and the roller load is 550 lbs. For the normal race, to apply a load of 550 lbs. to the top roller requires a bearing load of 1367 lbs. Even though sapphire has a considerably higher modulus than steel, the effect of the shallow insert is to increase slightly the load on the other four load bearing rollers. Had the sapphire been flush with the surface or proud, the insert would have had a considerable effect upon load distribution.

The change in film thickness due to the difference in materials, in rolling from steel to sapphire at constant load, can be calculated from equation 2.8, which gives the following relation:

$$\frac{h(\text{steel/steel})}{h(\text{sapphire/steel})} = .989$$

This is extremely small and can be neglected.

Film thickness in an E.H.D. contact is virtually independent of load, and therefore any alteration in load distribution will have an extremely small effect on film thickness. It is therefore concluded that the presence of a sapphire window will not significantly effect the conditions of lubrication within the bearing.

3.5 The Reflecting Surfaces

3.5.1 The Semi-Reflecting Coating.

The sapphire surface that forms part of the bearing track, was coated with a semi-reflecting layer of chromic oxide. The coating was deposited in a sputtering plant. In this process, the specimen to be coated is placed on an earthed plate, positioned below a target disc made of the coating material. The plant is then evacuated and a small quantity of argon gas introduced. A large potential is applied to the target disc, creating a plasma of highly excited argon ions, between the target and earth plate. Molecules of the target material are released under the resulting ion bombardment. These molecules are also in a state of high excitation, and any that hit the specimen will from an extremely strong bond with the surface.

This type of coating is extremely adhesive and therefore ideal for use under E.H.D. conditions. Chromic oxide is particularily suitable, for not only is it easily sputtered, but also it has a high refractive index (2.55) and is very hard. This coating has been used in exceptional circumstances without being damaged. Hedley (169) has successfully used this coating in a disc machine, in which high degrees of sliding occur at the heavily loaded contacts between a central sapphire disc and three steel discs. In this situation, conventional vacuum deposited coatings would have been stripped immediately.

In order to achieve maximum adhesion of the coating, the surface must be absolutely clean. The track surface was first cleaned with toluene and acetone, before the bearing ring was placed in the sputtering plant. After evacuation had been completed, the surface was sputter-etched. This is the reverse of the sputtering process, in which the surface now acts as the target, from which molecules are released, when bombarded with argon ions. In this way a layer of molecules is removed from the sapphire surface, which as it is still under high vacuum, remains chemically clean. The surface is now prepared for sputtering.

Chromic oxide is a dielectric meduim, and therefore there is a phase change of π when light is reflected at the oil/Cr_2O_3 interface. The Cr_2O_3/sapphire interface is a dense to rare reflection and there is no phase change.

It can be seen from figure 3.13, that if the optical thickness of the coating is $\lambda/4$, beams 1 and 2 will both be out of phase by π, relative to the initial beam. Constructive interference therefore occurs, and this is the condition for optimum reflectivity. For these conditions the reflectivity can be calculated from equations 3.6 and 3.12, and is 22% when the surface is in contact with oil.

During sputtering it is not possible to monitor the coating thickness. A test run was therefore conducted with a glass slide to calculate the deposition rate, which was assumed to be linear. The test coating thickness was measured by multiple beam interferometry. The deposition rate varies with distance of the substrate from the target. Lack of clearance inside the sputtering plant necessitated horizontally placing the race, so the surface of the window was at right angles to the target. In order to obtain an even coating, the race was turned over halfway through deposition. A coating of thickness 540 ± 30 Å was applied. This corresponds to an optical thickness of 1375 Å, which is a quarter of the wavelength of green light. Green was chosen, as photographic emulsion is most sensitive to this wavelength, and the strongest line of the laser, used for this study, was green.

On observing a roller in contact with the sapphire, the Hertzian region was black, indicating the coating to be of correct thickness. Although the coating is of compara-

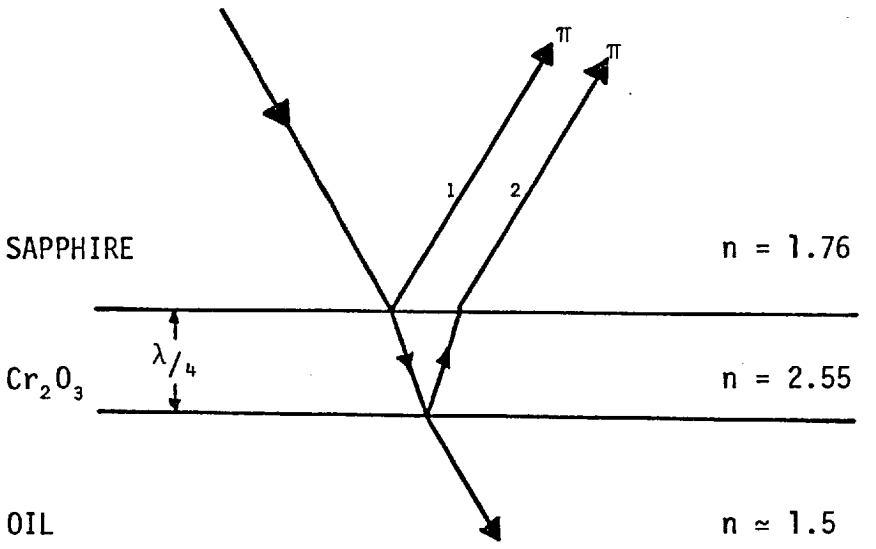

Figure 3.13 The semi-reflecting coating.

tively low reflectivity, there is no absorption in the Cr_2O_3 layer. Multiple beam interference takes place as more than two beams provide a significant contribution to the interference pattern. The polished rollers have a reflectivity of about 55% in oil. The combined reflectivity is therefore $\sqrt{55X22}$, which is equal to 36% Figure 3.3 shows the intensity distribution for multiple beam interference, and it can be seen that at 30% reflectivity the dark fringes are slightly narrower than the light fringes.

3.5.2 Anti-Reflection Coatings.

Supression of reflections occurring at the sapphire/air interface is extremely important in order to avoid image degradation. Also when using a laser, which has a long coherence length, these reflections will give rise to spurious interference patterns.

Figure 3.14 shows the mechanism of the anti-reflection coating. Magnesium fluoride was used, which is a dielectric having a refractive index of 1.38. The air/MgF_2 and the MgF_2/sapphire interfaces are both rare to dense reflections, and therefore both produce a phase change of π. Consequently, if the coating thickness is $\lambda/4$, the two beams 1 and 2 will be out of phase and destructively interfere. This results in an increase in transmission through the sapphire. Magnesium flouride is an ideal coating on sapphire. A single $\lambda/4$ coating reduces the

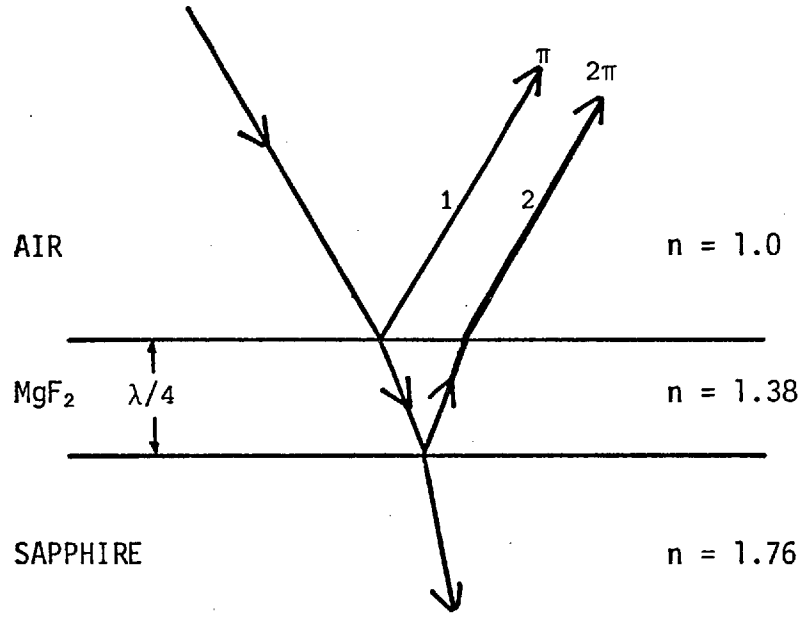

Figure 3.14 The anti-reflection coating.

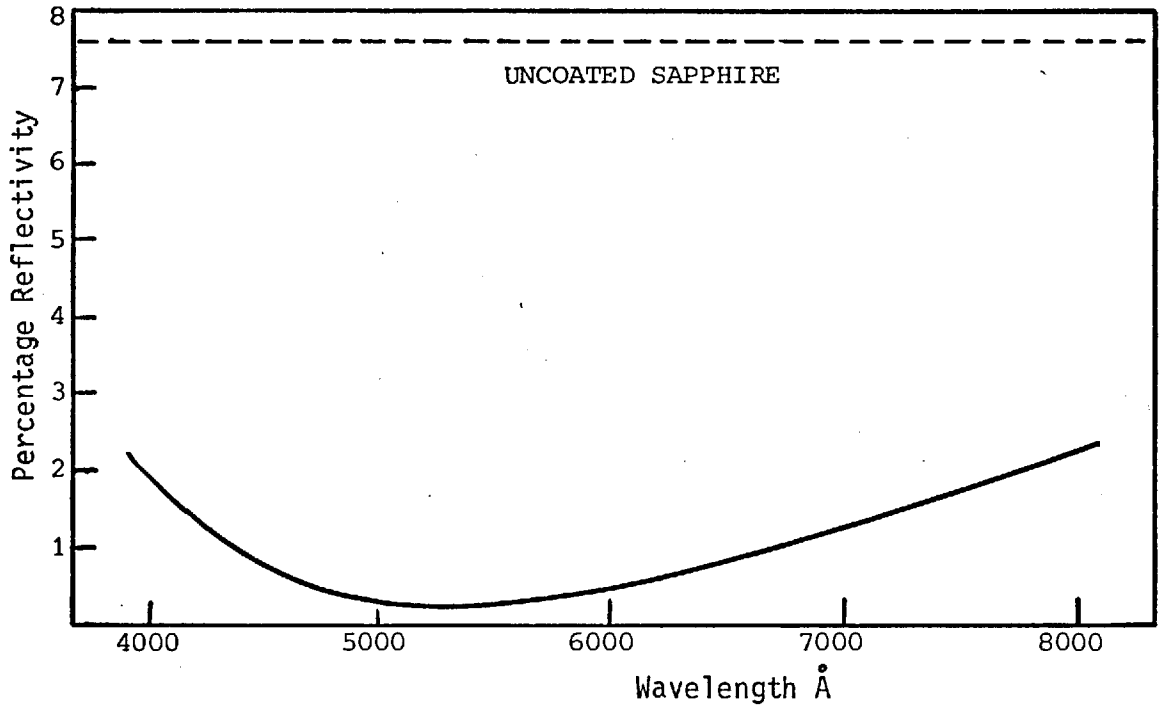

Figure 3.15 The variation of reflectivity with wavelength for the anti-reflection coating.

reflectivity of the air/sapphire interface from 7% to .15%. The anti-reflection coating had a thickness of 950 Å, which is equivalent to an optical thickness equal to a quarter of the wavelength of the strongest green line produced by the xenon laser (λ = 526 Å). Using equations 3.6 and 3.12, the variation in reflected intensity with wavelength has been calculated for a coating of this thickness. This is shown in figure 3.15, and it can be seen that the coating is extremely effective over nearly the complete visible spectrum.

There are many air/glass interfaces in the rest of the optical system. If these are not coated, the reflections will lead to a reduction in image intensity. All the microscope lenses were therefore also 'bloomed' with a quarter-wavelength coating of magnesium flouride.

3.5.3 The Rollers.

The standard rollers have a surface finish of about 3 μin. c.l.a. Figure 3.16 shows a 'Talysurf' trace of surface irregularities along one line of the roller surface. Also shown is a static interferogram of a standard roller loaded against the sapphire window. The fringe quality is poor, and this makes measurement of film thickness difficult. Figure 3.17 shows a static interferogram produced using a super-finished roller. These rollers, which have been honed, have a surface finish of about 2 μin. c.l.a. The fringe visibility is considerably improved, and

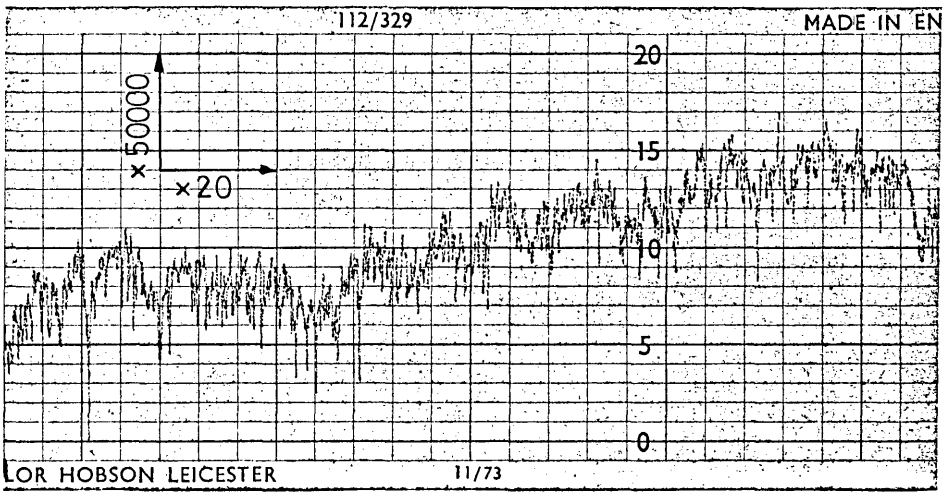

(a) "Talysurf" trace

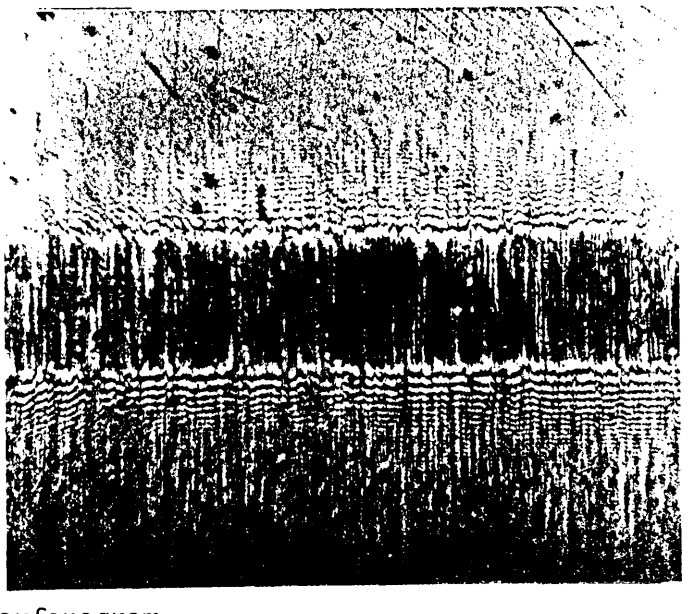

(b) Interferogram

Figure 3.16 "Talysurf" trace and interferogram of a standard roller.

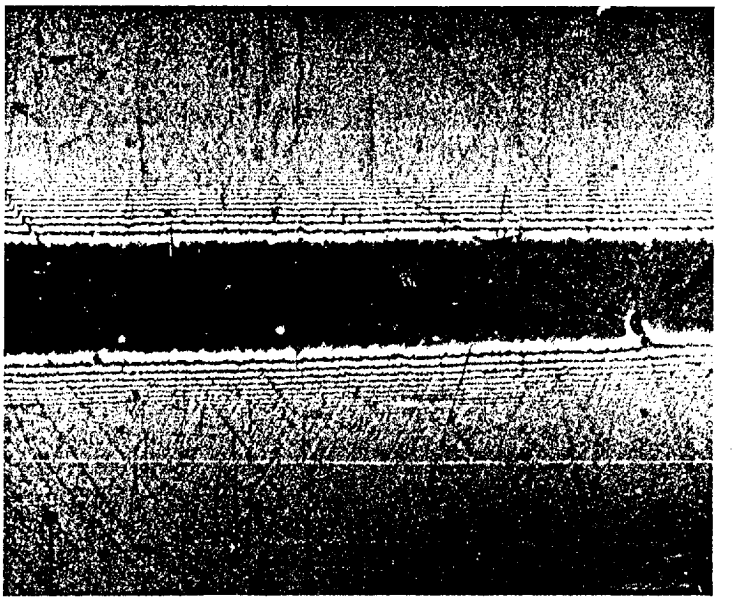

Figure 3.17 Interferogram of a super-finished roller.

is satisfactory for interferometric measurements. However it is possible, by polishing with diamond paste, to improve the surface finish of either the standard, or super finished rollers to about 1 μin. c.l.a. Figure 3.18 shows a 'Talysurf' trace and an interferogram, taken after polishing with 3 micron diamond paste. It is evident from the trace that the polishing has removed the asperity tips. The fringe visibility is extremely good.

Rollers were polished in the following manner: Three rollers were aligned in a 'vee' block and bonded together using cyanoacrylate cement. The rollers were then inserted in a collet chuck, such that the centre one was gripped. The protuding roller was then lapped by hand, using a simi-circular wooden lap covered with polishing cloth. When polishing of this one was complete, the outer rollers were reversed. It was found that super-finished rollers could be polished to a 1 μin. finish in approximately one minute. The standard rollers took slightly longer. A negligible amount of material is removed during this process. Superfinished rollers were used in preference to standard rollers, as the polishing process is shorter, and there is less likelihood of introducing geometrical inaccuracies. Also, when using super-finished rollers, it is unnecessary to polish every roller that is selected for viewing. It can be seen from figure 3.18 that the fringes are straight and parallel, and the Hertz width is approximately constant along the length of the roller. This

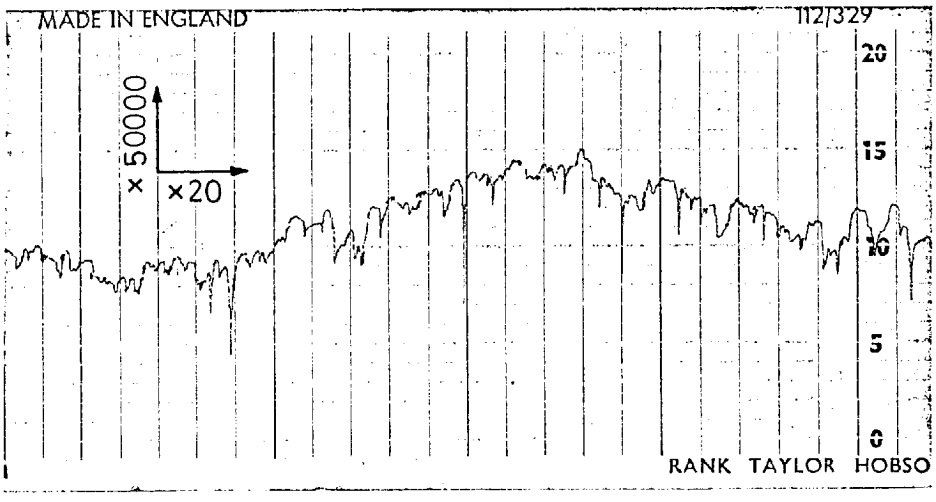

(a) "Talysurf" trace

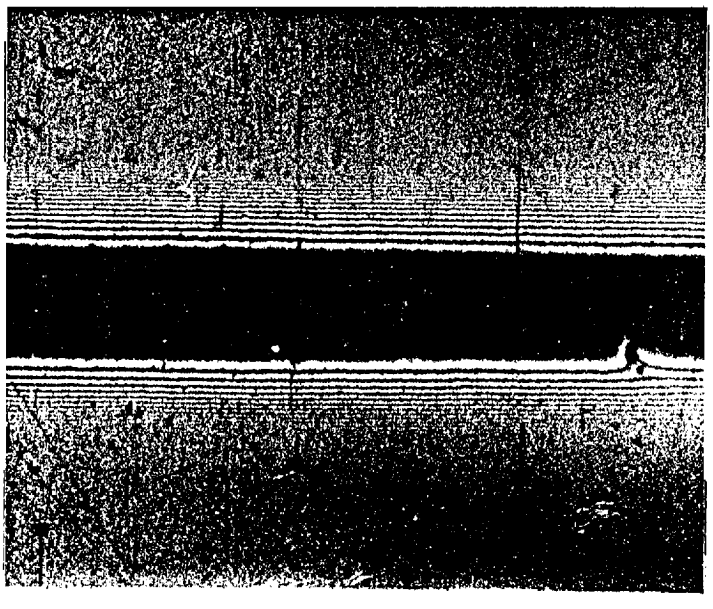

(b) Interferogram

Figure 3.18 "Talysurf" trace and interferogram of a polished roller.

indicates the polishing process was satisfactory.

During running, the polished rollers quickly became scratched. In order to maintain good fringe quality it was necessary to repolish the rollers after approximately five runs. Figure 3.19 shows a 'Talysurf' trace taken from the surface of a polished roller that had been run several times. The scratches are only superficial and can be removed extremely quickly with diamond paste.

3.6 The Microscope and Illuminator

3.6.1 The Microscope.

In order to observe inner and outer race contacts, a microscope of 2½ in. working distance was required, at a magnification of about X80. The microscope designed is similar in principle to that used by Wymer (80). This was a long working distance microscope which incorporated two additional lenses to reduce the required tube length, that otherwise would have been excessive.

To obtain the necessary working distance a new objective lens had to be manufactured. The design for this was based on a lens of ½ in. working distance and X10 magnification, produced by Ealing Beck Ltd. By scaling up the dimensions of this lens five times, a 1 in. diameter lens having a nominal working of 2½ in., was produced.

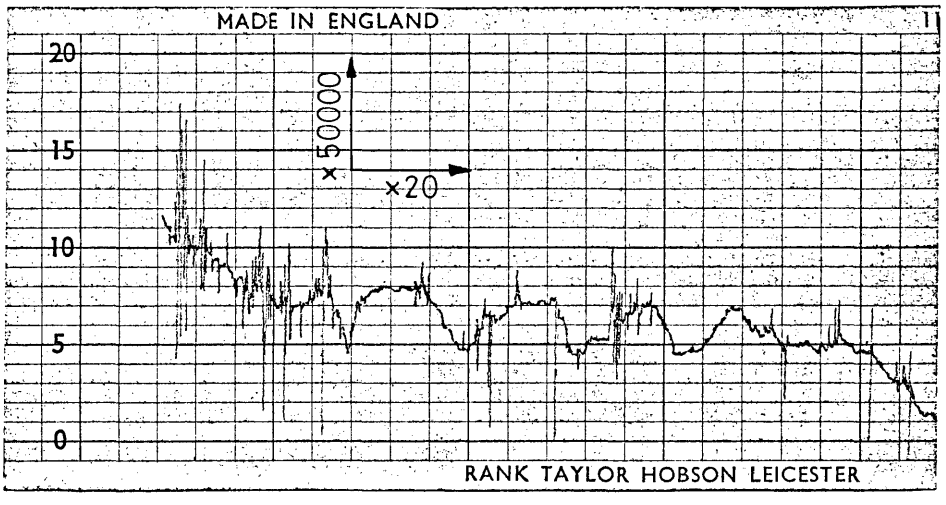

Figure 3.19 "Talysurf" trace of a polished roller after several test.

The new lens was found to have a magnification of X6.66. The numerical aperature (the sine of the half-angle subtended at the object by the objective aperature is equal to .18. The size of the objective is critical for multiple beam interferometry, as it controls the number of interfering beams collected by the microscope. It can be shown that a numerical aperature of .18 is sufficient to collect 30 reflected beams, when a thin wedge, angled to produce 100 fringes per centimeter, is observed. (Further details of this type of calculation can be found in ref. (170)). The new objective was therefore perfectly adequate for use in the interferometric system.

The two auxiliary lens (see figure 3.20) one positive and one negative, act as a telephoto lens combination. These have no effect upon the image, but serve only to reduce the required tube length from 31 in. to 9.7 in. The overall magnification is simply the product of the objective magnification and that of the eyepiece. A commercial eyepiece may be selected to give an overall magnification of up to approximately X150. This is the limit of useful magnification, determined by the numerical aperature of the objective.

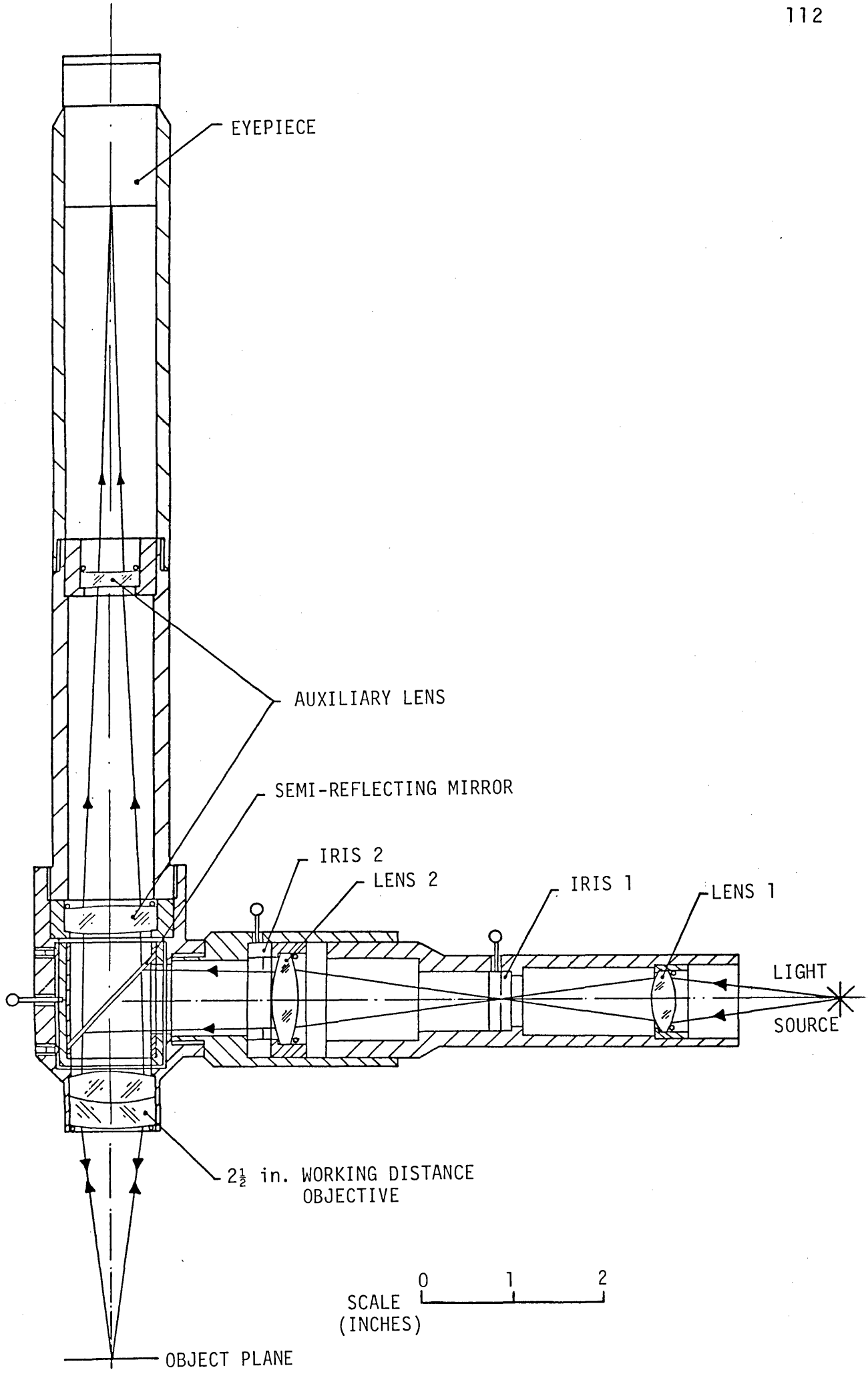

Figure 3.20 The microscope and incident illuminator

3.6.2 The Incident Illuminator.

A drawing of the microscope and illuminator is shown in figure 3.20. The illuminator was designed for use with a xenon flash lamp. As interferograms have to be photographed with a single pulse of extremely short duration, it is essential that the illuminator should provide maximum possible light intensity. To achieve this, the microscope field of view must be illuminated by an image of the source. In a system such as shown in figure 3.20, the source is imaged by the objective lens. The maximum intensity is then limited by the diameter of the objective.

A semi-reflecting mirror is used to inject light in a cone, such that the axis is coincident with the microscope axis. This mirror must be positioned above the objective to provide clearance for the illuminator. In order to avoid absorption losses, the reflecting side of the mirror was coated with titanium dioxide, which is a dielectric material. This gives a reflectivity of about 40%, which is only slightly lower than the optimum value of 50%. The upper surface of the mirror was 'bloomed' with an anti-reflection coating of magnesium fluoride. The mirror, which has a projected diameter equal to that of the objective lens, was positioned inside a cylinder and located by two thin sleeves. These sleeves were produced by slicing a thin walled cylinder at exactly 45^{o}. The outer cylinder was held in the microscope body by two sets of three grub

screws spaced at 120°, thereby providing adjustment in three dimensions. A small handle attached to the mirror holder, enabled the mirror to be rotated. The mirror was therefore fully adjustable, in order that alignment with the microscope and illuminator axes could be carried out after assembly.

The dimensions of the xenon lamp and housing necessitated that it was positioned about 6 in. from the microscope body. To satisfy this requirement, lens 1 was mounted in an extension tube, such that the distance from the centre of the source to the lens, was equal to twice its focal length. The source is then focused at an equi-distant point the other side of the lens. An Iris diaphragm (Iris 1) placed at this point acts as a field stop. This controls the effective source size, and hence the area of illumination. The position of lens 2 is such that an image of Iris 1 is formed at the microscope object plane. Therefore the distance of this lens from the iris is approximately equal to its focal length. Iris 2 is an aperture stop, and controls the area of the objective that is illuminated. This therefore limits the angle of illumination at the object plane, and hence the intensity. Maximum intensity was obtained by fully opening the iris, and thus illuminating the whole area of the objective. To ensure even illumination, the aperture stop was positioned at the focal plane of the objective. The image of the iris, formed by the objective, was then at infinity.

To set up the illuminator, the lamp was positioned and iris 1 closed to give a point source. The mirror was then adjusted until the field of view was illuminated by a central spot of light. The tube containing lens 1 and iris 1 was made a sliding fit within that containing lens 2 and iris 2. This was adjusted until the leaves of iris 1 were brought into sharp focus. Iris 1 was then opened until the field of view was just completely illuminated. The required intensity was produced by adjustment of Iris 2. At full aperture the illuminating cone has a semi-angle of 10^{o}. However after refraction at the air/sapphire and sapphire/oil interfaces, the maximum angle of incidence is about 7^{o}. This has only a very small effect upon fringe visibility, and a negligible effect upon fringe position.

3.7 The Light Sources

As the bearing was not run in a counter-rotating mode, it was necessary to observe the fringes stroboscopically. To freeze the motion of the fringes required a light source of extremely short pulse duration, capable of repetitive firing. A single flash of the source also had to be of sufficient intensity for photomicrography.

For measurement of the central film thickness, a roller movement of approximately half the contact width can be tolerated, as the colour of the central band can still be recognised. It was proposed to run at a maximum shaft

speed of 3000 R.P.M. This corresponds to a contact speed, relative to the window, of approximately 280 in./sec. For a contact width of .01 in., the pulse duration must be limited to about 17 μsec. However if the film thickness is to be measured at the exit constriction, the pulse duration must be considerably lower. At this point of the oil film, the separation between dark and bright fringes will typically be about .0003 in. Therefore to avoid complete blurring of fringe detail, the pulse duration should be less than 1 μ sec. Conventional flash lamps can be made to operate with pulse durations of this order, but the intensity is not sufficient for satisfactory photomicrography. 3000 R.P.M. is a relatively low speed for a roller bearing, and it was therefore proposed to develop a laser that could be used for future high speed tests, as well as for measurements at the higher speeds used in this study. For the initial low speed tests a xenon flash lamp was used.

3.7.1 The Xenon Flash Lamp.

The lamp together with the housing is shown in figure 3.21. This is a Thorn lighting type FA5 xenon discharge tube, which consists essentially of a compact arc (arc length : 0.12 in.) burning between tungsten electrodes, in a xenon atmosphere contained in a glass envelope. The spectral intensity distribution is very similar to that of daylight, and therefore this type of lamp is particularily

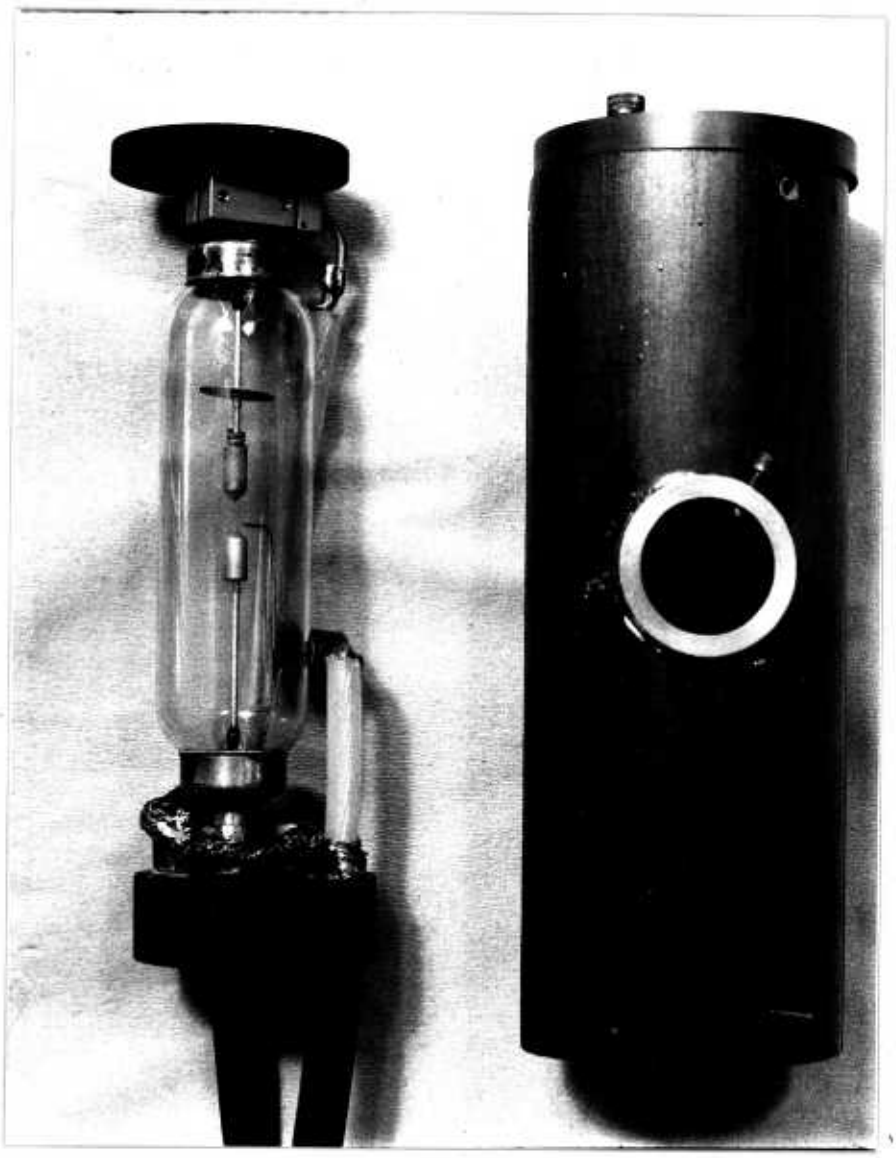

Figure 3.21 The xenon flash lamp and housing.

suitable for white light interferometry. To obtain monochromatic light, a narrow band filter was inserted in the illuminator. A Balzers B40, 5430 Å interference filter was found to be most suitable, as the narrow band width (100 Å) gave fringes of high visibility, and photographic emulsion is most sensitive to green light.

This type of lamp can be used to give short duration light pulses, by discharging a capacitor connected across the electrodes. The electrical energy dissipated in the flash is given by:

$$E = \tfrac{1}{2}CV^2$$

where C is the capacitance and V the applied voltage. The actual light energy produced is proportional to this value. The time duration of the flash is proportional to the product of the spark gap resistance, and the capacitance across the electrodes. To initiate the discharge, the gas is ionised by applying a very high voltage pulse (25 KV.) to the trigger electrode.

A commercially available power supply and triggering unit (Dawe Strobosun type 1203B), was modified to drive the lamp. This unit was designed for use with a small xenon lamp requiring a far smaller trigger pulse than the FA5. To obtain a 25 KV. trigger pulse required the application of a 300V. pulse to the primary side of the pulse transformer. It was therefore necessary to replace part of the transist-

orised triggering circuit with a relay valve, which was capable of switching this voltage. Details concerning the use of this valve are given by Wedeven (69). The FA5 could then be triggered from the existing variable frequency transistor multivibrator, or from an external signal. Use of the internal oscillator was required when setting up the optical system. External triggering requires a 10V negative going signal.

The flash repetition rate can be varied over three ranges up to a maximum of 250 flashes per second. The capacitance across the lamp is altered for each range, with a corresponding effect upon the flash duration. The capacitors are always charged to 1000V. The pulse duration (defined as the interval between points of $^1/_3$ maximum intensity) was approximately measured on an oscilliscope, using a phototransistor. These values, together with the energy dissipated, are given in figure 3.22. With the lamp externally synchronised, it is therefore possible to vary the pulse duration by switching ranges.

The lamp was enclosed within a Tufnol cylinder, and located at each end by thick Ebonite discs. This housing then provided adequate insulating protection. The discs were made a sliding fit within the cylinder, and the lamp electrode ends held in blind holes, drilled slightly off centre in the disc faces. A brass insert, bonded into the Ebonite housing, enabled the assembly to be directly mounted

RANGE	FREQUENCY (Hz)	CAPACITANCE (μ FARADS)	POWER (μ JOULES)	DURATION (μS)
1	0 - 25	3.35	1.675	50
2	0 - 83	1.1	.55	25
3	0 - 250	.35	.175	15

Figure 3.22 Pulse duration and energy dissipated by the xenon flash lamp.

on the illuminator. When in place, the position of the lamp could be adjusted by rotation, and by vertical movement of the end discs. When the arc was brought into line with the illuminator axis, the lower disc was locked by a grub screw. The upper disc was left free, to allow for expansion of the lamp.

3.7.2 High Speed Photomicrography with the Xenon Lamp.

Kodak high speed Extachrome reversal film was used for colour photography: Good exposure could be obtained from a single flash in range 1, by rating the film at 400 A.S.A. and using maximum aperture of Iris 2. For monochromatic work, the light intensity is greatly reduced by the filter. It was necessary to use Kodak 2475 recording film, and to rate this at 4000 A.S.A. With this film, adequate exposure could be obtained from a range 1 flash, using $^{2}/3$ maximum aperture of Iris 2. Range 2 required the use of full aperture, and range 3 resulted in under exposure.

3.7.3 The Xenon Laser.

Techniques of modulating (shuttering) a continuous working laser by electro-optic devices, were investigated. These were found to be unsuitable as complete extinction of the beam is not possible. For photomicrography an infinite extinction ratio is essential. The best modulators

currently available will give a 1000:1 extinction ratio. For satisfactory exposure, using a laser, 1 μjoule of energy is required. For a 1 μsec. pulse width, the minimum continuous working power required, is 1 watt. Therefore even with the modulator on (reducing the intensity), 1 μjoule will be produced in $^{1}/_{1000}$ sec., and the image will be completely obliterated during the time the camera shutter is open.

No commercially available pulsed laser in standard form, would fulfil the requirements of the interferometric system. A prototype laser was therefore developed by the Physics department of Imperial College, in collaboration with Chelsea Instruments Ltd. This was a pulsed xenon ion laser of the following specification:

Variable pulse rate:	0 - 50 p.p.s.
Pulse half width:	150 nanoseconds.
Peak power per pulse approx:	100 Watts (all wavelengths)
Wavelengths:	431, 495, 501, 519, 526, 535, 540, 596 nanometres.

The laser, shown in figure3.23, is similar in many respects to the xenon flash lamp. Two electrodes are situated at either end of the tube, about 1 metre apart. A 10kV discharge is initiated along the tube, by ionisation of the gas near one of the electrodes. This is achieved by applying a high voltage pulse, from a pulse transformer, to a coil wrapped around the quartz electrode casing. The passage of the discharge causes the gas in the tube to

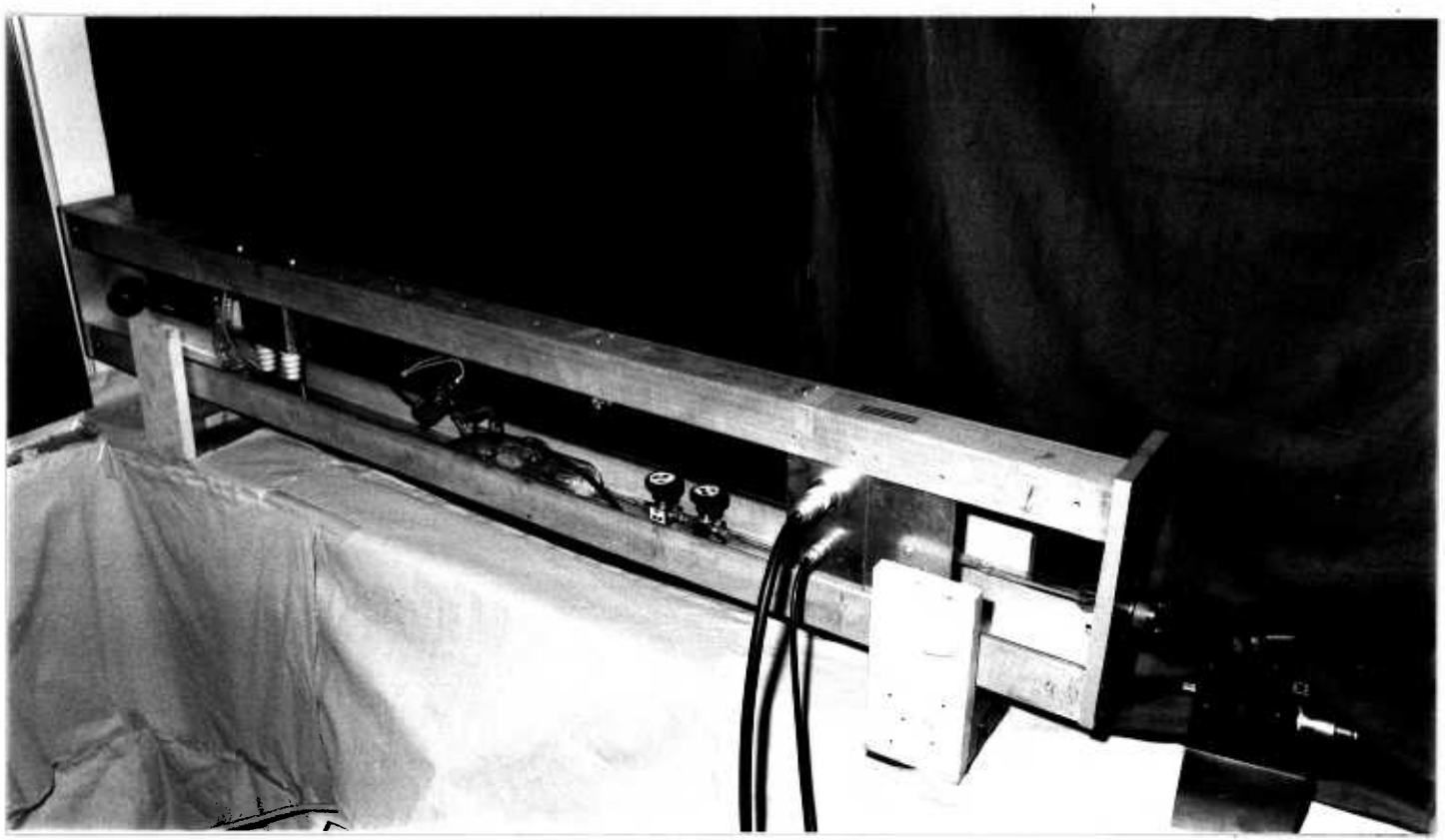

Figure 3.23 The pulsed xenon ion laser.

ionise, and when a certain ionisation threshold is exceeded, lasing begins. A semi-reflecting and a fully reflecting mirror are positioned outside either end of the tube. When the ions begin to lase, multiple reflections are directed by these mirrors up and down the tube. This further stimulates the ions, causing a rapid increase in lasing. As the discharge terminates, the ionisation level drops below the threshold and lasing ceases. The light pulse emerges from the semi-reflecting mirror.

There were two major problems involved in producing this laser. Firstly, the lasing action is critically dependent upon the gas pressure. This pressure must be extremely low, and it was found that during operation gas was removed by the electrodes. This gettering action altered the pressure sufficiently to prevent lasing. To overcome this problem, a separate gas reservoir was connected by two valves to the tube. The xenon gas in this reservoir was at a slightly higher pressure than that in the tube. To increase the pressure in the tube, the valve nearest the reservoir was opened, thereby releasing a small quantity of gas into the small tube separating the two valves. This valve was then shut, and the other opened, thereby releasing the gas into the tube. The tube pressure could be decreased by pouring liquid nitrogen into a flask surrounding the xenon reservoir. Both valves were then opened, and the tube pressure reduced to effectively zero. The valves were then

shut, and the liquid nitrogen left to boil away. The tube could then be refilled as already described. In this way the tube pressure could be optimised.

The second problem was caused by contamination of the gas, preventing lasing. This was overcome by fixing a getter pump to the tube. This type of pump will remove all but the rare gases. It operates continuously, but the action can be considerably accelerated by passing a current of about 0.5 Amps through a heater element in the pump.

The laser could be fired repetitively at variable frequency, or triggered from an external source. This requires a 10V. positive going pulse.

3.7.4 Illumination with the Laser.

The majority of the energy is radiated in the following lines: 4950 Å, 5260 Å, 5350 Å, 5400 Å. Individual lines were separated by reflection of the beam at a diffraction grating. The first order beams were then directed towards the microscope. It was found to be most satisfactory to direct the light into the bearing by reflection at a small fully reflecting mirror, positioned below the objective. Use of the semi-reflecting mirror inside the microscope, caused the beam to be focused by the objective lens. This resulted in a spot size smaller than the field of view. Also half the available intensity

was lost at the mirror. The small mirror and the mounting arrangement are shown in figure 3.24. The mirror, which was about $\frac{1}{8}$ in. square, was mounted on a shaft the end of which was located by a small steel ball. This ball could be moved up and down the slot drilled in the perspex block. Movement of the mirror was therefore completely three dimensional. The whole arrangement was held to the rig by the magnet.

When the laser beam was directed at near normal incidence, spurious fringe patterns were produced. These are thought to be caused by interference between beams reflected from the two sapphire surfaces. This is possible because of the long coherence length of the laser. However these patterns could be eliminated by adjusting the mirror to give non-normal incidence. This adjustment was extremely critical. The maximum angle of incidence used, never exceeded 10^{0} and therefore had a negligible effect upon fringe position.

This small mirror, which has only a small effect upon image contrast, can only be used below the objective for viewing the outer race contacts. No tests were carried out using the inner race. But in this situation, when the objective lens has to be positioned slightly inside the shaft, it was proposed to use the small fully reflecting mirror behind the objective, in place of the large semi-reflecting mirror.

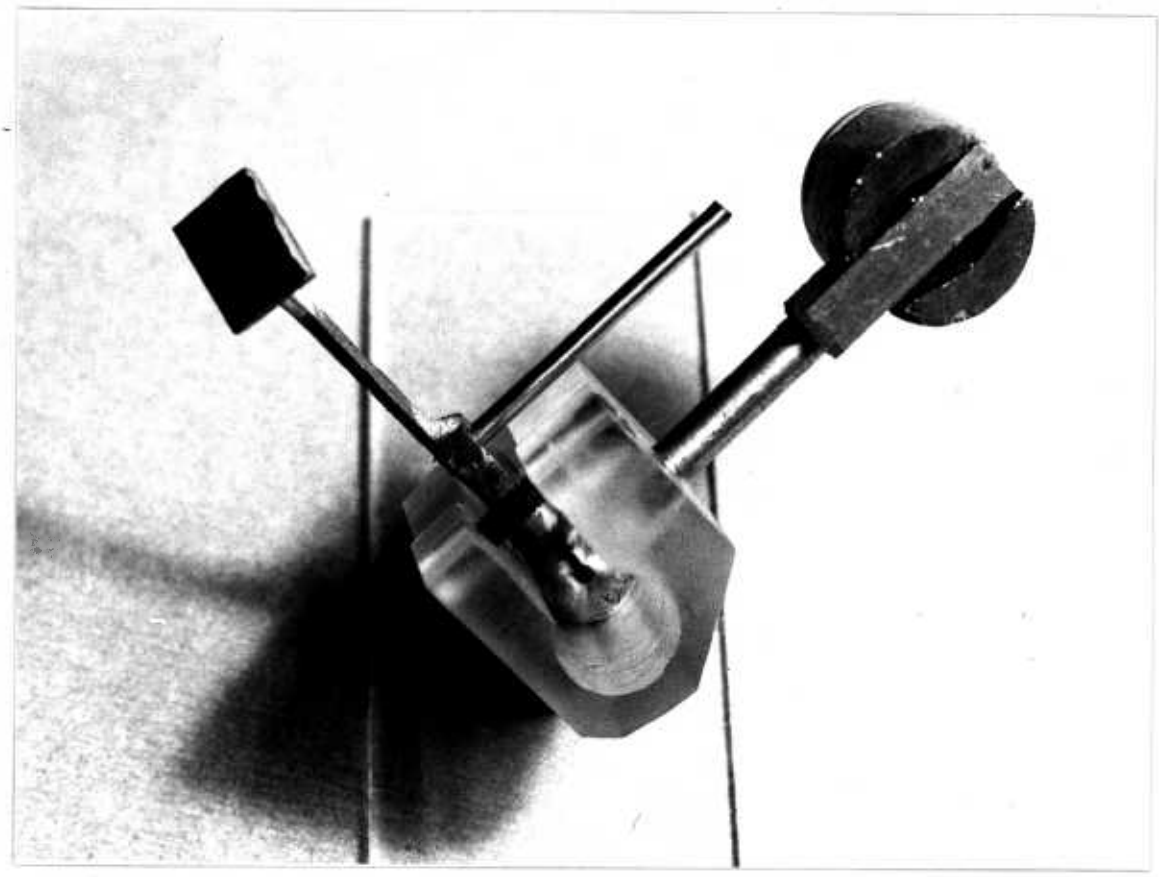

Figure 3.24 Small mirror for reflecting the laser beam.

3.7.5 High Speed Photomicrography with the Xenon Laser.

The two lines most frequently used were 4950Å (blue) and 5260Å (green). The extremely short flash duration necessitated using Kodak 2475 recording film. Good exposure was obtained, from a single flash, by rating this film at 4000 A.S.A.

3.7.6 Combined Illumination.

The fringes, resulting from laser illumination, were extremely sharp and of high visibility. However the position of the inlet boundary was far more distinct under flash lamp illumination. When using the laser and the small mirror below the objective, it is unnecessary to disturb the flash lamp set up. During a run it was possible to switch from the laser to the flash lamp, and thus revealing the position of the inlet boundary, and oil distribution on the track surface.

Under laser illumination, the fringe system is not localized. The microscope was therefore initially focused on the sapphire track surface, using the xenon flash lamp.

CHAPTER IV

EXPERIMENTAL SET UP

4.1 Mechanical Arrangement

4.1.1 Design Criterion.

The design of the bearing rig was based upon the following criterion:

(a) The capability of applying loads of up to 8000 lbs. to the test bearing, and the incorporation of load cells.

(b) Shaft speed infinitely variable between 0 and 3000 R.P.M.

(c) A rigid housing and mounting arrangement to minimise deflection and vibration.

(d) Optical access to all positions of the test bearing.

(e) Easy to dismantle for roller changes.

(f) A separate oil jet supply to the test bearing, isolated from supplies to the other bearings.

(g) Control of the oil flow rate to the test bearing from 0 to about 10 gallons per hour.

(h) Provision for oil temperature variation and adequate filtration.

(i) Provision for transducers for shaft and cage speed measurement and for flash synchronisation.

(j) Provision for thermocouples for temperature measurement of the oil jet and the surface of the sapphire window.

4.1.2 The Basic Test Bearing Rig.

The drawing shown in figure 4.1 illustrates front and side elevations of the basic rig. The housing (part A) was cast in 'Meehanite'. This satisfies criterion (C), and enabled the housing to be produced, in one piece with the minimum of machining.

The shaft was manufactured from EN24T, which is a semi-hardened steel of excellent mechanical properties. It was mounted between two bearings, one of which is a ball journal providing axial location. The other is the test roller bearing, which was positioned at the end of the shaft in order to minimize the optical path length required. The third bearing is a roller journal through which the load is applied. This is as close as possible to the test bearing in order to reduce misalignment caused by shaft deflection.

The outer race of the test bearing is seated within a mild steel collar (part C). This collar, which contains a 45^{o} mirror (see figure 4.3) placed above the sapphire window, can be rotated within the housing, such that the window may be fixed at any point around the circumference of the bearing. It is locked in position by a clamping ring (part B). Oil that has flowed through the bearing, drains through one of the 12 oil outlets drilled radially through the collar, and thence out of the housing. The oil supply to the test bearing is isolated from other

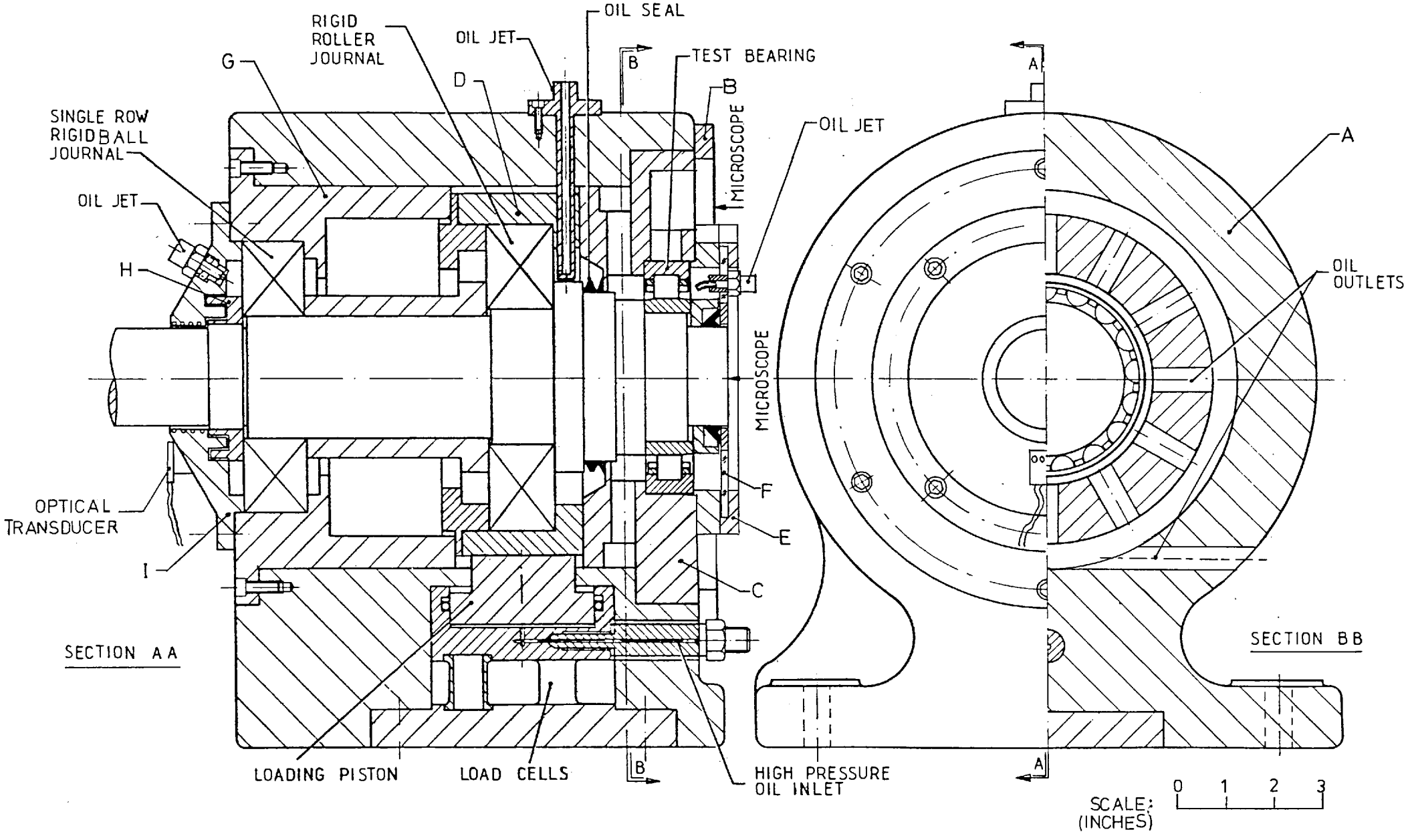

Figure 4.1 Drawing of the basic test bearing rig.

parts of the rig by a 'v-ring' seal rubbing against a lip on the collar. The bearing is enclosed by a perspex cover (part F), upon which are mounted the oil jet and transducers for flash synchronisation and speed measurement. This cover can be rotated and locked in place by a clamping ring (part E). The 'v-ring' seal acts upon a steel insert in the perspex cover.

The loading collar (part D) is free to move in a radial direction, in the line of the applied load, and is prevented from rotating by lugs on part G. The ball journal and the floating roller journal are locked onto the shaft by a nut (part H), which forms a labyrinth seal within the cover plate (part I). These two bearings are supplied by separate oil jets and have a common outlet situated between the two.

The outer races of all three bearings are a sliding fit within their respective housings. All the inner races are a light interference fit upon the shaft (about 0.0001 in.). Preliminary tests were carried out with a shaft ground so that the test bearing inner races were a sliding fit. Although this facilitated interchanging the test bearings, it led to considerable fretting of the shaft and a fluctuating load distribution. This problem was eliminated by manufacturing a new shaft, in order that these races would also be a light interference fit.

The complete shaft assembly, except the outer race of the test bearing, can be withdrawn from the front of the

housing, after removal of the screws securing part G. Test bearing rollers can therefore be easily changed, with a minimum of disturbance to the experimental set up. The outer race can be removed, with the shaft in position, by extracting part C from the rear of the housing.

4.1.3 The Loading System.

Load is applied hydraulically by means of a piston in cylinder arrangement. The diameter of the loading piston is 3 in. and therefore a load of 12,000 lbs. requires an oil pressure of 1700 p.s.i. An 'o' ring together with an anti-extrusion ring were used for sealing.

The loading cylinder is supported upon three load cells spaced at 120^{o} intervals. The cells were designed to give 1,000 micro-strain at a load of 12,000 lbs., and have a wall thickness of 0.0225 in. Each cell carries four strain gauges, two dummy gauges and two active gauges. The gauges are wired in the form of a 'bridge', each of the four 'arms' consisting of three gauges in series and having a resistance of 360 ohms.

A 24V stabilized power supply was built to supply the bridge, together with a facility for balancing. The output voltage was measured by a micro-voltmeter. The complete loading set up was independently calibrated in a testing machine up to a load of 12,000 lbs, and was found to have a sensitivity of 7.1 μV. per lb.

Initially the load was applied by means of a small hand pump fitted with a non-return valve. This was unsatisfactory as the load was not held constant, there being some oil leakage either from the loading cylinder or at the non-return valve. The problem was overcome by using a 10 cubic in. 'hydro-pneumatic' accumulator in conjunction with a bottle of compressed nitrogen. The acculumator essentially consists of a cast shell containing a separator bag. The bag was directly connected to the nitrogen bottle via an extremely fine needle valve. A similar valve provided an outlet to atmosphere. The acculumator shell was filled with oil and connected to the loading cylinder. The oil could be pressurised by inflating the acculumator bag with nitrogen, and the pressure monitored on a gauge fitted below the acculumator fluid port. A small leakage of oil from the loading cylinder results in a negligible reduction of load, because of the high compressibility of the gas. The arrangement can be seen in figure 4.1 and in figure 4.10.

4.1.4 The Rig Mounting.

The rig was mounted on a discarded lathe bed. This provided an extremely rigid mounting for the rig, associated optical equipment, the drive motor and pump, and ancillaries. The headstock was removed and a plate machined to fit over the slides. The bearing rig was bolted to this plate, which can be moved along the slides and clamped in

any desired position. The whole bed was placed upon four anti-vibration rubber pads, which helped considerably to reduce vibration. The mounting arrangement can be seen in figure 4.5 and figure 4.10.

4.1.5 The Drive System.

The rig is driven by a 3 h.p. variable speed d.c. motor, and electronically controlled by a Fenner 'Speed Ranger'. This gives a speed holding capability of better than 2% of top speed, for any change of load within the motor rating. The drive is transmitted by a timing belt fitted over 'taper lock' toothed pulleys. As the specified maximum motor speed is 2000 R.P.M., the number of teeth on each pulley are in the ratio 2:3, giving a theoretical maximum shaft speed of 3000 R.P.M. The motor is secured by rubber mountings to a steel plate which is located below the slides, and bolted to a lip above the bed sump. The belt is guided through the slides by an idler pulley, which also serves as a tensioner.

4.1.6 The Pumping System.

Figure 4.2 shows a schematic diagram of the flow circuit. The pump, which is capable of delivering 1.5 gallons per minute at 500 p.s.i., was mounted below the drive motor in the bed sump. The 3 gallon tank contains a 1.5 kV . immersion heater, which is thermostatically controlled. The main filter has a 25 micron element of sintered bronze.

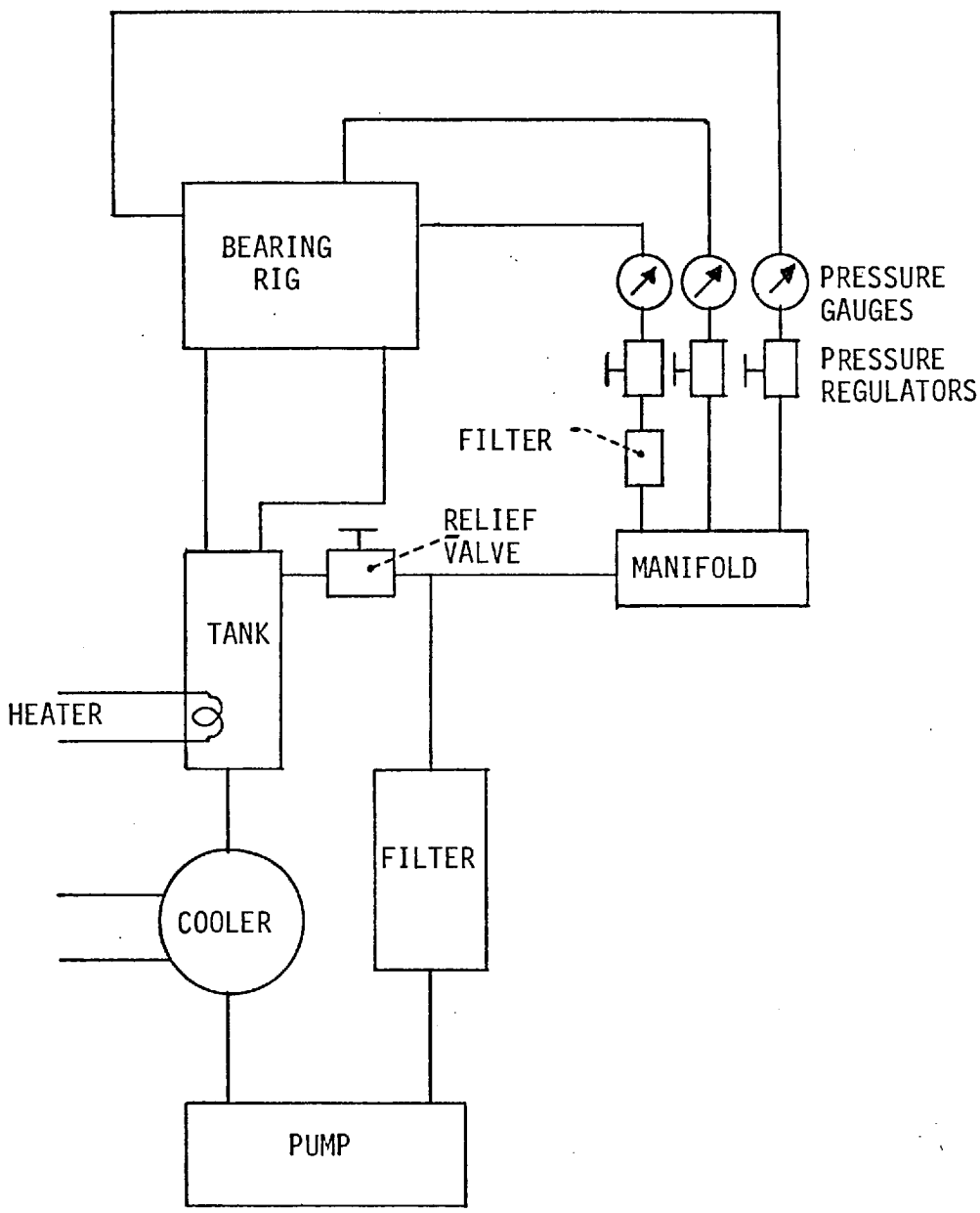

Figure 4.2 Schematic diagram of the flow circuit.

The relief valve can be adjusted to give a manifold pressure between 0 and 100 p.s.i. The oil flow rate to each bearing is controlled by Norgen miniature pressure regulators, adjustable from 0 to 50 p.s.i. These regulators are designed to work with gases, but were found to work equally well with oil. The regulators together with pressure gauges and the relief valve, can be seen mounted on the rig in figure 4.10.

In initial tests, the oil supplied to the test bearing was only filtered through the main 25 micron filter. When quite severe scratching of the sapphire surface occurred, the pressure regulator for the test bearing oil supply was replaced with a miniature filter regulator containing a 5 micron sintered bronze element. This modification virtually eliminated any further deterioration of the sapphire surface.

With this secondary filter in place, the maximum flow rate that could be delivered to the test bearing, using the thicker of the two test oils (lubricant 1), was about 5 gallons per hour. The test bearing jet has a diameter of $^1/_{16}$ in. and is directed at the cage pilot area, when the LRJ 65 bearing is in place. Oil flows out of the rig and is returned to the tank under the action of gravity.

4.1.7 Speed Measurement.

Shaft speed was measured using a sub-miniature 'Skanner' (Skan-A-Matic type S-351SR) to detect reflective marks on the drive pulley. This 'Skanner' consists of a light source and a photo-transistor spaced close together

in a single unit. It was mounted upon the front cover plate of the bearing rig, and directed at the rear face of the drive pulley. The positioning is illustrated in figure 4.1. Sixteen strips of silver tape were stuck to the back face of the pulley. The circuitry to drive this 'Skanner' was incorporated with that for flash synchronisation, and is shown in figure 4.9. The output from the photo transistor is fed directly into a digital tachometer, and the time base set to 3.75 seconds in order to give speed readings in R.P.M.

The cage speed was measured by means of a magnetic transducer, with the probe placed as close as possible to the roller surfaces. The positioning of the transducer is shown in figure 4.3. At low speeds the signal from this transducer is not large enough to trigger the counter. It was therefore fed first into an operational amplifer and thence to the counter. This circuitry was again incorporated with that for flash synchronisation and is shown in figure 4.9. The LRJ65 (this bearing was used for all tests) has 16 rollers, and therefore both shaft speed and cage speed are measured in R.P.M. The counter has the facility to display the ratio of the two inputs, and therefore direct measurements of slip can be made.

The accuracy of speed measurement depends upon the number of signals per revolution, which in this case is 16. In the mid-speed range this gives an accuracy of about .5% for the gate time of 3.75 seconds.

4.1.8 Temperature Measurement.

Nickel-chromium/nickel-aluminium thermocouples, in conjunction with a Comark electronic thermometer (type 1604) were used for temperature measurement. This type of thermometer can be read to $0.1^{o}C$. Two thermocouples were used, one positioned in the test bearing oil jet, and the second upon the sapphire window, at the oil exit side of the test bearing. This thermocouple is sheathed in steel and was clamped so as to be sprung loaded against the sapphire surface. The bead was insulated from the steel sheath with silicone rubber. The plug connecting the leads to the thermocouple is visible in figure 4.7.

4.2 Optical Arrangement

4.2.1 The Fully Reflecting Mirrors.

Figure 4.3 illustrates the basic optical arrangement for viewing the outer and inner race contacts (the incident illuminator illustrated does not correspond to that actually used). The fully reflecting mirrors have a projected diameter sufficient to allow all parts of an area equal to the length of the roller X a distance of ten Hertz widths, to be viewed at a total cone angle of 20^{o}. The sizes of all the viewing slots were also based upon this condition.

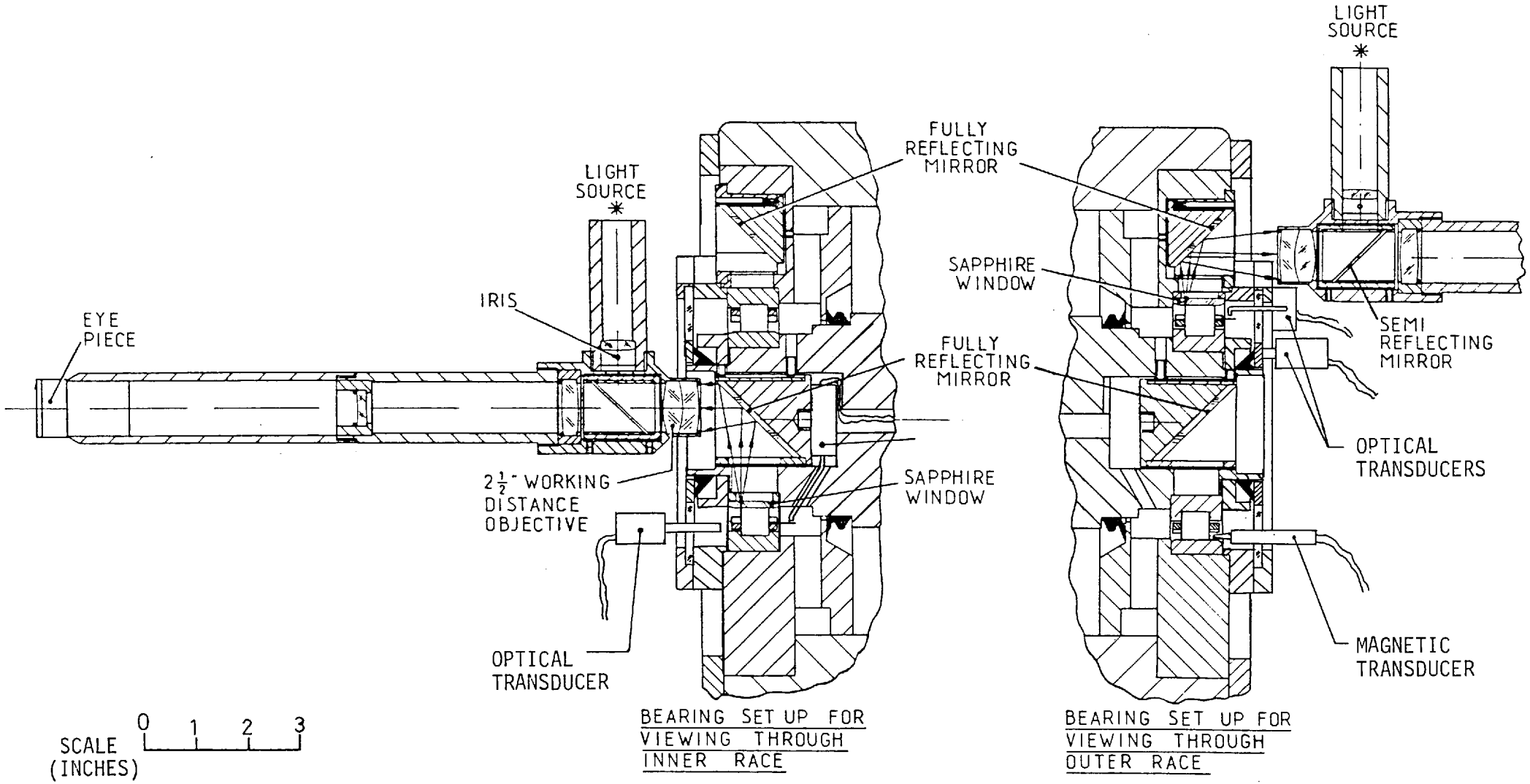

Figure 4.3 Drawing of the optical arrangement for viewing the outer and inner race contacts.

The mirror faces were coated with aluminium and have a protective coating of silicon dioxide. The mounts were made from brass and have a face machined flat and at 45^{o}. The mirrors were bonded to these mounts upon three pads of 'Silocet,' spaced at 120^{o}. 'Silocet' is a rubber based cement which, when set, allows slight movement; it was used to ensure that there would be negligible distortion of the mirror surfaces.

The mirror for outer race viewing is enclosed in a brass slieve located, above the sapphire window, in collar C. The slieve contains three adjusting screws spaced at 120^{o}. A lip at the back of the mirror mount is pressed against these screws by a spring, and thus the mirror is fully adjustable. It is shown in position in figure 4.4. Rotation of the collar enables the outer race contacts to be viewed at any position around the bearing.

The rotating mirror for inner race viewing is similarily enclosed within a brass slieve, to which the mirror mount is fixed. The slieve is located in the centre of the shaft, so that the mirror is correctly positioned in line with the shaft viewing slot and sapphire window. It is fixed by two sets of three grub screws, again spaced at 120^{o}, to enable the mirror to be adjusted. These screws locate in slots, machined along the slieve, to ensure no rotation of the mirror relative to the shaft. The mirror can be seen in position in figure 4.4.

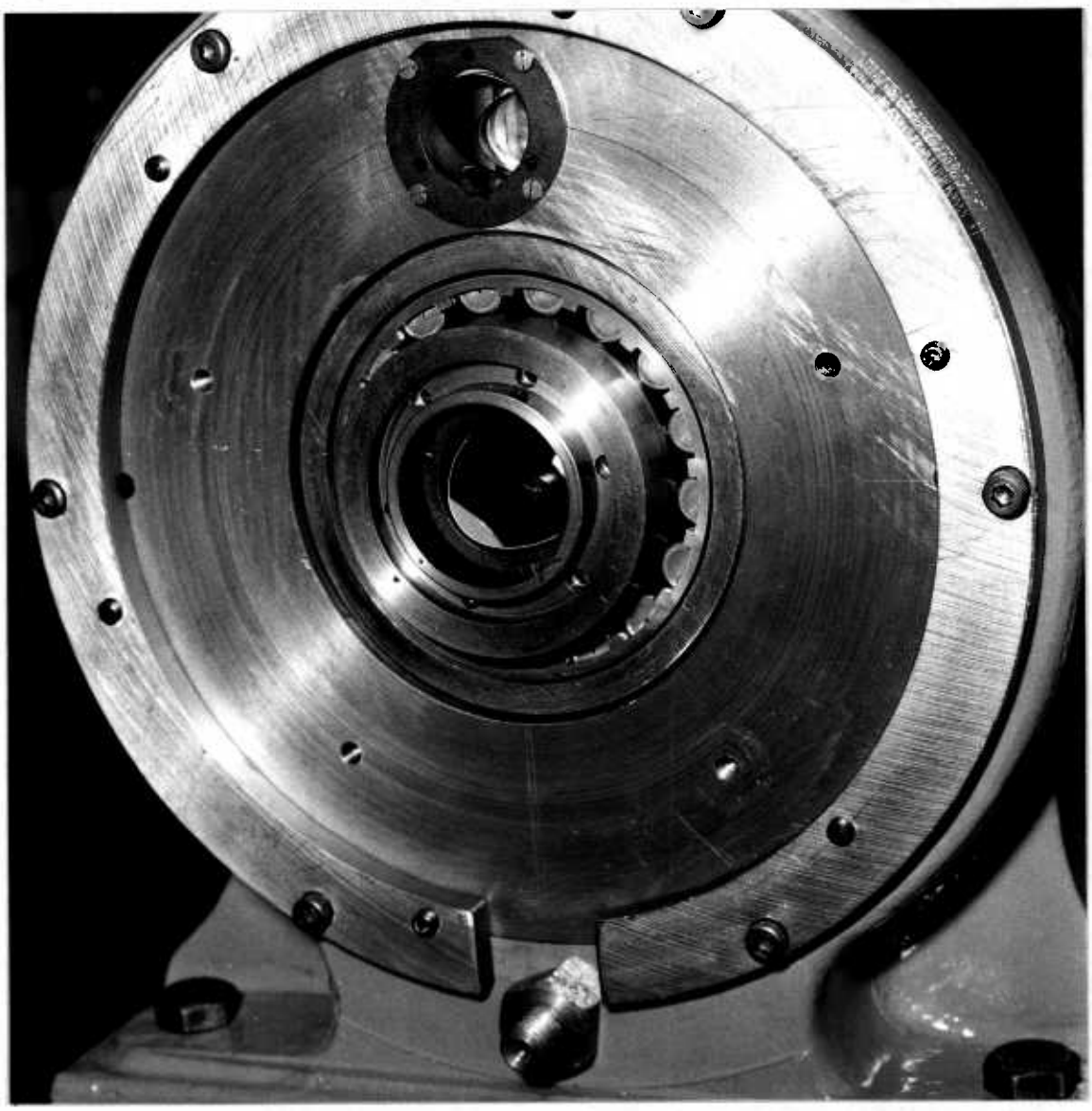

Figure 4.4 The fully reflecting mirrors positioned in the rig.

4.2.2 The Microscope Mounting.

The microscope mounting was bolted to the original lathe cross slide. The slides then performed the same function as those on an optical bench. Movement of the saddle enabled the microscope to be moved up to, or away from the rig, whilst always keeping it aligned. There is sufficient movement of the cross slide to allow the microscope to be positioned to view through the outer race, at any angle around the circumference.

The mounting arrangement can be seen in figure 4.5. The microscope was mounted upon a commercially available three way movement, which was used for fine adjustment in the horizontal and vertical directions. This whole assembly was supported by a bracket from a vertical pillar, bolted in the place of the original tool post. The bracket can be slid up and down the pillar and clamped in any position; this provided a means of coarse height adjustment. In order that the microscope may be aligned with the rig, the pillar can be revolved in the horizontal plane, and also one section of the bracket can be revolved in the vertical plane. The bottom of the bearing can be viewed through the outer race by moving the bracket to the top of the pillar and mounting the whole assembly 'up-side down'.

The method of mounting the microscope upon the lathe bed formed a rigid fixing, giving optical access to all parts of the bearing, and allowing full 3-dimensional adjustment.

4.2.3 Arrangement for Laser Illumination.

The laser was mounted on a ledge alongside the rig and the beam deflected using a diffraction grating. The set up is shown in figure 4.5. The small fully-reflecting mirror, used to reflect the beam in front of the microscope objective for outer race illumination, is shown in position in figure 4.7. Further details concerning illumination with the laser are given in section 3.7.4.

4.2.4 Arrangement for Viewing and Image Recording.

The images could be viewed by eye or on a television monitor. Recording could be made on 35 mm. film or on videotape. Figure 4.5 and figure 4.10 illustrate the set up. A Sony television camera attachment, type MVA-1, was placed in the end of the microscope instead of the conventional eye-piece. This attachment contains a fully reflecting mirror, which enables the optical path to be switched from ocular to a video camera or to a still camera. The use of this attachment gave the following approximate overall magnifications, when used in conjunction with the X6.66 2½ in. working distance objective:

Ocular	. . . . . X 80
35 mm. Still camera	. . . . . X 18
Television Monitor	. . . . . X 140

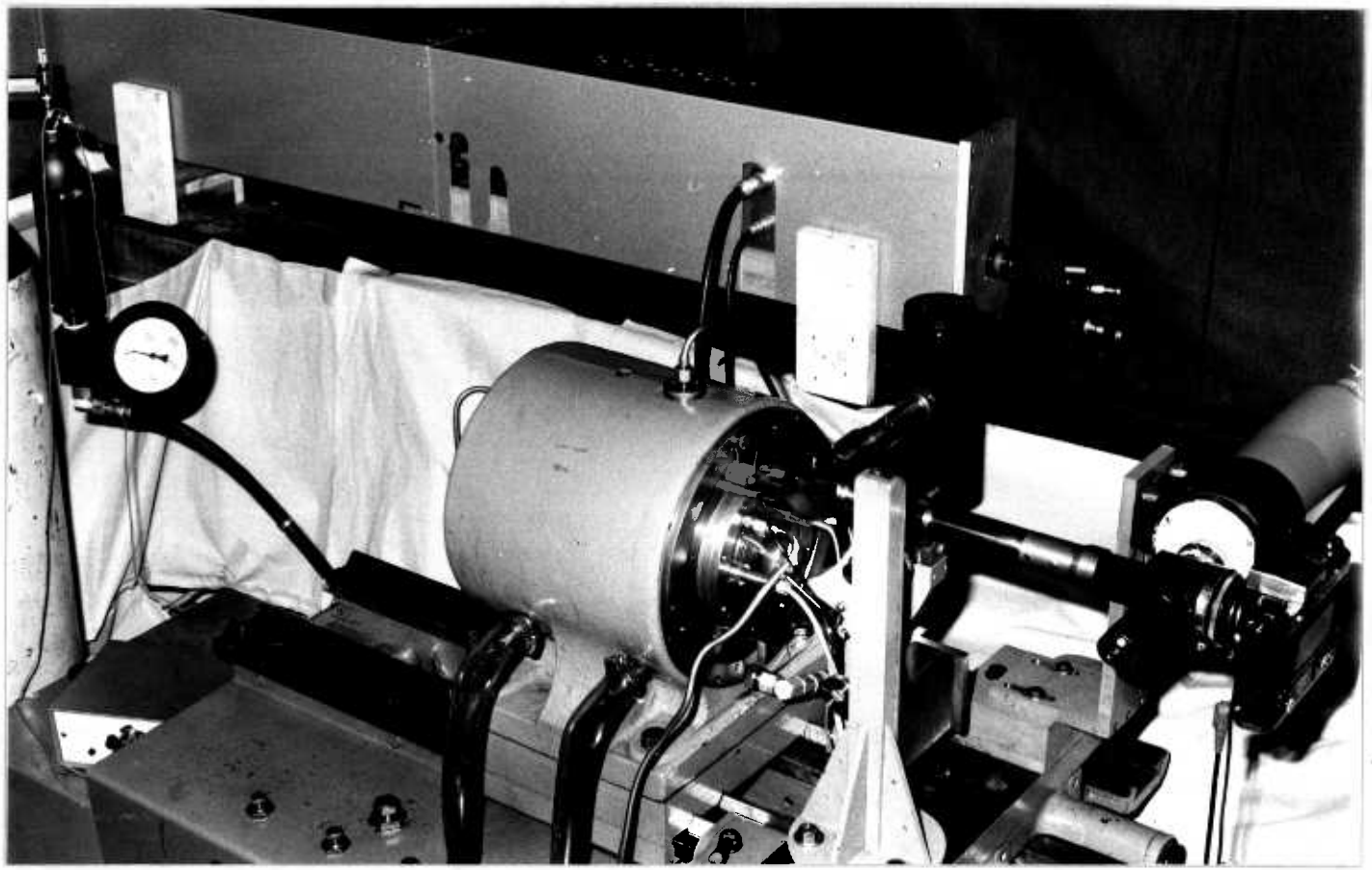

Figure 4.5 Optical arrangement.

These magnifications enabled a distance of about five Hertz widths to be viewed either side of a contact placed in the centre of the field of view.

The television camera was supported upon a bracket bolted to the cross slide. Once this was in position, the microscope could only be moved horizontally by movement of the saddle or cross slide; however the support it gave to the end of the microscope considerably increased the overall rigidity of the microscope mounting.

4.2.5 Photomicrography.

A motor driven Nikon F 35 mm. camera was used for still photomicrography. The automatic wind on facility enabled photographs to be taken in quick succession, without disturbing the optical set up. The shutter speed control was set at 'Bulb' and the motor drive at single shot.

When a photograph was required, the optical path was switched to the camera, and the flash synchronisation circuit connected through the contactor that is operated by the camera shutter. The remote shutter button was then pressed and held down. This action opened the shutter and closed the points of the contractor. A triggering pulse from an appropriate roller passing over the sapphire window could then initiate a single flash of the lamp or laser. After the flash, the shutter was closed by releasing the button, which also caused the film to be wound on. Another flash could not be initiated until the flash synchronisation

circuit had been re-set. There was therefore no possibility of multiple exposure. Details concerning flash synchronisation are given in section 4.3.

4.2.6 The Television and Video Recording System.

The use of closed circuit television was a considerable aid to viewing, and the video-recorder enabled every image to be recorded. While the rig is actually running, it is sometimes difficult to monitor the colour of the central Hertzian region, and the position of the inlet boundary may be quite erratic. Upon playback, every frame can be studied individually, the fringe order followed, and any change in conditions observed step by step. The use of the recorder is essential for viewing through the inner race window, as it is not possible to achieve a stroboscopic effect with the window at exactly the same orientation every revolution of the shaft.

Because of the very short duration of the flash and the use of monochromatic light, it was necessary to use a vidicon camera tube of high sensitivity. An E.M.I. tube type 9677B was found to give an extremely good image. Maximum contrast was obtained by adjusting the beam current and the target voltage, with controls situated on the camera control unit. Because of the stroboscopic nature of the light source, it was necessary to override the automatic gain controls on the camera control unit and on the video-recorder. The scanning of the photocathode was not

synchronised with the flash lamp. This was found to be unneccessary as there is sufficient capitance to enable an image to be formed after the flash has occurred. The effect of this was to cause some frames to be of lower contrast than those produced when the scanning and flash were simultaneous. To prevent overlap of the images, and subsequent lack of contrast, it was found desirable to limit the flash repetition rate to a maximum frequency of about 15 flashes per second. A facility to enable the maximum flash repetition rate to be adjusted was incorporated with the flash synchronisation circuitry, and details are given in section 4.3.4.

The sound-track on the tape was used to record a commentary detailing the running conditions during a test.

4.3 Flash Synchronisation

4.3.1 Introduction.

It was proposed to synchronise the flash using an integrated circuit timer, which would enable the timing of the flash to be adjusted to view a substantial distance before and after the actual contact area. At the maximum roller speed of approximately 350 in. per second, a delay of 140 μ. seconds is required to allow viewing 0.05 in. in front of the contact. The repeat accuracy of the timer is $\pm \frac{1}{2}\%$, and a repeatability of the roller position to within

± 0.002 in. was required. Assuming no jitter in the initiation of the actual flash discharge, this requirement demanded that the position of the roller could be sensed to within ± 0.0015 in.

The following methods for sensing roller position were attempted and found to be unsatisfactory. Firstly a fiber optic 'Skanner', having a coaxial light source and sensor, was used to detect the polished ends of the cage bars that interspace the rollers. Because of the large reflecting area (about 0.1 in.), any variation in the intensity of the reflected light reaching the sensor, which could be caused by oil or movement of the cage towards the 'Skanner', altered the point at which the flash was triggered. Also there is a certain amount of movement of the rollers within the cage pockets.

Secondly a similar 'Skanner' was positioned between the cage and outer race and used to detect the roller edges. This too was unsatisfactory for similar reasons.

Thirdly a magnetic transducer was placed with the probe between the cage and outer race and close to the roller faces. To avoid variation in the signal amplitude, caused by axial movement of the rollers, the signal was differentiated before being fed into the triggering circuit. The advantage of this method was that it was unaffected by the presence of oil. However repeatability of object position was still unsatisfactory, and at shaft speeds below about 50 R.P.M. the amplitude of the signal was not

sufficient for accurate triggering.

The method that was successfully used is outlined below.

4.3.2 Synchronisation of the Outer Race Contacts.

A fiber optic 'Skanner' was used to detect needles located in the centre of four rollers, equi-spaced around the bearing. A schematic drawing of the 'Skanner' (Skan-A-Matic type S2005-3) is given in figure 4.6(a). The semi-rigid snout, that contains the coaxial fiber bundle, can be bent to any desired shape. At the optimum distance of 0.01 in. from the target, the field of view is 0.02 in. Figure 4.3 illustrates the positioning of this 'Skanner,' and figure 4.7 shows the 'Skanner' in place on the rig. The needles have a diameter of 0.03 in. and, since the curved surface is viewed, the reflected light pulses are extremely sharp.

Ordinary sewing needles were used, as these are exceptionly stiff and have a surface finish of high reflectivity. They were inserted into the rollers in the following manner: A hole of 1/8 in. diameter was spark eroded approximately through the centre of the rollers, and a soft plug of mild steel inserted. A 0.03 in. diameter hole was then drilled through the plug while the rollers were rotated in a collet chuck. Before insertion, the needles were ground such that 1/4 in. would protrude from the end of the rollers. A drop of cyanoacrylate cement

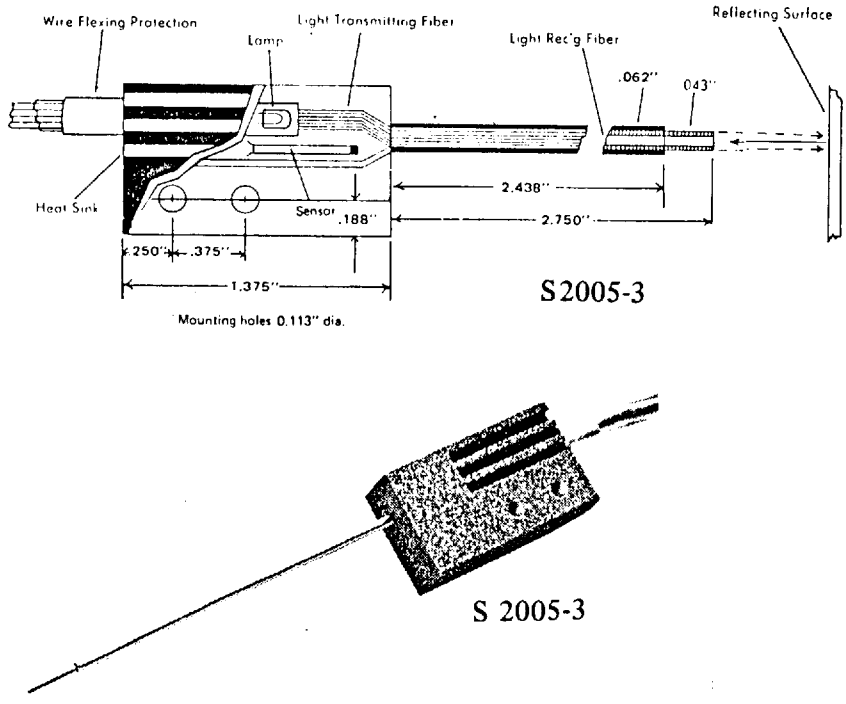

(a) "Skanner" to detect needles.

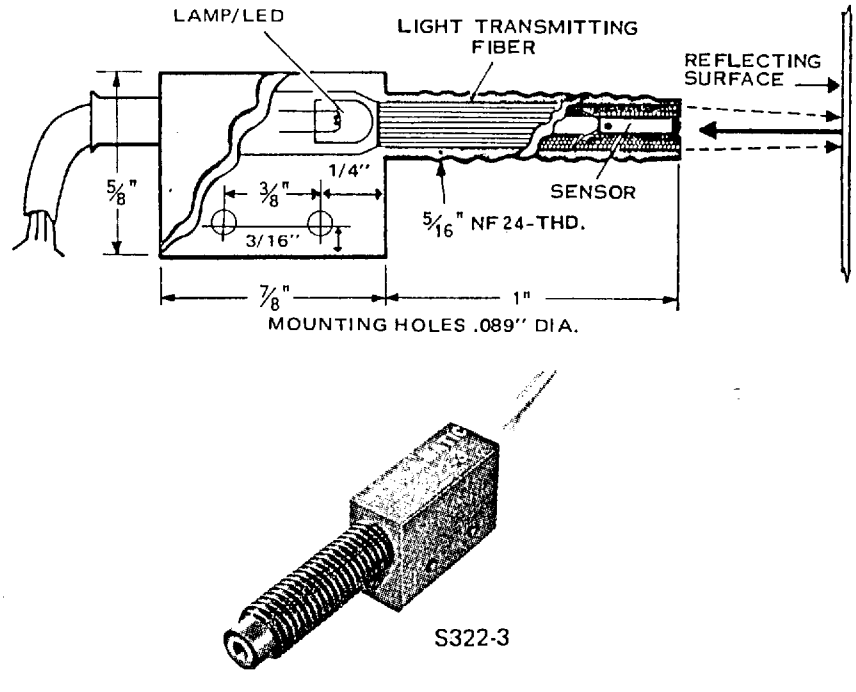

(b) "Skanner" to detect cage mark.

Figure 4.6 Schematic drawings of the fiber optic "Skanners" for flash synchronisation.

ensured that they were bonded in position.

In order that an individual roller could be selected for viewing, a second fiber optic 'Skanner' (Skan-A-Matic type S322-3) was positioned so as to detect a mark on the cage, when that particular roller was over the sapphire window. This 'Skanner' is illustrated in figure 4.6(b), and can be seen in position in figure 4.7. The reflective mark on the cage was made by polishing and lacquering this portion of the brass cage. This was then masked and the rest of the cage side sprayed matt black.

This arrangement gave consistantly good flash synchronisation. Both with the xenon flash lamp and the laser, there was found to be an inherent delay of about 500 μ seconds between the time of the application of the triggering signal to the discharge unit, and the initiation of the actual flash. Therefore to achieve synchronisation at the highest speed, it was necessary to place the 'Skanner' about 0.125 in. in front of the centre of the field of view. A small variation in this inherent delay could have been responsible for the inaccuracy of about $\pm$ 0.003 in. in repeatability of roller position. The circuitry for this system of synchronisation is outlined in Section 4.3.4.

4.3.3 Synchronisation of the Inner Race Contacts.

No work was attempted with the inner race fitted with the sapphire window. However it was proposed to synchronise, either by sputtering a 0.001 in. manganin strip

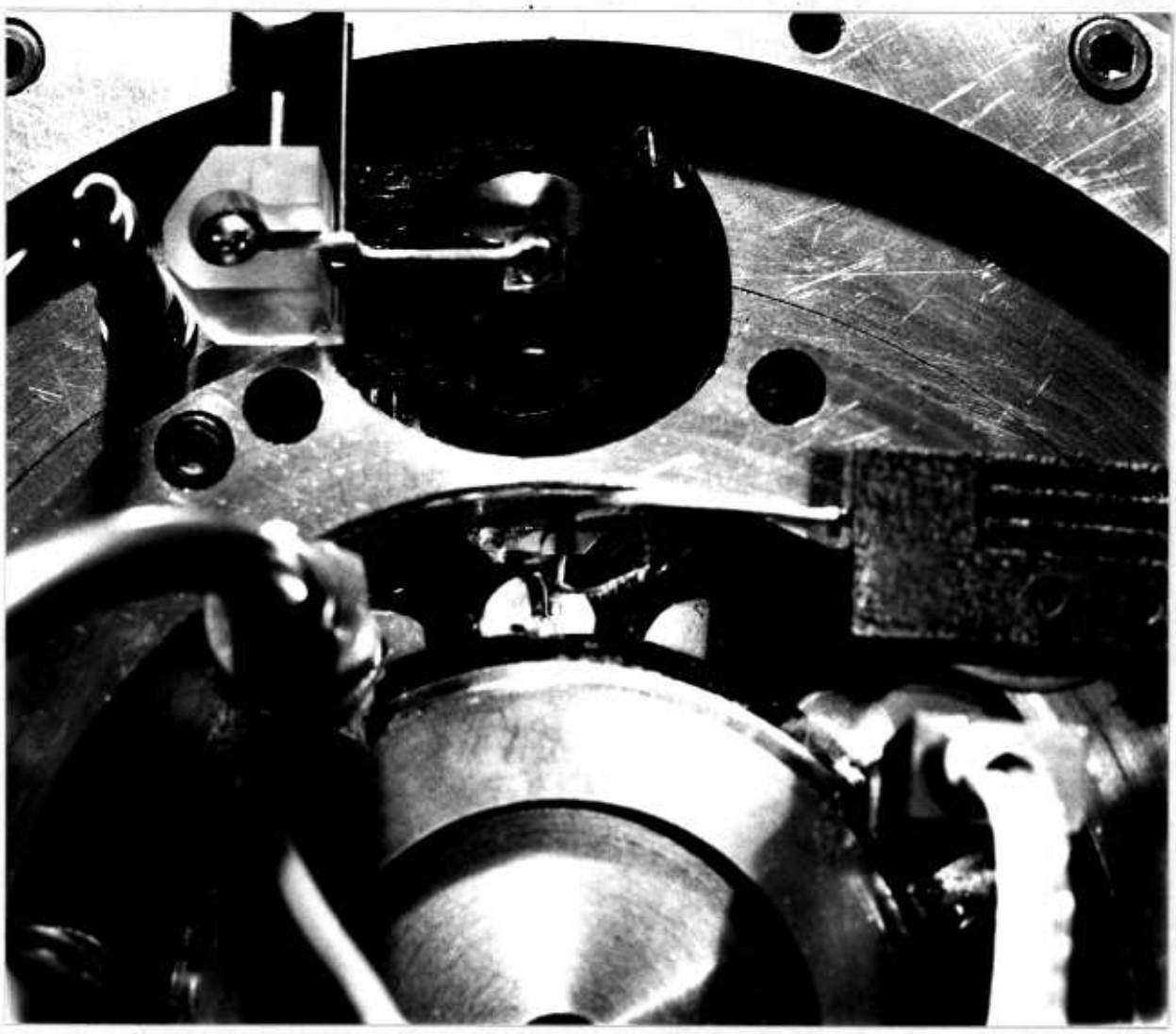

Figure 4.7 Positioning of the transducers and mirrors for viewing the outer race contacts.

(similar to that used in (89)) across the race upon the sapphire surface, or by using a fiber optic 'Skanner' rotating within the shaft and detecting needles, as for the outer race. Manganin is pressure sensitive, and therefore triggering could only take place in the loaded region. For this reason the latter method is regarded as more suitable.

Figure 4.3 illustrates the proposed set up and shows the position of the 'Skanner' within the shaft. Slip rings are required for the 'Skanner' connections. A second 'Skanner' is mounted to detect a reflecting mark on the inner race locking ring. This 'Skanner' can then be used to position the window, so that the flash will occur at a desired orientation. At a particular shaft speed, the flash frequency will be inversily dependent upon the positioning accuracy required. For the LLRT65 bearing, a reflecting mark that covers an arc of 35^{o} will ensure a flash every revolution of the inner race, if all the rollers are fitted with needles. The circuitry for this synchronisation arrangement is identical to that used for the outer race tests, and is described below.

4.3.4 Circuitry for Flash Synchronisation.

The circuit was designed to fulfill the following requirements:

(a) Trigger either the flash lamp or the laser, after a time delay continuously variable from 0 to 100 milliseconds.

(b) The capability of only triggering the light source when a particular roller is over in the window. (For inner race viewing this infers the capability of only triggering when the window is at a certain orientation).

(c) Synchronisation of the flash with the camera shutter, such that a single triggering pulse is produced when the camera shutter is open and an appropriate roller is over the window.

(d) When desired to limit the flash repetition rate.

(e) Amplify the signal from the magnetic transducer in order to trigger the digital counter at low speeds.

(f) Provide the power required to drive the 'Skanners' and integrated circuits.

Figure 4.8 illustrates a logic diagram of the electronic set up and displays the signal shapes at various points of the circuit. The complete circuit diagram is shown in figure 4.9.

The power supply gives a stabilized supply of $\pm$ 12V. to the operational amplifiers, + 12V. to the integrated circuit timers and + 24V. to supply the 'Skanner' phototransistors and reference voltages. The 'Skanner' 5V. lamps are supplied directly from the rectifier through dropping resistors. The operational amplifiers are connected to operate as level detectors. When the reference level is connected to the negative input, the output swings from - 12V. to + 12V. as soon as the signal exceeds the

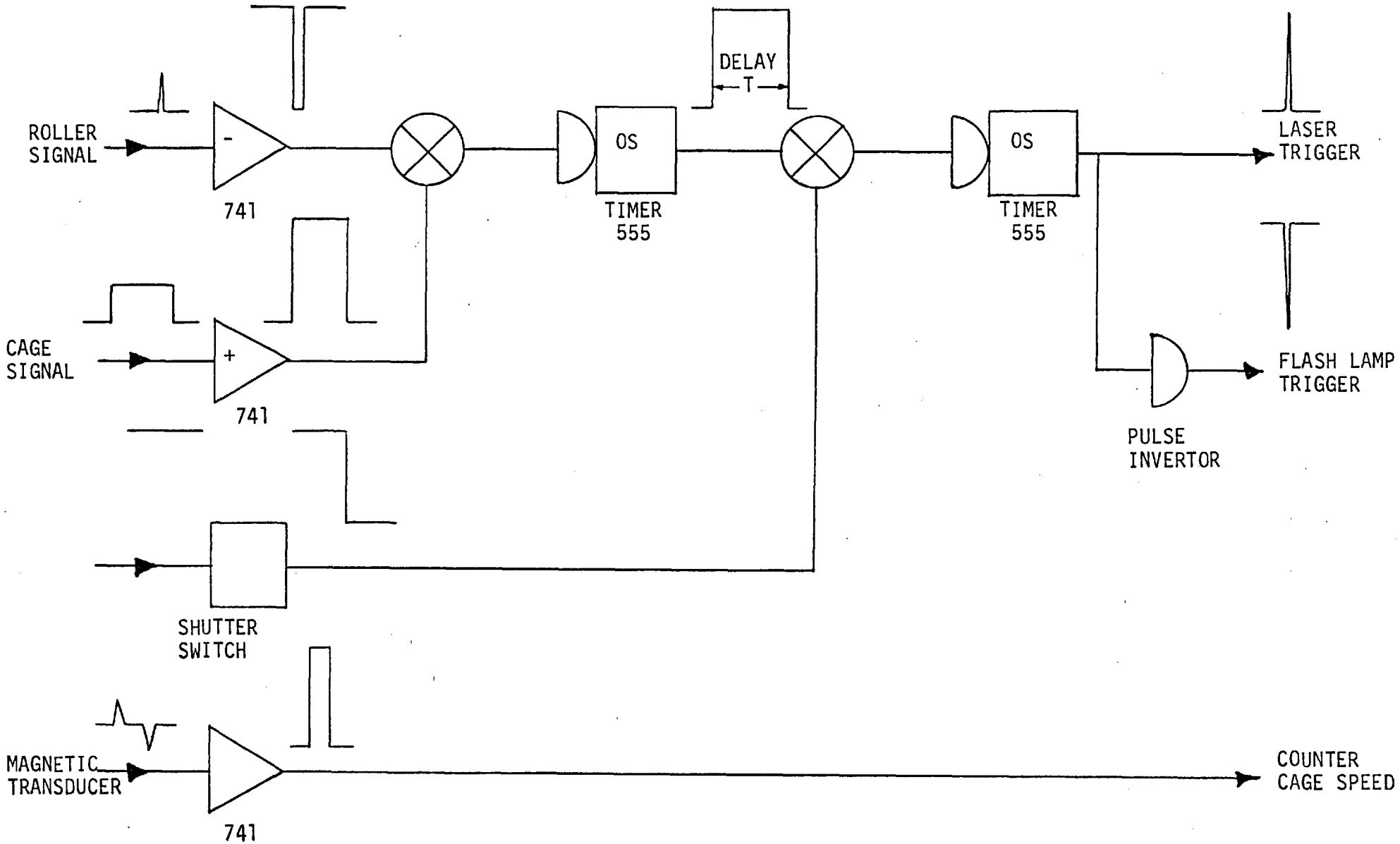

Figure 4.8 Logic diagram of the unit for flash synchronisation.

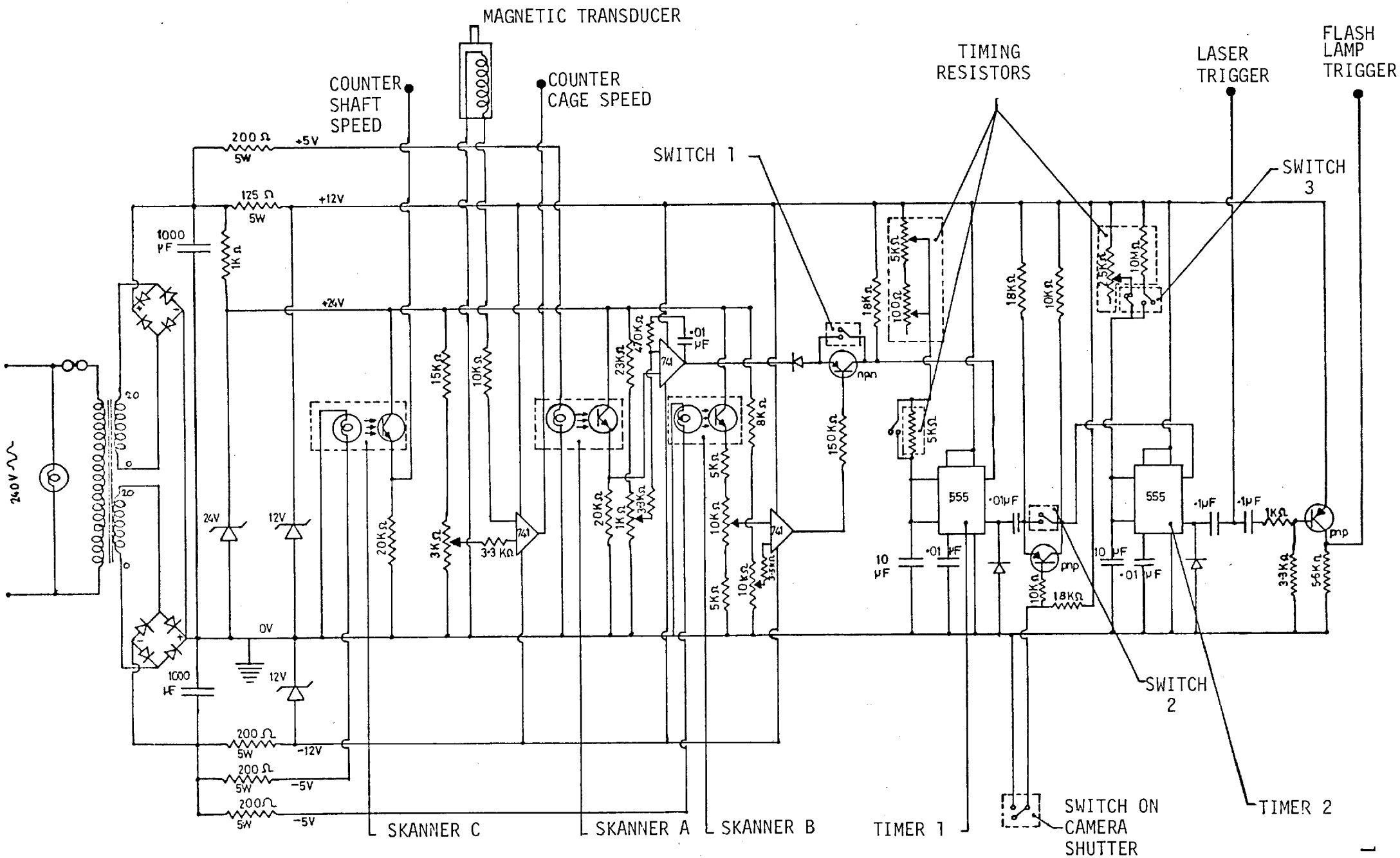

Figure 4.9 Circuit diagram of the unit for flash synchronisation.

reference level, or vice-versa if the reference is connected to the positive input. The timers are connected to operate on a one shot (monostable) basis.

Two timers are used and connected in series, the first of which controls the flash time delay. A linear ten turn 5k. ohm potentiometer provides a coarse control, giving a delay range adjustable from 0 to 55 milli-seconds The linear ten turn 100 ohm potentiometer acts as a fine delay control, one turn of which alters the delay by 110 μ seconds. The additional 5k. ohm resistor can be switched in to add a further 55 milli-seconds delay. The second timer controls the maximum flash repetition rate, and is used when photographing to produce a single trigger pulse and then block all following pulses.

The passage of a needle under the field of view of 'Skanner' A causes the application of a positive pulse to the negative input of the amplifier, and when the reference level (this is adjustable) is exceeded, the output swings from + 12V. to - 12V. If the mechanical switch 1 is closed, this negative going signal triggers the first timer. If the mechanical switch is open, this signal can only reach the timer input if the transistor is conducting. This will be the case only when 'Skanner' B is detecting the cage mark, during which time a positive signal is applied to the transistor base.

As soon as the timer is triggered, the output swings from 0 to + 12V. At the end of the timing period the

output drops back to zero V., and if the mechanical switch 2 is closed, this negative going signal triggers the second timer. If this switch is opened, the signal can only pass when the transistor is conducting. This only occurs when the camera shutter is open. As soon as this second timer is triggered the output rises to + 12V., and remains up during the timing period set by the timing resistance. While the output is high the timer cannot be re-triggered.

For normal stroboscopic application, the 25k. ohm variable resistor is connected and controls the maximum flash repetition rate, which can be limited to 4 flashes per second. At all times it is necessary to set this resistor, such that the timing period of the second timer is larger than that of the first. This is necessary to prevent voltage spikes, induced by the firing of the lamp or laser, re-triggering the firing circuit and producing unstable operation.

For the purpose of photography, switch 2 is opened and the 10 mega-ohm timing resistor connected by switch 3 (switch 3 is double pole and connected so that this action disconnects the 25k. ohm resistor). When the camera shutter is opened, timer 2 is triggered by the next pulse from timer 1. Any further pulses are then blocked for a period of two minutes, unless the timer is reset by switching back to the smaller 25k. ohm resistor. The positive edge of the output pulse from timer 2, produces a 12V. positive spike upon passing through the capacitor. This spike is used to trigger

the laser. The second timer does not therefore increase the firing delay. The flash lamp is triggered by inverting this pulse, and so producing a negative going spike (12V to zero V.).

4.4 The Complete Arrangement

The complete experimental arrangement, and layout of all the associated equipment is shown in figure 4.10. The position of the speed control and the delay control is such that they can be adjusted simultaneously, enabling the contact to be continuously held in the centre of the field of view.

4.5 Experimental Procedure

4.5.1 Setting Up the Rig.

The following procedure was adopted for assembly, and setting up the rig for outer race viewing:

(a) Thoroughly clean the test bearing components and insert the appropriate rollers.

(b) Position the outer race, align the viewing slot with the slot in the race housing, and clamp in position with the end cover.

(c) Position the shaft assembly within the main housing and slide the test bearing inner race and rollers into the outer race.

Figure 4.10 Complete experimental arrangement.

(d) Align the microscope with the rig.

(e) Apply a small load, bring a roller over the window and focus the microscope on the fringes.

(f) Adjust the incident illuminator and position of the lamp to obtain maximum illumination intensity.

(g) Close the aperture stop to obtain the desired intensity.

(h) Adjust the fully-reflecting mirror to give an even number of fringes either side of the contact, and so that the fringes are in focus along the length of the contact.

(i) If the laser is to be used, position the small mirror and diffraction grating to give a clear fringe system at the chosen wavelength.

(j) Position the television camera.

(k) With the lamp or laser firing at a moderate rate, adjust the beam current and target voltage to obtain optimum contrast.

(l) Focus the picture by moving the vidicon tube within the camera.

(m) Adjust the position of the needle detecting 'Skanner' relative to the centre of the window, to allow synchronisation at maximum speed, and place so as to obtain maximum signal.

(n) Flush the test bearing with filtered oil for several minutes before running.

4.5.2 Test Procedure.

The following test procedure was adopted for film thickness measurement:

(a) Set the thermostat for the desired oil temperature, or switch on the oil cooler. Run oil through the bearings for several minutes before start up to allow the temperature to stabilize.

(b) Apply the load.

(c) Bring the roller selected for photography over the window and photograph.

(d) Adjust the oil flow to the test bearing.

(e) Set the delay to maximum and start the tape.

(f) Start the rig and adjust the speed to synchronise the flash. Record the fringe order or colour, speeds and temperatures. Photograph the contact.

(g) Increase the speed, while decreasing the delay, until the next fringe order or colour is observed. Record the conditions and photograph.

(h) Repeat (g) until the maximum speed of the rig is reached.

As the speed is increased, viewing is aided by switching the delay unit to trigger only when the selected roller is over the window. Near maximum speed, the flash frequency must be limited. When the run is complete the tape can be replayed for a detailed examination of the state of lubrication at each step.

CHAPTER V

FILM THICKNESS MEASUREMENTS

5.1 Preliminary Experimental Work

5.1.1 Colour Calibration for White Light.

Chromic oxide is a dielectric coating and it is therefore possible, when using monochromatic light, to calculate directly the film thickness corresponding to each fringe position. However no colour calibration for this type of coating had previously been conducted.

The calibration procedure was similar to that used by Wymer (80). The curved side of a 60 ft. radius plano-convex glass lens had been sputtered with chromic oxide at the same time as the sapphire track surface. The lens was placed in a loading collar (the weight of the collar provided the load of about 5lbs.), and the curved surface rested against an optically polished steel flat. The gap between the glass and steel was filled with a small quantity of oil. Figure 5.1 shows the calibration set up. Owing to the large radius of curvature of the lens, the fringe system could be viewed by eye, and was photographed using a 35 mm. camera fitted with a 135 mm. lens on a bellows attachment. The xenon flash lamp was used as the light source.

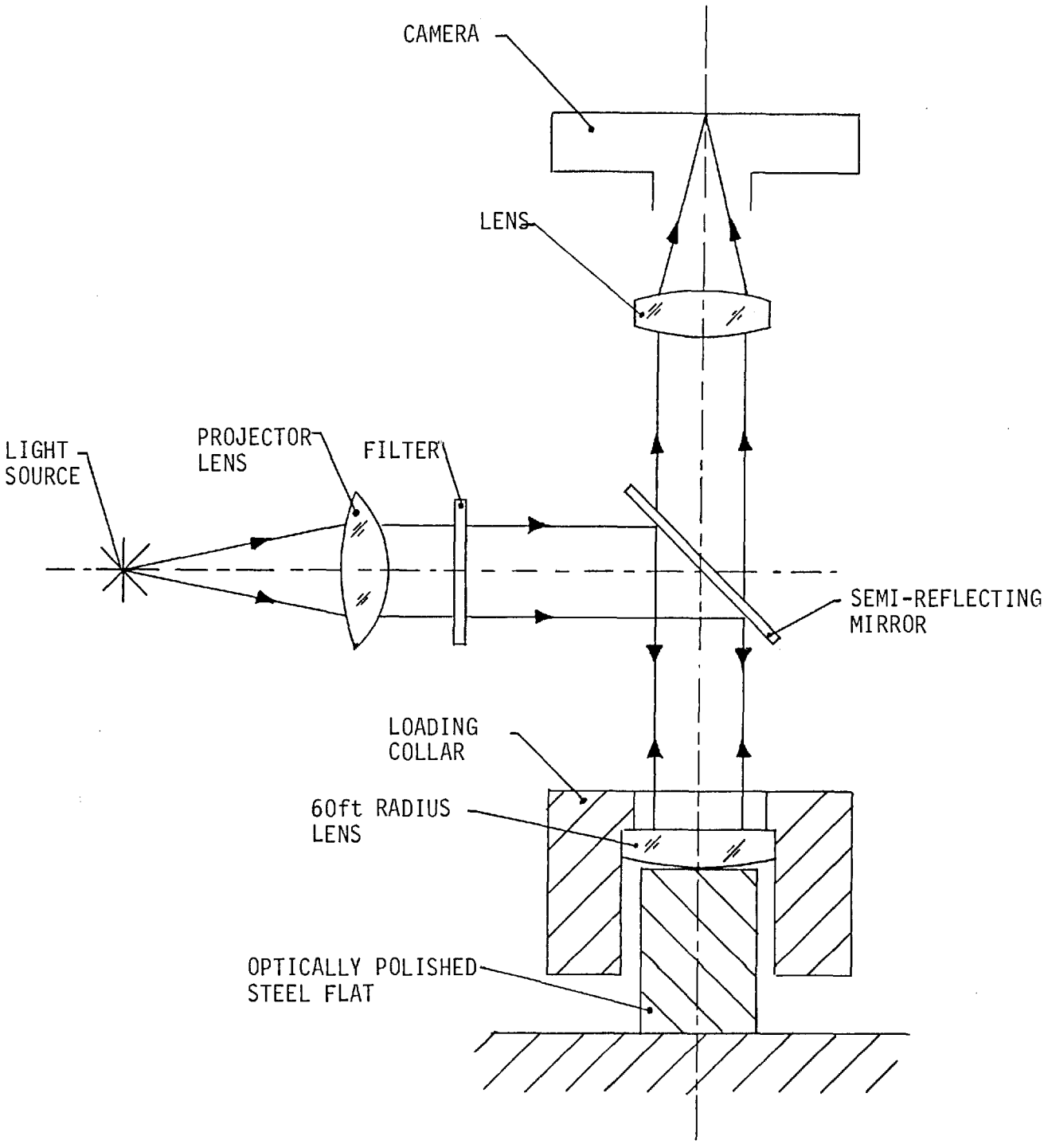

Figure 5.1 Arrangement for the white light calibration.

The white light interference patterns were photographed using Kodak high speed Extachrome film, developed in a identical manner to that used in the actual tests. In order that the gap shape could be determined a narrow band interference filter was placed in front of the lamp,and the monochromatic interference fringes photographed. Figure 5.2 shows a photograph obtained in this manner. These two photographs represented an identical situation, as it was only necessary to place a filter in the system. The photographs were then projected onto polar graph paper, such that the centre of the contact corresponded with the centre of the paper. The photographs were arranged to be coincident by noting the position of two marks on the loading collar. The fringe radii for the monochromatic and the coloured systems were noted for 8 different angles, and the means taken. The gap shape was calculated from equation 3.13 and thus the optical thickness,corresponding to the position of each coloured band,could be directly determined. The results are shown in figure 5.3. The only errors are those produced during measurement of fringe radii,and extrapolation between the monochromatic fringe positions. It is estimated that the calibrated fringes provide the correct optical thickness to within about 6% for the centre of the first yellow band,and about 2% for the centre of the 4th green band.

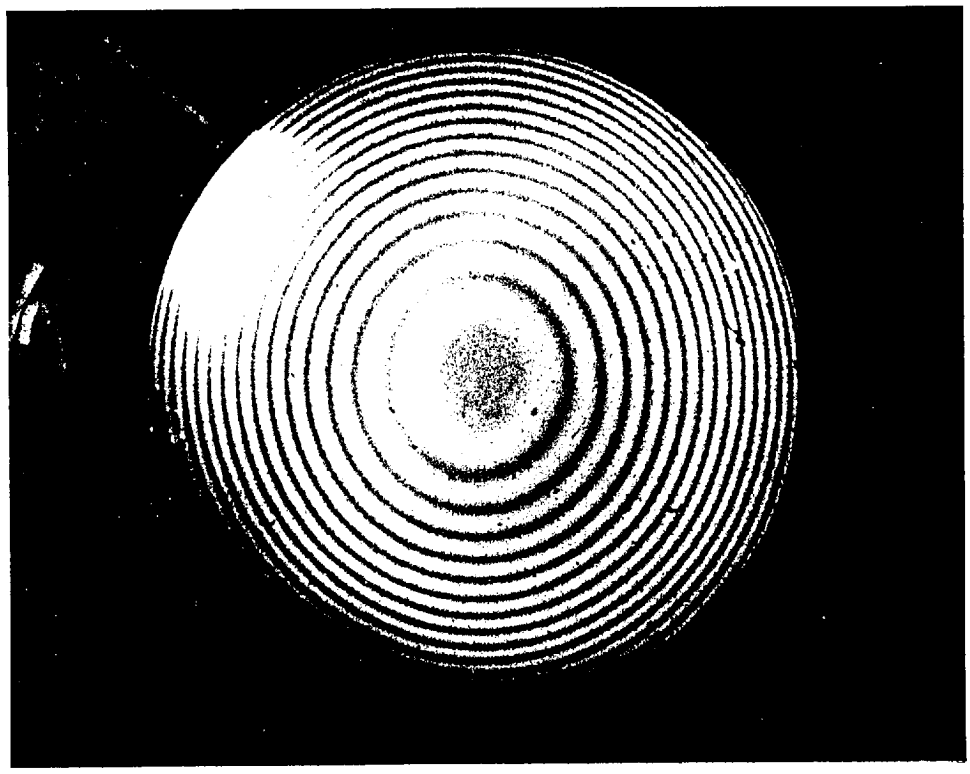

Figure 5.2 Monochromatic fringes that illustrate the gap shape for the white light calibration.

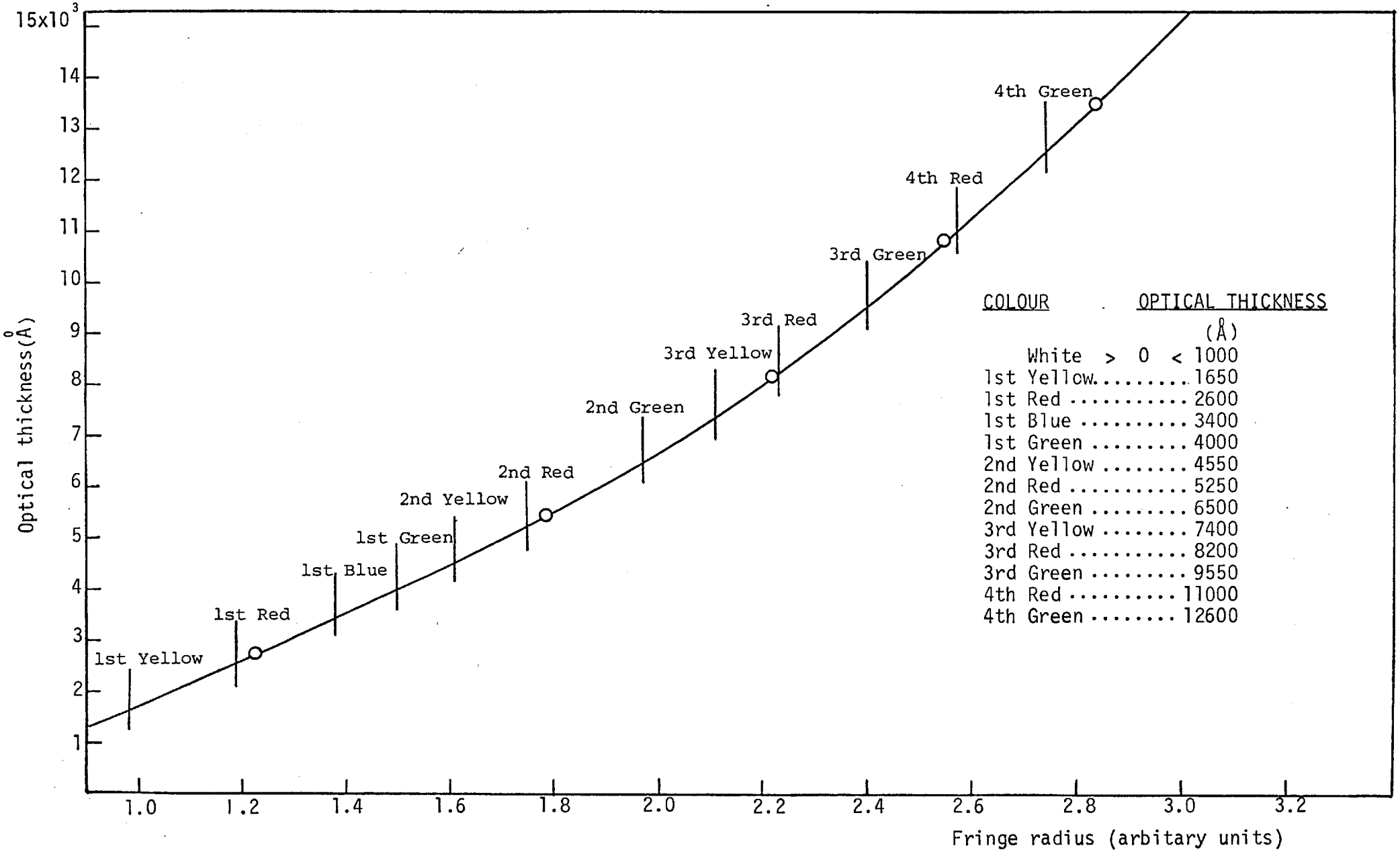

Figure 5.3 Results of the white light calibration.

5.1.2. Measurement of Lubricant Properties.

Two lubricants were used for the basic film thickness measurements. Lubricant 1, designated Shell A, was a high viscosity index mineral oil as used in reference (64), and known to exhibit Newtonian behaviour. Lubricant 2, designated Mobil B, was a mineral oil containing a commercial phosphorus/sulphur additive package.

To evaluate the film thickness measurements, it was necessary to know the viscosities, densities, and refractive indices of the lubricants, and their variation with temperature and pressure. Viscosity and density data for Lubricant 1 was given by the suppliers. Values of refractive index and the pressure-viscosity coefficient (measured in a rolling contact rig) for this oil, are given by Wymer (80). No data was available for Lubricant 2 and direct measurements were made.

Viscosity was measured at several temperatures using a suspended level viscometer, enclosed in a temperature controlled bath. Density was measured with a specific gravity bottle, and refractive index with an Abbé refractormeter that could be temperature controlled.

The pressure-viscosity coefficient (α) of Lubricant 2 was determined by a method similar to that used by Foord et al. (66). Lubricant 1, of known α value, was used as a reference fluid. The two oils were run in a small point contact rig, and central film thickness measured as a function of speed at constant load. The results were then plotted in

dimensionless terms. At any value of the speed parameter U*, the separation of the lines is entirely dependent upon the difference in α values of the two oils. Westlake (75) has found HO* to be proportional to $\alpha^{\cdot 55}$. Therefore the α value of the test oil can be related to that of the reference fluid, by the following relation:

$$\alpha = \alpha_{ref} \left[\frac{ho}{(ho)_{ref}}\right]^{1\cdot 8}$$

Values of the lubricant properties are given in Appendix 3.

5.2 Determination of Dimensionless Parameters

To obtain correlation with other experimental and theoretical studies, the results were expressed in terms of the non-dimensional parameters as used by Dowson and Higginson (30).

5.2.1 Film Thickness Parameter.

This is defined as:

$$H^* = \frac{h}{R}$$

To determine the absolute film thickness h, the measured optical film thickness must be divided by the refractive index of the oil within the contact. The refractive index at the oil inlet temperature (for pure

rolling the temperature rise within the contact is small (90)) was corrected for pressure assuming a Hertzian pressure distribution. The following procedure was used: the variation of refractive index with density was found from the Lorenz-Lorentz (174) relation.

$$\frac{1}{\rho}\left(\frac{n^2 - 1}{n^2 + 2}\right) = \text{constant}$$

The refractive index n_0, and density ρ_0, at atmospheric pressure are known, therefore:

$$n = \left(\frac{1 + 2A}{1 - A}\right)^{\frac{1}{2}}$$

where:

$$A = \frac{\rho}{\rho_0}\left(\frac{n_0^2 - 1}{n_0^2 + 2}\right)$$

This relation predicts refractive indices within about 1.5% of measured values (175) at pressures between 0 and 200,000 p.s.i.

The density ratio was obtained from Hartung's empirical formula for hydrocarbons (see Chu and Cameron (176)):

$$\frac{\rho}{\rho_0} = 1 + \frac{42.8 \times 10^{-6} \times p^{.75}}{(\nu_{100})^{.0385}}$$

where ν_{100} is the viscosity in centi-Stokes at 100°F. and p is the pressure in pounds per square inch. This

expression has been shown to predict densities within 2% of experimental values (177). The error involved in obtaining the actual film thickness, using these expressions refractive index, is therefore about 3%.

R is the reduced radius of the contact, and is used to represent the contact geometry as mathematically equivalent to that of a cylinder of radius R, near a plane. For an outer race contact, the reduced radius is defined by the relation:

$$R = \frac{R_0 r}{R_0 - r}$$

The value of R was calculated from the bearing dimensions given in Appendix I.

5.2.2 Materials Parameter.

This is defined as:

$$G^* = \alpha E'$$

E' is the reduced elastic modulus, and represents the elastic properties of the equivalent cylinder near a rigid plane. It is defined by the relation:

$$\frac{1}{E'} = \frac{1}{2}\left[\frac{1-\sigma_1^2}{E_1} + \frac{1-\sigma_2^2}{E_2}\right]$$

In this case the material combination is sapphire and steel, the elastic properties of which are given in Appendix 2.

The values used for the pressure-viscosity coefficients of the two oils are given in Appendix 3.

5.2.3 Speed Parameter.

This is defined as:

$$U^* = \frac{U\eta_0}{E'R}$$

U is the mean of the surface velocities relative to the contact. In all tests the cage speed was epicylic and it was therefore assumed that, in the loaded region of the bearing, no slip was occurring at either the outer or inner race contacts. For the outer race contacts the mean velocity is given by:

$$U = R_0 \omega_c$$

or

$$U = \frac{\omega_c (Ri + 2r)}{2 (1 + r/Ri)}$$

The dynamic viscosity of the oil at the inlet temperature η_0, is difficult to access accurately, as the temperature within the actual contact inlets could not be directly measured. Thermocouples were used to measure the jet temperature, and the temperature of the sapphire surface at the edge of the track. In one instance, at the top of

the speed range, these readings differed by as much as $10^{o}C$, which corresponds to a 60% variation in viscosity at those particular conditions. The kinematic viscosity at both temperatures, was computed from the Walter-ASTM formula (given in ref. (178)) which can be expressed as follows:

$$\log \log (\nu + 0.6) = K - C \log T \quad \ldots\ldots 5.1$$

where ν is the viscosity in centi-Stokes, T is the absolute temperature in degrees Kelvin and K and C are constants. The constants were evaluated by substitution of two known viscosities ν_1 and ν_2 at temperatures T_1 and T_2 (see Appendix 3) into the following equations:

$$C = \frac{\log \log (\nu_1 + 0.6) - \log \log (\nu_2 + 0.6)}{\log T_2 - \log T_1}$$

$$K = \tfrac{1}{2} \left[\log \log(\nu_1+0.6) + \log \log(\nu_2+0.6) + C(\log T_1+\log T_2) \right]$$

This formula was found to give adequately accurate predictions of the viscosity-temperature characteristic. The dynamic viscosity η_0, expressed in Imperial units (Reynolds), was found by multiplying the kinematic viscosity ν (centi-Stokes) by the specific gravity (corrected for temperature) and a conversion factor of 1.4503×10^{-7}.

For each test result, two values of the speed parameter were computed corresponding to the two temperature readings.

5.2.4 Load Parameter.

This is defined as:

$$W^* = \frac{W}{LE'R}$$

The roller load could have been indirectly estimated from the knowledge of the load applied to the shaft (measured by the calibrated load cells), and of the load distribution around the test bearing (see section 3.4.6). However any variation in roller size would produce a large change in the load distribution, and it was considered to be far more accurate to calculate the load per unit length of the contact, at the particular point under the microscope field of view, by measuring the static contact width and using Hertz (8) theory. This states that:

$$\frac{W}{L} = \frac{b^2 \pi E'}{8R}$$

Although this theory can only be rigorously applied to the case of perfectly smooth surfaces, Greenwood and Tripp (179) have shown that, for real surfaces, the departure from the Hertzian pressure distribution will only be small at high loads. The surfaces in question are polished to a surface finish of 1 μ in. c.l.a., and are under relatively high load. It is estimated that the error in calculating the load in this manner is not more than 5%.

The contact width was measured in the following manner: load was applied to the shaft and the particular

roller selected for viewing, positioned over the window. A photograph was taken of the contact and projected onto a large piece of graph paper, and the width of the projected image marked. To determine the magnification, a photograph was taken under identical conditions of a graticule ruled with 100 lines per millimetre, and this was projected onto the graph paper in exactly the same manner.

5.3 Experimental Results

Results were computed for five of the film thickness tests.

Two test runs, A and B, were conducted with a jet feed of lubricant 2, and a test bearing load of 875 lbs. The oil flow rate of 9 gallons per hour was sufficient to immerse completely the lowest roller in the bearing. High speed black and white photographs of the interferograms were taken of test A, using the laser as the light source. A series of these photographs, that illustrate the film building up as the speed increases, are shown in figure 5.4. Test B was carried out under similar conditions using the xenon flash lamp as the light source. Six of the photographs taken during this run are presented in figure 5.5, five of these clearly illustrate the position of the inlet boundary.

TEST A, Pmax = 149,400 p.s.i., Laser (λ = 4950 Å)

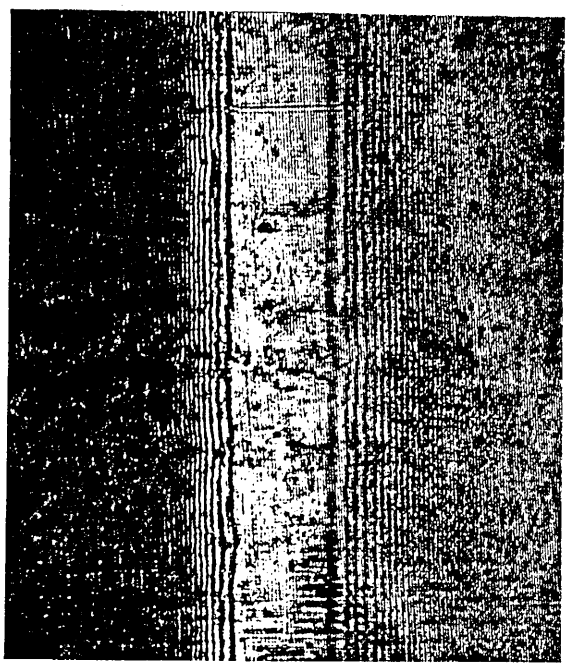

(a) 91 R.P.M.
h_0 = 9.0 μ in. (2nd bright fringe)
h_1 = 6.1 μ in. (1st dark fringe)

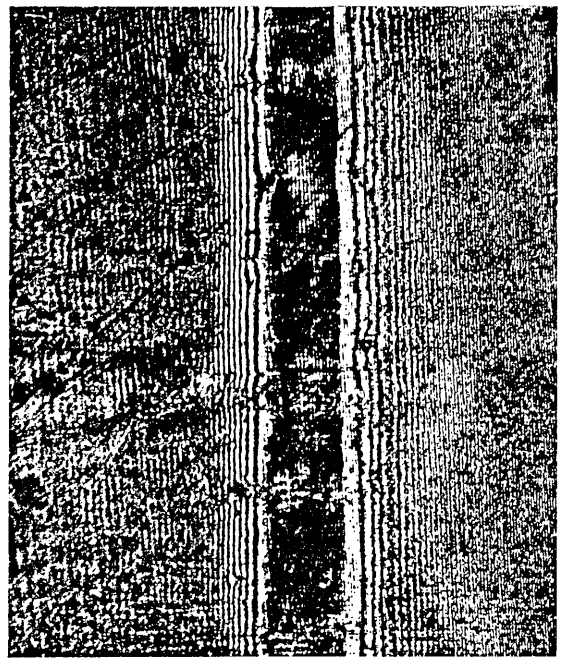

(b) 162 R.P.M.
h_0 = 12.0 μ in. (2nd dark fringe)
h_1 = 9.1 μ in. (2nd bright fringe)

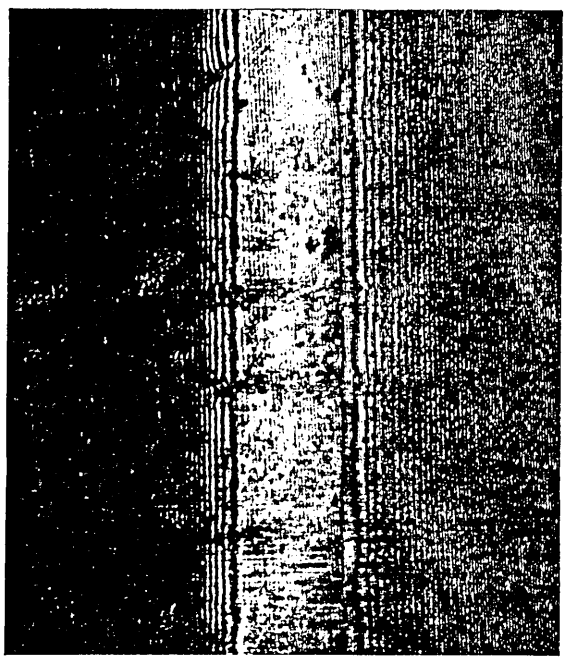

(c) 233 R.P.M.
h_0 = 13.5 μ in. (3rd bright/
2nd dark fringe)
h_1 = 10.6 μ in. (2nd bright/
2nd dark fringe)

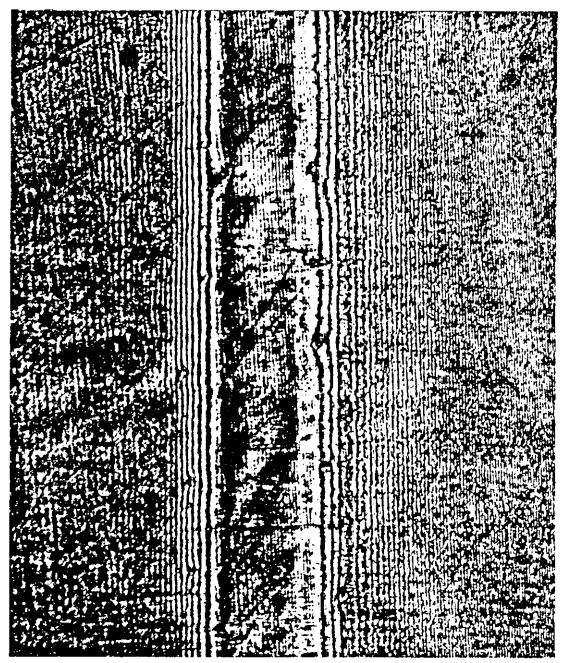

(d) 331 R.P.M.
h_0 = 16.6 μ in. (3rd dark/
3rd bright fringe)
h_1 = 13.7 μ in. (2nd dark/
3rd bright fringe)

Figure 5.4 Photomicrographs, taken under laser illumination, illustrating film build-up in Test A.

Jet feed lubricant 2, Hertz width (static) = 0.008 in.

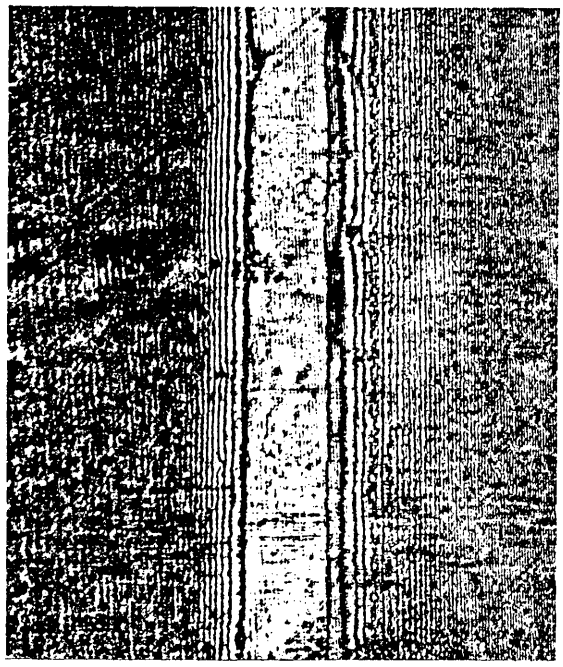

(e) 503 R.P.M.
h_0 = 21.1 μ in. (4th bright fringe)
h_1 = 15.2 μ in. (3rd bright fringe)

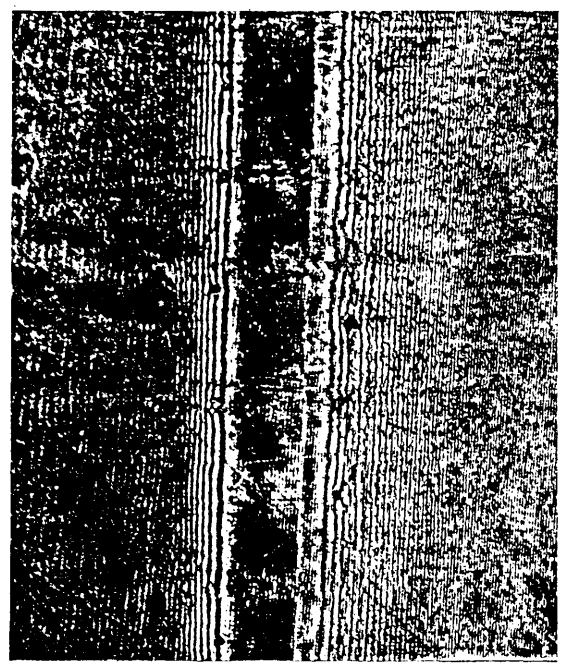

(f) 643 R.P.M.
h_0 = 24.1 μ in. (4th dark fringe)
h_1 = 18.3 μ in. (3rd dark fringe)

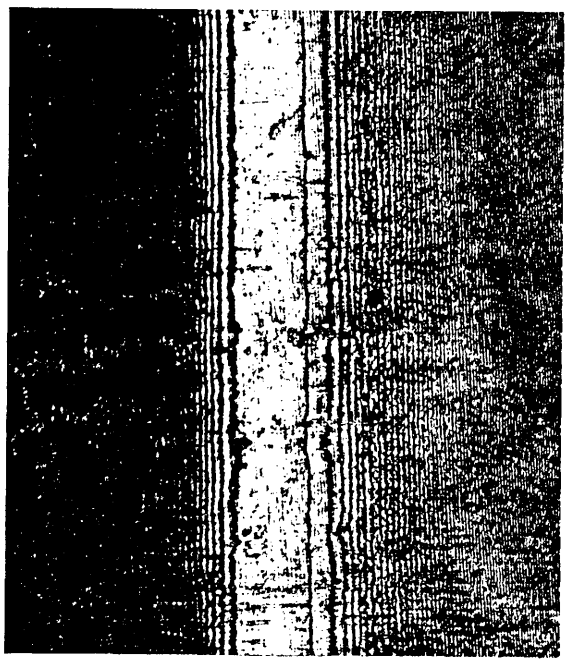

(g) 1105 R.P.M.
h_0 = 27.2 μ in. (5th bright fringe)
h_1 = 21.3 μ in. (4th bright fringe)

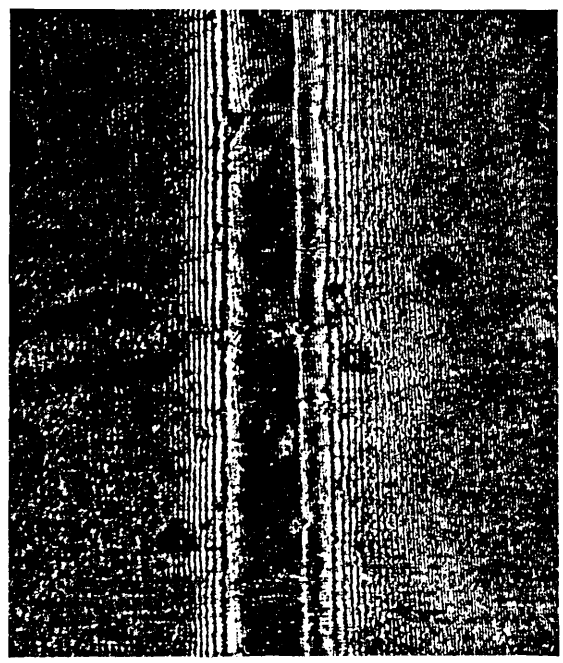

(h) 2155 R.P.M.
h_0 = 30.2 μ in. (5th dark fringe)
h_1 = 24.4 μ in. (4th dark fringe)

Figure 5.4

TEST B, Pmax = 149,400 p.s.i., flash lamp (λ = 5460 Å)

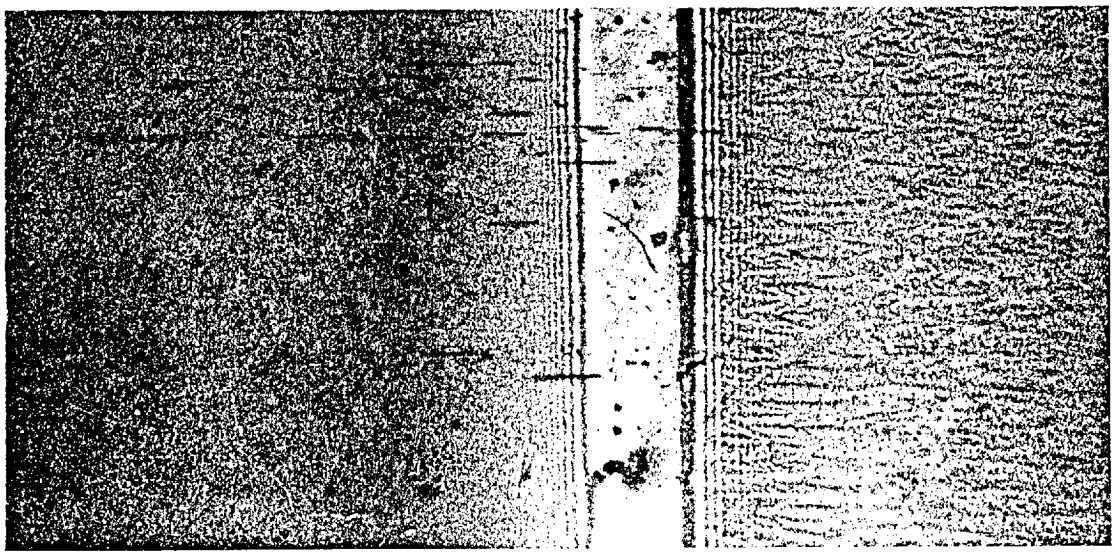

(a) 216 R.P.M., h_0 = 16.6 μ in. (3rd bright fringe)
h_1 = 13.4 μ in. (2nd dark fringe)

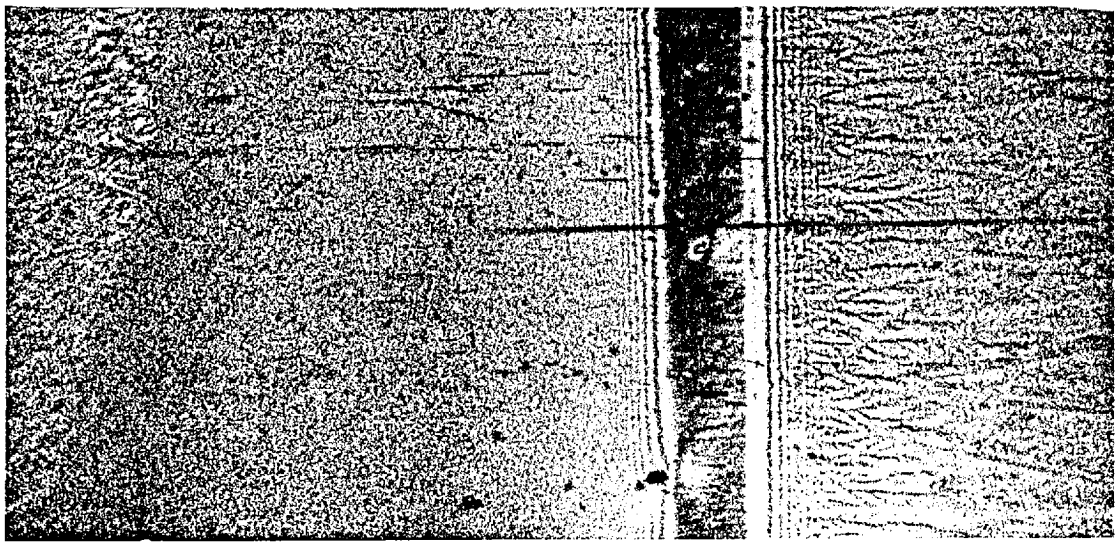

(b) 305 R.P.M., h_0 = 19.9 μ in. (3rd dark fringe)
h_1 = 15.1 μ in. (3rd bright/2nd dark fringe)

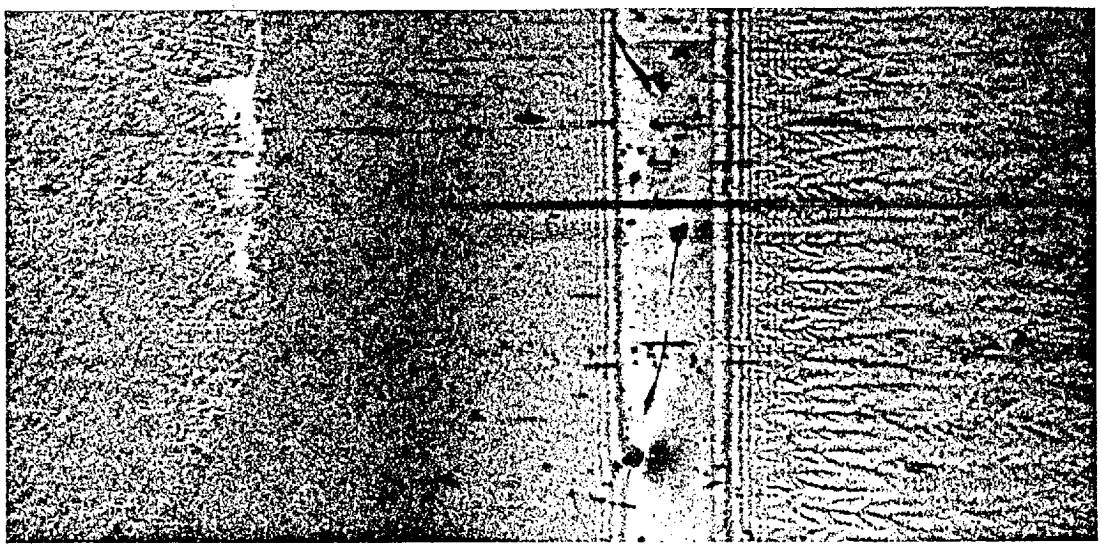

(c) 405 R.P.M., h_0 = 23.2 μ in. (4th bright fringe)
h_1 = 16.7 μ in. (3rd bright fringe)

Figure 5.5 Photomicrographs, taken under flash lamp illumination, during test B.

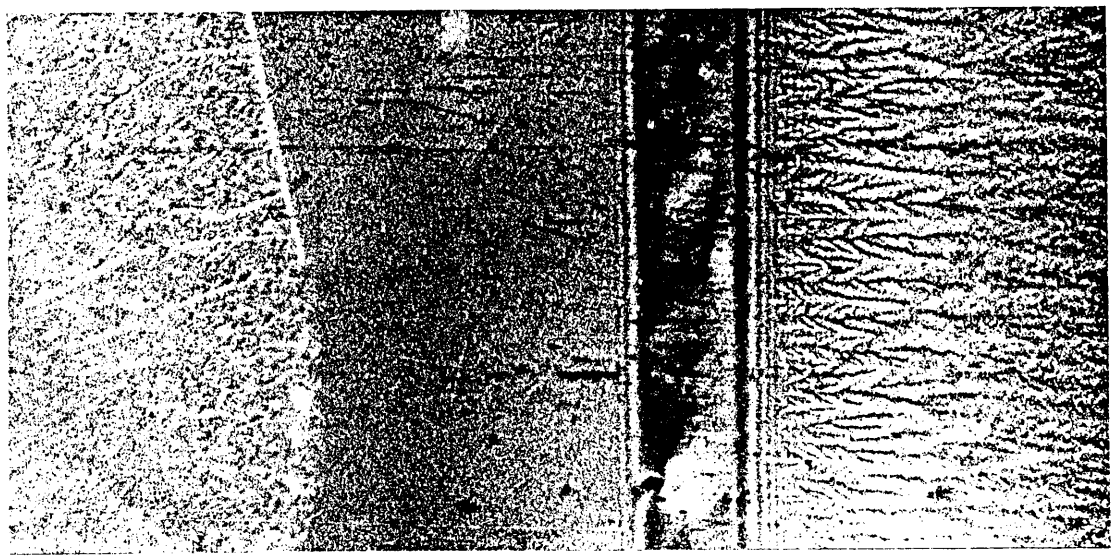

(d) 532 R.P.M., h_0 = 26.5 μ in. (4th dark fringe)
h_1 = 20.1 μ in. (3rd dark fringe)

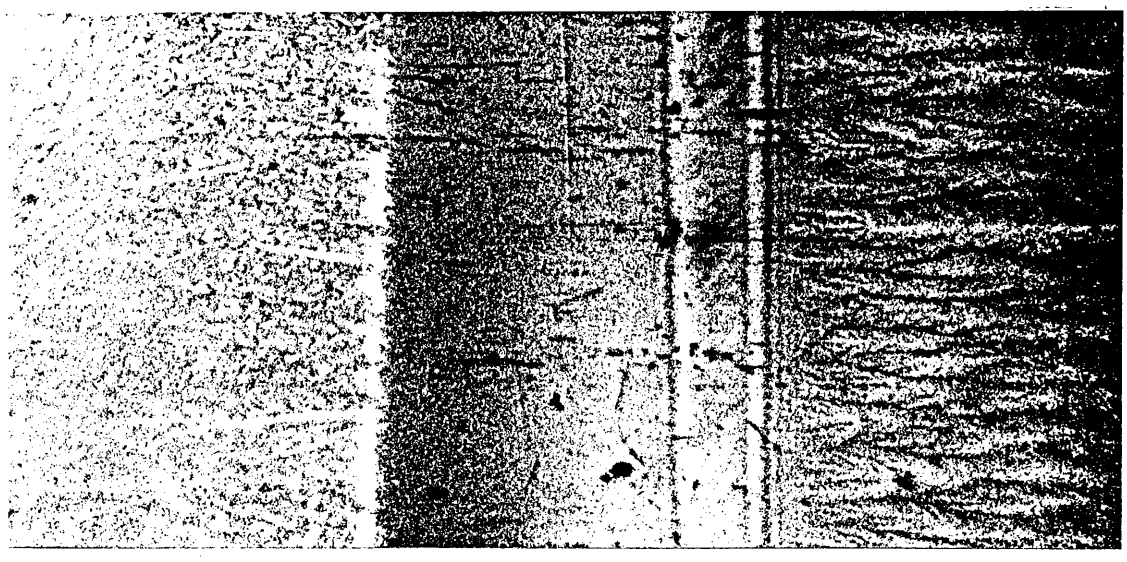

(e) 743 R.P.M., h_0 = 29.9 μ in. (5th bright fringe)
h_1 = 23.5 μ in. (4th bright fringe)

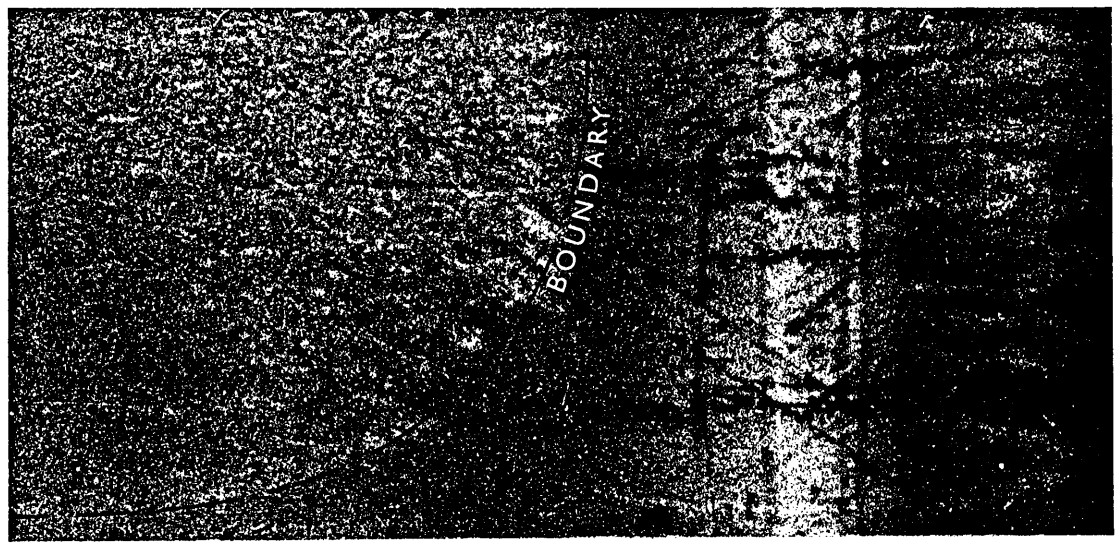

(f) 1542 R.P.M., h_0 = 30.0 μ in. (5th bright fringe)
h_1 = 23.5 μ in. (4th bright fringe)

Figure 5.5

Test C was conducted with a jet feed of lubricant 1, and a test bearing load of 875 lbs. The oil flow rate of 5 gallons per hour was again sufficient to completely immerse the lowest roller in the bearing. Four of the photographs taken during this run, using the laser as the light source, are presented in figure 5.6. Test D was carried out with zero oil flow and a test bearing load of 875 lbs. A quantity of lubricant 1 (about.8 cubic in.), sufficient to cover the outer race track at the bottom of the bearing, was placed in the race housing. Three of the photographs, taken during this run using the flash lamp as the light source, are presented in figure 5.7. Test E was conducted under similar conditions to test C, but with a jet feed of 5 gallons per hour of lubricant 1, supplied at 50°C. This test was carried out in order to determine the variation of the pressure-viscosity coefficient α, with temperature.

The basic experimental film thickness results are plotted against shaft speed in figures 5.8, 5.12, 5.16, 5.20, and 5.24. Also shown in these figures is the variation of sapphire temperature, oil temperature and the inlet boundary distance (measured when visible). The inlet boundary distance, taken from the edge of the Hertz zone, was measured from the photographs in the same manner as used for obtaining the Hertz width (see section 5.2.4). In some cases it was measured directly from the television monitor. (The magnification was found by recording an image of the graticule,

TEST C, Pmax = 149,400 p.s.i., laser (λ = 5350 Å)
Jet feed lubricant 1, Hertz width (static)
= 0.008 in.

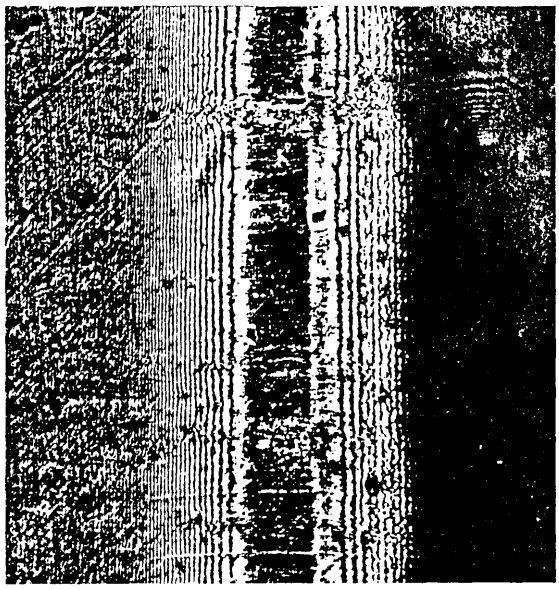

(a) 207 R.P.M.
h_0 = 26.0 μ in. (4th dark fringe)
h_1 = 19.7 μ in. (3rd dark fringe)

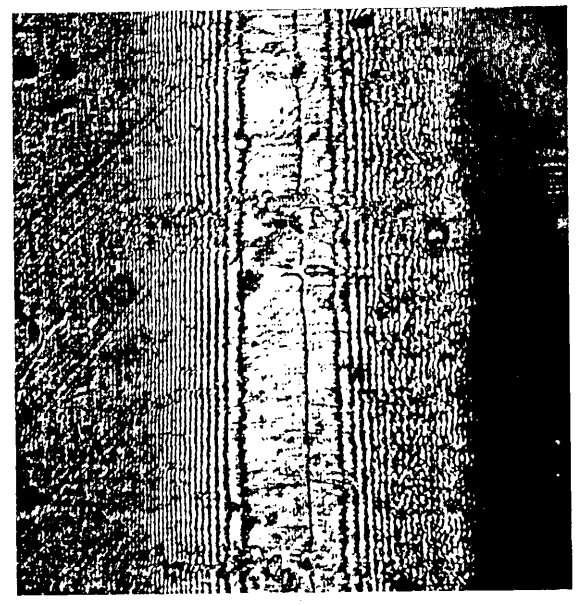

(b) 444 R.P.M.
h_0 = 35.8 μ in. (6th bright fringe)
h_1 = 29.7 μ in. (5th bright fringe)

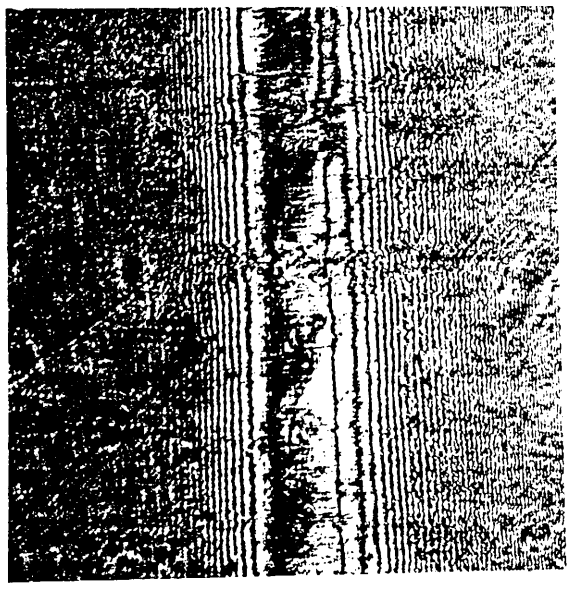

(c) 1678 R.P.M.
h_0 = 37.5 μ in. (6th dark/
6th bright fringe)
h_1 = 29.7 μ in. (5th bright fringe)

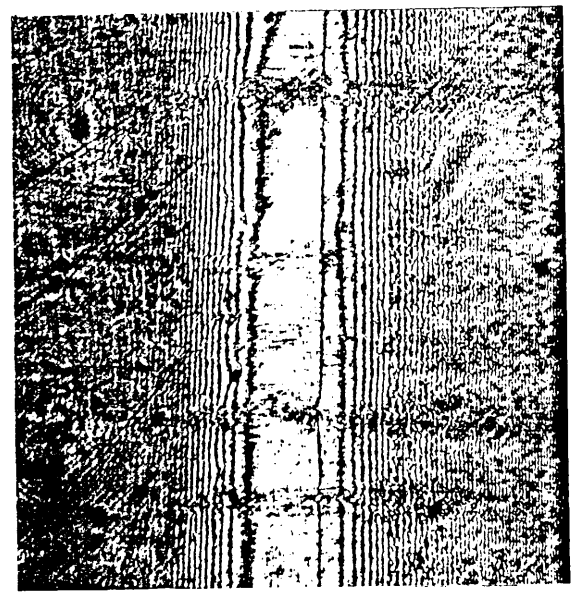

(d) 2022 R.P.M.
h_0 = 36.0 μ in. (6th bright fringe)
h_1 = 29.8 μ in. (5th bright fringe)

Figure 5.6 Photomicrographs, taken under laser illumination, during test C.

TEST D, Pmax = 149,400 p.s.i. flash lamp (λ = 5460 Å), lubricant 1, Hertz width (static) = 0.008 in.

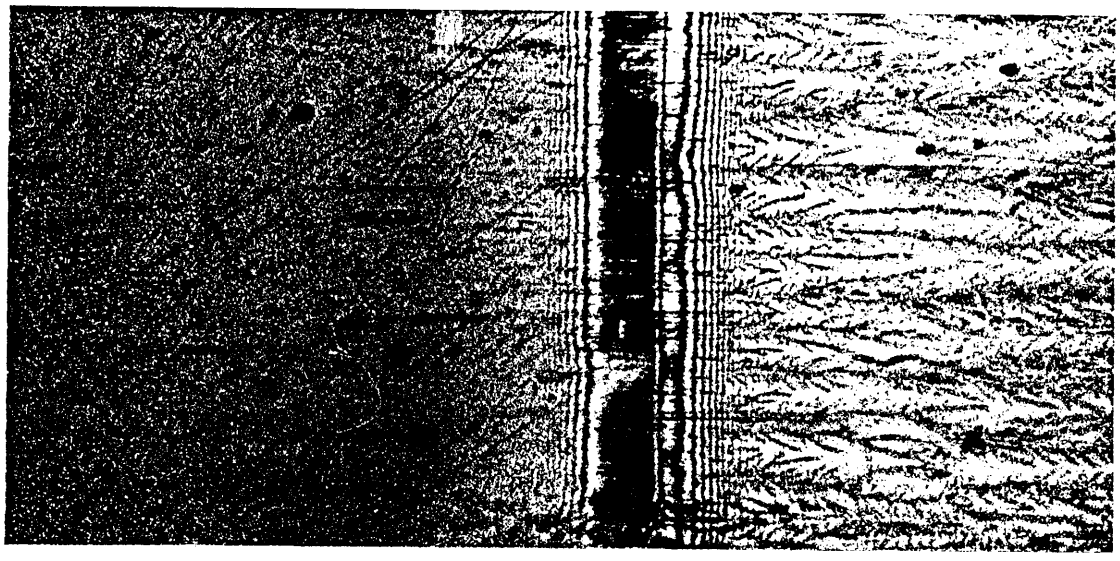

(a) 250 R.P.M., h_0 = 46.1 μ in. (7th dark fringe)
h_1 = 36.6 μ in. (6th bringe fringe)

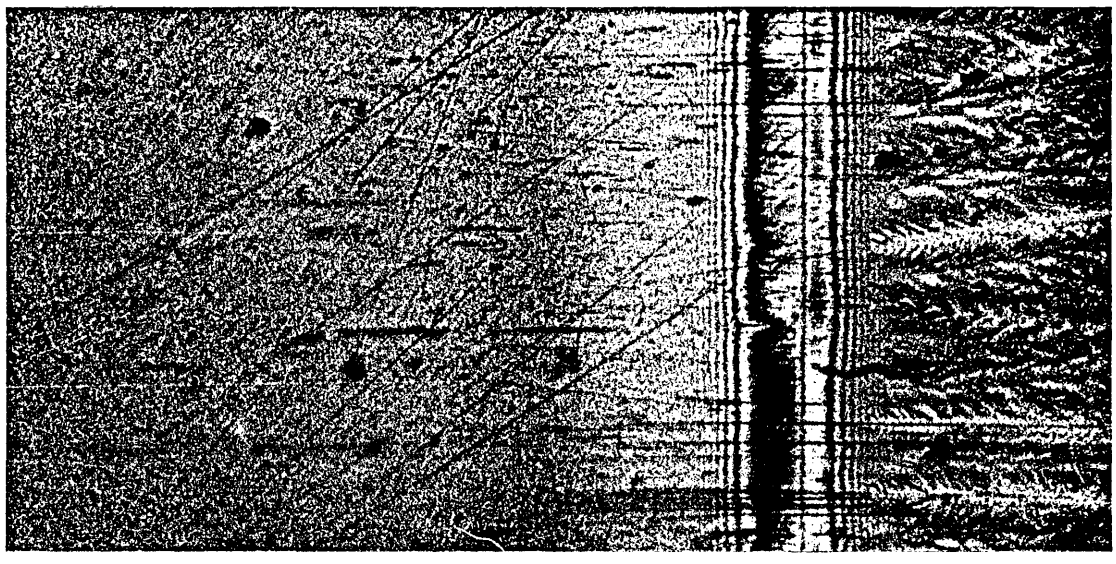

(b) 417 R.P.M., h_0 = 52.8 μ in. (8th dark fringe)
h_1 = 41.6 μ in. (6th dark/7th bright fringe)

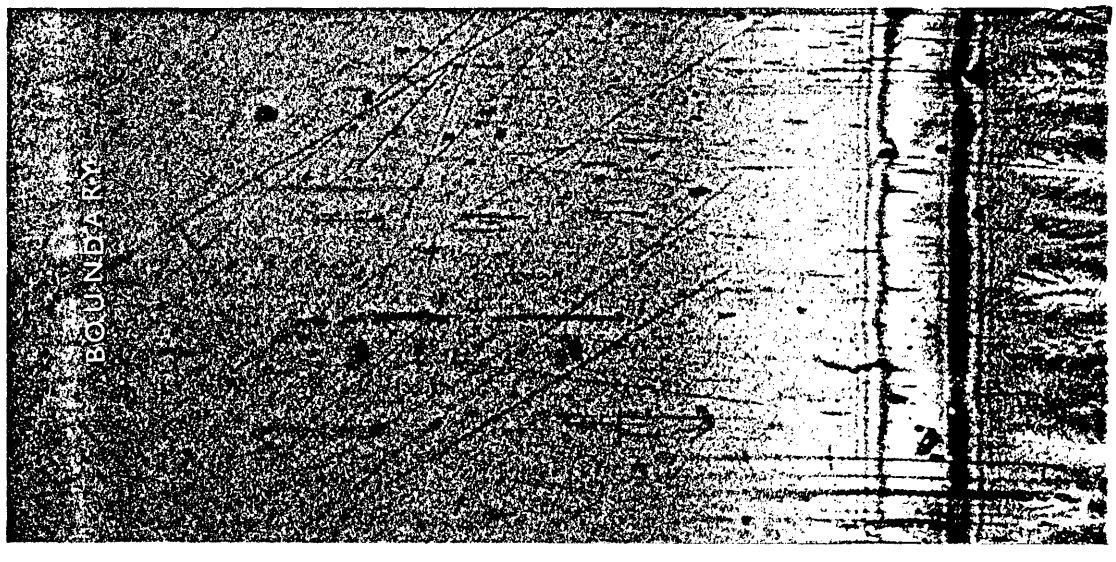

(c) 532 R.P.M., h_0 = 49.5 μ in. (8th bright fringe)
h_1 = 40.0 μ in. (6th dark fringe)

Figure 5.7 Photomicrographs, taken under flash lamp illumination, during test D.

ruled with 100 lines per millimeter). As the position of the inlet is sometimes highly erratic, the inlet distance was measured for several revolutions, at a particular shaft speed, and the minimum value plotted.

The experimental results, expressed in terms of the dimensionless parameters H* and U*, are plotted in figures 5.9, 5.13, 5.17, 5.21, and 5.25. The value of the viscosity η_0, used to calculate the parameter U*, was determined at the temperature measured by the thermocouple positioned on the edge of the sapphire surface. For the purpose of comparison, values of U*, based on viscosities calculated at the jet temperature, have also been plotted in figure 5.17.

5.4 Comparison with Other Experimental and Theoretical Studies

5.4.1 Comparison with Isothermal solutions.

Lines representing Wymer's (81) empirical solutions for H_0* and H_1*, equations 2.9 and 2.10; the Grubin (22) solution for H_1*, equation 2.7; and Dowson and Higginson's (30) theoretical solution for H_1*, equation 2.8, have been plotted for comparison with the experimental results in figures 5.9, 5.13, 5.17 and 5.21. These solutions were plotted assuming no variation of the pressure-viscosity coefficient α, with temperature.

5.4.2 Comparison with Thermal Solutions.

Film thickness predictions were also made using a thermal solution developed by Murch and Wilson (172). In this analysis a modified Reynold's equation, that takes into account the effects of viscous heating, is used in place of the conventional Reynold's equation, in a Grubin type analysis of the E.H.D. inlet zone. A viscosity model of the following form is used:

$$\eta = \eta_0 e^{\alpha p - \gamma (T - Ts)} \qquad \ldots\ldots\ldots \quad 5.2$$

where: η is the viscosity at temperature T and pressure p.

η_0 is the viscosity at zero pressure and surface temperature Ts.

γ is a temperature coefficient of viscosity.

The equation they obtained is expressed as follows:

$$\overline{H} = \overline{S}^{.73} \left(3.94 + \overline{L}^{.62}\right)^{-1} \qquad \ldots\ldots\ldots \quad 5.3$$

$\overline{H}$, $\overline{S}$ and $\overline{L}$ are non-dimensional parameters obtained as follows:

$$\overline{H} = \frac{\pi h_0 L E'}{4W} \qquad \text{Film thickness parameter.}$$

$$\overline{S} = \frac{.75 U \eta_0 \alpha b L^2 \pi^2 E'^2}{W^2} \qquad \text{Speed parameter.}$$

$$\overline{L} = \frac{U^2 \eta_0 \gamma}{k} \qquad \text{Thermal loading parameter.}$$

The thermal conductivity k of lubricant 1 is given in ref.(171) as 0.117 watt/m^{0}c. at 40^{0}C. No data on the thermal

conductivity of lubricant 2 was available and, as it is unlikely that there is a significant difference, the same value was used for both oils. The temperature coefficient of viscosity was calculated for each oil using equation 5.2, and the data given in Appendix 3.

When the thermal loading parameter $\bar{L} = 0$, equation 5.3 can be written as follows:

$$\bar{H} = 0.254\ \bar{S}^{.73} \qquad \ldots\ldots\ldots \quad 5.4$$

This relationship is equivalent to the usual isothermal Grubin result given by equation 2.7. In order that predictions of the minimum film thickness could be made from the Dowson and Higginson solution, taking into account the effects of viscous heating, the effective viscosity of the oil at entry η_0' was calculated from the Murch and Wilson approach. Values of η_0' were obtained by calculating from equation 5.4 the values of $\bar{S}'$ required to give the same film thickness as predicted by equation 5.3. The effective viscosity is then given by:

$$\eta_0' = \frac{\bar{S}'}{\bar{S}}\ \eta_0 \qquad \ldots\ldots\ldots \quad 5.5$$

Using the Dowson and Higginson solution, the minimum film thickness is influenced by viscosity according to equation 2.8 i.e.,

$$\frac{H^*{}_1'}{H^*_1} = \left(\frac{\eta_0'}{\eta_0}\right)^{.7} \qquad \ldots\ldots\ldots \quad 5.5$$

Where $H^*_1{}'$ is the dimensionless minimum film thickness taking account of the effects of viscous heating. Substituting equation 5.5 gives the following relation which was used to obtain predictions of minimum film thickness:

$$H^*_1{}' = H^*_1 \left(\frac{\bar{S}'}{\bar{S}}\right)^{.7} \qquad \ldots\ldots\ldots \quad 5.6$$

To obtain the inlet temperature rise, predicted by the Murch and Wilson theory, the temperature corresponding to the oil viscosity of $\eta_0{}'$ was calculated from equation 5.1. The measured surface temperature was then subtracted from this value. In calculating the oil inlet temperature from the effective inlet viscosity, no account was taken of the variation of density with temperature. As the temperature rise is relatively small, the error introduced is negligible.

The thermal predictions, expressed in terms of the usual dimensionless parameters, are plotted for comparison with the experimental values of central and minimum film thickness in figures 5.10, 5.14, 5.18 and 5.22. In figures 5.11, 5.15, 5.19, and 5.23, the theoretical film thickness predictions and experimental results are plotted against shaft speed. Also shown in these figures is the predicted inlet temperature rise.

The predictions obtained for lubricant 2 from the Murch and Wilson analysis and the corrected Dowson and Higginson equation (figures 5.10, 5.11, 5.14, 5.15), have

been calculated assuming a constant value of the pressure-viscosity coefficient α. The film thickness predictions for lubricant 1, shown in figures 5.18, 5.19, 5.22 and 5.23, also allow for the variation in α value with temperature. The relationship was found by comparing the experimental results obtained for central film thickness in tests D and E. These results are plotted together in figure 5.25. For both of these tests, at values of U* below 9×10^{-11} there is negligible reduction in film thickness due to viscous heating, as predicted by the Murch and Wilson analysis. Therefore for any value of U* less than 9×10^{-11}, the separation between the curves can be solely attributed to the difference in α value. The reference value of α is 1.46×10^{-4} in.^{2}/lb. at 20.5^{o}C. Values of α were calculated relative to this reference value for three points, on the line representing test E, corresponding to surface temperatures of 36^{o}C, 42^{o}C, and 49.5^{o}C. The same reference value of α was used for all three points since, in this range, the surface temperature in test D only varies from 18^{o}C. to 20.5^{o}C. and such a small temperature variation is assumed to have a negligible effect on the reference value. Wymer (81) has found experimentally that the central film thickness is influenced by the α value according to equation 2.9 ie.,

$$\frac{H^*_0}{H^*_{0\,\text{ref.}}} = \left(\frac{\alpha}{\alpha_{\text{ref.}}}\right)^{.58}$$

TEST A
(Lubricant 2)

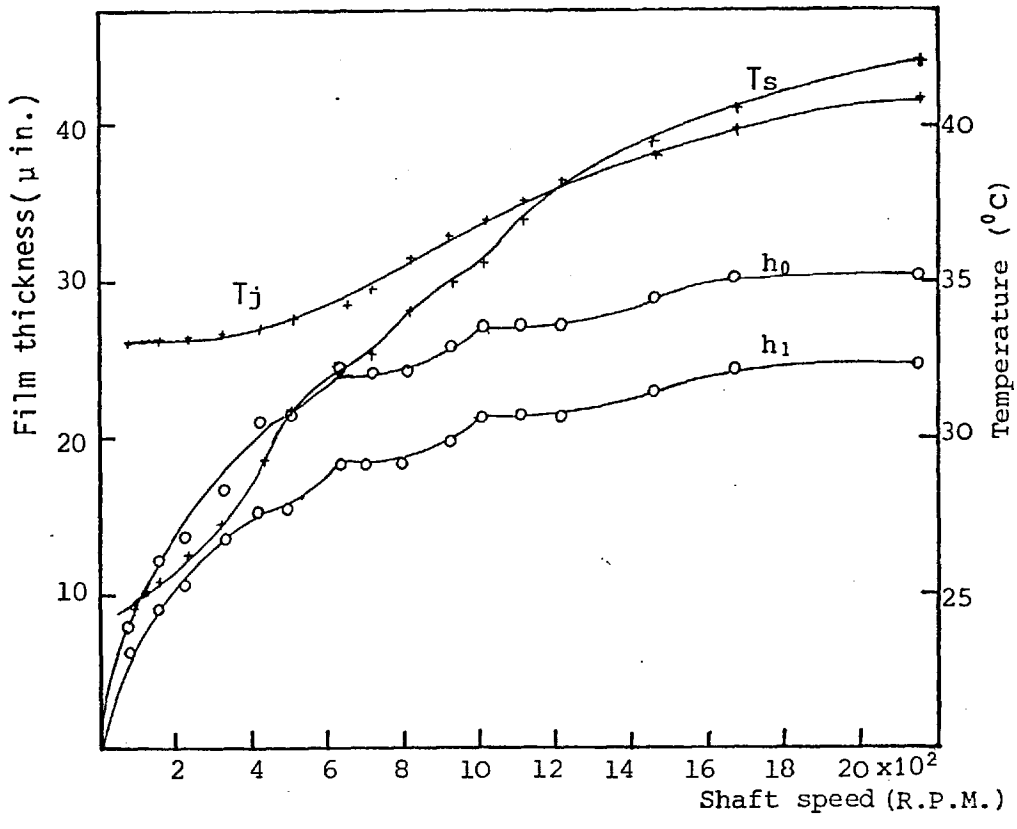

Figure 5.8 Experimental results plotted against shaft speed.

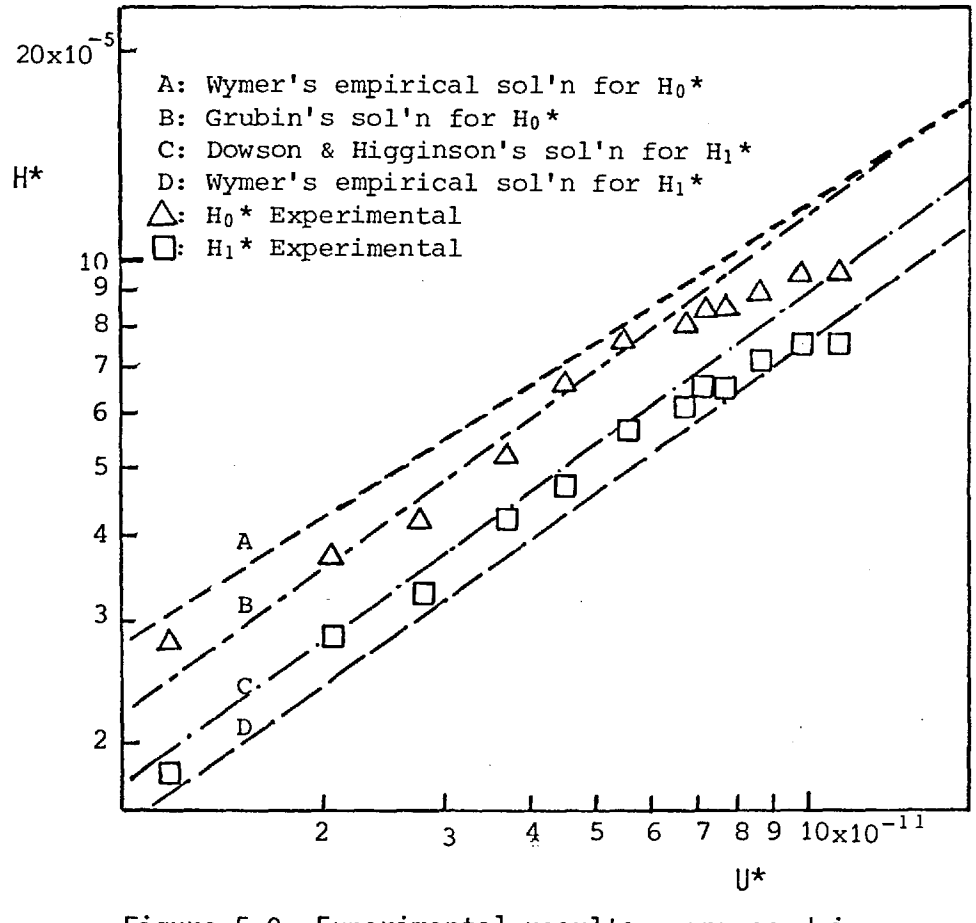

Figure 5.9 Experimental results, expressed in dimensionless terms, plotted for comparison with isothermal theory.

TEST A
(Lubricant 2)

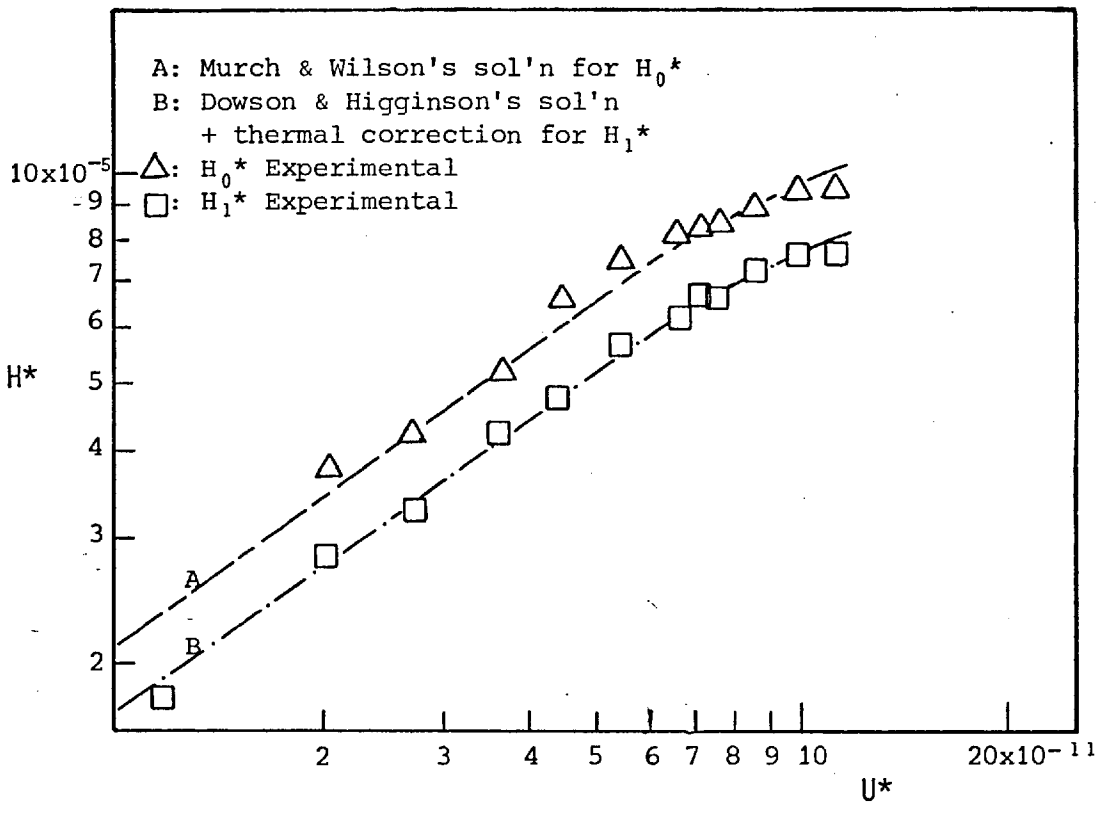

Figure 5.10 Experimental results, expressed in dimensionless terms, plotted for comparison with thermal theory.

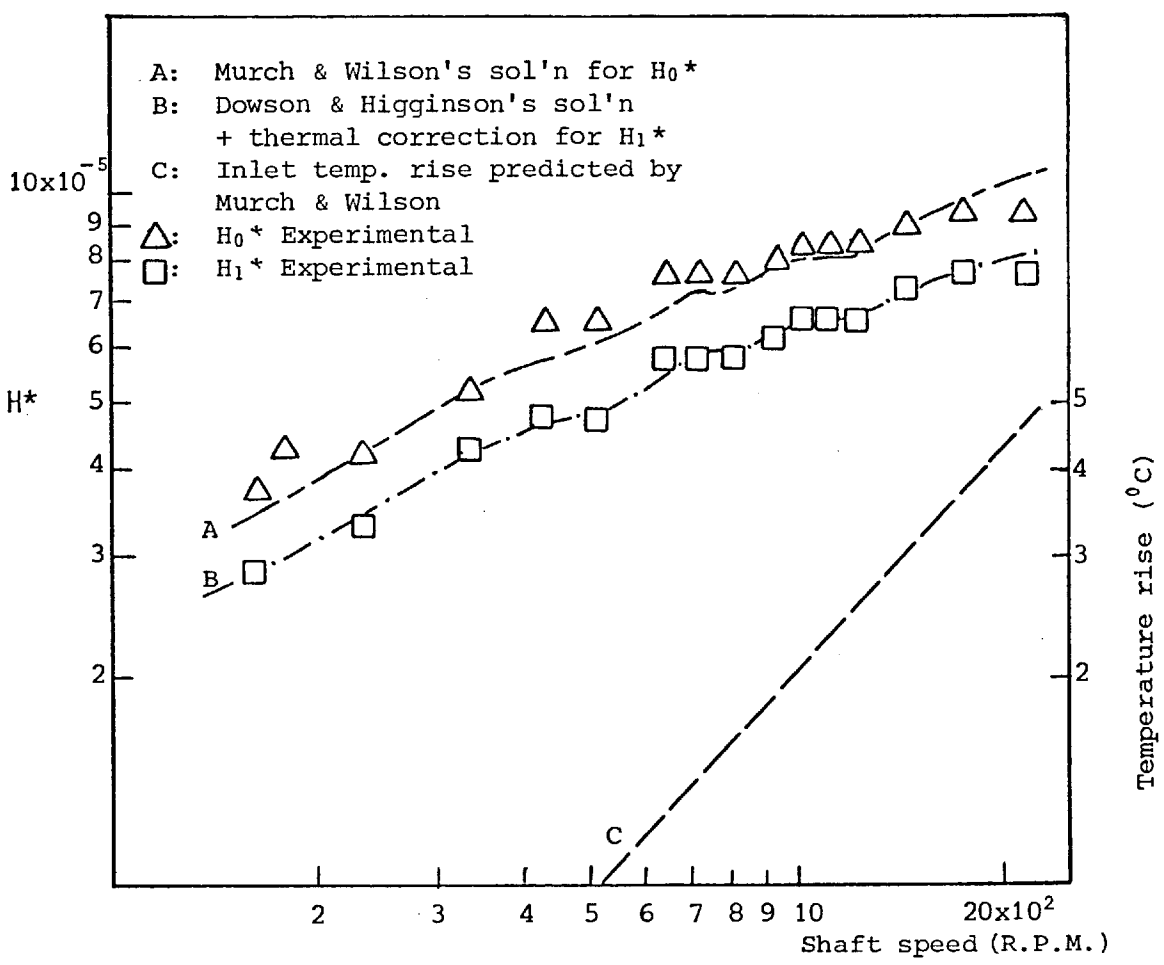

Figure 5.11 Experimental values of dimensionless film thickness plotted against shaft speed for comparison with thermal theory.

TEST B
(Lubricant 2)

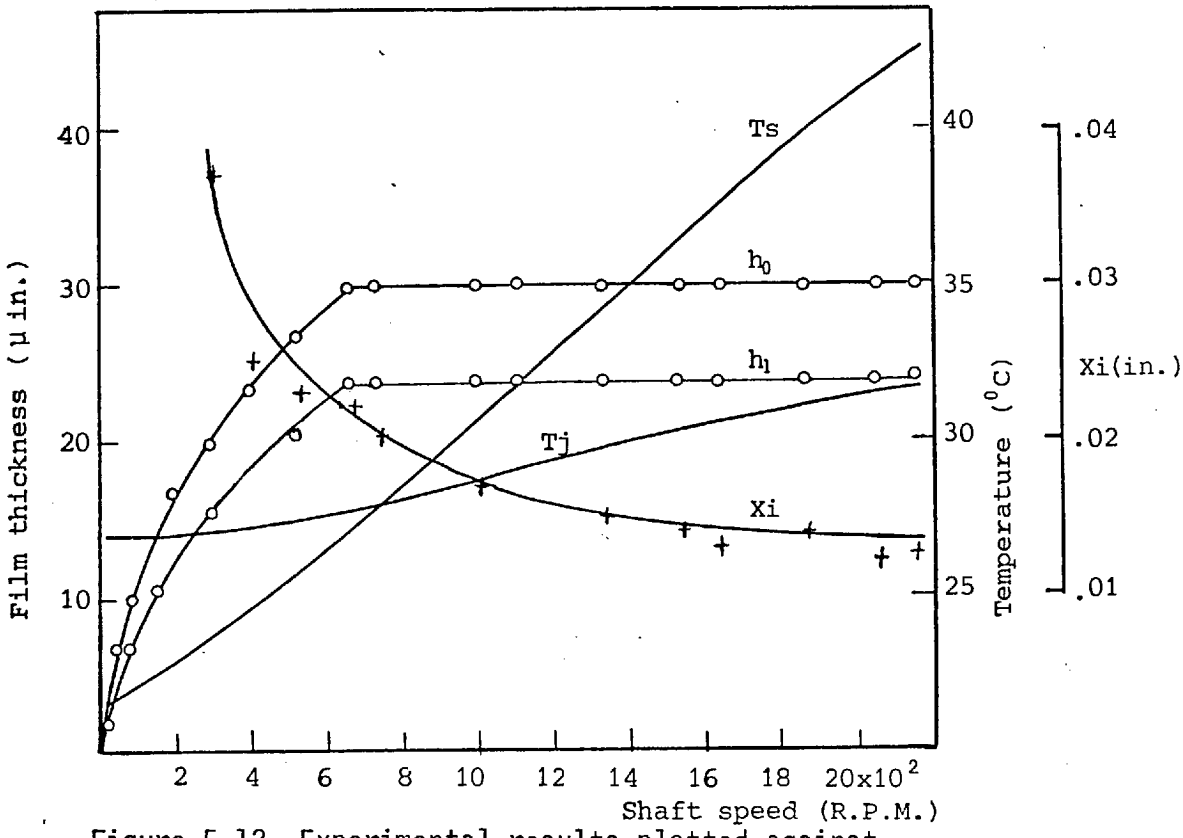

Figure 5.12 Experimental results plotted against shaft speed.

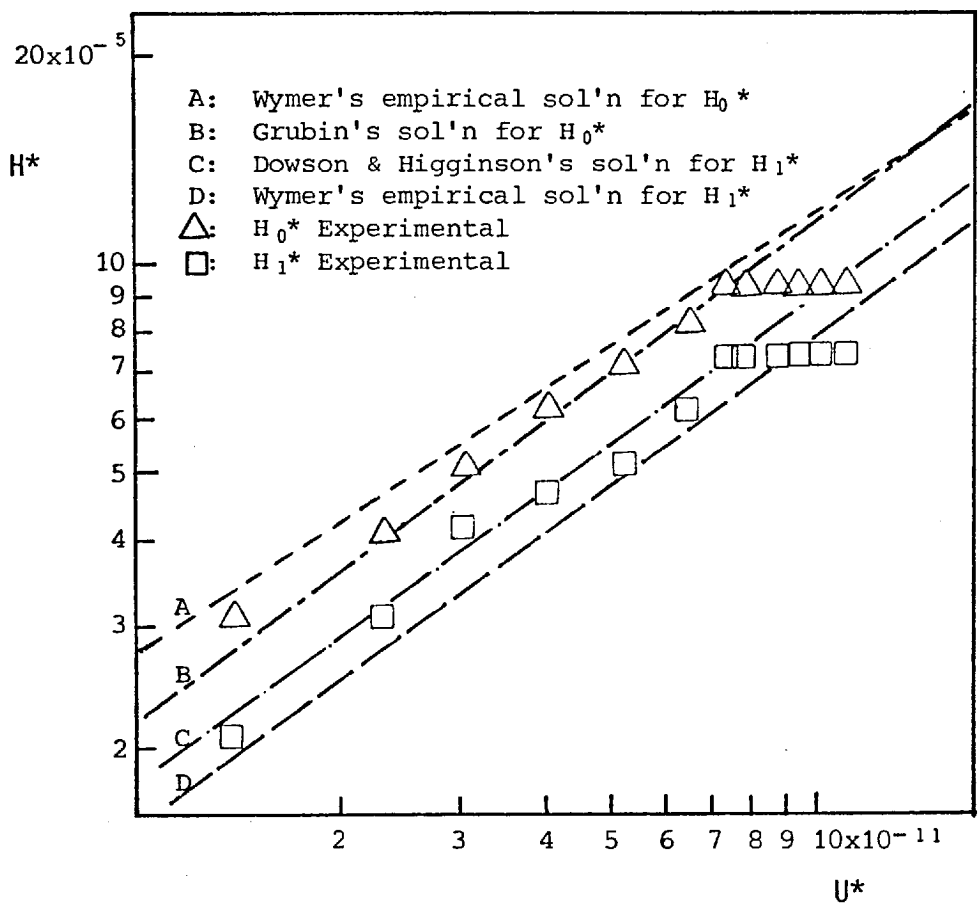

Figure 5.13 Experimental results, expressed in dimensionless terms, plotted for comparison with isothermal theory.

TEST B
(Lubricant 2)

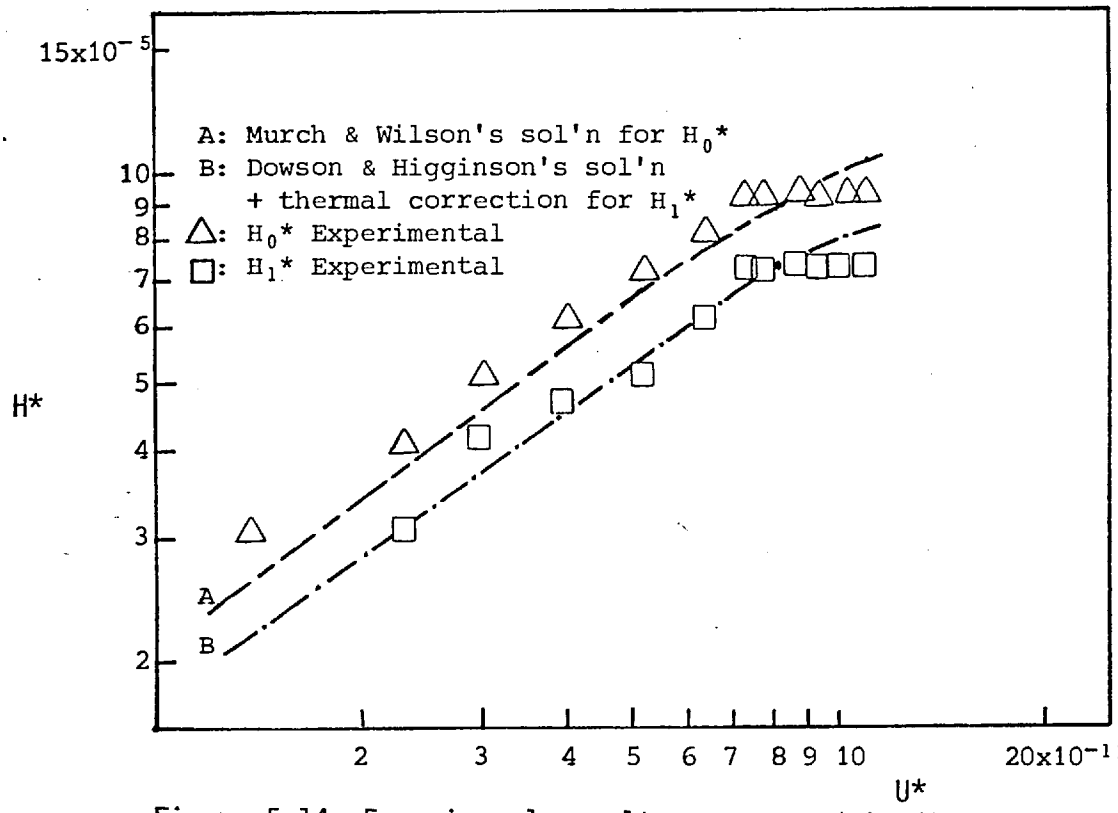

Figure 5.14 Experimenal results, expressed in dimensionless terms, plotted for comparison with thermal theory.

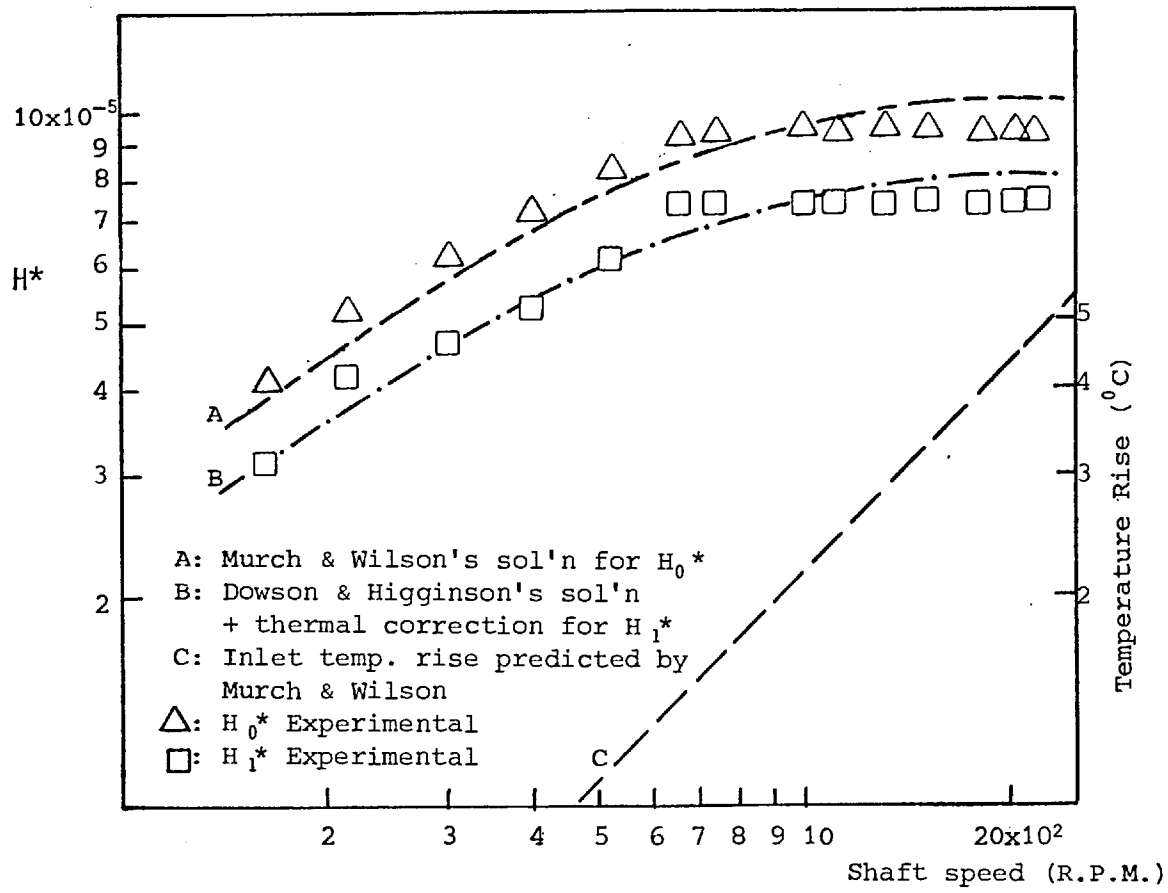

Figure 5.15 Experimental values of dimensionless film thickness plotted against shaft speed for comparison with thermal theory.

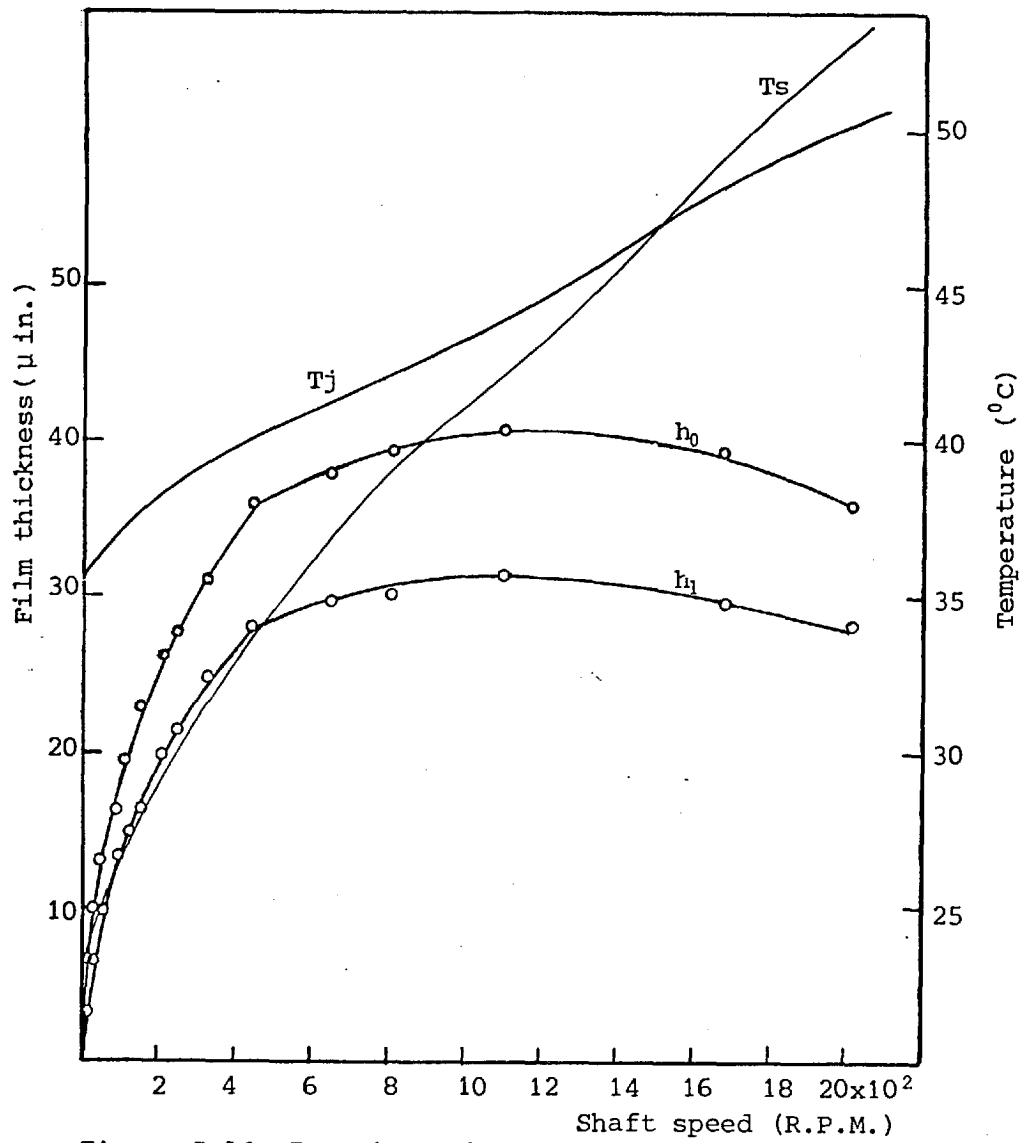

Figure 5.16 Experimental results plotted against shaft speed.

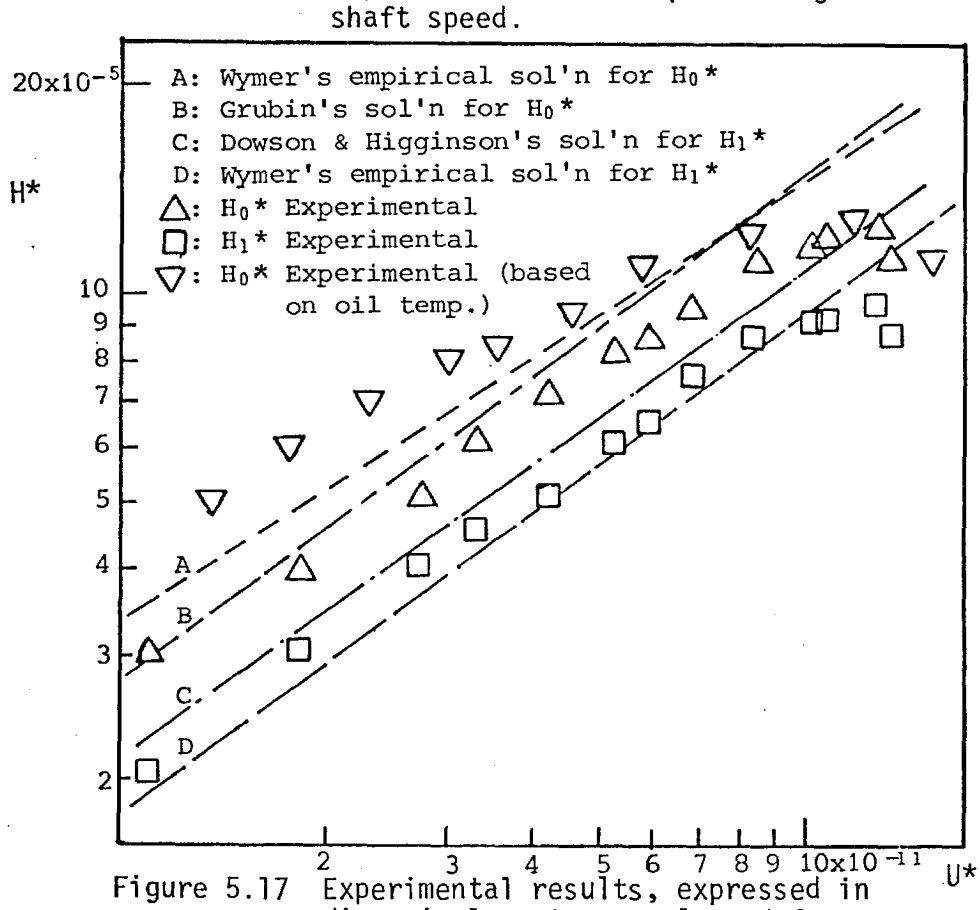

Figure 5.17 Experimental results, expressed in dimensionless terms, plotted for comparison with isothermal theory.

TEST C
(Lubricant 1)

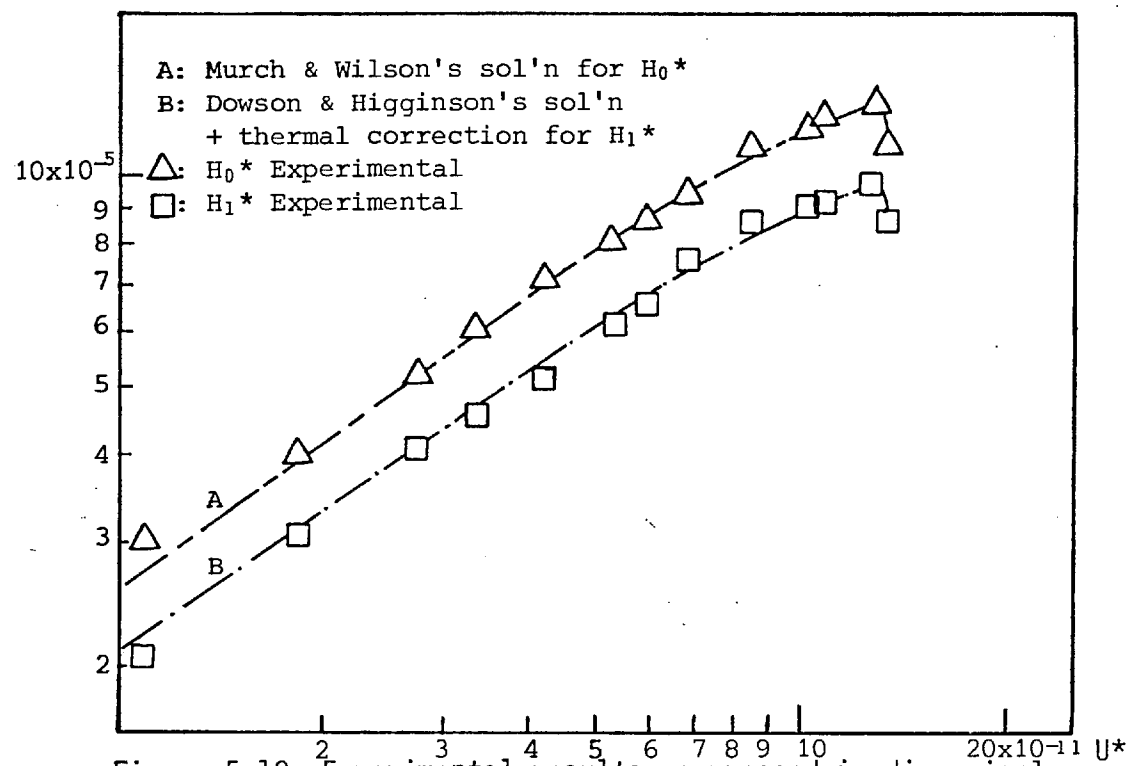

Figure 5.18 Experimental results, expressed in dimensionless terms, plotted for comparison with thermal theory, allowing for the variation of α value.

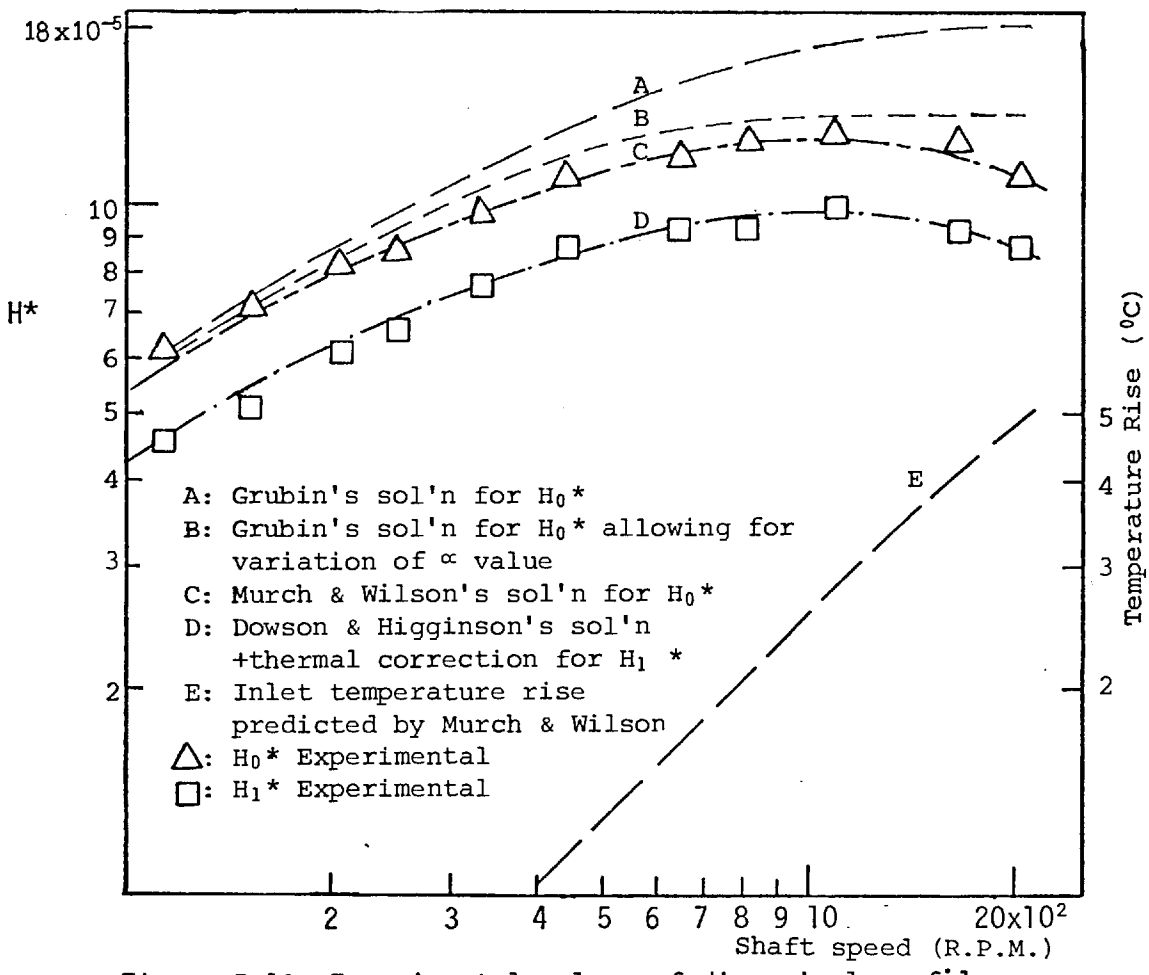

Figure 5.19 Experimental values of dimensionless film thickness plotted against shaft speed for comparison with thermal theory allowing for α value variation.

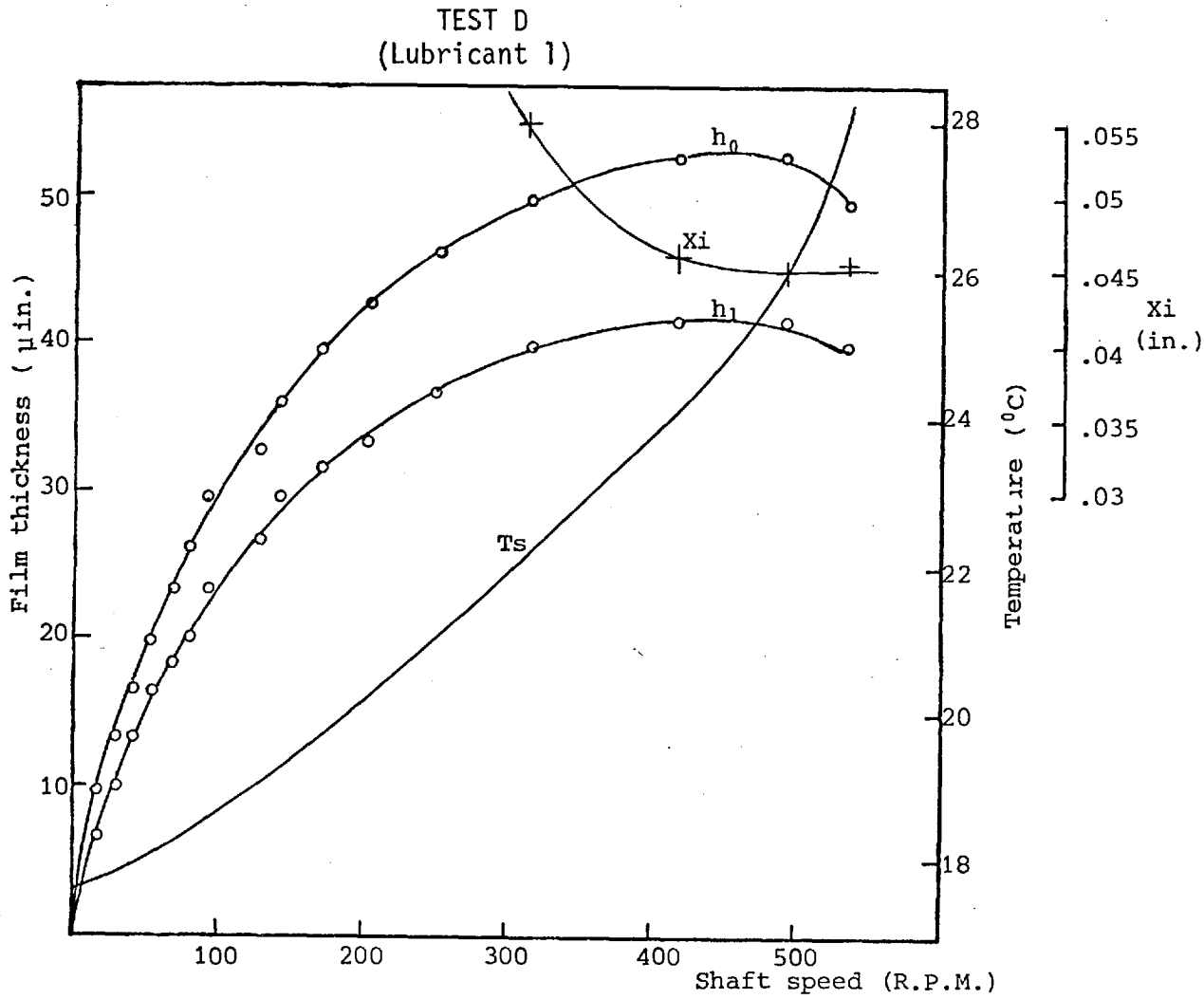

Figure 5.20 Experimental results plotted against shaft speed.

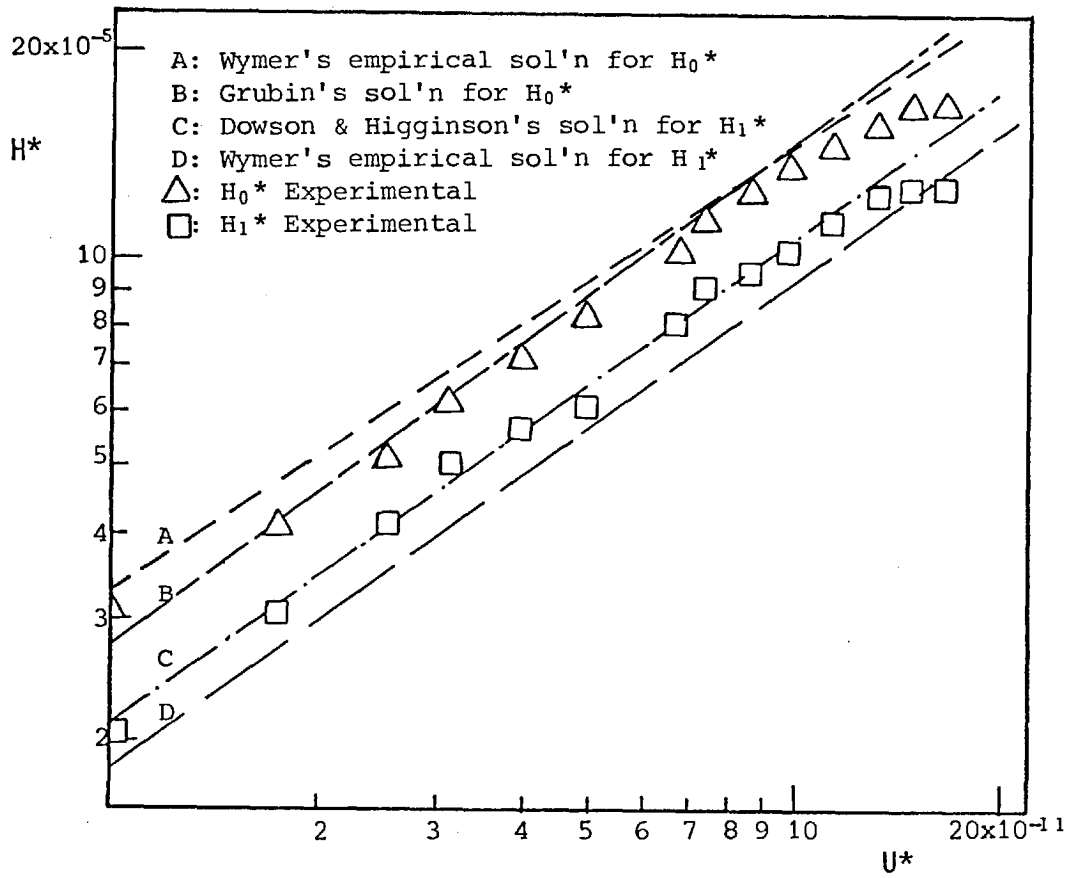

Figure 5.21 Experimental results, expressed in dimensionless terms, plotted for comparison with isothermal theory.

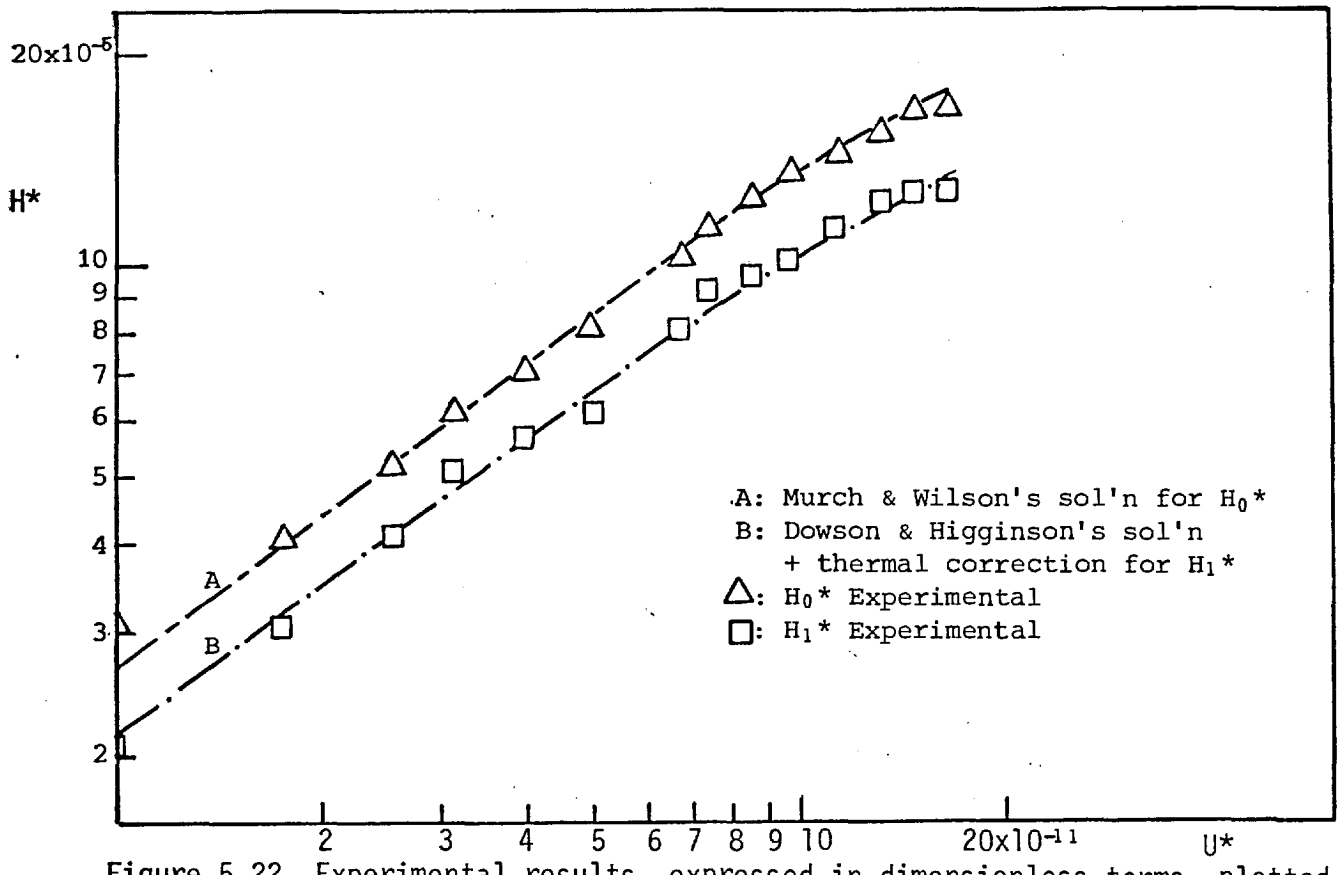

Figure 5.22 Experimental results, expressed in dimensionless terms, plotted for comparison with thermal theory, allowing for the variation of α value.

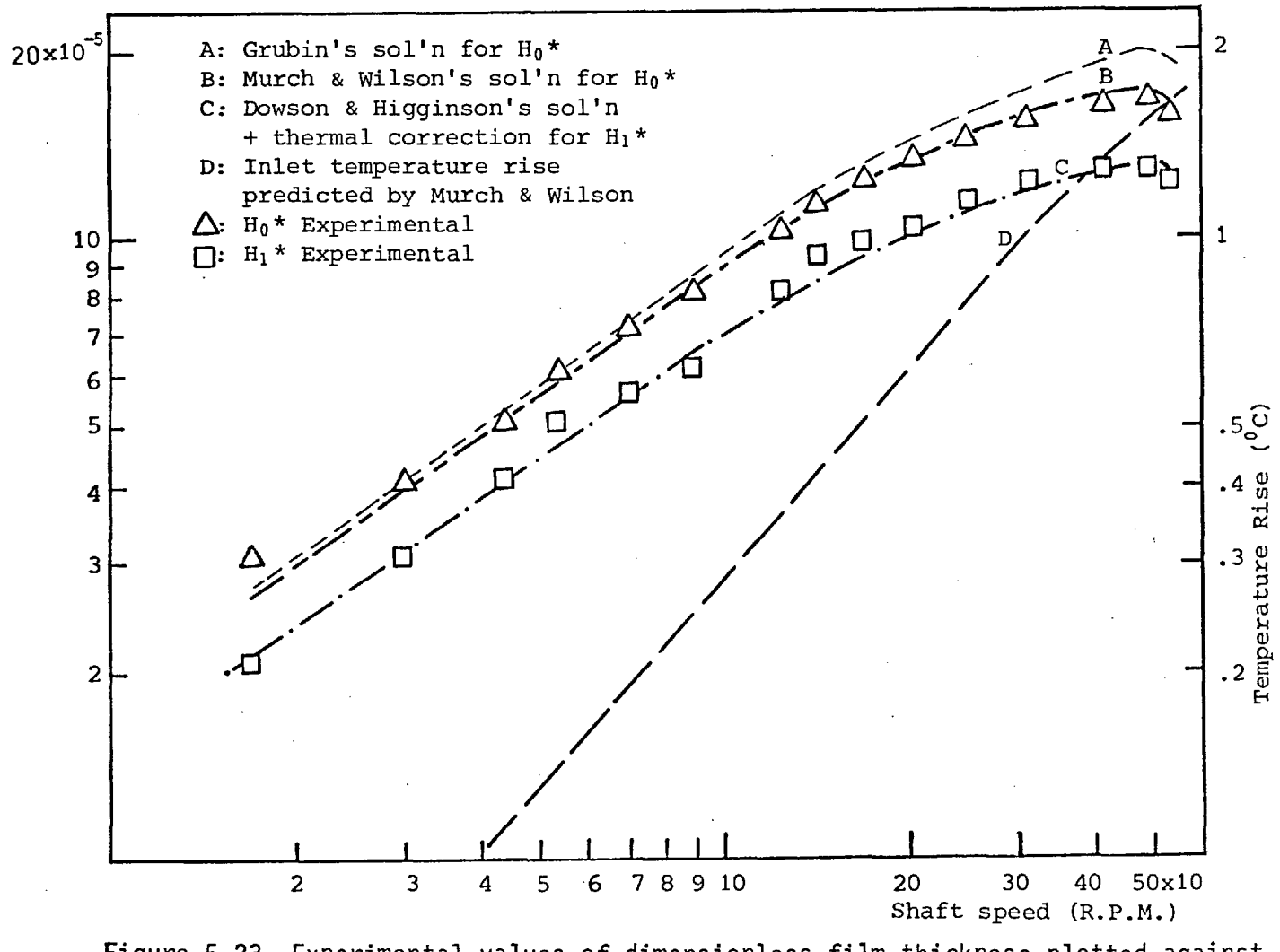

Figure 5.23 Experimental values of dimensionless film thickness plotted against shaft speed for comparison with thermal theory allowing for α value variation.

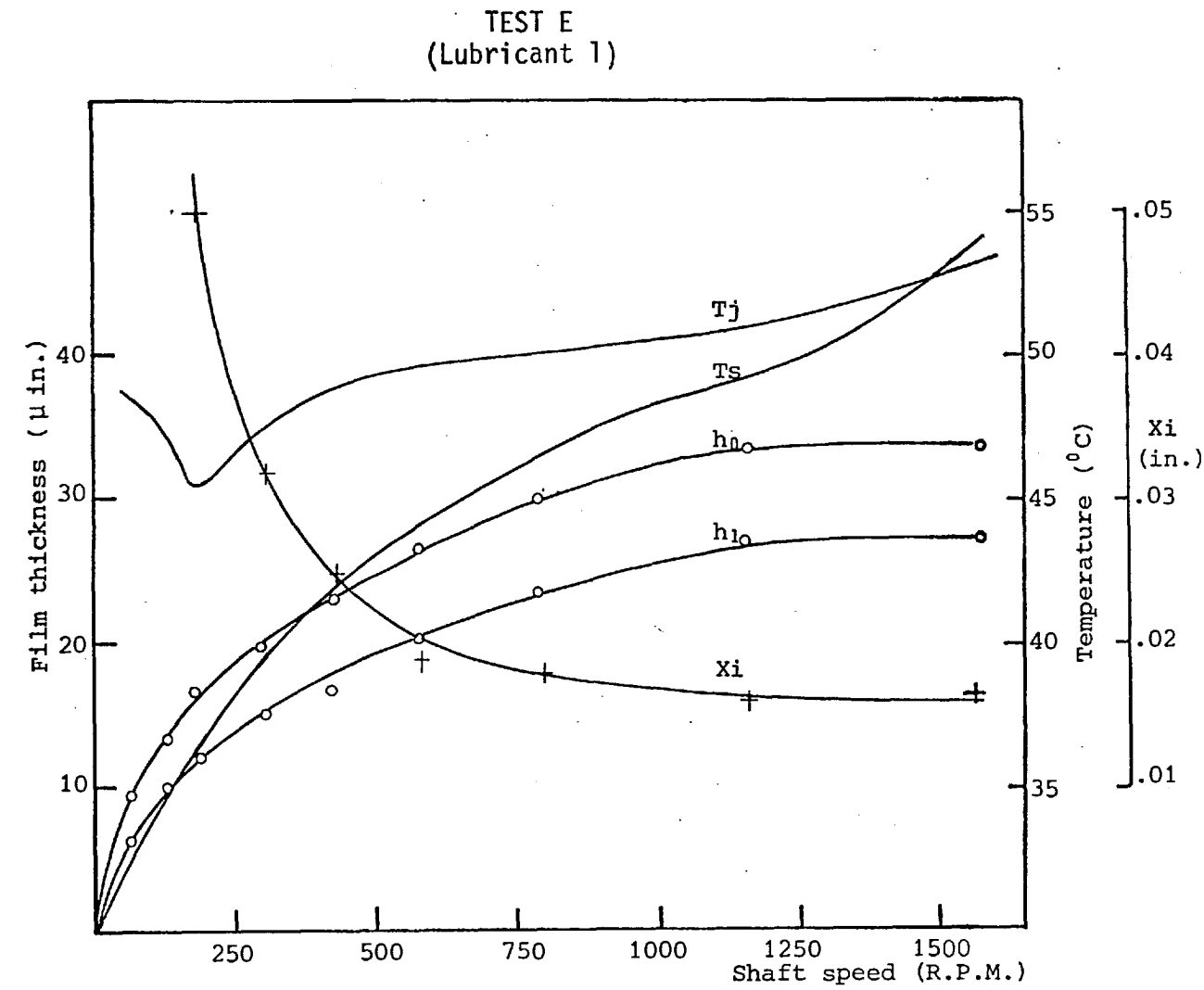

Figure 5.24 Experimental results plotted against shaft speed.

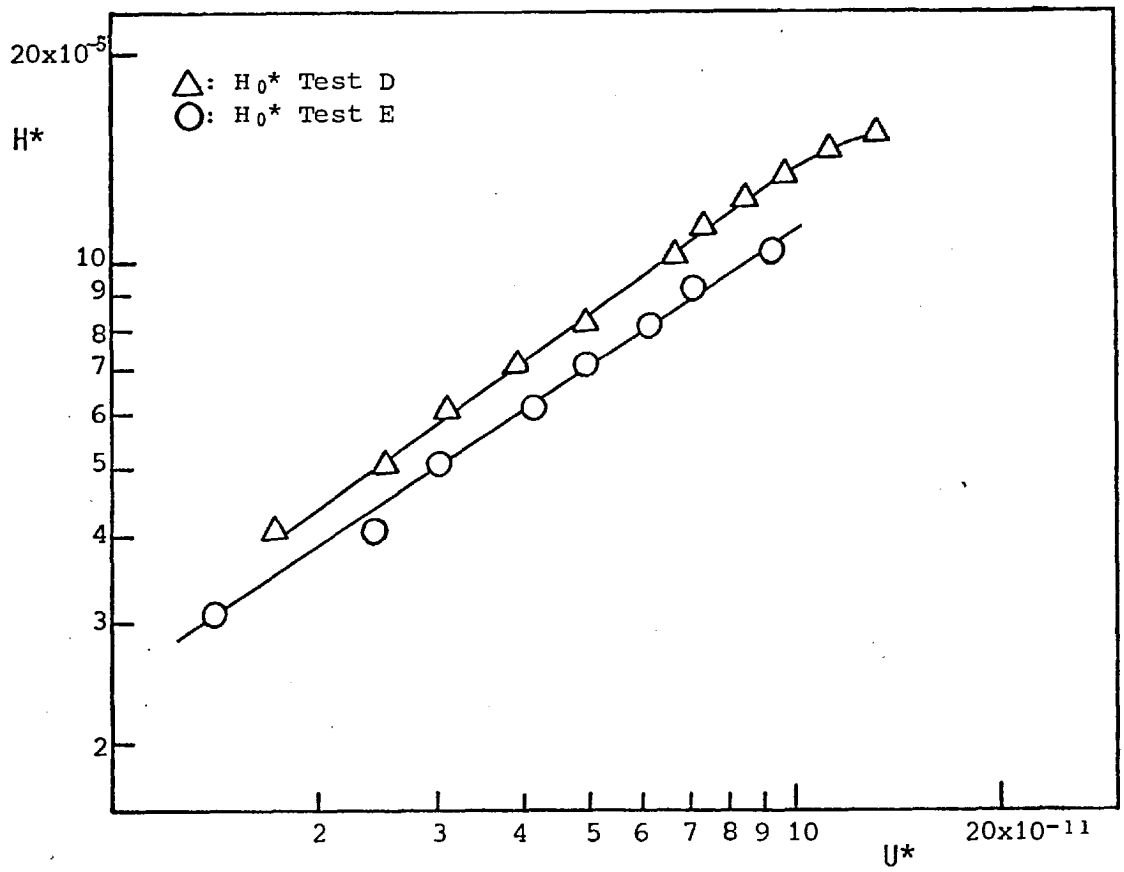

Figure 5.25 Experimental results, expressed in dimensionless terms, plotted for comparison with results of test D.

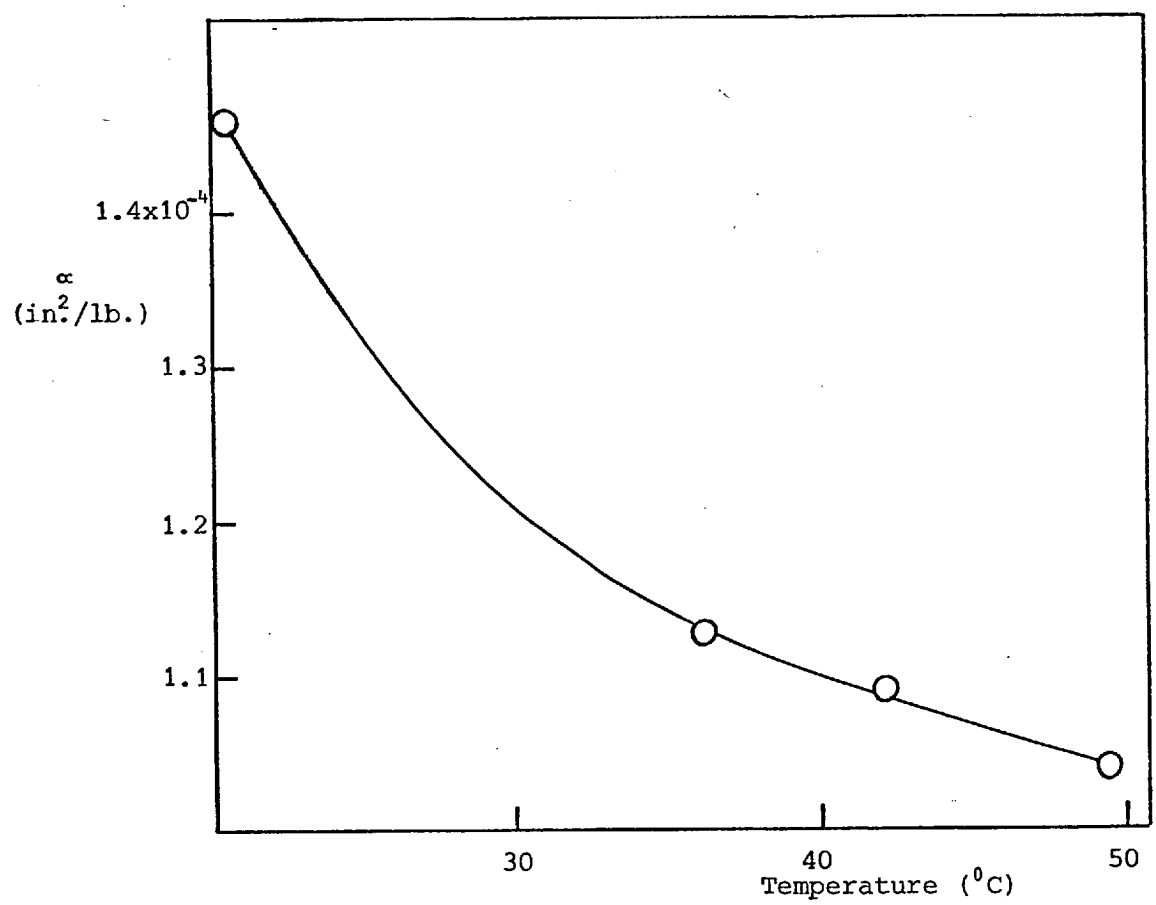

Figure 5.26 Variation of the pressure - viscosity coefficient of lubricant 1 with temperature.

Therefore for a particular value of U*:

$$\alpha = 1.46 \times 10^{-4} \left(\frac{H^*_0}{H^*_{0\,ref.}} \right)^{1.724}$$

This equation, where H_0^* is taken from test E, and $H^*_{0\,ref.}$ from test D, within the specified ranges of U* and temperature, was used to obtain the variation of α value with temperature for lubricant 1. The results are plotted in figure 5.26. For the purposes of computation these results were represented by the following relationship, which closely fits the experimental curve:

$$\alpha = \frac{4.71 \times 10^{-4}}{T_s^{.39}}$$

Where T_s is the surface temperature measured in ^oC.

5.5 Discussion

A study of the interferograms presented in figures 5.4 to 5.7 reveals the typical film shape of an E.H.D. contact, in which the central region of constant film thickness is followed by an exit constriction along the rear edge of the contact.

The absence of a constriction at the contact inlet suggests the smooth transition of the roller onto the sapphire insert. If there was a normal approach velocity,

caused by an uneven transfer from the steel surface to the sapphire, it is likely that a slight additional constriction would be formed at the front edge of the contact (49).

At the contact ends the exit constriction broadens to form side constrictions. At the load used in these tests, the reduction in film thickness occurring at the side constrictions was no greater than that occurring at the exit constriction. The rollers, of standard commercial type, have been carefully blended to alleviate these side constrictions. As the film thickness increases, the deviation from the Hertzian shape becomes more pronounced, and the exit constriction occupies a greater area of the contact.

Upon leaving the contact it can be seen that the oil cavitates, and is left on the sapphire surface in the form of streamers. The oil remains on the track in this form, until the streamers are swamped by an inflow of oil or by oil in the inlet region of the following contact. In figure 5.5 the cavitation streamers, left from a preceeding contact, are clearly visible in the contact entry region. As the film thickness increases, the point at which cavitation occurs moves further away from the rear edge of the contact. This again indicates the departure from the Hertzian pressure curve, as the film thickness increases with speed.

It is evident from figures 5.8 and 5.24 that the film thickness is directly influenced by the surface temperature and not by the jet temperature. In figure 5.8 it can be seen that the irregular shape of the film thickness curves reflects the variations in the shape of the surface temperature curve. Figure 5.24 illustrates that a sharp drop in the jet temperature has no effect upon the shape of the film thickness curves. In figure 5.17 the experimental results for H^*_0 have been plotted against values of U* based on an oil inlet viscosity calculated at the jet temperature. This results in points that show an inconsistent relationship between film thickness and speed. This behaviour is obviously expected, as the temperature of the oil at the contact inlet will be directly influenced by any change in surface temperature. Convincing evidence that the inlet viscosity is governed by the surface temperature has also been given by Crook (34).

A comparison of figures 5.16 and 5.20 reveals that considerably larger film thicknesses were obtained with zero flow to the bearing, than with jet feed. Although the higher value of oil temperature, responsible for the low film thickness, is caused by oil churn, it is likely that had the bearing been left to run with no supply, the surface temperature would eventually have risen over and above the temperatures resulting from jet feed.

At low values of the dimensionless speed parameter

U* (below 6 x 10^{-11}) the experimental values of film thickness are accurately predicted by the isothermal theories of Grubin and Dowson and Higginson (see figures 5.9, 5.13, 5.17, 5.21). Measurements of central film thickness fall consistently below the curve representing the empirical solution of Wymer, and the slope of a line joining the experimental points, at low values of U*, is greater than that of Wymer's solution. The measured values of minimum film thickness fall consistently above Wymers' empirical curve, although the dependence on U* is the same. The average value of the ratio of minimum film thickness to central film thickness, obtained from the experimental results, is equal to .78. This is extremely close to the value of .75 quoted by Dowson and Higginson (31).

At values of U* above 6 x 10^{-11} the slope of the experimental results begins to decrease, and in some cases even becomes negative, as is the case in test C (figure 5.17). At the maximum value of U* reached in this test, the experimental values of central and minimum film thickness are 39% lower than those predicted by the isothermal theories of Grubin and Dowson and Higginson. This considerable reduction in film thickness, which is occurring at relatively low speed of 2020 R.P.M., is not caused by starvation. At this speed, although the position of the inlet boundary was extremely unstable, there appeared to be no variation in film thickness. If the contact was starved, small fluctuations in the position of the inlet boundary would cause

a large change in film thickness. Figure 5.5(f) shows a photograph taken at a shaft speed of 2060 R.P.M. during test B. Although the position of the inlet boundary varies from a minimum of 0.012 in. to over 0.06 in. along the length of the contact visible in the photograph, it can be seen there is no change of fringe order. For these conditions, at the minimum boundary distance, the theory of Wolveridge, Baglin and Archard (119) predicts a 5% drop in film thickness from the fully flooded value. This is considerably less than a drop of 30%, which is the discrepancy between the film thickness predicted by isothermal theory and the experimental result. A 5% drop in film thickness would not be sufficient to cause a change in fringe order, which confirms the experimental observations.

The thermal analysis of Murch and Wilson (172) (equation 5.3), and the corrected Dowson and Higginson equation (equation 5.6), give extremely accurate predictions of film thickness at the higher values of U*. The thermal predictions for tests C and D (figures 5.18, 5.19, 5.22, 5.23) have also allowed for the variation of α value with temperature, and this results in almost exact predictions of central and minimum film thickness over the whole range of the speed parameter U*. In figure 5.19, curve A represents the isothermal solution of Grubin for central film thickness at constant α value. Curve B is Grubin's solution allowing for the variation in α, and curve C is the Murch and Wilson

solution allowing for α value variation. At a shaft speed of 2022 R.P.M. the drop in α value accounts for a 24% drop in film thickness and thermal effects cause a further 20% drop. No account of the variation of α value has been made in the theoretical predictions for the tests with lubricant 2 (figures 5.10, 5.11, 5.14, 5.15). This would explain the remaining discrepancy in tests A and B, at the higher speeds and correspondingly higher temperatures.

It is evident from a comparison of figures 5.19 and 5.23 that the higher the viscosity of the oil, the lower the speed at which thermal effects make a significant reduction in film thickness. In test C thermal effects are not significant until speeds are over 650 R.P.M., whereas in test D they begin to effect film thickness at speeds above 200 R.P.M. The drop in film thickness that occurs above speeds of 1000 R.P.M. in test C, is solely caused by thermal effects. Any further increase in speed merely has a detrimental effect on film thickness. All the experimental results show that the film thickness ceases to increase with speed at comparatively low values of shaft speed. This is caused by a combination of increasing surface temperature and viscous heating, which drop the inlet viscosity, and a decreasing α value. A similar effect has been found by Dyson and Wilson (180) who comment "There is a tendency for the experimental values to stop increasing with increasing theoretical film thickness".

In figures 5.11, 5.15, 5.19, and 5.23, the inlet temperature rise as predicted by the thermal approach, has also been plotted against shaft speed. These values are in good agreement with those obtained experimentally by Orcutt (91). Wilson and Murch (172) have found that as the thermal loading parameter was increased, the pressure gradient in the inlet zone decreases. This results in the effective length of the inlet zone increasing from about 2.5 Hertz widths, under isothermal conditions, to around 15 Hertz widths, under conditions of high thermal loading, which they predict could lead to premature starvation. However the experimental results do not show this effect. An explanation of why this is not evident is that as the edge of the parallel section is approached, the velocity distribution becomes almost constant. It would therefore be expected that as starvation becomes increasingly severe, the temperature rise in the inlet, due to viscous heating, would become correspondingly lower. Thus the two effects balance each other.

CHAPTER VI

FURTHER INVESTIGATIONS INTO THE LUBRICATION OF THE OUTER RACE CONTACTS

6.1 Introduction

Recent theoretical studies (119, 120, 123), and experimental work (47, 69, 81, 127, 137) in which low values of film thickness have been attributed to lubricant starvation, have caused considerable speculation as to whether rolling element bearings operate frequently under starved conditions. It is evident from the results of the film thickness tests, that starvation was not causing a drop in film thickness. This is surprising when the difficulty encountered by other workers in avoiding starvation (81), is considered. Also as the oils used in this study were of comparatively high viscosity, the early onset of starvation was expected. Efforts to bring about starvation by shutting off the oil supply, only resulted in a stabilizing effect on the position of the inlet boundary. Even leaving the bearing to run with no additional supply, had no further effect on the boundary position.

Recently considerable attention has been focused on the question of lubricant starvation. Prediction of film thickness, under starved conditions, can be accurately made if the position of the inlet boundary is known. However in practice this is not the case, and interest is now

centred on predicting where the air/liquid interface will form for a given set of operating conditions (123, 127). In order to try to resolve the way by which oil that is continually being lost from the bearing surfaces, is replaced, several tests were conducted to elucidate the mechanisms involved.

6.2 Position of the Inlet Boundary

Measurements of the inlet boundary distance, made during the film thickness tests, are plotted against shaft speed in figures 5.12, 5.20, 5.24. Only the minimum distance is plotted, this being measured from the edge of the parallel contact zone, midway across the length of the contact. The highly erratic behaviour of the boundary, which occurred at the higher speeds when oil was being supplied, was caused by drops of oil, flung onto the outer race by centrifugal force, some of which wet the surface. A comparison of figure 6.1(a) and 6.1(b) shows the effect of switching off the oil supply. The photograph illustrated in figure 6.1(a), which was taken when the oil jet was on, shows an unstable inlet boundary position. When the jet was switched off, the boundary assumed a steady position, as illustrated in figure 6.1(b). However the minimum distance was virtually unaffected by changes in the oil flow rate, and by plotting this distance the effects of oil flinging can be discounted.

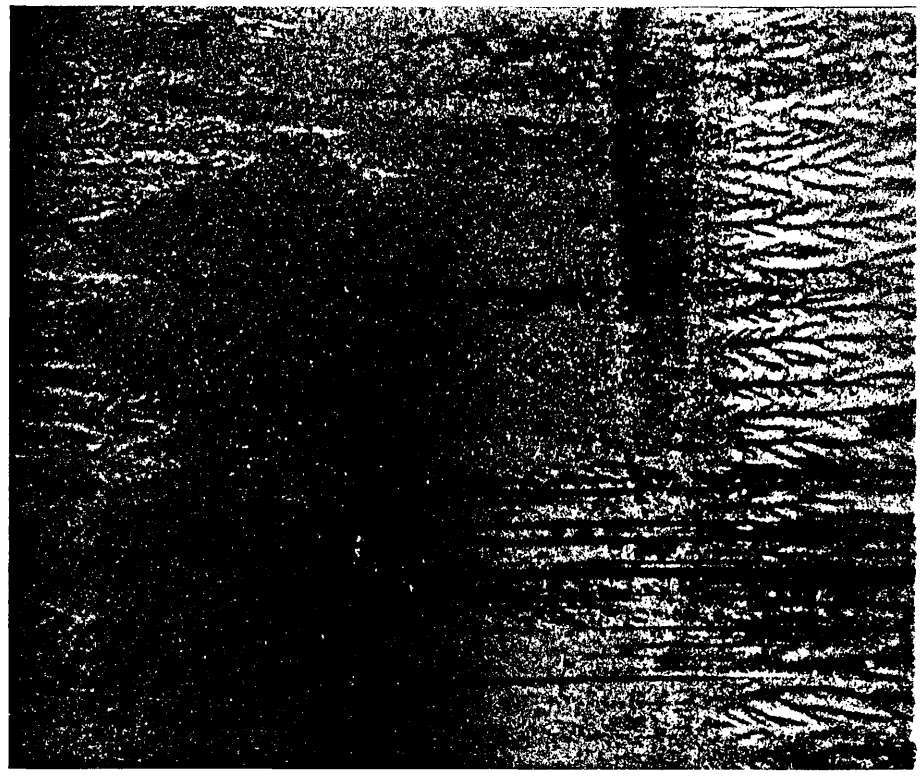

(a) Oil on

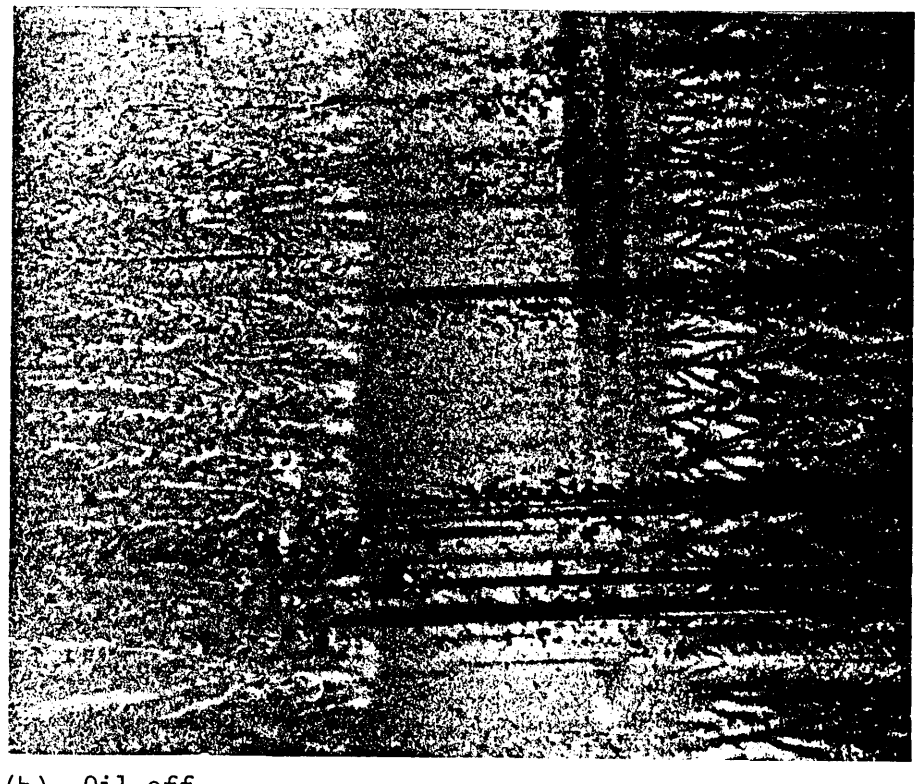

(b) Oil off

Figure 6.1 The effect of lubricant supply on the inlet boundary.

The reduction in the inlet boundary position with increasing speed, is consistent with the behaviour observed by other workers (47, 123, 137). Provided the inner race contacts are running at the same film thickness as the outer contacts; this will be the case as long as the surfact temperatures are the same, there is no starvation, and no oil is lost from the roller surfaces; the only way that oil can be lost from the outer contacts is by leakage around the sides in the inlet zone, or by side leakage within the actual contact. Side leakage within the high pressure contact zone can be neglected in comparison with that lost around the contact edges in the inlet region (this has been shown experimentally, to be considerable in section 6.43). At a constant speed, the rate at which lubricant is lost will be proportional to the boundary distance. The boundary will form in such a position that an equilibrium is established between oil in-flows to the contacts, and the out-flow around the edges. The out-flow is proportional to speed and therefore, provided the in-flows are less dependent upon speed (if at all), the boundary distance will decrease with increasing speed.

It was noted from the experimental results that the inlet boundary distance tended to be larger for higher viscosity oil (compare figures 5.20 and 5.24). This result was totally unexpected as it is contary to other experimental findings (47, 123), and to the generally accepted

theory that increased oil viscosity will lower the rate of oil replenishment.

In order to determine whether there was any definite relationship between inlet distance, speed, and viscosity, the measurements of the boundary position, made in tests B, D, and E, were plotted against η_0/U. Figure 6.2, in which the majority of the experimental points are closely represented by the solid line, confirms that the behaviour of the boundary can be described by a relationship in which the inlet distance is proportional to the viscosity, and inversely proportional to the speed.

The experimental results bear no relation to the starvation theory recently put forward by Chiu (123), (see section 2.4). Although his analysis does not include line contacts, it does predict that at a shaft speed of 2000 R.P.M. there will be no refilling of the rolling track from the edges. The theory in fact suggests that the 'delay time' is larger than the contact time interval. This infers that oil is still being drawn out of the contact during the whole time interval. If the mechanism of oil replenishment suggested by Chiu is applied here, then severe starvation would be expected. This is clearly not the case.

A current hypothesis, put forward by Dowson (127), (see section 2.4), is that under conditions of little or no

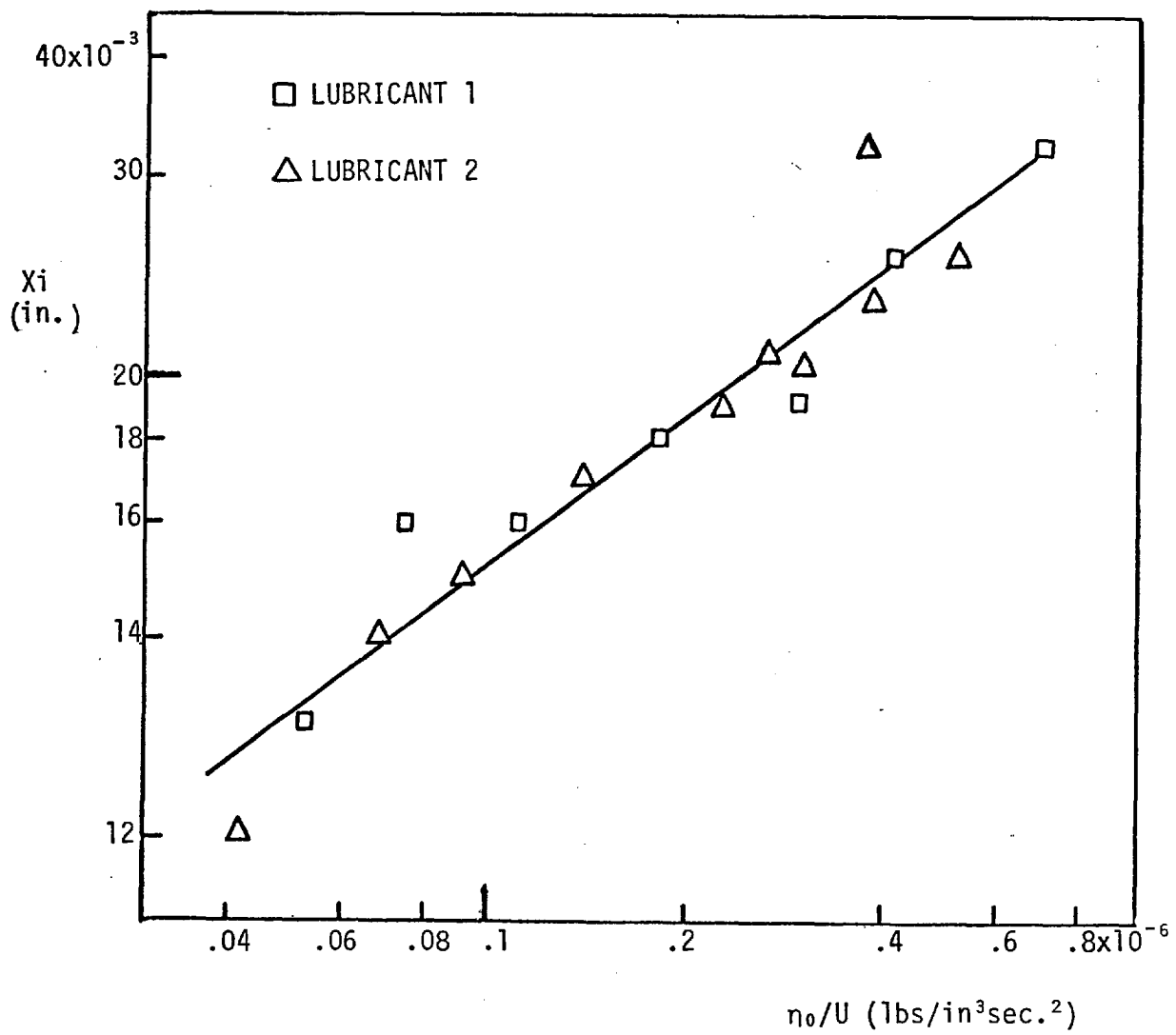

Figure 6.2 Inlet boundary distance Xi, plotted against n_0/U

lubricant supply, the boundary will form at the position of 'zero reverse flow'. In pure rolling this would cause a reduction in film thickness of 29%. At a central film thickness of 30 μin. the calculated position of 'zero reverse flow' is approximately 0.003 in. from the edge of the contact. Even when the oil supply was cut off, the boundary was never formed at a distance of less than 0.012 in., and Dowson's suggestion is not upheld.

In order to confirm the surprising finding that the inlet distance is greater at higher viscosities, the bearing was run at speeds up to 2000 R.P.M. using a small quantity of oil with a viscosity of 8500 cS at 20°C. At all speeds, the position of the inlet boundary was out of the field of view of the microscope, confirming the original findings. Two photographs of this test, taken from the video monitor, are illustrated in figure 6.3. Although interference fringes are hardly visible, because of the extremely thick film, it can be seen from the shape and starting position of the cavitation fingers, that the film thickness is larger at 86 R.P.M., than at 1980 R.P.M. The shape of the cavitation fingers, shown in figure 6.3(a), is very similar to those that occur in journal bearings (compare with those shown in ref. (181)), and the large gap between the edge of the contact and the start of cavitation, suggests that the state of lubrication has become completely hydrodynamic. At the higher speed (figure 6.3(b)), cavi-

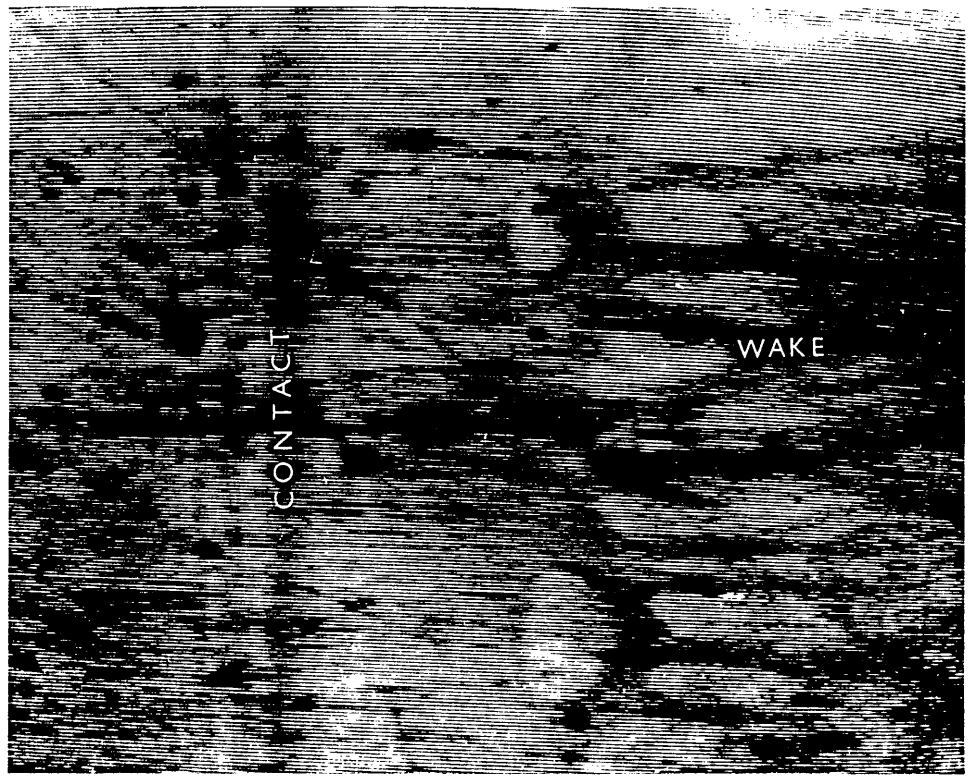

(a) 86 R.P.M.

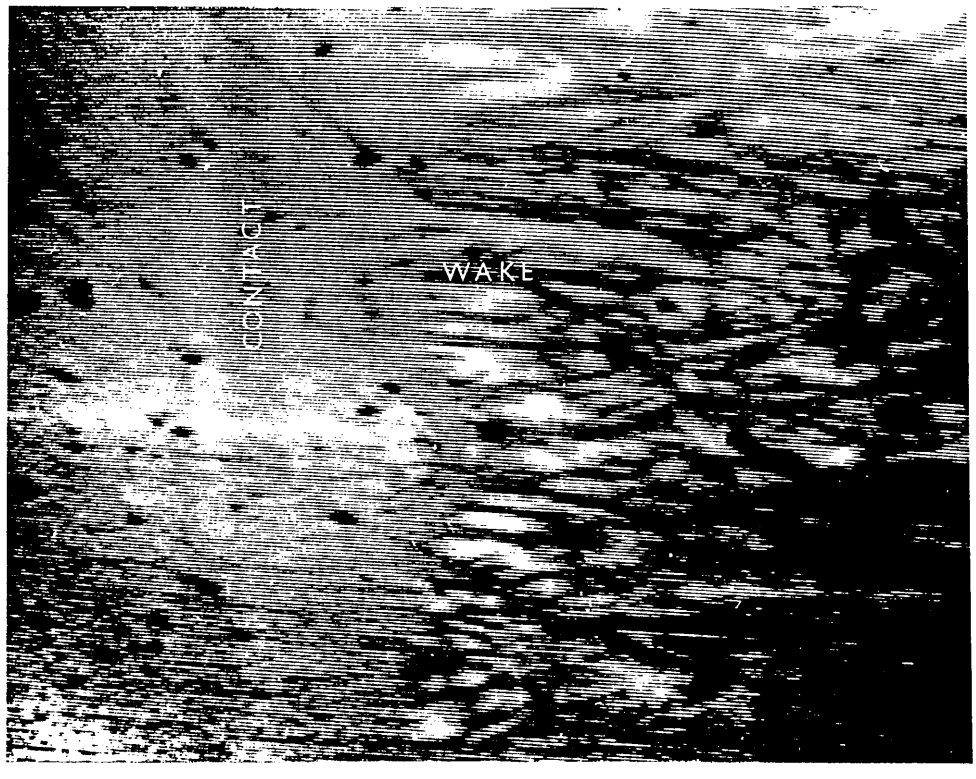

(b) 1982 R.P.M.

Figure 6.3 Appearance of the contact, when running with 8500 cS oil.

tation starts closer to the contact, and the fingers are smaller. This is more characteristic of an E.H.D. contact.

The density, α value, and the variation of viscosity with temperature were not measured, and therefore to estimate the theoretical film thickness, values of these quantities were assumed to be the same as for lubricant 1. The thermal theory of Murch and Wilson (172) predicts a central film thickness of 210 μin. at a speed of 86 R.P.M. and at a surface temperature of 23°C. At 1982 R.P.M., and a temperature of 49°C, the theory predicts a central film thickness of 160 μin. This is inspite of an overall increase in the product of viscosity and speed.

6.3 The Effects of Starvation

6.3.1 Experimental Results.

Severe starvation was induced by limiting the quantity of oil in the bearing to one drop per roller, which is a total volume of approximately 0.01 cubic in. White light was used to enable small changes in film thickness to be measured, and the position of the inlet boundary was obtained in the same way as described in section 5.2.4. Four photographs, that illustrate the reduction in inlet distance with increasing speed and film thickness, are shown in figure 6.4. The effect of an addition of oil, at constant speed, is shown by the photographs presented in figure 6.5.

(a) 31 R.P.M.
1st Red, Xi = .027in.
h_0 = 6.3 µin.

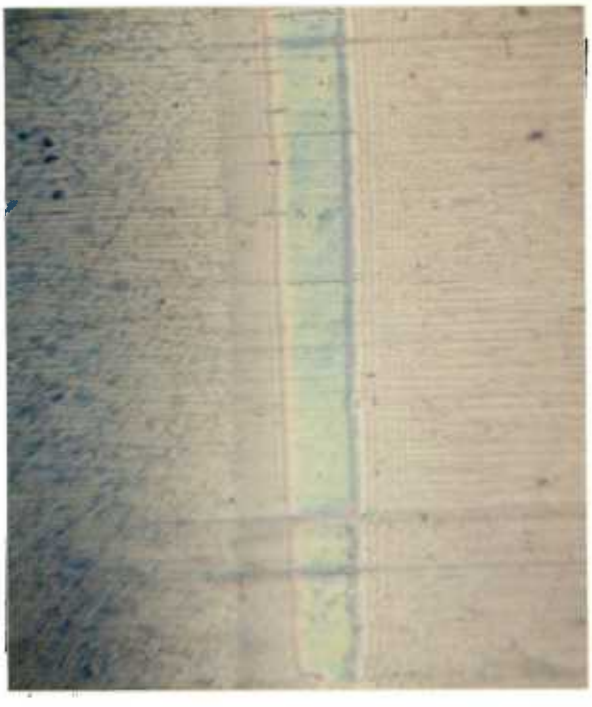

(b) 70 R.P.M.
1st Green, Xi = .0049in.
h_0 = 9.7 µin.

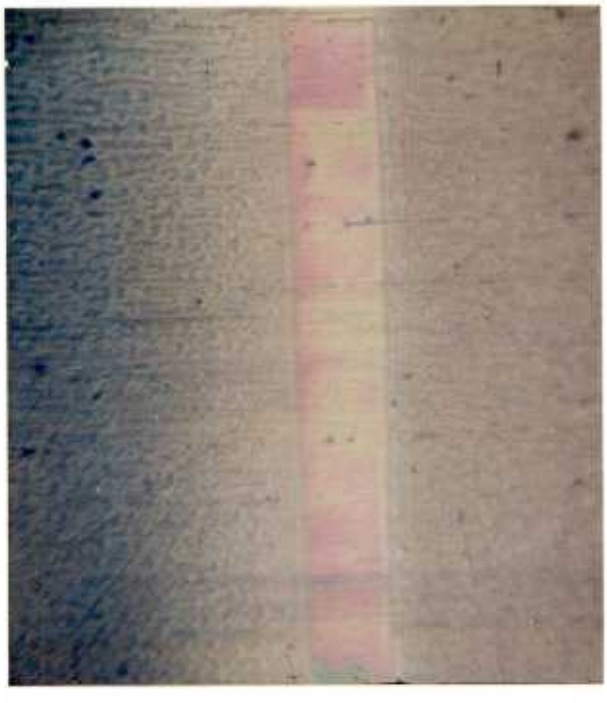

(c) 293 R.P.M.
2nd Red, Xi = .0014in., h_0=12.7 µin.
2nd Yellow, Xi = .0009in., h_0=11.0 µin.

(d) 576 R.P.M.
2nd Green, Xi = .0015in., h_0=15.8 µin.
2nd Red, Xi = .0006in., h_0=12.8 µin.
2nd Yellow, Xi = .0002in., h_0=11.1 µin.

Figure 6.4 Photomicrographs, taken with white light, illustrating the effect of increasing speed under starved operating conditions.

Shaft speed = 322 R.P.M., Hertz width (static) = 0.008in.
Initially one drop of lubricant 2 per roller,
0.3 cubic in. added during test.

(a) 2nd Red
Xi = .001 in., h_0 = 12.7 µin.

(b) 3rd Red
Xi = .0045 in., h_0 = 19.9 µin.

(c) 3rd Green/3rd Red
Xi = .006 in., h_0 = 21.5 µin.

(d) 3rd Green
Xi ≃ ∞, h_0 = 23.2 µin.

Figure 6.5 Photomicrographs, taken with white light, illustrating the effect of an addition of oil under starved operating conditions.

In figure 6.6 the experimental results are compared with the semi-analytical solution of Wolveridge, Baglin and Archard (119), and with Wymer's (81) empirical solution (equation 2.12). The following non-dimensional parameters have been used:

Film thickness parameter: $\beta = \frac{h_n}{h_\infty}$

Inlet distance parameter: $\Psi_i = \frac{b^{1/3}}{(2Rh_\infty)^{2/3}} X_i$

where: h_∞ is the fully flooded central film thickness. Xi is the inlet distance, measured from the edge of the Hertzian contact area. The value of h_∞ was obtained from the Grubin solution and, as the speeds were relatively low, no thermal correction was used. It can be seen from the film thickness results presented in Chapter V that, at low speeds, agreement with the Grubin solution is good.

6.3.2 Discussion.

The scatter in the experimental results reflects uncertainty in the prediction of h_∞, and in assessing the exact location of the boundary at very small inlet distances. Over the whole range of Ψ_i, the drop in film thickness is less than that predicted by Wolveridge et al. (119), although it is only at values of Ψ_i below 0.4 that the discrepancy becomes large. When the inlet boundary approaches the edge of the Hertzian region, the theory predicts a far greater drop off in film thickness than was found experimentally.

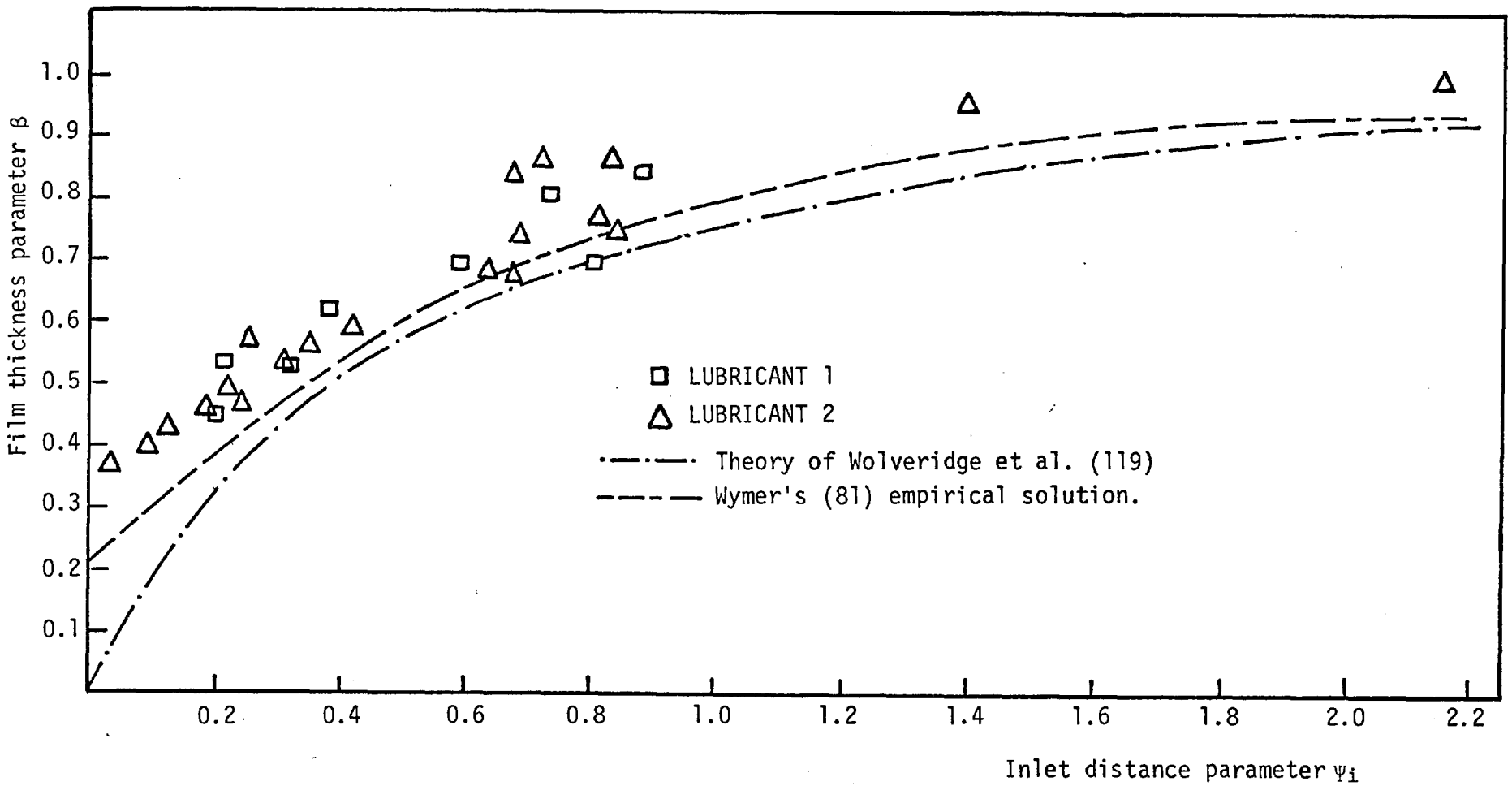

Figure 6.6 Comparison of starvation results with other theoretical and empiral solutions.

Wymer (81) has found the same behaviour and his empirical formula predicts a finite film thickness (0.21 h_∞) at zero inlet distance. However his results were obtained in conditions such that only small regions of the contact were severely starved. Thus the load carried by these areas was considerably reduced, and supported by the surrounding fully flooded contact. The local reduction in contact width in the starved regions, gave the appearance that the boundary had actually entered the Hertzian contact zone. It can be seen from the photographs presented in figure 6.4 that the inlet boundary never quite reaches the edge of the parallel region, and there is always a region of convergence that is responsible for the film formation. The theory of Wolveridge et al. (119) assumes a Hertzian shape, and this is not truly representative of the actual shape close to the boundary of the Hertzian flat. Castle and Dowson (120) have produced a complete numerical solution for starved conditions, but were unable to obtain convergence at values of Ψ_i less than 0.5.

The dependence of film thickness on the position of the inlet boundary (Xi) at constant speed, is illustrated by the photographs presented in figure 6.5. A comparison of (a) and (b) demonstrates that in a severely starved situation a small increase in Xi will cause a large increase in film thickness. However when the boundary is about one Hertz width away from the edge of the contact, any further increase has only a very small effect upon film thickness.

This is evident from a comparison of photographs (c) and (d) of figure 6.5.

Figures 6.4 and 6.5 also show the effect of starvation on the exit constriction. As starvation becomes increasingly severe, the constriction becomes narrower and less pronounced, until it disappears and there is uniform film thickness across the whole contact (see figure 6.4(d)). In figure 6.7 the ratio h_1/h_0 has been plotted against the inlet distance parameter Ψ_i. Again there is considerable scatter, but the results consistently show that the ratio tends to unity as Ψ_i becomes small. This effect has been predicted theoretically by Castle and Dowson (120) for a constant value of H^*_{∞}, and the ratios calculated from their results are represented by the solid line in figure 6.7. These values are higher than those obtained experimentally, as their analysis is based on a low value of H^*_{∞}, for which the ratio of minimum to central film thickness, under fully flooded conditions, is equal to 0.87 (an average value of 0.79 was obtained from film thickness measurements under fully flooded conditions). Wedeven (47, 69) has observed the same behaviour in a point contact situation.

It is also evident from a comparison of the two photographs presented in figure 6.8 that starvation alleviates the side constriction. Although the central film thickness has remained the same, the exit and side constrictions have almost completely disappeared. Increasing

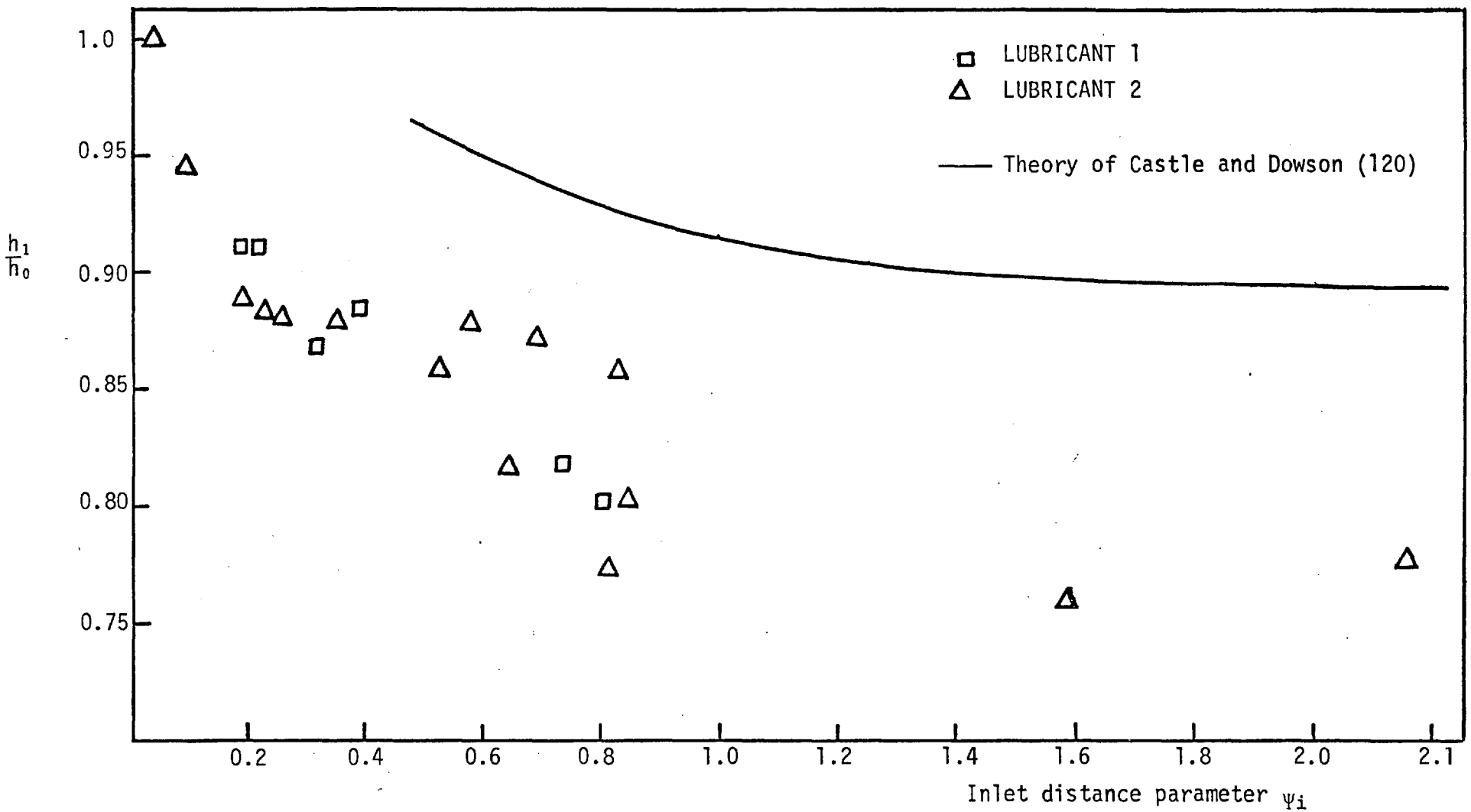

Figure 6.7 Plot of h_1/h_0 against inlet distance parameter.

One drop of lubricant 2 per roller
Hertz width (static) 0.008in.

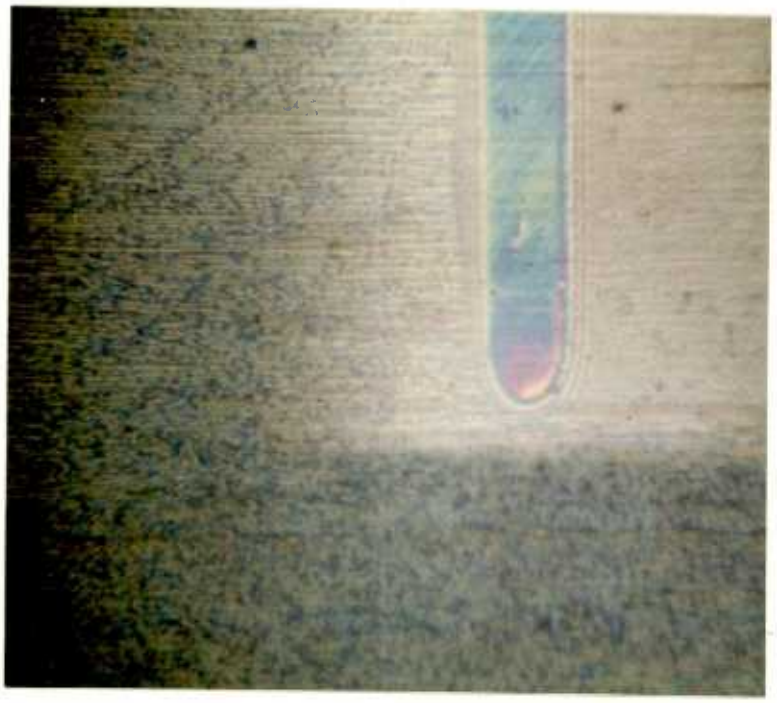

(a) 106 R.P.M.
1st Blue, h_0 = 8.2 µin.
1st Red, h_1 = 6.3 µin.

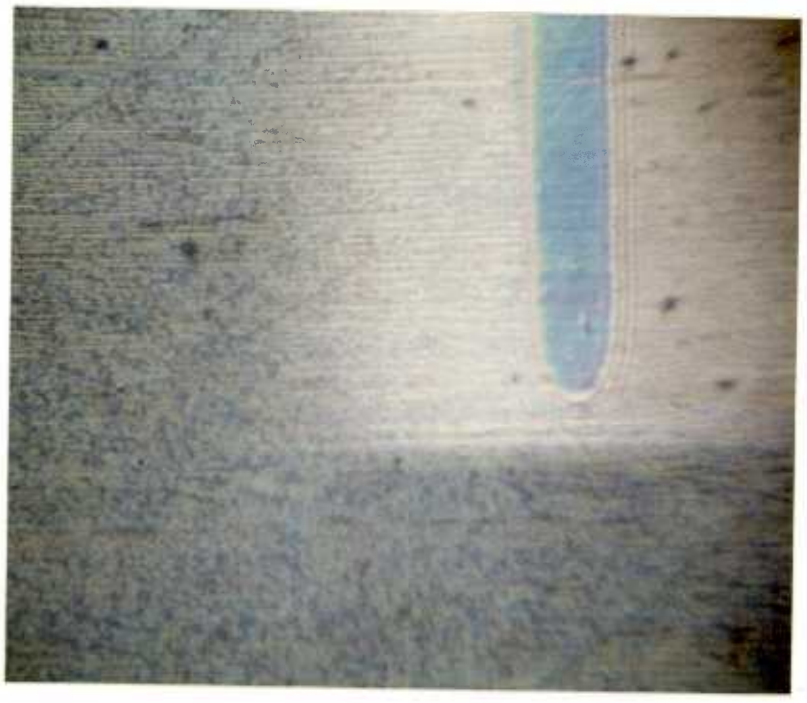

(b) 187 R.P.M.
1st Blue, h_0 = 8.2 µin.
1st Blue, h_1 = 8.2 µin.

Figure 6.8 Interograms, produced using white light, illustrating the effect of acute starvation on the side and exit constrictions.

the speed, and hence the degree of starvation, has had the beneficial effect of removing the constrictions, even though the contact is supported by a substantial oil film (8 μin.). Under conditions of acute starvation the film thickness is limited by the amount of oil brought into the contact region by the bearing surfaces. As there is effectively no inlet region, oil that is on the edge of the track surfaces on the roller and the race, is carried straight into the high pressure contact zone, and cannot be lost around the roller edges. Therefore there is no pressure drop off in the entry region, at the contact edges, and no side constriction is produced. These observations again emphasise that the inlet conditions control the film thickness and contact shape.

In these experiments, where the supply of lubricant was inadequate for fully flooded operation, the limiting film thickness was determined by the amount of oil available. As this limiting film thickness is approached, the quantity of oil available in the inlet regions is decreased, and the degree of starvation becomes increasingly severe. Thus the film thickness becomes less and less sensitive to changes in speed, and the other parameters that control film thickness in E.H.D. contacts. Under these conditions the film thickness is extremely sensitive to any additional supply of oil. Figure 6.9 (taken from the television monitor) shows the effect of a small quantity of oil reaching the inlet of an extremely starved contact. The fringe pattern, which is approximately symmetrical, reflects

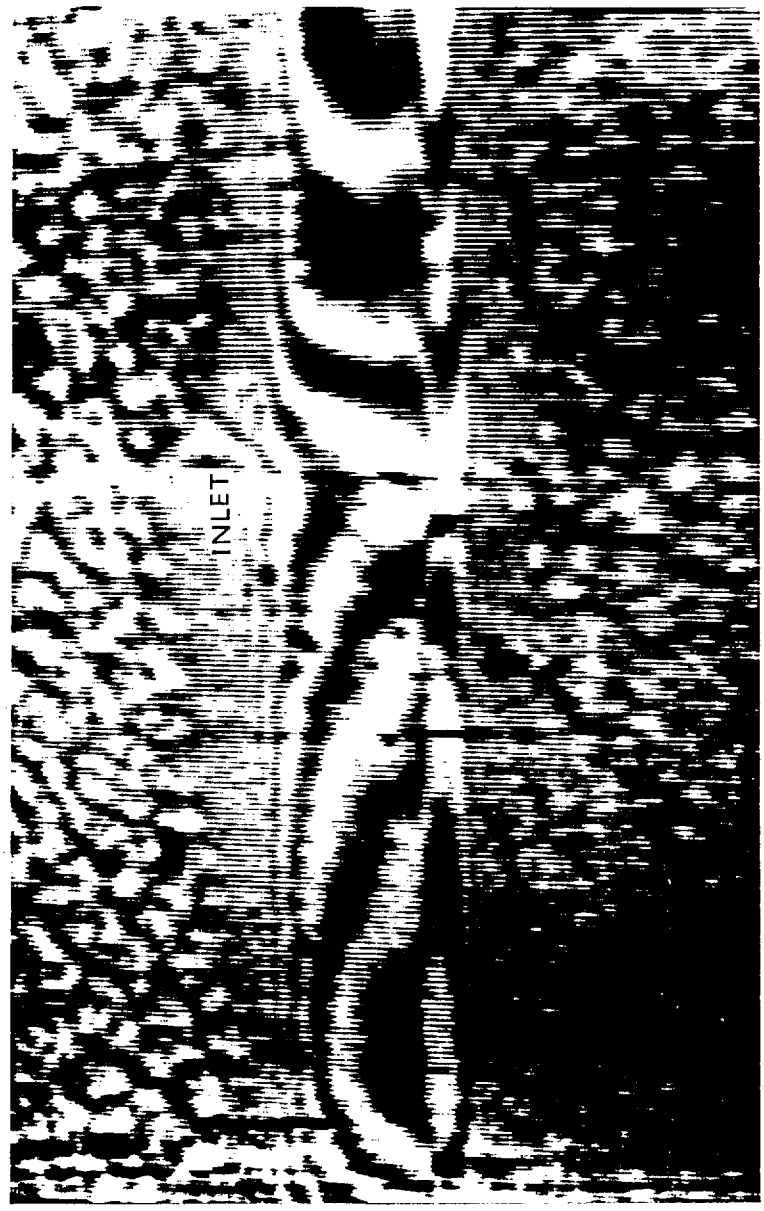

165 R.P.M. (3000 cS mineral oil)

Figure 6.9 Interferogram illustrating the effect of a drop of oil reaching the inlet of a starved contact.

the shape of the inlet boundary, and illustrates the contact adjusting to the new inlet conditions.. The shape of the fringes shows that the film thickness is not constant across the normally parallel region of the contact, and this is an indication of the highly transient conditions. A drop of oil, entering the inlet region of an acutely starved contact causes a rapid change in film thickness, and a torque jog. It is for this reason that torque jogs are associated with positional instabilities in gyro bearings.

6.4 Additional Experimental Observations

6.4.1 The Effect of Uneven Roller Spacing.

Chiu's starvation theory (123) for point contact is based on the hypothesis that the position of the inlet boundary and hence the degree of starvation, is controlled by the rate at which oil, from the track sides, replenishes the depleted area immediately after the passage of a contact. He proposes that the degree of fluid replenishment is dependent upon the contact time interval, the oil/air surface tension and the oil viscosity. If Chiu's theory is correct, greater boundary distances would be expected at the contact edges, than in the centre. At low shafts speeds this was frequently the case (see figure 6.10(a)). At constant speed, the time between contacts is dependent upon the roller spacing and therefore, in order to ascertain whether this mechanism

of lubricant replenishment was causing the increased boundary distance at the edges, two diametrically opposite rollers were removed from the bearing. Under constant running conditions the time delay of the flash could be adjusted to view, either a roller preceded by a normal spacing, or a roller preceded by a double spacing.

Throughout the speed range there was no consistent difference between the shape, or position of the boundary, across the whole contact length of these two rollers. To determine whether this type of replenishment action was being masked by the copious supply of lubricant, the bearing, with the two missing rollers, was run under starvation conditions. Again the roller spacing was observed to have no effect on the inlet boundary.

These findings suggest that the mechanism of lubricant replenishment is independent of the roller spacing, and that the make-up flow, required to replenish the oil that was being continually lost around the contact sides, was provided by the rollers.

6.4.2 The Effect of the Roller Edges on Lubricant Supply.

It was noted that if the bearing was run with oil supply at low speeds, the inlet boundary would adopt a shape that curved away from the contact ends. This concave shape indicates that replenishment is taking place from the contact edges. If the oil supply was switched off, the boundary

would reverse to a convex shape, in which the ends of the contact were depleted of oil. The two photographs presented in figure 6.10 illustrate this effect. As the speed was increased, a concave boundary would tend to straighten, and eventually reverse to a convex shape. The higher the viscosity of the oil, the lower the speed at which this change in shape occurred.

The concave boundary at the roller edges is similar in shape to that which occurs, in the inlet region, at either side of a point contact. Therefore, to elucidate the mechanism of oil replenishment that appeared to be occurring atthe contact edges, the television camera was arranged to view directly the rolling contact, formed between a rotating glass plate and steel ball, in a counter-rotating rig. This rig comprised of a single ball loaded against the lower side of a driven flat glass plate, in a thrust bearing arrangement. The ball was supported on cones that contacted the ball far enough apart so as not to effect the lubricant films, left on the ball surface from the contact at the plate. The arrangement is shown in figure 6.11. The magnification on the video monitor of approximately X20, enabled the complete oil distribution around the contact to be viewed. The lubricant used for this study was a phosphate ester (Reolube L752) and was aerated, using an emulsifier, to allow flow visualisation. This lubricant, of moderately high viscosity (3600 cS at 25^{o}C), was used because of its stabilising effect upon the foam. About 0.25 cubic in. was applied to the disc

348 R.P.M. (lubricant 2)

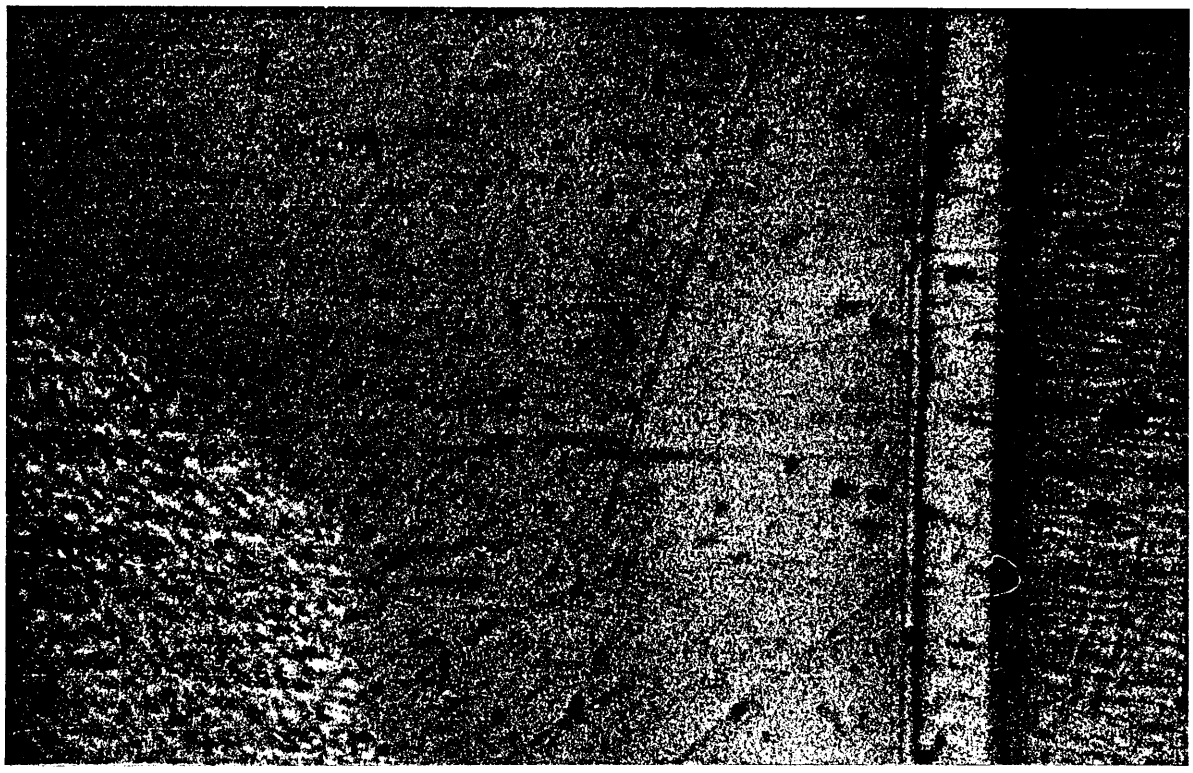

(a) Oil jet on

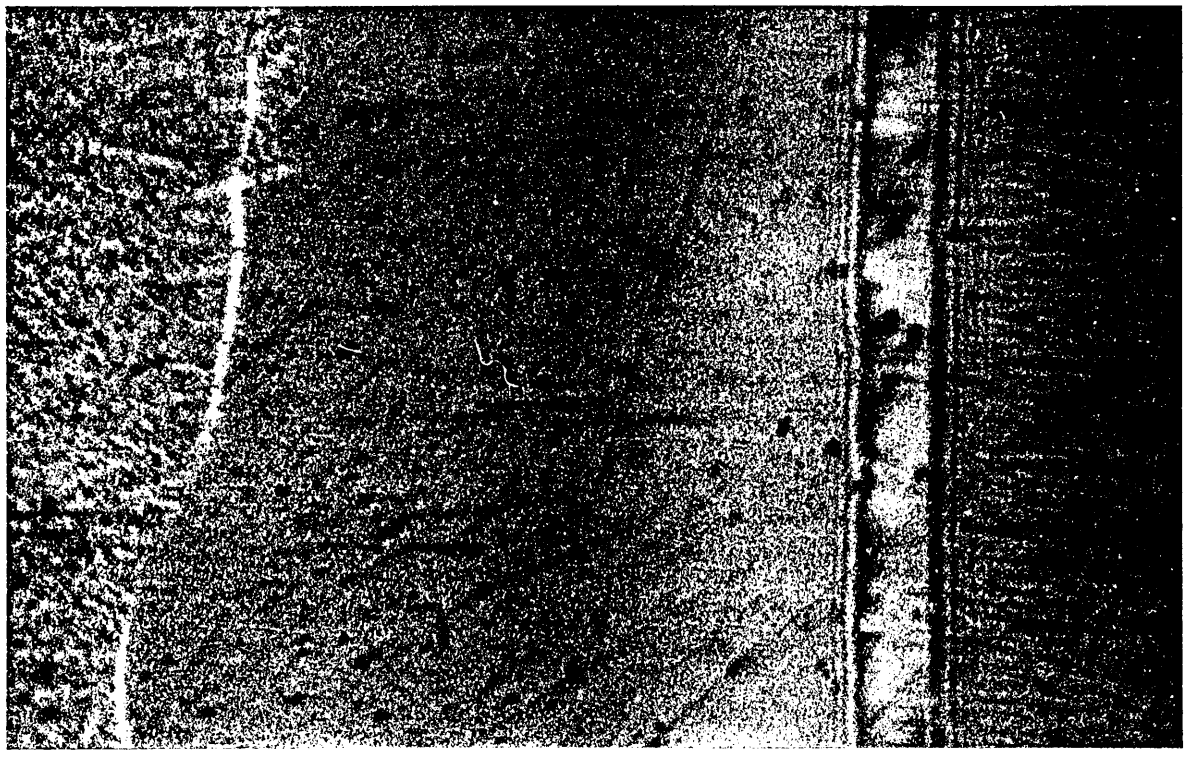

(b) Oil jet off

Figure 6.10 Photomicrographs illustrating the effect of oil supply on the boundary shape at the edge of the contact.

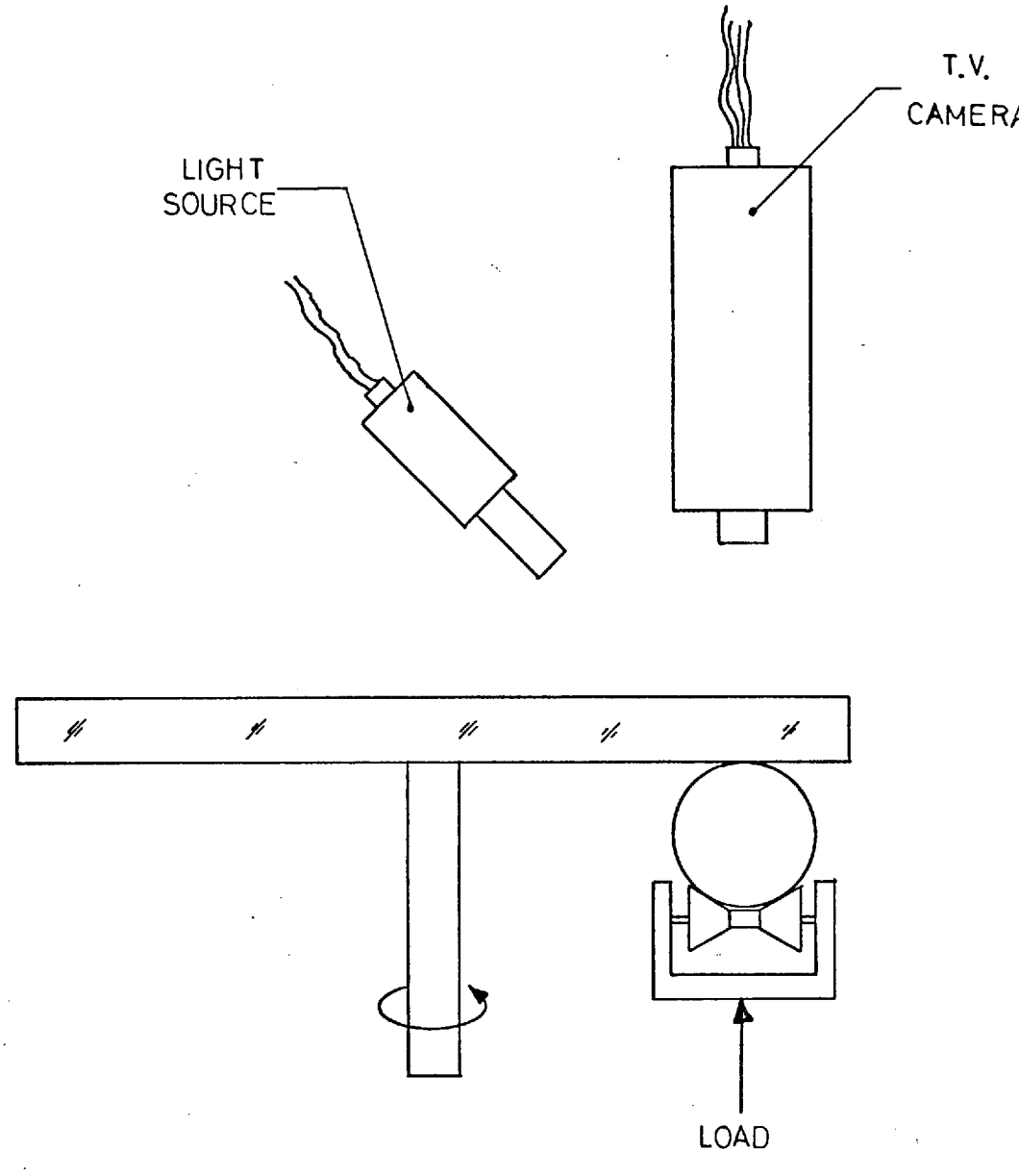

Figure 6.11 Experimental arrangement for visualisation of the flow around a point contact.

surface. Optimum reflectivity from the bubbles was obtained by illumination at oblique incidence, and when the rig was set in motion the passage of the bubbles around the contact region gave the appearance of the streamlines. A photograph taken from the video monitor, is presented in figure 6.12. Although the streamlines, revealed by the path of the bubbles, are not well defined (to illustrate this effect the tape must be run continuously), the shape of the oil boundaries around the contact region is clearly visible. The 'butterfly' shape is characteristic of the oil distribution around this type of contact, and is stable at all but the lowest speeds.

At extremely low speeds the two bands of oil, that have passed around the contact region, merge and form a meniscus around the rear of the contact. This meniscus encloses the wake, and ensures that the track is completely replenished with oil. If the speed is increased this system becomes unstable, and turbulent effects cause the oil to split into two distinct side bands. The speed at which this occurs is principally dependent upon the viscosity of the oil. Once the meniscus has split, the side bands of lubricant do not merge until the following inlet region. The oil that has passed through the contact is left on the surface of the ball and race in the form of streamers, which are interspaced by air. Figure 6.14 illustrates the appearance of the cavitation streamers, just before the inlet boundary, at the edge of one of the contacts in the test roller bearing.

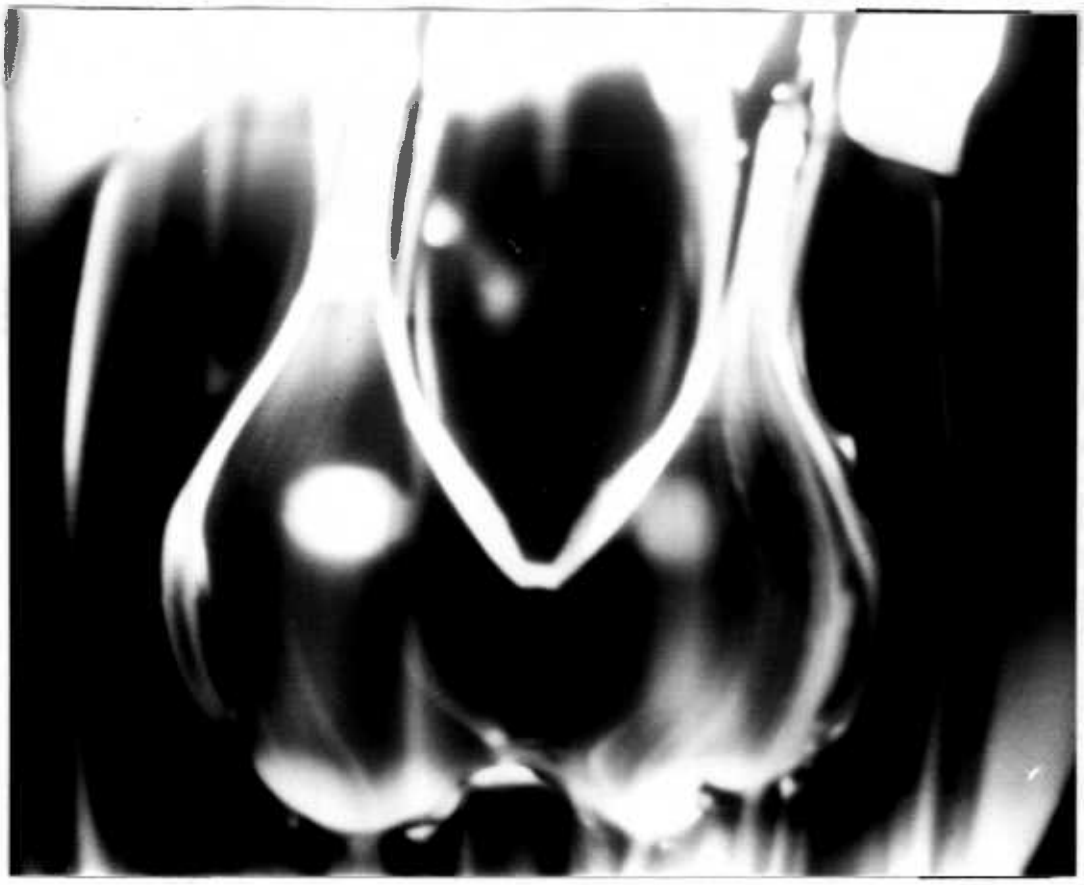

Figure 6.12 Photograph taken from the video moniter, illustrating the distribution of oil around a point contact.

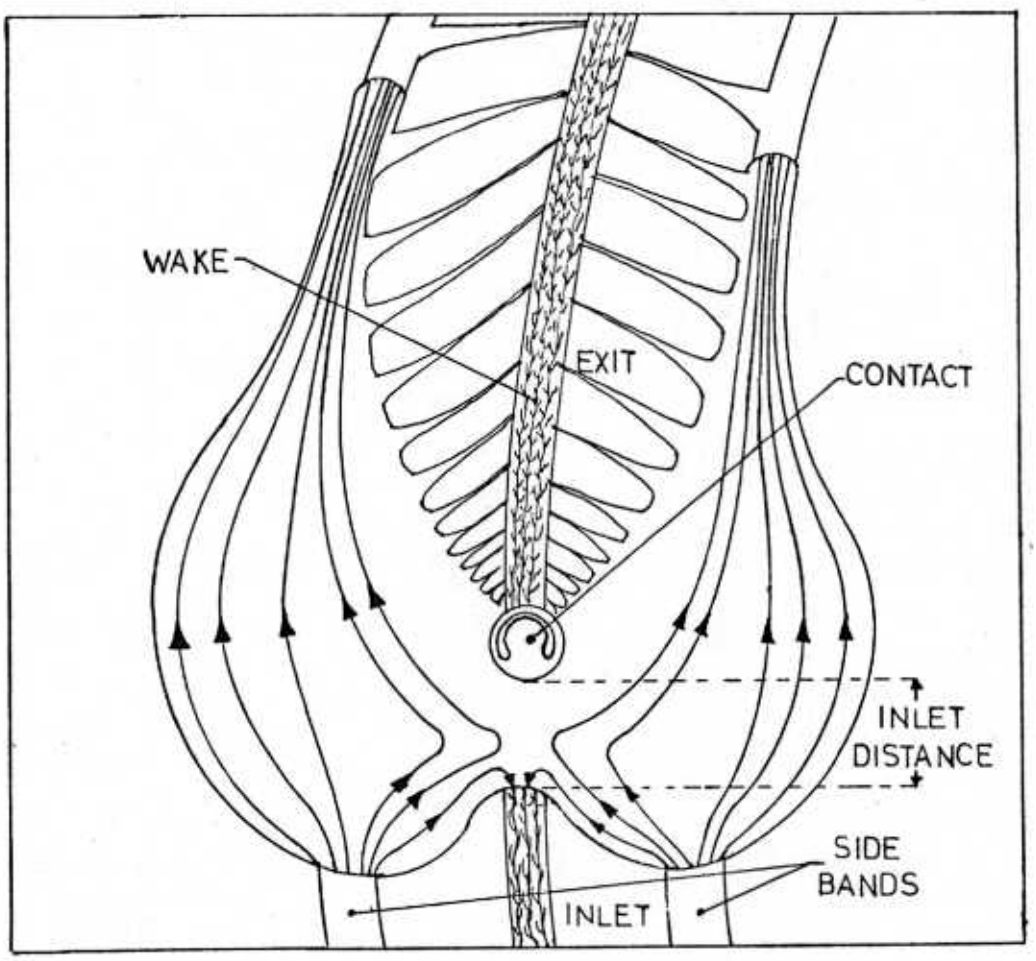

Figure 6.13 Shape of the streamlines, as traced by the bubble movement around a point contact.

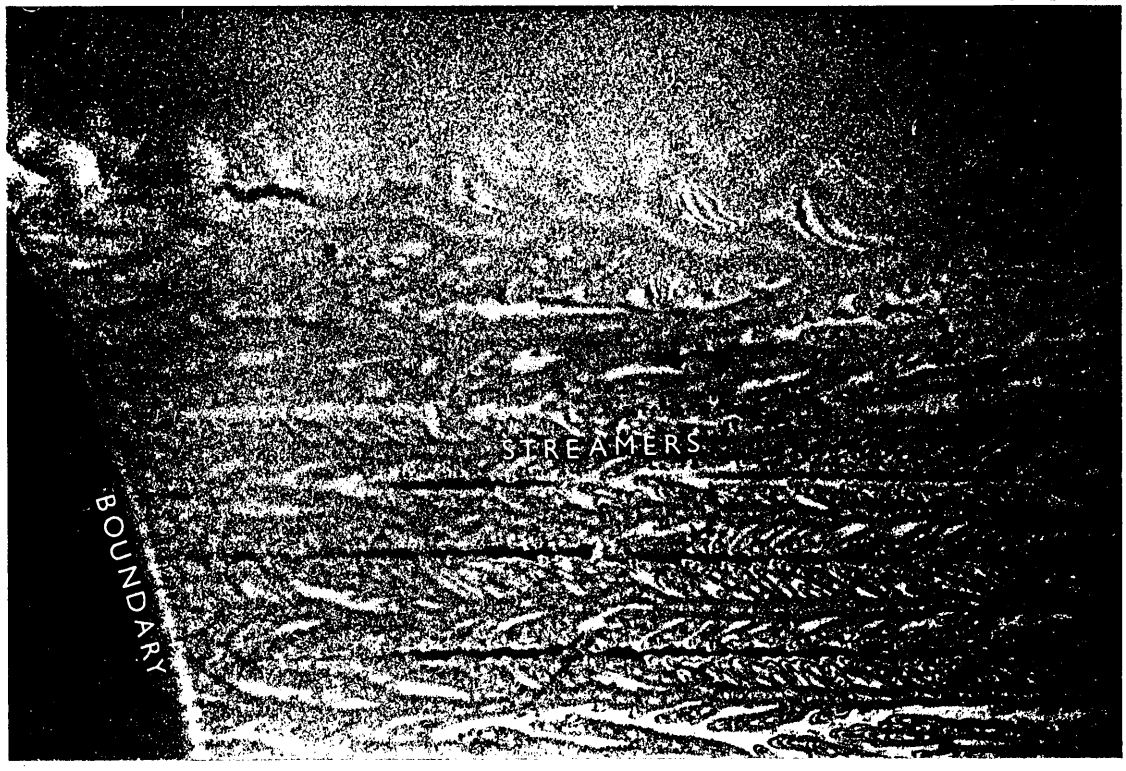

419 R.P.M. (Lubricant 1)

Figure 6.14 Photomicrograph illustrating the appearance of the cavitation streamers just before the inlet boundary.

There is no interconnection of the streamers, and therefore no path by which the track can be replenished from the side bands during the contact time interval, which is the mechanism that has been suggested by Chiu (123).

The form of the streamlines, as traced by the movement of the bubbles, as well as the position of the contact and appearance of the wake, are shown in figure 6.13. No bubbles were visible in the immediate vicinity of the contact, where it is presumed the gap was smaller than the bubble diameter. At constant conditions the positions of the boundaries are stable, which indicates that flows to and from the system are in equilibrium. The combined thickness of the lubricant side bands, held on the surfaces of the ball and race, is greater than the gap at either edge of the contact. Therefore when this fluid enters the converging region it is forced to spread laterally, causing the side bands to merge with oil in the inlet region. The majority of the flow passes around the edges of the contact area, and the remainder is entrained in the inlet to replace that lost, from this region, by side leakage. It was observed that the air bubbles, that were drawn into the contact entry region, moved close to the inlet boundary and followed the boundary curve until they were in line with the contact. At this point the direction of motion reversed and the bubbles appeared to vanish. This indicated that the fluid was being caught up in one of the vortices that exist in

this region where reverse flow occurs (see figure 2.8).

To the rear of the contact the surfaces diverge, and the lubricant is drawn together by surface tension to form two thin webs, that straddle the gap between the ball and the race. The oil that has passed close to the sides of the contact area, where the gap is correspondingly smaller, cavitates and is split into large streamers, that are left on the surfaces at either side of the wake produced by the oil that has been through the actual contact. The rearmost boundaries mark the end of the webs, beyond which the oil is completely divided between the ball and plate, and is moved at the surface speed.

At a steady film thickness the amount of oil leaving the contact area is equal to the amount supplied to the contact by the track surfaces, provided there is no loss and it is assumed that there is negligible fluid replenishment, from the track sides, during the contact time interval. The re-appearance of the cavitation streamers in the entry region indicates this to be the case, and therefore the position of the inlet boundary is determined solely by the requirement that a balance must be maintained between the rate at which oil is lost from the entry region, and the rate at which it is entrained.

It was observed that, for otherwise constant conditions, an increase in speed caused a decrease in the inlet boundary distance. This is not thought to be caused by a

change in E.H.D. film thickness. The side bands of fluid act as reservoirs, that remove or supply oil to the track surfaces, if changing conditions alter the film thickness. This process, which only takes place around the contact region, requires removal or supply of a volume of oil that is extremely small, and will result in a negligible change in the volume of oil contained in the side bands. The flow rate of oil approaching the contact, in the side bands, is directly proportional to the speed, and therefore, if the filling of the entry region was only controlled by the spreading of these bands, as they pass into the convergent region, an increase in speed would not be expected to effect the boundary position. The rate at which oil is lost from the entry region is proportional to speed and boundary distance. It is proposed that the rate of entrainment is less dependent upon speed, and therefore as the speed is increased, the inlet boundary must form closer to the contact to maintain equilibrium. Surface tension forces may be partially responsible for the entrainment phenomena, and these will only depend upon the boundary shape. This mechanism of fluid replenishment would explain why starvation can occur even though considerable quantities of oil are still contained in the side bands.

The contact at the edges of a blended roller is similar to a point contact, and a concave inlet boundary indicates that the edges are supplying oil to the entry region in the manner as described above. To examine

whether oil was being held by the blend on the roller edges, the television camera was mounted to view the side of the bearing through the perspex cover, and stroboscopic illumination was provided. Large side bands were observed on the outer race, at either side of the track, and when oil was continuously supplied to the bearing at a flow rate of about 5 gallons per hour, these bands occupied the whole of the gap between the outer race and the cage. Also immediately apparent, at either side of the track in the exit region, were the webs of lubricant, formed between the roller and the outer race. A photograph, taken from the video monitor, illustrating these webs is presented in figure 6.15. The webs, identical to those formed in the point contact situation, show that oil was being carried on the roller blend.

To determine whether the curved edge was influencing the inlet boundary, the blend was removed from one edge of a roller by grinding. A central region of $^{1}/_{4}$ in. diameter was left to locate on the side of the cage. As the rollers were already slightly barrelled (as well as blended), the effective length of the contact was not shortened, so a severe edge constriction was avoided. The removal of the blend was found to have a consistent effect on the boundary shape at the contact end. The two photographs presented in figure 6.16(a) and (b) were taken under identical conditions, and show that no oil was being en-

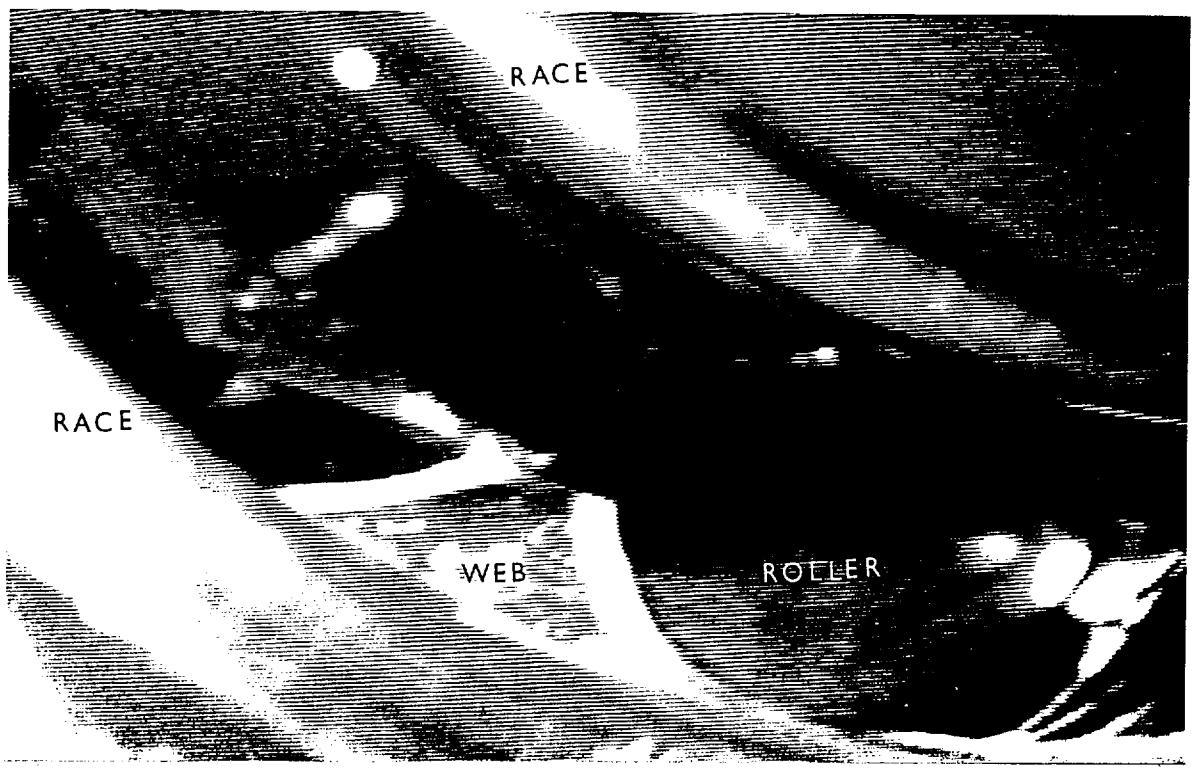

Figure 6.15 The appearance of the lubricant webs at the roller edges.

403 R.P.M. (Lubricant 2)

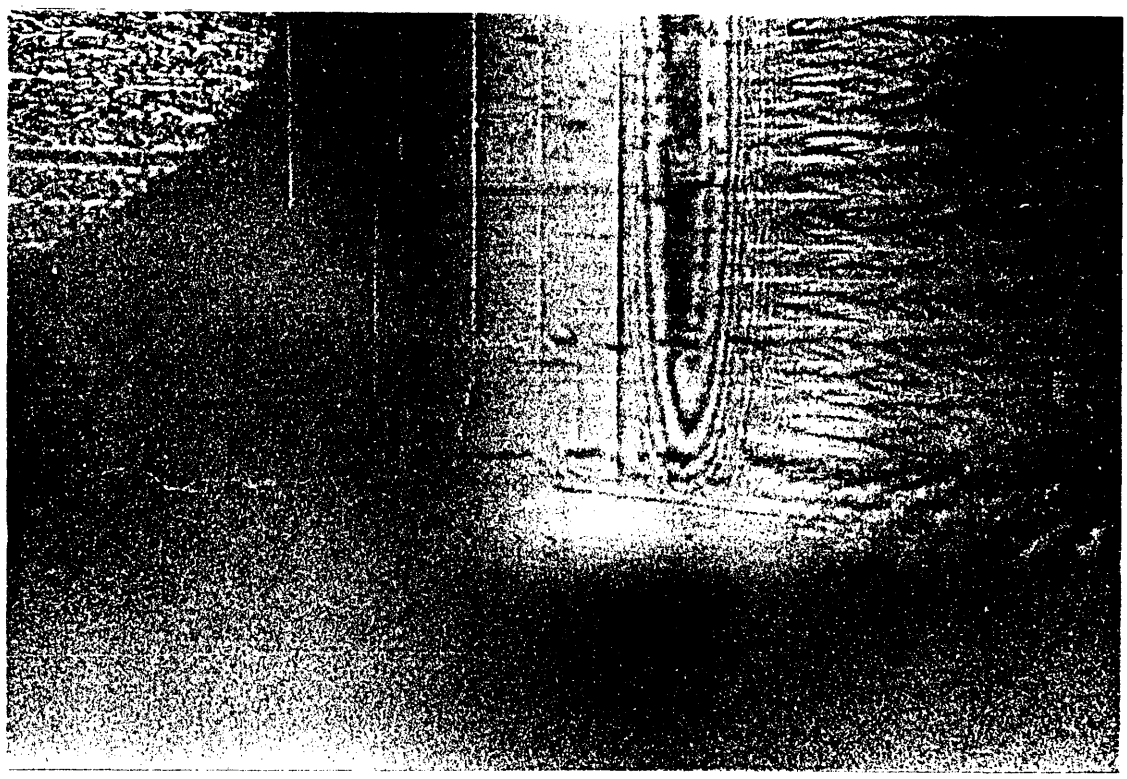

(a) blended

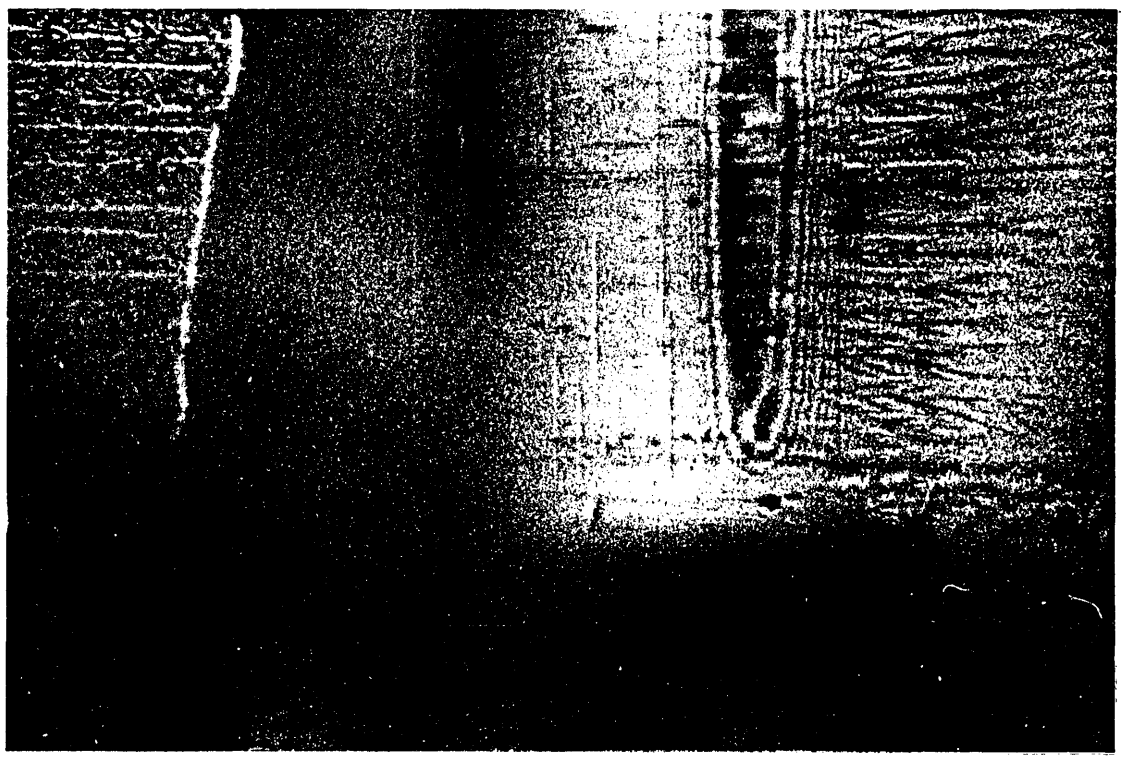

(b) unblended

Figure 6.16 The effect of blending on the shape of the inlet boundary.

trained by the edge of the unblended roller.

Under starvation conditions it was noticed that a roller having a shorter contact width, ran more acutely starved. This was caused because the short contact was unable to be supplied from the side bands. Two photographs, taken from the video monitor, illustrating this effect are shown in figures 6.17(a) and (b).

The function of the edges in supplying oil to the contacts was demonstrated by running the bearing under severely starved conditions, and placing a small quantity of oil (about 0.03 cubic in.) near the edge of the track. Simultaneous observations were made, under stroboscopic illumination, of the rollers through the perspex cover, and of the contact edges through the sapphire window. The oil was observed to flow gradually towards the roller edges, and as soon as pick up occurred,characterized by the formation of the webs, the inlet boundary and the film thickness were seen to build up from the contact sides. Once oil was brought into the entry region, the inlet pressure build up assisted in moving it along the length of the contact, until an even film thickness was obtained. The photograph presented in figure 6.18 illustrates the end of a contact running at a film thickness 80 μin. larger than that at the centre. At constant speed the rate at which oil moved along the contact was found to be extremely dependent on viscosity. An oil, having a viscosity of 400 cS at 100^{o}F, took several

178 R.P.M. (Lubricant 2)

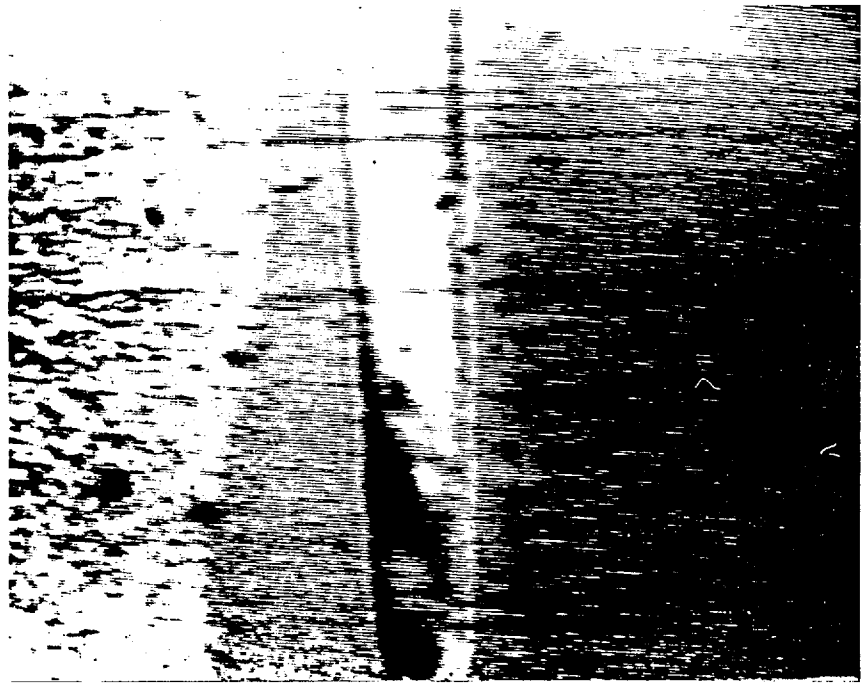

(a) long contact

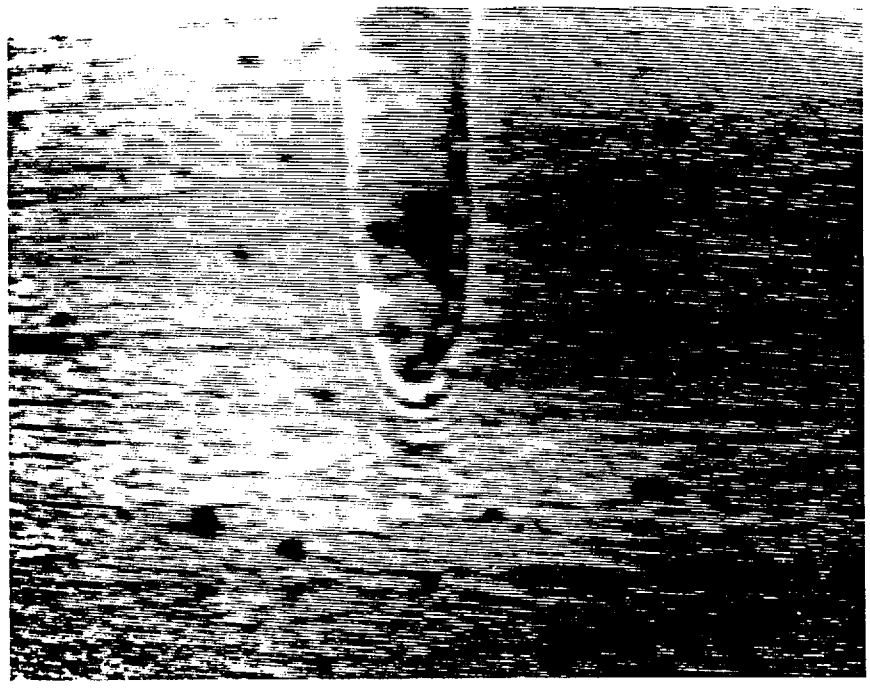

(b) short contact

Figure 6.17 The effect of a short contact on lubricant supply to the inlet region, under starved operating conditions.

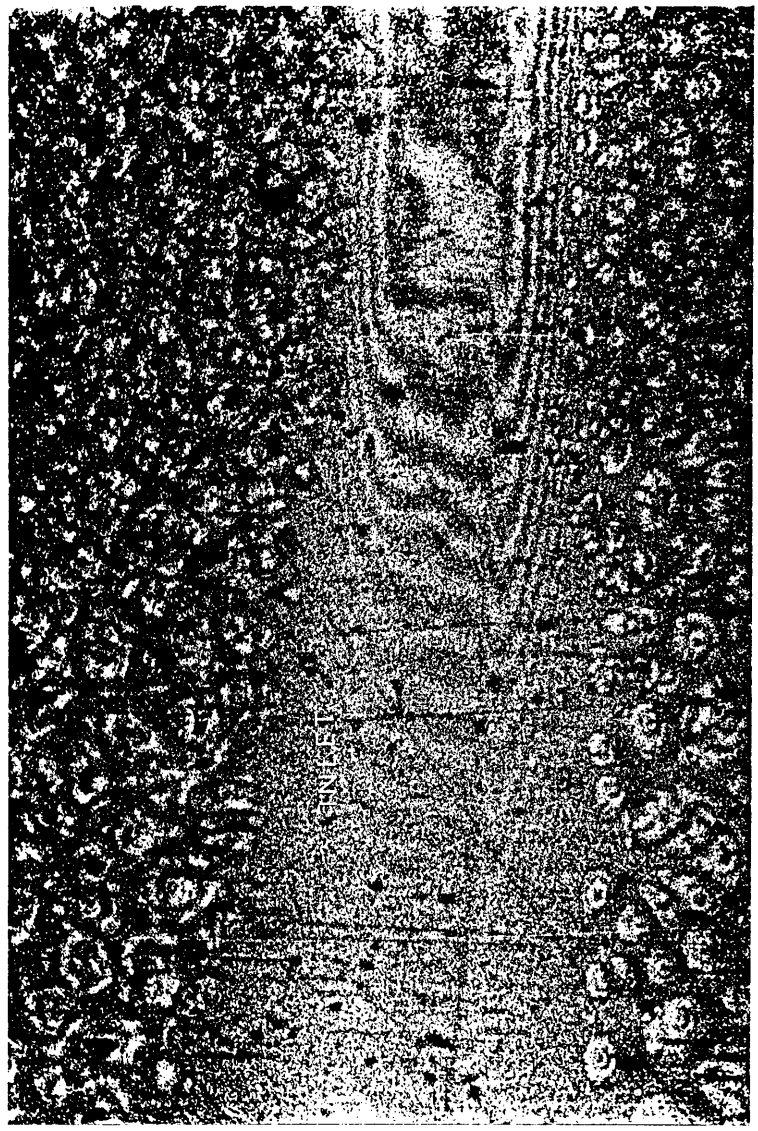

160 R.P.M. (oil : polyphenyl ether, 5P4E)

Figure 6.18 Photomicrograph illustrating pick up by the roller edges causing oil to be supplied to the contact inlet region.

minutes before an even film thickness was formed, whereas lubricant 2 (75 cS. at 100°F) took only a few seconds.

6.4.3 Isolation of the Central Contact Region from the Edges.

To determine the effect of isolating the central contact region from the roller edges, two circumferential slots were ground at either side of a roller, as illustrated in figure 6.19. The slots were ground $^{3}/_{32}$ in. wide, $^{1}/_{8}$ in. deep, and $^{3}/_{32}$ in. from the roller ends. The edges of the slots were slightly chamfered, to remove burns.

Although there was no means by which oil, entrained by the roller edges, could reach the inlet zone of the central contact region, fully flooded conditions were still maintained at the centre of this roller. There was no consistent difference in boundary distance for the isolated contact, and the other contacts in the bearing; this still being the case when the oil supply was switched off. The contact at one edge of the central region is illustrated by the photograph presented in figure 6.20(a). The severe constriction is caused by the unblended edge. The inlet boundary, at either end of the isolated central contact, was always a convex shape, indicating that no fluid replenishment action was taking place from the edges. However there was frequently a small discontinuity in the shape of the boundary, that always occurred in line with the edge. This is evident in figure 6.20(a), and was most likely caused by a small quantity of the oil that was lost by side leakage,

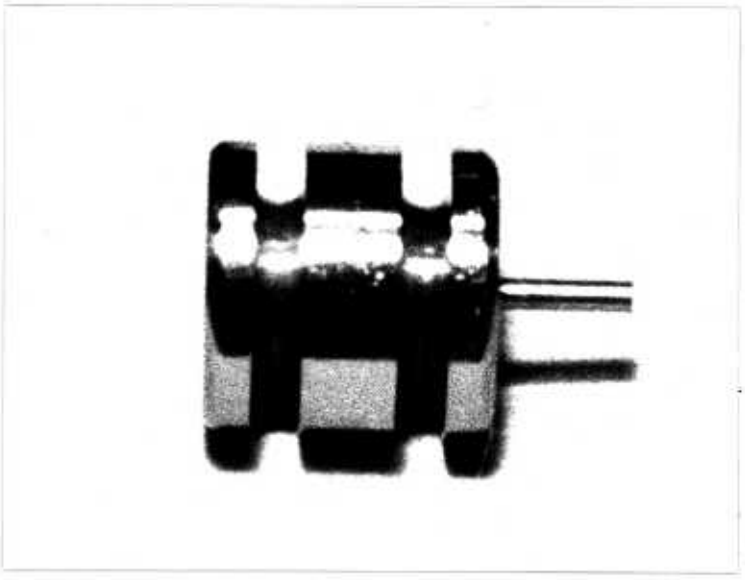

Figure 6.19 The roller with circumferential slots.

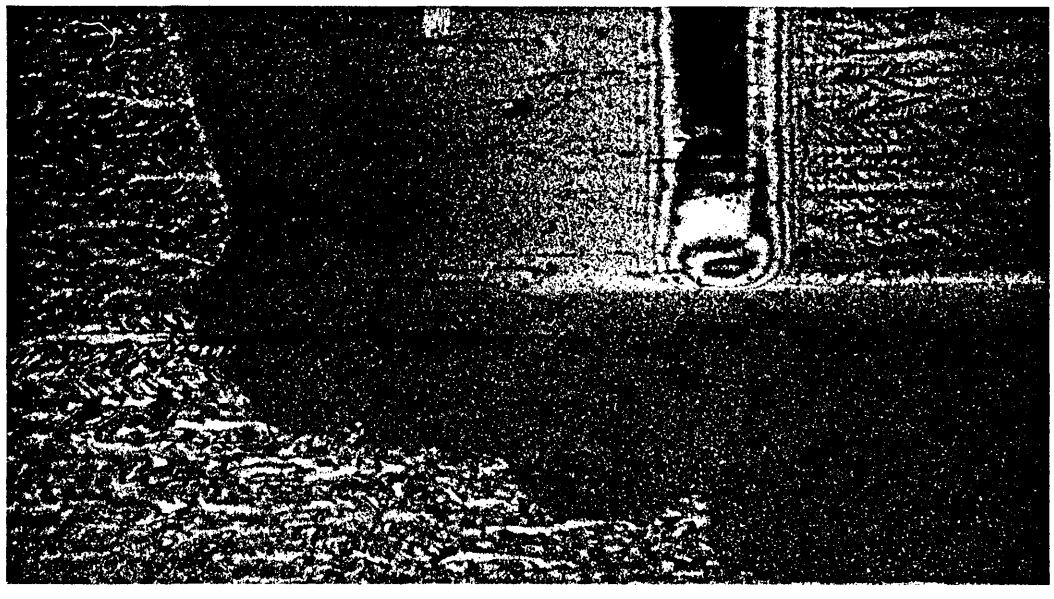

(a) contact at one edge of the slot

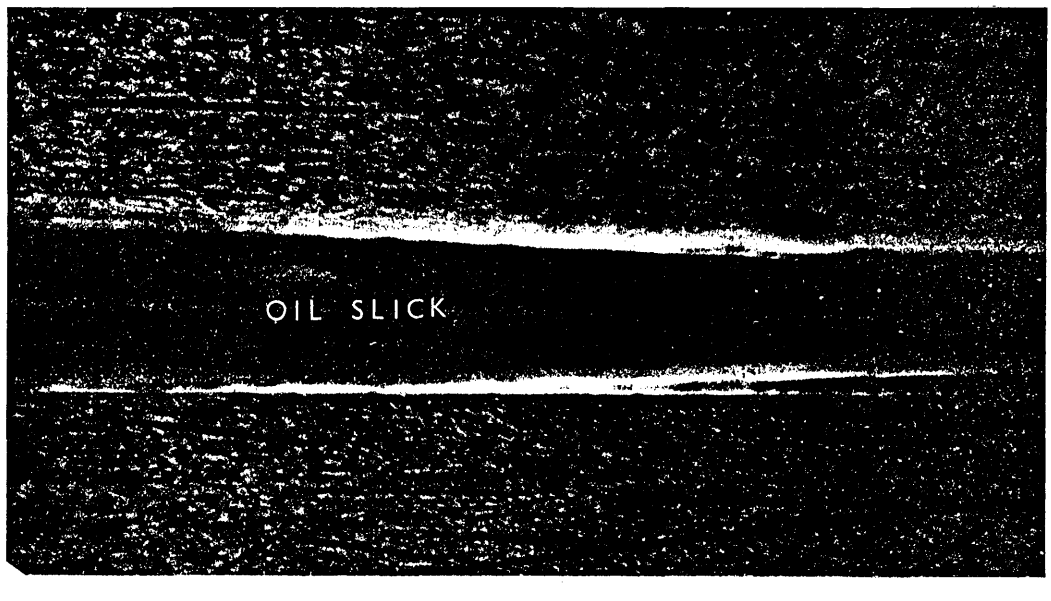

(b) oil slick left on the track surface

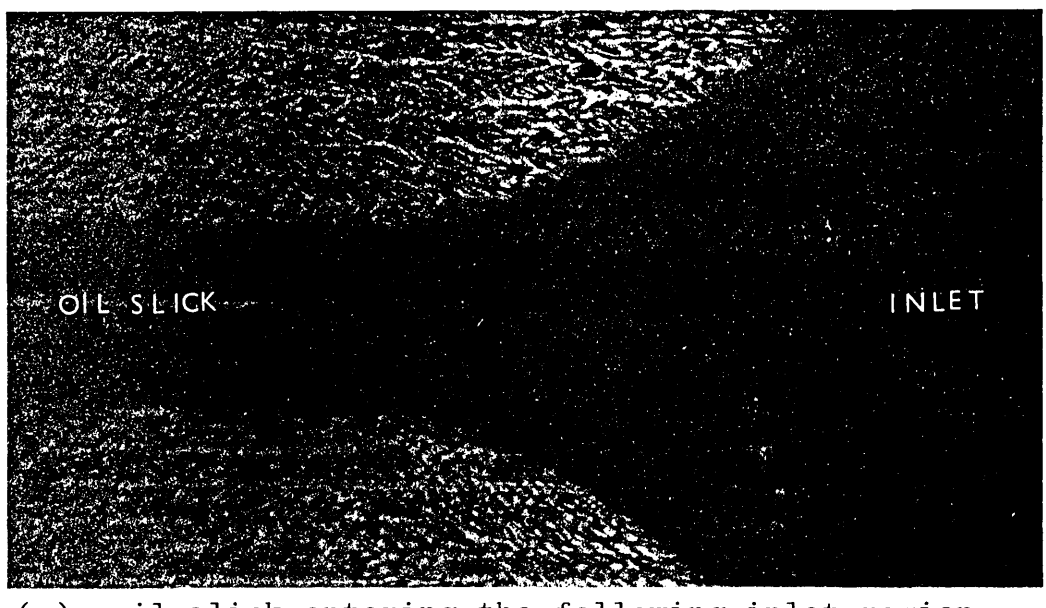

(c) oil slick entering the following inlet region

Figure 6.20 Photomicrographs illustrating the effect of a circumferential slot.

being returned to the entry zone by the edge of the slot.

Use of this special roller clearly demonstrated that considerable losses occur, from the entry region, around the sides of a contact. The oil that was lost around the four contact edges, created by the two slots, was left on the track surface in the form of slicks, as shown by figure 6.20(b). These slicks increased considerably the volume of oil contained in the entry region of the following contact. Figure 6.20(c) illustrates one such slick supplying oil to the following entry region. The rate of oil loss through the slots, as shown by the degree of excess filling of the following entry region, was proportional to the inlet boundary distance, and under starvation conditions no slicks were visible on the track surface.

When the bearing was run with only a small initial supply of lubricant (about 0.3 cubic in.), the boundary distance, at the central contact of the special roller, was considerably smaller than that at other contacts. This is illustrated by a comparison of the two photographs presented in figure 6.21. The situation is similar to that shown by figure 6.17.

When ample lubricant was available, large quantities of oil were continually being lost around the edges of this isolated contact, without causing a drop in boundary distance. This indicated that oil was being supplied by mechanisms other than edge entrainment.

184 R.P.M. (2000 cS mineral oil)

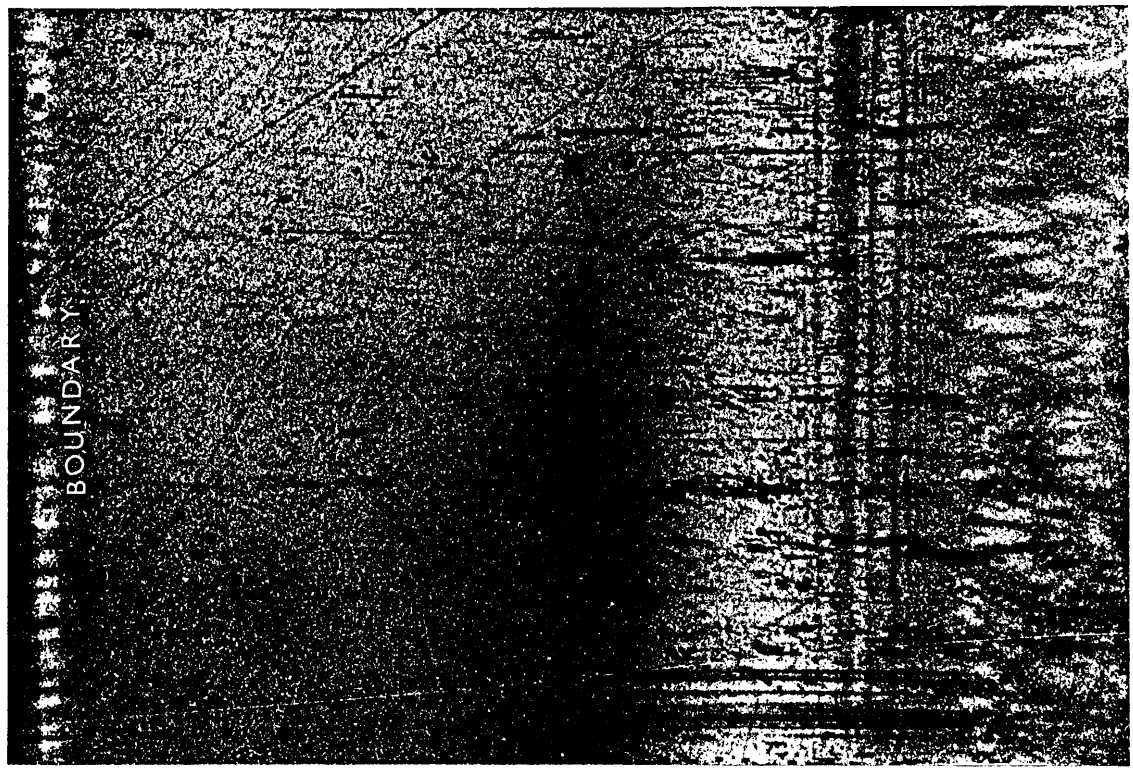

(a) complete contact

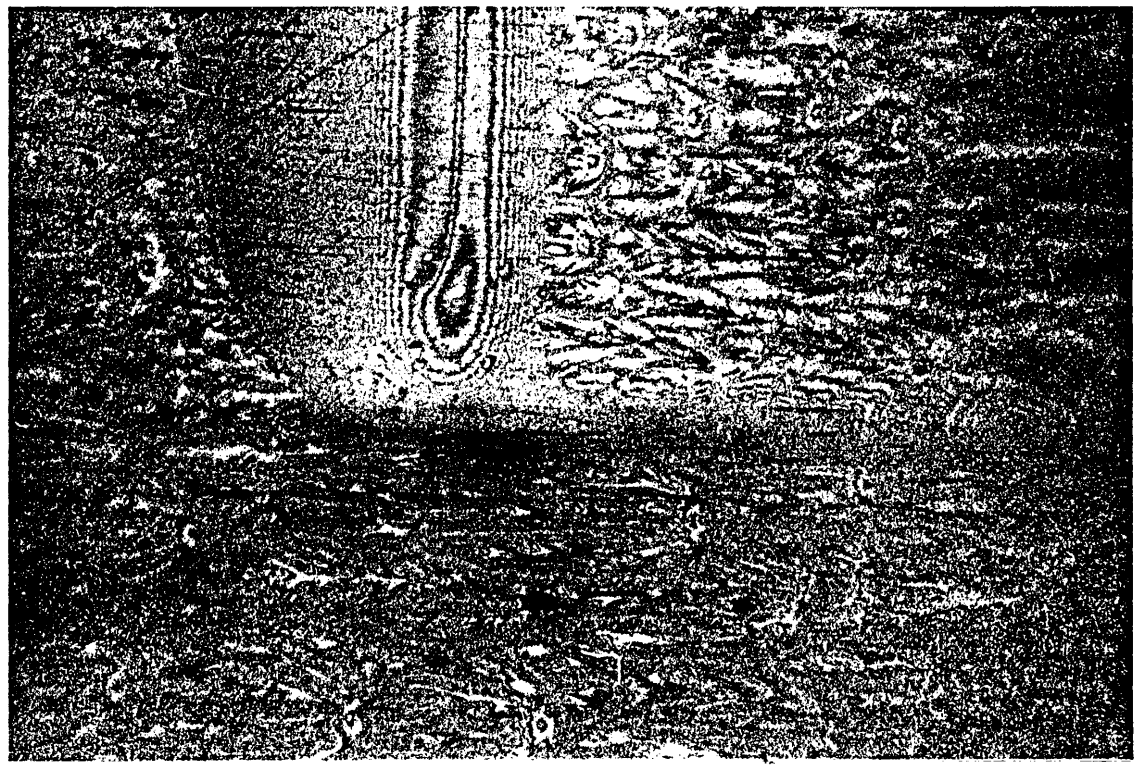

(b) isolated central contact

Figure 6.21 Photomicrographs illustrating the effect of isolating the central contact region under conditions of minimal oil supply.

6.4.4 Isolation of the Roller Surface from the Cage.

This experiment was carried out to determine whether the additional oil, that was obviously supplying the central isolated contact (as described in section 6.4.3), was transferred to the roller surfaces by the cage. The roller surfaces were isolated from the cage by enlarging the cage pocket, and positioning the roller with an axle. This axle was inserted through the roller centre, and the protruding ends were located in two slots, machined in brass inserts, bonded to either side of the cage. The arrangement is shown in figure 6.22.

There was no consistent difference in the inlet boundary distance for a roller mounted in this manner, and for other rollers in the bearing. To confirm that the cage was not responsible for the supply of oil to the central region of the 'slotted' roller, this roller was positioned in the modified cage. These experiments demonstrated that the cage was not significantly influencing the supply of oil to the contacts.

6.4.5 Lubrication of the Unloaded Region.

To investigate the lubrication of the unloaded region, the microscope and sapphire window were positioned so the lowest point of the bearing could be viewed. In this section, the only loading at the outer race contacts is caused by the roller weight, and by centrifugal force. In

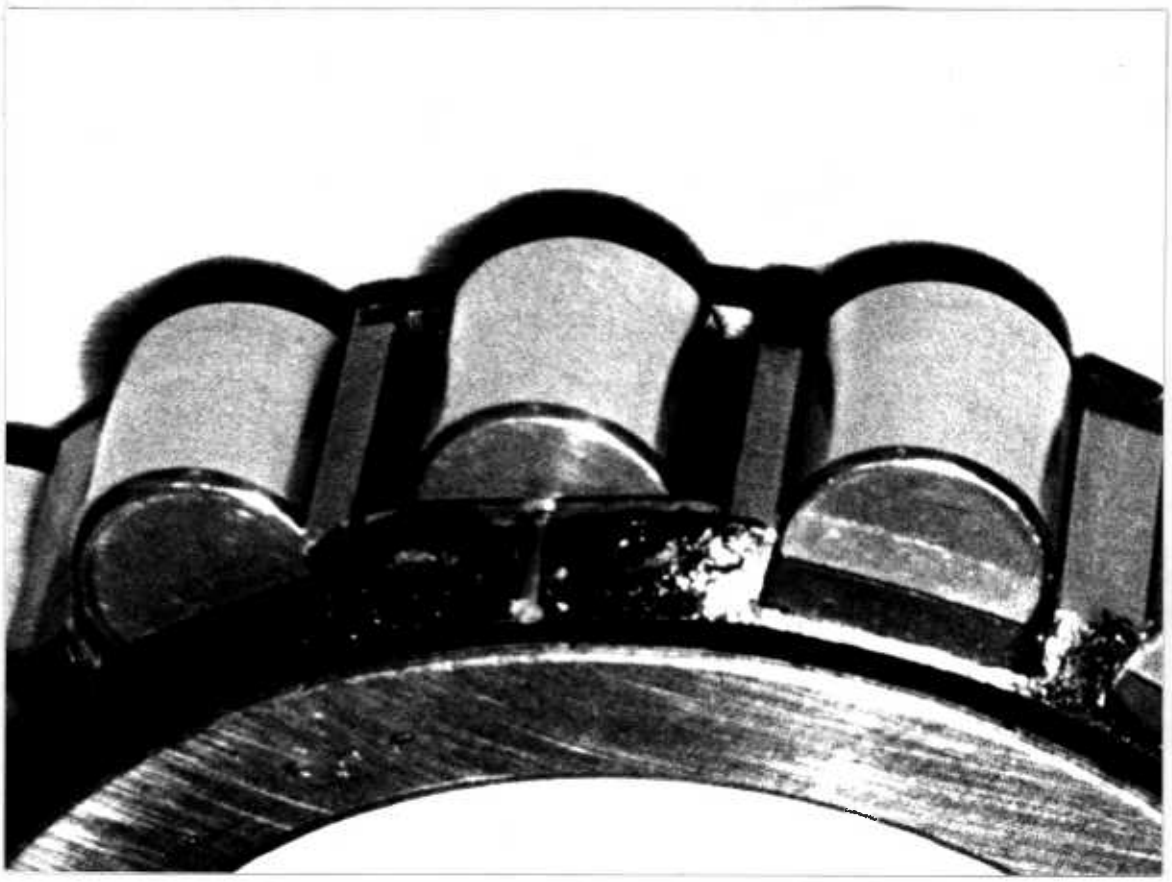

Figure 6.22 Arrangement to isolate a roller from the cage spacing bars.

this configuration, the centrifugal force would not be great enough to cause E.H.D. lubrication, until speeds of about 10,000 R.P.M. are reached (see equation 6.1, section 6.5). The absence of a parallel contact area, and the very thick films developed in this region, prevented measurement of film thickness; however the cavitation streamers, and the inlet boundary could be observed.

The two photographs, presented in figure 6.23, were taken at a shaft speed of 1950 R.P.M. and illustrate the change in conditions when the oil supply was switched off. When oil was supplied (figure 6.23(a)), only a few cavitation bubbles were produced in the contact exit region and no inlet boundary or fringes were visible. Soon after the oil supply was stopped, well defined cavitation streamers, that extended to the inlet boundary of the following contact, were left on the track surface, and faint fringes just became visible (figure 6.23(b)). At this speed centrifugal force causes a roller load of 1.5 lbs. and, for these conditions, the classical theory of Martin (equation 2.1) predicts a film thickness of 700 μin. The bearing has a diametrical clearance of .0 02 in., and a film thickness of this magnitude could be accommodated at both the inner and outer contacts, without causing any additional loading. The absence of any visible frings, when oil was being supplied, suggests that the film thickness was greater than 250 μin. At these very large film thicknesses, the position of the inlet boundary begins to have a substantial effect upon the

1952 R.P.M. (Lubricant 1)

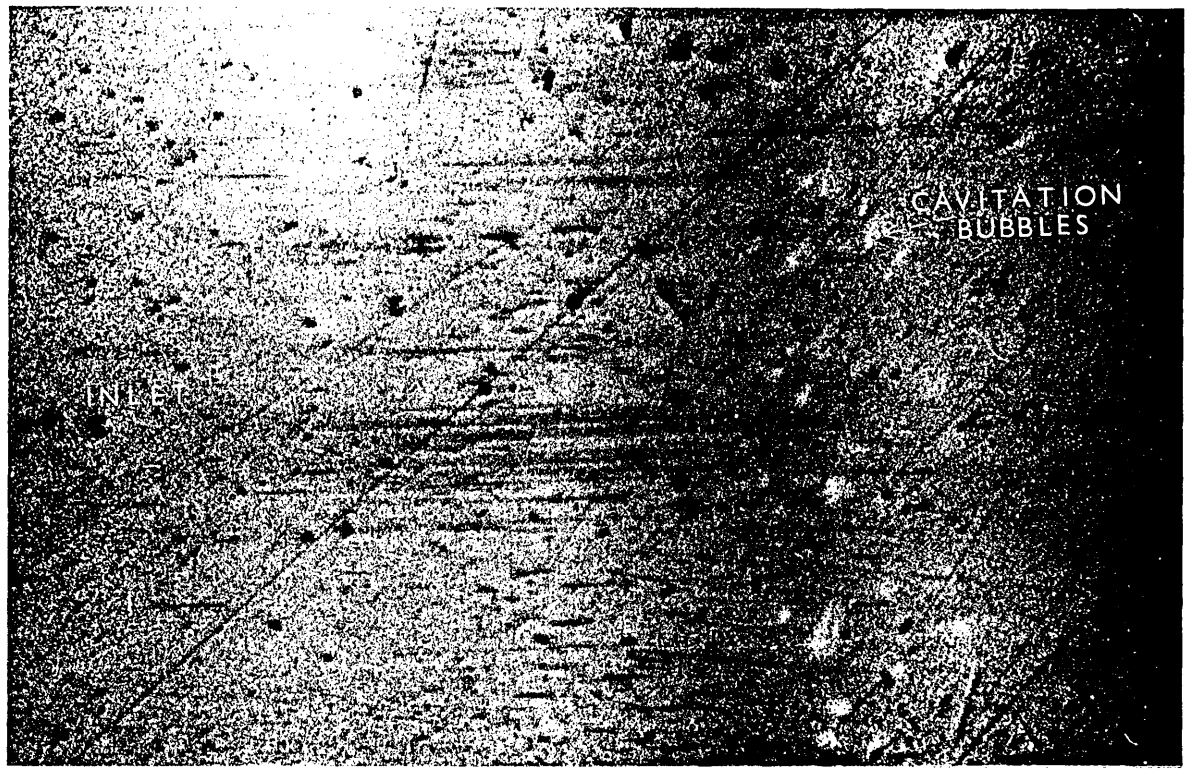

(a) oil jet on

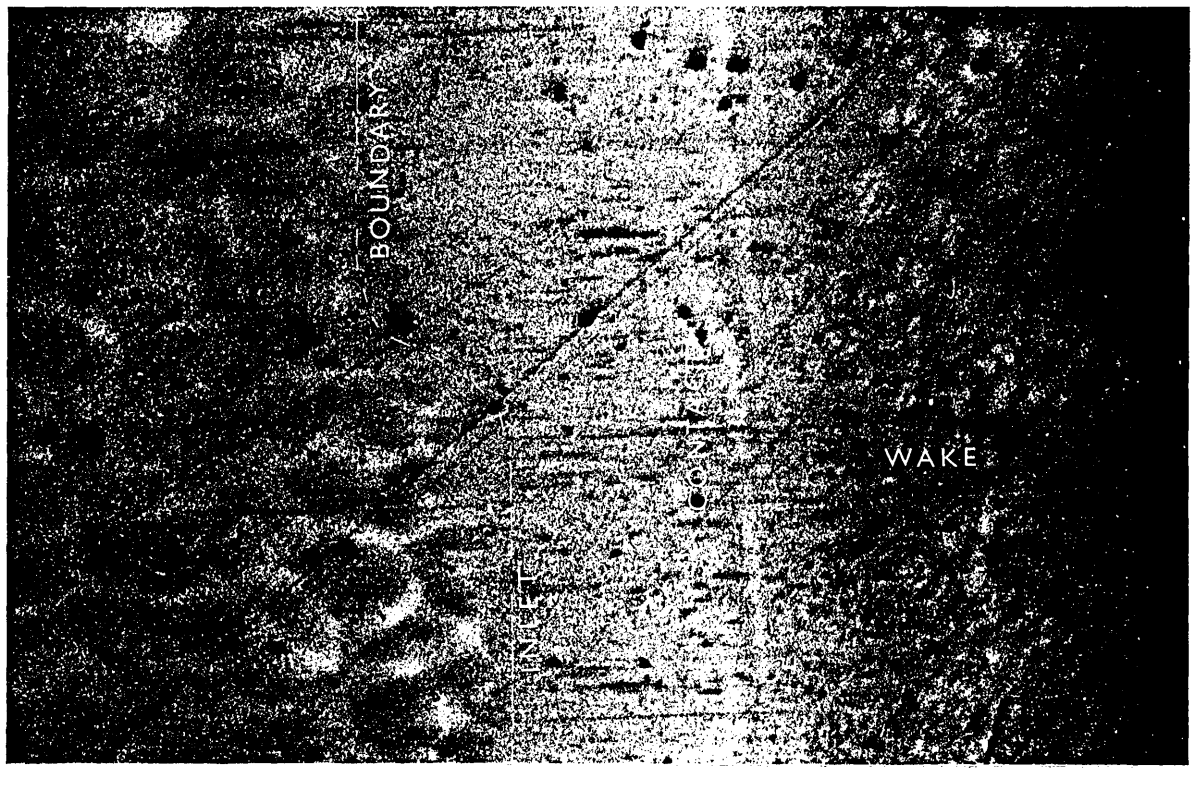

(b) oil jet off

Figure 6.23 Photomicrographs illustrating the appearance of the cavitation streamers in the unloaded section.

film thickness at much larger values of Xi, than for normal E.H.D. conditions. Although it is not possible to measure accurately the inlet boundary distance for the system portrayed in figure 6.23, it is estimated, from the theory of Wolveridge, Baglin, and Archard (119) for classical conditions, that starvation is causing a 70% drop in film thickness, assuming the boundary distance to be constant along the contact length. If the fully flooded film thickness is assumed to be 700 μin., then an actual film thickness of 210 μin. is predicted. This would be consistent with the observation of faint fringes.

Unlike the cavitation streamers formed under E.H.D. conditions, the large streamers, observed in the unloaded region, when the contacts were running fully flooded appeared to reform into a continuous layer of oil, soon after the contact exit. The photograph presented in figure 6.24 illustrates this effect. Although this part of the bearing was usually completely immersed in oil, the wake appeared to reform at a constant rate across the width of the track. This would suggest that the reforming process was caused by surface tension effects, and not by oil flowing through the bearing. This flow could not be observed, and may have been obscured by the continuous layer of oil on the track surface. A comparison of figures 6.23(a) and (b) shows that the oil supply was having a considerable influence on the amount of oil contained in the contact inlets, in this part of the bearing.

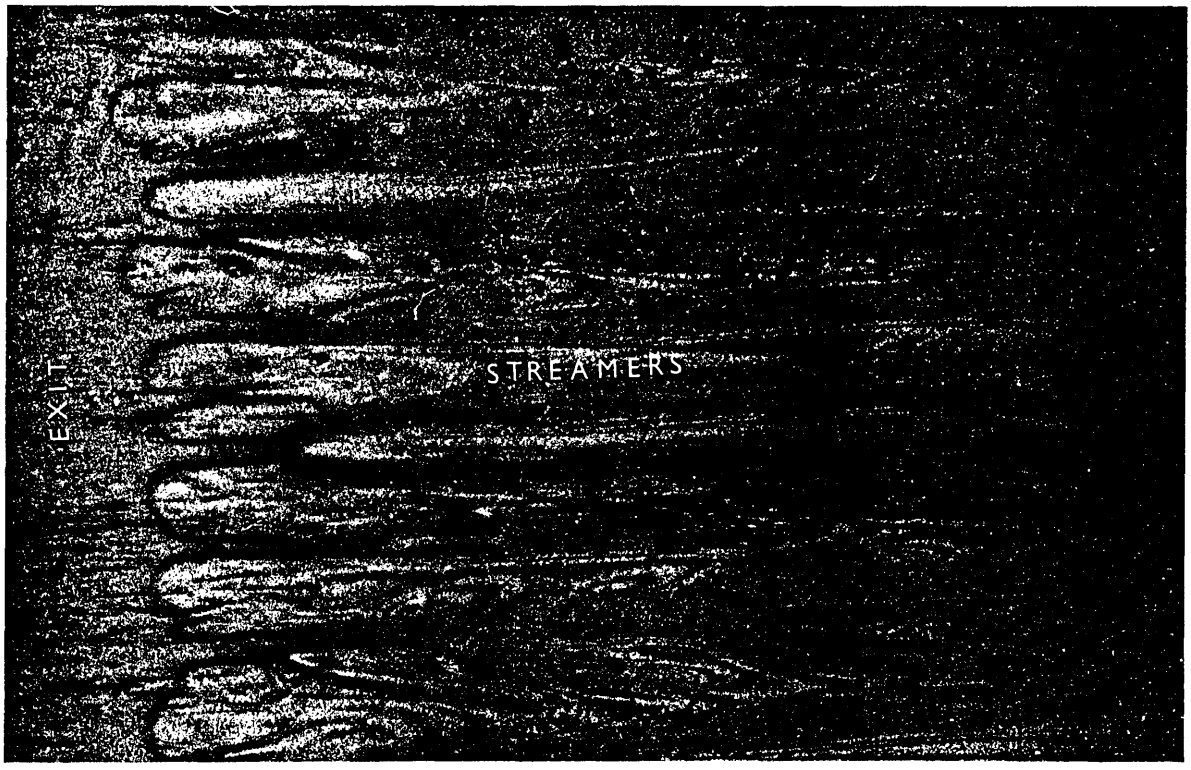

328 R.P.M. (Lubricant 2)

Figure 6.24 Photomicrograph illustrating reforming of the cavitation streamers in the unloaded section.

The large oil films that are formed on the roller surfaces during their passage through the unloaded section, will supply oil to the contact entry regions in the E.H.D. zone at the top of the bearing. This effect is further discussed in section 6.4

6.4.6 The Effect of a Small Roller.

During a test, in which the contacts in the loaded region of the bearing were being studied, it was noted that one of the rollers was virtually unloaded. This contact was supported by a hydrodynamic oil film, and the large cavitation streamers, left on the track surface, had increased considerably the volume of oil contained in the inlet of the following contact. The photograph presented in figure 6.25(a) illustrates the lightly loaded contact. The fringes are quite distinct, and it is estimated that the film thickness was of the order of 100 μin. The concave boundary shape suggests that the edges were supplying oil. When the speed was increased,the boundary distance decreased and in some instances the wake, from the previous contact, broke through the contact area. This effect is illustrated in figure 6.25(b). The area in which this occurs is unsupported by a fluid film, but as there is effectively no elastic deformation, there is no change in film thickness.

The rig was run to a maximum speed of 600 R.P.M., with this roller in the bearing. At this speed, although the boundary position was more unstable, the lightly loaded

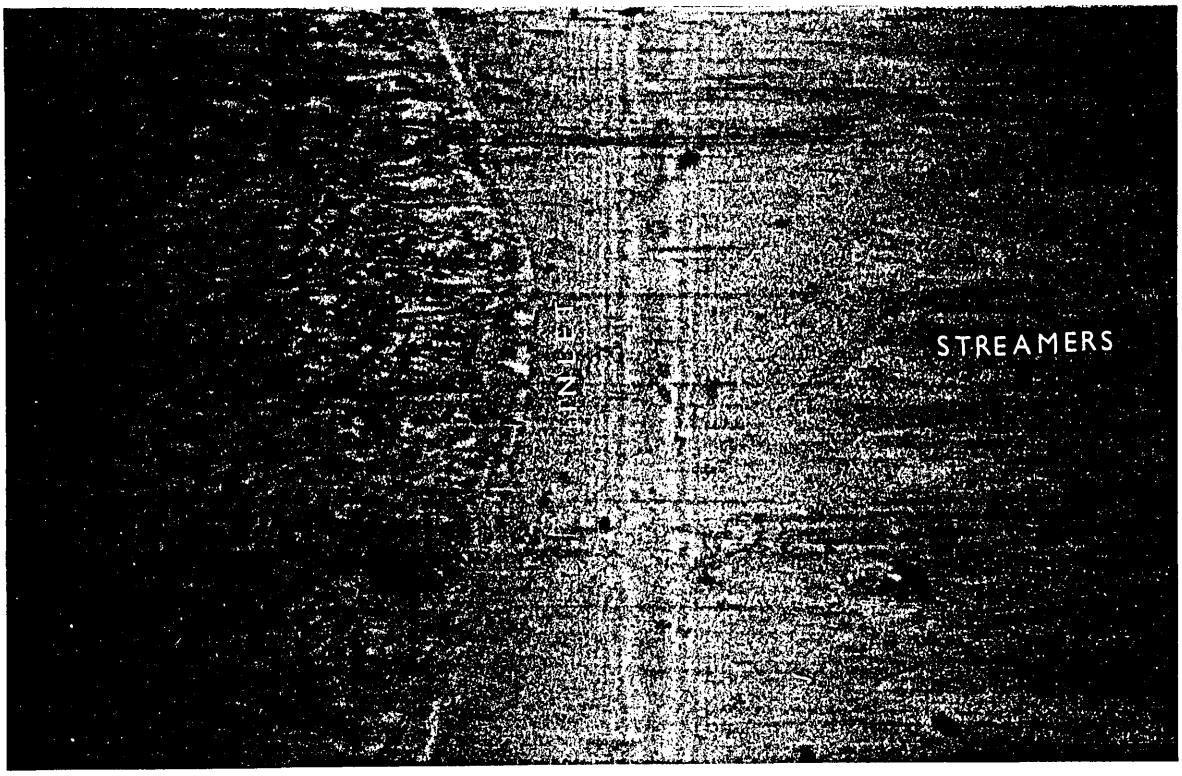

(a) 310 R.P.M.

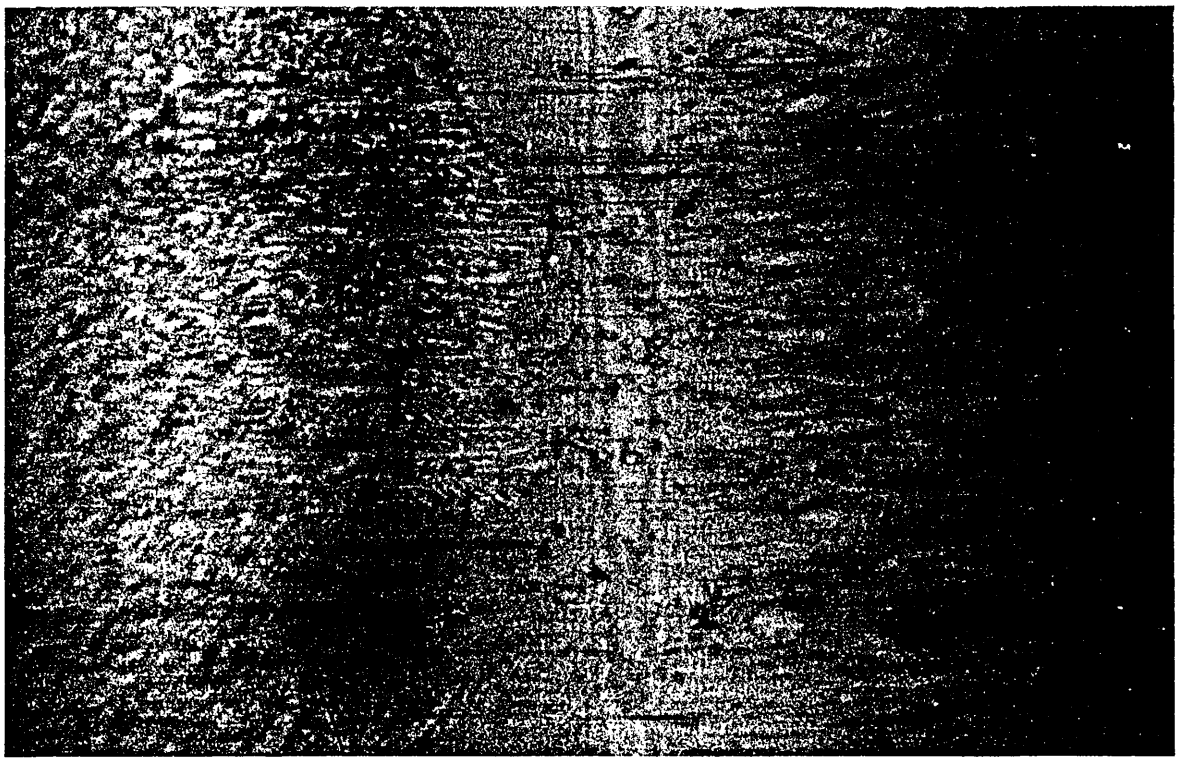

(b) 354 R.P.M.

Figure 6.25 Photomicrograph illustrating a lightly loaded roller.

contact was still running on a substantial hydrodynamic oil film, and filling the inlet of the following contact. Upon completion of the test, the roller was removed and found to be 0.0005 in. undersize.

6.4.7 Oil Globules In Between Rollers.

Further information, concerning the movement of oil within the bearing, was obtained using stroboscopic illumination to 'freeze' the motion of the rollers, and viewing through the perspex end cover.

When oil was being continuously supplied to the bearing, the gaps between the rollers were completely obscured by the large side bands, that were formed at either edge of the outer race track. When the supply was cut off, the side bands gradually diminished in size, and large globules of oil could be observed in the roller gaps. The appearance of these globules is shown by the photograph presented in figure 6.26(a). When there was still a large quantity of oil contained in the side bands, the globules extended the whole length of the contact, and occupied about $^1/_3$ of the gap between the rollers. At low speeds (around 300 R.P.M.), in the side of the bearing where the rollers move downwards, gravity caused the globules to drop out of the entry regions into the exit regions of the preceding rollers. (This is illustrated in figure 6.26(a)), the direction of motion is from right to left). This observation indicates that the oil contained in these globules was not

500 R.P.M. (Lubricant 1)

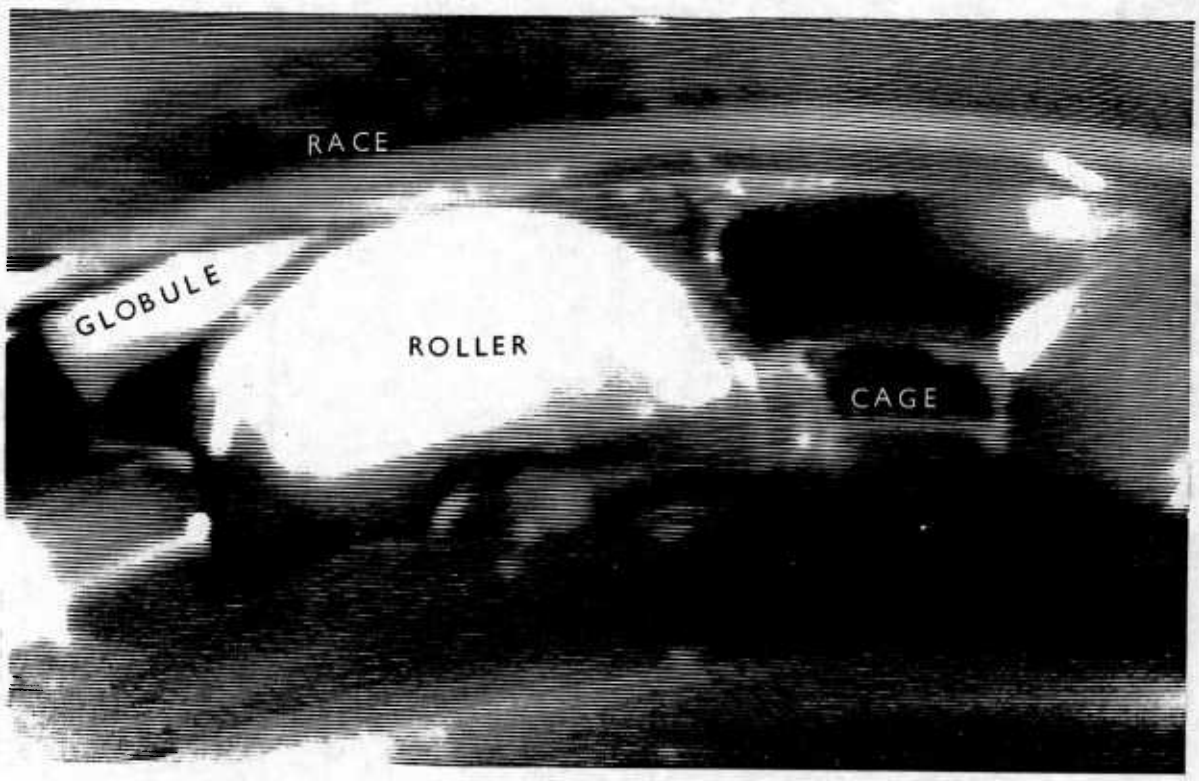

Figure 6.26 The appearance of oil globules in between rollers.

contacting the bearing surfaces; in which case shear forces would have been expected to hold the globules in the entry regions. At higher speeds the globules were flattened by centrifugal force, and remained in the roller entry regions during a complete revolution. In this situation it is probable that the shear forces, induced by the velocity gradient across the air films, are greater than the weight of oil contained in the globule. It was observed that, when the side bands were sufficiently large, some of the oil that had been picked up by the roller edges was scraped off by the cage spacing bars. This oil accumulated on the top surface of the spacing bars, until it was flung off by centrifugal force. Usually this was captured by the globules, as is illustrated by figure 6.26(b), (taken from the video monitor). Any oil that was thrown off, and not engulfed by the globules, was observed to bounce off the track surface, and was lost out of the sides. If the bearing was left to run with no further supply of oil, this process diminished the size of the side bands, and thus the rate at which oil was supplied to the globules. Since oil was being lost from the globules out of the sides of the bearing, they too diminished in size, and several minutes after the oil supply had been cut off, only a few droplets were left. These appeared to move at random along the length of the rollers.

Although these globules could not be seen, when viewing the contacts through the sapphire window, simul-

taneous observation through the sapphire and the perspex cover, confirmed that they were not wetting the track surface. Even though a globule extended far in front of the inlet boundary, the cavitation streamers left on the track surface from the preceding contact, were not effected by it's presence. A space could also be seen behind the globules, and therefore there could be no connection with the inlet boundary.

6.4.8 The Effect of Scratchs, Pits, and Debris.

Scratchs, pits, and debris, passing through the contact were observed to cause a decrease in film thickness. The photograph presented in figure 6.27 illustrates a scratch on the roller surface passing through the contact. The central film thickness is 24 μin., and the minimum film thickness in the constrictions at either side of the scratch, is 13 μin. The constrictions are similar in shape to those occurring at the contact edges of an unblended roller, and are produced for similar reasons. In the entry region the scratch inhibits the pressure build up, as it acts as an escape path. This combined with the pressure relaxation, produced by the pressure of the scratch in contact zone, causes constrictions to form at either side of the scratch. Wymer (81) has observed a similar effect produced by a scratch in a glass plate.

In figure 6.28 a debris particle can be seen entering a contact region, causing the central film thickness

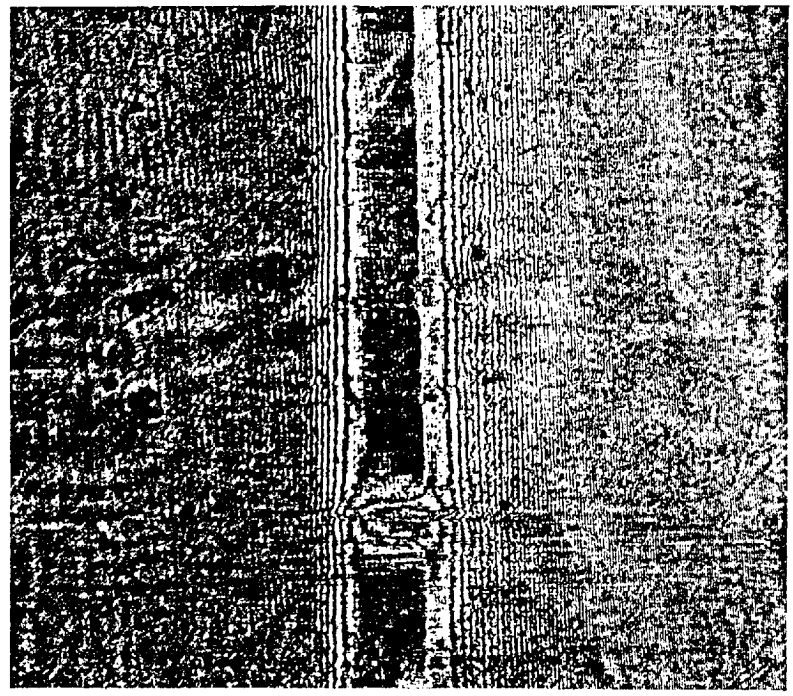

719 R.P.M. (Lubricant 2)

Figure 6.27 Photomicrograph illustrating a scratch passing through the contact.

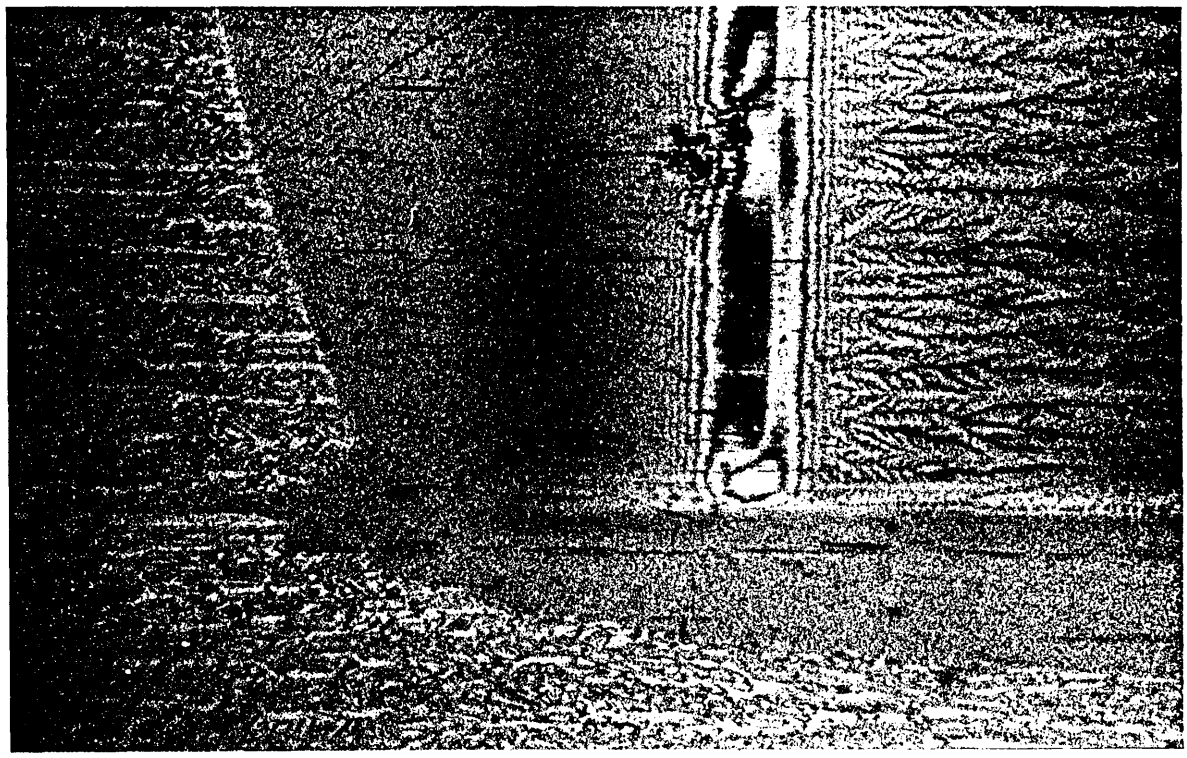

520 R.P.M. (Lubricant 2)

Figure 6.28 Photomicrograph illustrating debris entering the contact region.

to reduce from 26 μin to 23 μin. This reduction is produced because the debris particle is carrying a proportion of the load, and causing a relaxation of pressure in the contact zone.

Figure 6.29 shows a pit, which is approximately 0.002 in. in diameter, and of unknown depth, entering the contact region and causing a reduction in film thickness from 27 μin. to 21 μin. It appears from this photograph (taken from the video monitor), that the pit is draining oil when it interconnects the high pressure contact area and the inlet region. The shaft speed was 115 R.P.M. and, for this to be the case, the drainage would have to take place during a time period of 80 μ seconds. An approximate calculation was carried out to determine whether this would be a feasible static mechanism, using the following form of Reynold's equation in one dimension:

$$\dot{Q} = \frac{h_0^3}{12\eta} \frac{dp}{dx}$$

where: η is the lubricant dynamic viscosity at the average contact pressure.

$\dot{Q}$ is the flow rate per unit length.

For the case represented by figure 6.29, the volume of oil that appears to have been lost from the contact region, is approximately equal to 1.6×10^{-10} cubic in.; and the central film thickness, h_0, is 27 μin. At the average contact pressure of 115,000 p.s.i., the dynamic viscosity of the oil

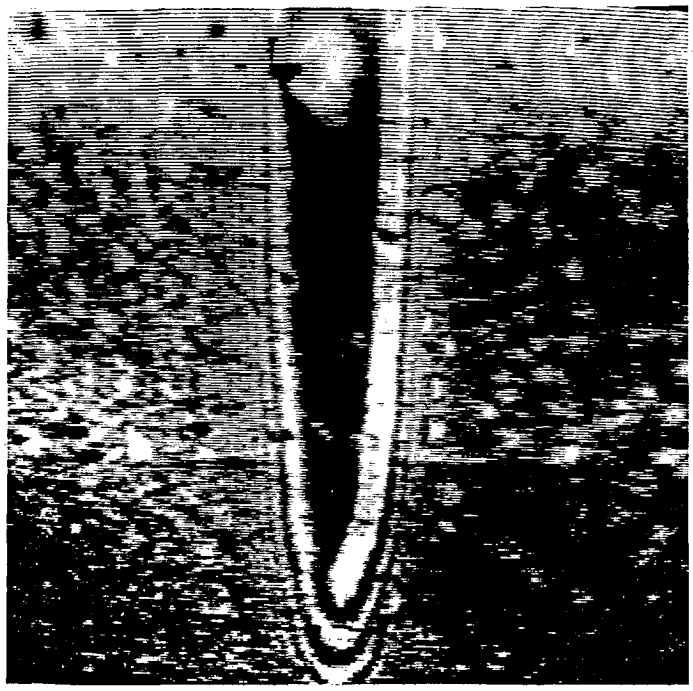

115 R.P.M. (Synthetic paraffin)

Figure 6.29 Photomicrograph illustrating a pit entering the contact region.

would be in the region of 10^5 Poise (the lubricant was a synthetic paraffin, details of which are given by Westlake (73)). The pressure gradient, required to force this volume of oil out of the contact region in the available time, is approximately equal to 5×10^{11} lbs/in^3. This is over four orders of magnitude greater than the actual pressure gradient, which would typically be in the region of 20×10^6 lbs/in^3 (see figure 2.10).

The drop in film thickness must be caused by the sudden pressure relaxation occurring around the pit as it enters the contact zone. The same pit is also visible in figures 5.5(a, b, c, d). In figure 5.5(b) it can be seen that the pit has had a small influence on the film thickness, before it has reached the edge of the contact area, indicating that it is inhibiting the inlet pressure build up.

Scratchs and pits reduce the film thickness over an area considerably greater than that occupied by the defect, and thus increase the likelihood of further damage occurring in this surrounding area.

6.5 Discussion

The experiments described in section 6.4 show that the additional oil, required to prevent starvation of the contacts in the loaded section, when oil was being lost from the inlets at a greater rate than it was being supplied by the edges, could only have been supplied by the roller surfaces, and by oil carried over in the inlets from the unloaded region. The film thickness in the unloaded section

was observed to be of the order of several hundred micro-inches, and therefore the excess oil on the roller surfaces will be supplied to the inner and outer contact inlets as the rollers come under load. At a bearing load of 875 lbs., as used in the film thickness tests, three rollers are loaded (when one roller is over the window at the top of the bearing). The roller spacing is 22.5^{o} and, if it is assumed that the film thickness is constant throughout the loaded region, each roller will supply oil to the inner and outer contacts for half a revolution, which corresponds to 24^{o} movement around the bearing. The rollers begin to come under load at about 30^{o} from the point of maximum loading, and the surfaces would therefore have just finished supplying oil when the rollers come over the sapphire window, positioned at the top of the bearing. If the film thickness at the unloaded and loaded contacts is 200 μin. and 30 μin. respectively, and assuming that at the contact exits the film divides equally between the track surface and roller surface, then excess oil to a depth of 85 μin. will be carried by the roller surface into the loaded region. In this case a volume of 7.5×10^{-5} cubic in. per unit length of the roller surface, is supplied to both the inner and outer contacts. This volume is sufficient to fill an empty inlet region to a distance of 0.05 in. from the edge of the Hertzian contact zone.

In the unloaded section the rollers are supported on hydrodynamic oil films, and in this region classical

theory applies. At all but the lowest speeds the weight of the roller can be neglected in comparison with the loading produced by centrifugal force. As this loading force is proportional to the square of the cage speed, the film thickness is proportional to viscosity, and inversely proportional to speed (see equation 2.1). Immediately after a contact, oil is left on the roller surface in the form of cavitation streamers which, in the unloaded section, are several hundred micro-inches thick. Centrifugal force will tend to increase the height of the streamers, and whether or not oil will be lost from these streamers, during the roller contact time interval (time for a half a revolution of the roller, if there is an oil film between the inner race and roller), will depend upon the balance between centrifugal force, viscous forces, and surface tension. Smart and Ford (126) have measured the mean equilibrium surface film thickness, formed on a 73 mm. spinning steel cylinder, using a diester gas turbine lubricant. In the test bearing configuration, centrifugal forces are caused by the rotation of the rollers, and by the rotation of the cage. These forces will act in the same direction on the fluid, held on the roller surface, that is about to enter an outer race contact. To simulate these combined centrifugal forces at a shaft speed of 2000 R.P.M., a 73 mm. cylinder would be required to rotate at 2400 R.P.M. At this speed Smart and Ford measured an equilibrium film thickness of 200 μin., and the fluid bubbles that were formed on the surface, without

being flung off, must have been considerably longer than this mean value. It therefore seems unlikely that any oil would have been lost from the large streamers, formed on the roller surface in the unloaded region, during the short contact time interval.

In the loaded section, it was observed that the position of the inlet boundary, at the centre of the contact, was virtually unaffected whether the oil supply was on or off. This suggests that the amount of oil, that is already contained in the inlets as the rollers enter the loaded area, is also unaffected by the supply. At the bottom of the bearing, which is immersed in oil when there is continuous supply, the boundary was affected if the supply was switched off. Some of the supply was therefore being entrained in the inlet regions during the passage through this part of the bearing. However at large inlet distances, oil is rapidly lost around the contact sides, and the same equilibrium boundary distance, as in the case when there was no supply, would be quickly formed. Also very large inlet distances may be unstable, and the oil engulfed in the globules. For otherwise constant conditions, the higher the viscosity of the oil, the greater the film thickness in the unloaded section, and the greater the volume of oil that is carried by the roller surfaces into the loaded region. This is consistent with the experimental finding that the boundary distance was proportional to viscosity. If the speed is in-

creased, for otherwise constant conditions, the film thickness is the unloaded section decreases, and less oil is brought into the loaded region by the rollers. This too is consistent with the experimental finding that the boundary distance decreases with increasing speed. Entrainment of oil, into the inlets, by the roller edges has been neglected; as whether or not this was occurring was observed to have little influence on the position of the inlet boundary, in the loaded region, at the centre of the contact. The effect of entrainment on the boundary position, was being masked by the large amounts of oil supplied by the surfaces.

The manner by which the contact inlets are replenished in the unloaded section, when there is no oil supply, was not investigated. However as oil tends to accumulate in this region, because of gravitational forces, it is likely the side bands are larger, and replenishment by the edges will be more effective than in the loaded section. Also because of the very large cavitation streamers, which sometimes reform before the next contact, there may be a small amount of track refilling in the manner suggested by Chiu (123). Because of the large clearance in the bearing, it is unlikely that any fluid film can be formed between the inner race and the rollers in the unloaded region, and no additional oil would have been supplied, by the inner race, to the contacts in the loaded section.

If the curve drawn in figure 6.2 could be used to describe the position of the inlet boundary at lower values of η_0/U, an inlet boundary position of 0.006 in. would be predicted for a shaft speed of 5.000 R.P.M., and a lubricant viscosity of 9 cS. (this would be a typical viscosity for a diester lubricant in a gas turbine application.) Assuming a contact width of 0.008 in., and a α value of 1.2×10^{-4} in.^{2}/lb., Grubin's isothermal theory predicts a central film thickness of 19.7 µin. under fully flooded conditions. The thermal theory of Murch and Wilson predicts a 19% drop in film thickness to 16 µin., and at the boundary distance of 0.006 in. starvation will only cause a further 8% drop to 14.8 µin. However at higher speeds, centrifugal force will become significant, and cause E.H.D. lubrication in the unloaded region. The centrifugal force Fc, for each roller in the test bearing (assuming no cage slip), is given by:

$$Fc = 0.398\ N^2 \times 10^{-6} \text{ lbs.} \qquad \ldots\ldots 6.1$$

where: N is the shaft speed in R.P.M. Shaft speeds in gas turbines are frequently as high as 30,000 R.P.M. and at this speed centrigugal force creates a roller loading of 358 lbs. at the outer race, and the film thickness is effectively constant. Assuming that there is no oil film between the inner race and the rollers in the unloaded section, no additional oil would be supplied by the roller surfaces, and starvation effects must be significant. This is likely to be the

case even though there is copious lubricant supply, as the majority of oil that passes through the bearing does so in the form of globules, which neither wet the surfaces, nor supply oil to the inlets. Such globules have also been observed in the contact by Crook (53), and by Dowson (127). They have been seen in point contact by Kingsbury (124). Crook does not comment on the implications of the globules; Dowson suggests they transport lubricant to and from the inlet region in order that, under changing conditions, the inlet boundary position always conforms with the position of zero reverse flow; Kingsbury suggests that the globules are supported on a hydrodynamic air film, that prevents them entering the inlet region. It was evident from the experimental work described in section 6.4.7 that these globules are supported by an air film. They are prevented from merging with oil contained in the inlet region, because of the air pressure build up that occurs in the gap between the globule and oil inlet boundary. The formation of these globules emphasises the difficulty in effectively supplying oil to the contact inlets. The most effective method of directly replenishing the inlet regions is to ensure that the oil wets either the race, or roller surfaces in between loaded contacts. It is for this reason that large quantities of oil were supplied to the following entry region by the undersize roller (see section 6.4.6). However at high speeds centrifugal forces would cause the contact between this roller and the outer race to operate in the E.H.D. regime,

and there would be no further benefit to the following contact. In a high speed bearing an arrangement such as shown in figure 6.30 would be a possible means of ensuring fully flooded lubrication. The cage is manufactured so that the top surface of the bars, that interspace the rollers, is a hemispherical shape, and is positioned extremely close to the outer race surface (not contacting). If these bars were made slightly longer than the rollers, oil would be entrained from the side bands into the convergent entry region, between the cage and the race, and a hydrodynamic film would occur that supplied oil to the following contact in the same manner as the undersize roller.

In a standard bearing, such as used for this study, at all speeds there will be clearance between the inner race and the rollers, in the unloaded section. At high speeds this gap will not be normally filled by an oil film, and the surface film thickness on the inner race will be approximately equal to half the film thickness occurring in the loaded region. If several high velocity oil jets were spaced around the unloaded region, and directed at this gap, it is likely that some of the oil would fill the inlets. Once oil was contained in the inlets of the inner race contacts, it would be trapped between the race and roller, and could not be thrown out by centrifugal force. Thus large hydrodynamic oil films would be created that supplied oil to roller and race surfaces. Provided the inlets could be

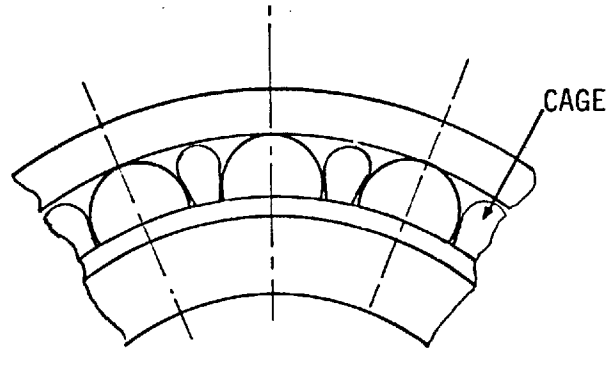

Figure 6.30 A cage for applying oil to the race surface.

filled in the unloaded section, and the films retained on the surfaces, this would ensure fully flooded operation of the bearing.

With the usual methods of oil supply (jet directed at the cage pilot area, oil bath), as soon as the outer race contacts enter the E.H.D. regime at all positions around the bearing, entrainment of oil by the edges becomes the primary mechanism by which the inlets are replenished. In a ball journal this will occur at relatively low speeds, and is always the case in preloaded bearings, or bearings that run under axial or thrust loading. If there is only a small initial supply it is the only mechnaism of inlet replenishment. Meyer and Wilson (134) have measured film thickness in a small preloaded instrument ball bearing, using an oil of similar viscosity to lubricant 1; the film thickness at 4000 R.P.M. was 50% lower than that predicted by isothermal theory. Although they were unable to measure the position of the inlet boundary, starvation would have been causing a significant drop in film thickness.

Not only is a blend on a roller edge important for alleviating the side constriction, it also is essential for retaining the side bands, and providing a convergent region for spreading the bands at either side of the contact. The presence of the side bands is essential if oil is to be entrained by the roller edges, the mechanism of which has been elucidated in section 6.4.2. Horsch (111), Wedeven

(47), and Dowson (127), have also observed similar bands and suggest that they function as reservoirs, that supply oil to the inlets. In roller bearings, guiding lips will interfere with the formation of these bands and should be relieved to provide a space at the edges of the track. In the case of a roller journal, relieved lips on the inner race would prevent the side bands from being flung off by centrifugal force. However this recommendation does not apply if oil can be supplied directly to the inlets, since their presence will have the benefical effect of reducing the rate at which oil is lost around the contact ends. On the rolling elements, centrifugal force will cause oil, that is picked up by the roller ends, to flow radially and merge with oil already contained on the blend. In ball bearings, spin will assist oil replenishment as the oil that is picked up from the race side bands, and left on the ball surface at either side of the wake, will periodically be brought across the direction of rolling. However in a starved situation this would lead to a fluctuating film thickness.

When no other oil reaches the inlet regions, other than that entrained by the sides, the position of the inlet boundary is controlled solely by the equilibrium between the rate at which oil is lost around the contact edges, and the rate at which this can be replenished. Provided there is sufficient oil to fill the side bands, and to fill the inlets to the equilibrium position, and to provide the

the surface films, the spacing or number of the rolling elements has no effect on formation of the boundary. Also because oil is only lost around the contact ends, the length of the contact has no influence on the boundary position. High surface tension lubricants are likely to enhance fluid replenishment from the side bands.

Under conditions of severe starvation, when only a few drops of oil are initially supplied to the bearing, the film thickness is limited by the amount of oil available in the rolling track. It is evident from the experimental work described in section 6.3 that, in line contact, substantial oil films can still be formed when the inlet boundary has effectively reached the edge of the contact region. In some line contact systems it may be an advantage to run under severely starved conditions, as rolling friction is substantially reduced, traction increased (128, 165), and the side and edge constrictions removed. During starved operation of the test bearing, there was negligible loss from the entry regions, and the film thickness remained steady at constant running speed. However it was not possible to allow the rig to run for long periods to ascertain whether film decay would occur, as running time had to be kept to a minimum to preserve the sapphire surface. Under these conditions, side leakage from the high pressure contact zone may be a major source of loss, in the manner suggested by Kingsbury (122). In lightly loaded bearings,

slip often occurs at the inner race contacts (162), in particular with bearings having large diametrical clearance (126). Under starved operating conditions this could lead to a serious reduction in film thickness at the inner race contacts, as the rate at which oil is brought into these contacts by the roller surfaces, is reduced.

CHAPTER VII

CONCLUSION

7.1 Summary of the Main Conclusions

(a) Optical access to the contacts of a commercially available cylindrical roller bearing, was achieved by the insertion of a sapphire window across the whole width of the outer race track. This bearing has been run for many hours, at loads and speeds representative of an actual bearing, with minimal deterioration of the sapphire surface. The feasibility of inserting windows for optical studies of bearing lubrication has therefore been demonstrated. An inner race with a sapphire window was also prepared, but not run.

(b) The rig, capable of applying loads of up to 4 tons to the test bearing, and running at speeds up to 2200 R.P.M., has proved to be ideal for optical studies of this nature. The associated optics enables the inner and outer race contacts to be viewed at all angles around the bearing. The images can be viewed by eye, or on a television monitor, and can be recorded on 35 mm. film or on videotape. A method of flash synchronisation has been devised that is consistently accurate and

which, for the outer race, enables either one, or several selected contacts to be viewed every time they pass over the window. For the inner race, it enables contacts to be viewed wherever one of the selected rollers is over the window, or only when the race is in a particular orientation; and a selected roller is over the window. In both cases any position in between contacts can be studied.

(c) A prototype pulsed xenon ion laser, designed by the Physics department of Imperial College, has been shown to be a light source ideal for this type of application, in which a short pulse is required to 'freeze' the motion of the contact.

(d) Using pulsed light sources, the technique of optical interferometry has been successfully applied to measure the film thickness at the outer race contacts. Also the distribution and movement of oil within the bearing, has been studied by viewing the track surface through the sapphire window, and viewing one side of the bearing through the perspex end cover.

(e) At low speeds the measured values of central and minimum film thickness can be accurately predicted by the isothermal theories of Grubin and of Dowson and Higginson. However as the speed is increased, the film thickness increases at a progressively

slower rate, and becomes substantially lower than isothermal predictions. The speed at which the drop off begins to occur, decreases with increasing viscosity. The reduction in film thickness was not caused by starvation which, at the highest speeds, would only account for a 3% drop. Accurate predictions were made over the whole range of speed and viscosity, using an equation developed by Murch and Wilson that allows for the effects of viscous heating in the inlet zone, and taking into account the reduction in α value with increasing overall bulk temperature. At all speeds switching off the oil supply had no effect on film thickness, and only a stabilisinginfluence on the position of the inlet boundary.

(f) Thick hydrodynamic films, that are formed in the unloaded region, cause considerable quantities of oil to be carried by the roller surfaces into the loaded region and supplied to the contact inlets. At higher speeds, oil supplied in this fashion prevents starvation of the loaded contacts. The film thickness in the unloaded region, and hence the volume of oil supplied to loaded contacts and the length of the inlet boundary, is proportional to viscosity and inversely proportional to speed. Rolling element spacing has no effect on the inlet boundary shape or position. Running an undersize

roller caused hydrodynamic film formation in the loaded region, and flooding of the following contact.

(g) Besides alleviating the side constrictions, the blends on the roller edges are essential for retention of the side bands. In the vicinity of the inlet region the combined height of the side bands, contained on the rollers and the race, is less than the available gap. Therefore when the bands meet, they are spread laterally and merge with the oil in the contact inlet region, causing a boundary which is longer at the edges than in the centre. Entrainment of oil into the inlets is aided by surface tension forces, and takes place along the edge of the boundary. In a sparsely lubricated bearing, in which all the contacts are operating in the E.H.D. regime, this entrainment mechanism is the only way in which the inlets can be replenished. The inlet boundary then forms in a position such that an equilibrium is maintained between the oil that is being lost around the contact edges, and that which is entrained from the side bands. There is no replenishment action in between contacts in the manner that has been suggested by Chiu, and neither the rolling element spacing, nor the contact length, influence the boundary position.

(h) When there is a copious supply of oil to the bearing, the majority of the oil flows ir between the contacts in the form of globules. These globules are supported on hydrodynamic air films, and are prevented from entering the inlet region by air pressure build up. They do not wet the surfaces and have no influence on the bearing lubrication.

(i) In high speed rolling element bearings, such as operate in aircraft gas turbines, all the outer contacts operate in the E.H.D. regime, and it is therefore likely that starvation causes a substantial drop in film thickness.

(j) Severe starvation of the test bearing could only be induced by limiting the initial supply of oil to one drop per roller. The reduction in film thickness, caused by an inadequate volume of oil in the inlet region, is accurately predicted by theoretical solutions, except at very small inlet distances. Substantial oil films can still be maintained even when the boundary is effectively at the edge of the Hertzian zone, and this results in alleviation of both the edge and side constrictions.

(k) Scratchs and pits cause a reduction of film thickness over an area considerably greater than that occupied by the defect, and can therefore lead to increased wear rates.

7.2 Suggestions for Future Work.

(a) Investigate the lubrication of the bearing using greases.

(b) Investigate the lubrication of the inner race contacts, in both the loaded and unloaded regions. Determine whether the inlets can be filled, in the unloaded region, using an oil jet.

(c) Investigate the effect of guide lips on lubricant supply, and loss in the inlet region.

(d) Experiment with cage design to simulate the effect of an unloaded roller.

(e) Investigate the edge entrainment phenomena in a line contact using a counter-rotating thrust bearing, with the bubble technique to trace the streamlines. Determine the influence of surface tension and edge blending, on entrainment flow and inlet boundary position.

(f) Run the outer race with the sapphire window in conjunction with oversize rollers, or an oversize inner race, so that all contacts are equally loaded. Examine the effect of speed, viscosity, and supply rate, on the inlet boundary position.

(g) Investigate the lubrication of an angular contact bearing through an outer race window. Determine the influence of spin on lubricant supply.

(h) Using the pulsed laser, study the lubrication of a rolling element bearing at speeds up to 50,000 R.P.M.

(i) Investigate experimentally and theoretically, the effect of pits of various dimensions.

(j) Investigate the reasons for the discrepancy between theoretical predictions and measured values of film thickness in line contact, at very small inlet boundary distances.

APPENDIX 1 : BEARING DIMENSIONS (in inches)

(a) LRJ 65 with outer race window.

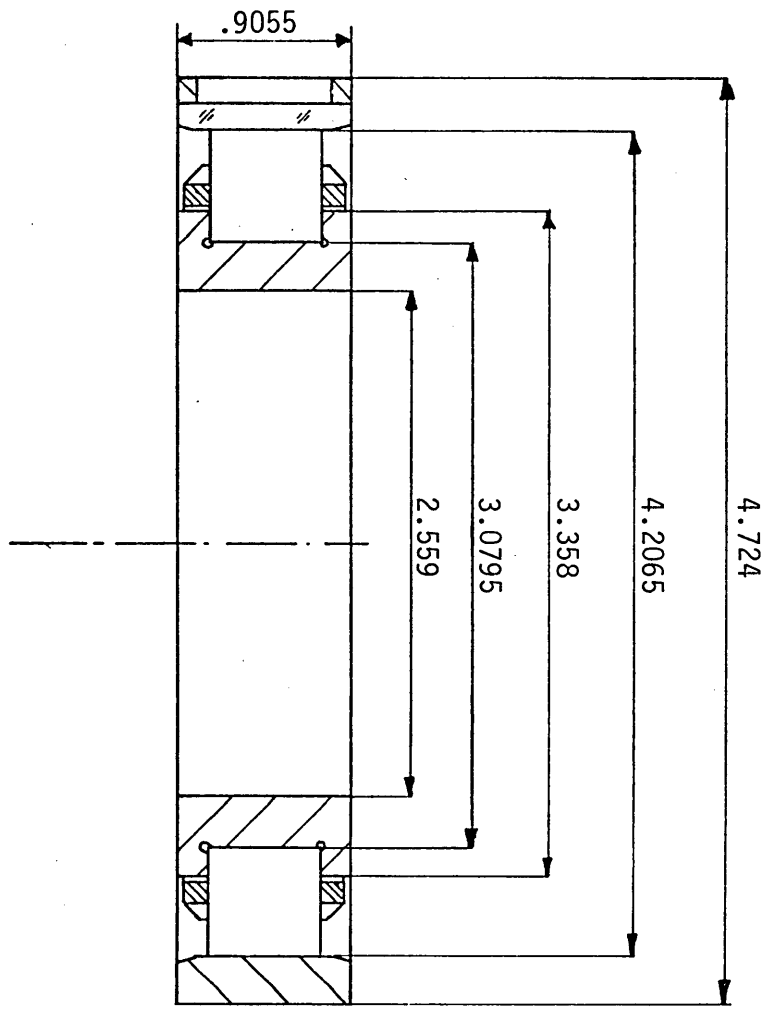

16 rollers 9/16 in. diameter

(b) LLRJ 65 with inner race window.

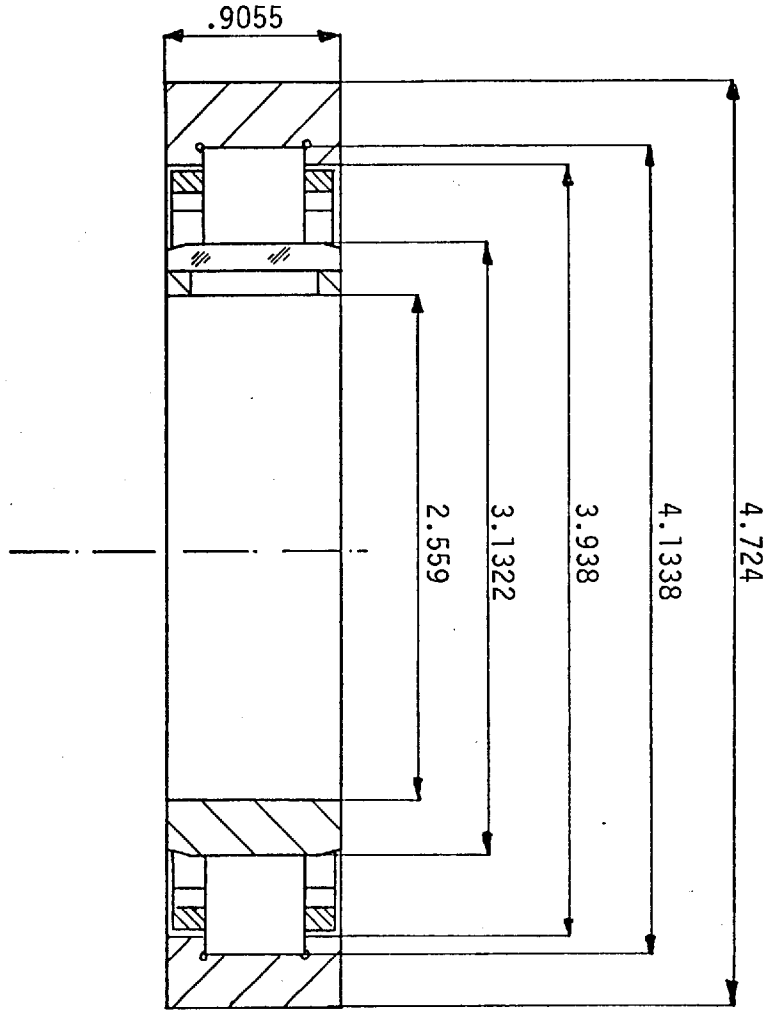

17 rollers $\frac{1}{2}$ in. diameter

APPENDIX 2 : MATERIAL PROPERTIES OF SAPPHIRE AND BEARING STEEL.

	STEEL	SAPPHIRE(Al_2O3)
Young's modulus :	33.4×10^6 p.s.i.	50×10^6 p.s.i.
Compressive strength :	-	300×10^3 p.s.i.
Modulus of rupture :	-	55×10^3 p.s.i.
Hardness :	910 Vickers	2100 Knoop
Coefficient of linear expansion (per ^0C) :	11×10^{-6}	8.4×10^{-6}
Refractive Index :	-	1.768

APPENDIX 3 : LUBRICANT PROPERTIES.

(a) Lubricant 1.

Type :	High viscosity Index mineral oil
Source :	Shell Oil Co.
Viscosity :	177.3*cS at 100°F
	15.4*cS at 210°F
	Viscosity index = 95*
Density :	0.895* gm/cc at 60°F
Refractive Index :	1.4897 gm/cc at 20.5°C
	1.4830 gm/cc at 39.0°C
Pressure-Viscosity Coefficient (α) :	1.46 x 10^{-4} in^2/lb at 20.5°C
Thermal Conductivity (k) :	.117* watt/m°C at 40°C

(b) Lubricant 2.

Type :	Mineral oil containing a commerial Phosphorus/Sulphur additive package
Source :	Mobil Oil Co.
Viscosity :	75.0 cS at 100°F
	9.6 cS at 210°F
	36.1 cS at 130°F
Density :	0.892 gm/cc at 22.5°C
	0.875 gm/cc at 46.8°C
	0.856 gm/cc at 78.0°C
Refractive Index :	1.4850 at 22.2°C
	1.4785 at 40.5°C
	1.4650 at 78.4°C
Pressure-viscosity Coefficient (α) :	1.05 x 10^{-4} in^2/lb at 21°C

* Supplier's data

REFERENCES

1. PAUL, G., and CAMERON, A., "Time-dependent viscosity effects measured on an impact microviscometer", Nature 1974, Vol.248, p.219 - 220.

2. MARTIN, H.M., "Lubrication of Gear Teeth", Engineering Lond. 1916, Vol.102, p.199.

3. LANCHESTER, F.W., Conference on lubrication at the Physical Society , 1919. Referred to by Stanton, Engineering 1927, Vol.127, p.312.

4. SCHERING, H. and VIEWEG, R. "Über die Beurteilung der Lagerschmierung nach elektrischen Mesungen". (The use of Electrical Measurement in the Study of Bearing Lubrication). Zeits. Für Ang. Chemie. 1926, Vol.39, p.1119.

5. ARCHBUTT, L., and DEELEY, R.M., "Lubrication and Lubricants", Automobile Engineer, 1927, p.120.

6. WAY, S., "Pitting due to Rolling Contact", Trans. ASME. J. Appl. Mech., 1935, Vol.57, p.A49 - A58.

7. HYDE, J.H., Proc. Royal Society of London, 1920, Vol.97A, p.240.

8. HERTZ, H. "On the contact of elastic solids", and "On the contact of rigid elastic solids and on hardness", reprinted in "Miscellaneous Papers", translated by Jones, D.E. and Schott, G.A., Macmillan Co. Ltd., London, 1896, p.146 - 183.

9. PEPPLER, W. "Untersuchungen über die Druckubertragung bei belasteten und geschmierten umlaufenden achsparallelen Zylindern", Maschinenelemente-Tagung, Aachen 1935. VDI Verlag 1936 (Berlin), p.42.

10. PEPPLER, W., "Drucküübertragung und geschmiert zylindrischen Gleit und Wälzflächen", VDI ForschHft 1938, p.391.

11. MELDAHL, A., "Contribution to the theory of the lubrication of gears and the stressing of the lubricated flanks of gear teeth", Brown Boveri Rev. 1941, Vol.28 (no.11), p.374.

12. NEEDS, S.J., "Boundary film investigations", Trans. ASME 1940, Vol.62(No.7), p.331 - 345.

13. ROSENFELD, L. "Ball and Roller Bearings", Automobile Engineer, October 1944, p.421 - 425.

14. LARSON, C.M., "Discussion of Flow Properties of Lubricants Under High Pressure", Trans. ASME, October 1941, p.638.

15. GATCOMBE, E.K., "Lubrication characteristics of involute spur gears - a theoretical investigation", Trans. ASME 1945, Vol.67, p.177.

16. BRIX, V.H., "Electrical Study of Boundary Lubrication", Aircraft Eng. 1947, Vol.19, p.294 - 297.

17. HERSEY, M.D. and LOWDENSLAGER, D.B., "Film thickness between gear teeth. A graphical solution of Karlson's problem", Trans. ASME 1950, Vol.72 (No.7), p.1035.

18. BLOK, H., "Fundamental aspects of thin film lubrication", Ann. N.Y. Acad. Sci. 1950, Vol.53, p.779.

19. CAMERON, A. "Hydrodynamic theory in gear lubrication", J. Inst. Petrol. 1952, Vol.38, p.614.

20. McEWEN, E., "The effect of variation of viscosity with pressure on the load-carrying capacity of oil films between gear teeth", J. Inst. Petrol. 1952, Vol.38, p.646.

21. LANE, T.B. and HUGHES, J.R., "A study of the oil film formation in gears by electrical resistance measurements", Brit. J. Appl. Phys. 1952, Vol.3, p.315 - 518.

22. GRUBIN, A.N., "Fundamentals of the hydrodynamic theory of lubrication of heavily loaded cylindrical surfaces", Symposium: Investigation of the Contact of Machine Components, Central Scientific Institute for Technology and Mechanical Engineering (TsNIITMASh), Book no.30, Moscow 1949, p.115 - 166, (D.S.I.R. Translation).

23. PETROUSEVICH, A.I., "Fundamental conclusions from the contact-hydrodynamic theory of lubrication", Izvestia Uzbekist. Fil. Akad. Nauk SSSR (OTN) 1951, Vol.2, p.209, (Ministry of Defence translation No.293).

24. CAMERON, A., "Surface failure in gears", J. Inst. Petrol. 1954, Vol.40, p.191.

25. LEWICKI, W., "Some physical aspects of lubrication in rolling bearings and gears", Engineer 1955, Vol.200, p.176 - 178 and 212 - 215.

26. EL-SISI, S.I. and SHAWKI, G.S.A., "Measurement of oil-film thickness on gear teeth", J. Basic Eng., Trans. ASME 1958, Vol.80 (Series D, No.1), p.12.

27. CROOK, A.W., "Simulated gear tooth contacts", Proc. Instn. Mech. Engrs. 1957, Vol.171, p.187 - 214.

28. DOWSON, D. and HIGGINSON, G.R., "A numerical solution to the elastohydrodynamic problem", J. Mech. Engng. Sci. 1959, Vol.1 (No.1), p.6.

29. DOWSON, D. and HIGGINSON, G.R., "The effect of material properties on the lubrication of elastic rollers", J. Mech. Engng. Sci. 1960, Vol.2 (No.3), p.188.

30. DOWSON, D. and HIGGINSON, G.R., "New roller-bearing lubrication formula", Engineering, Lond. 1961, Vol.192, p.158.

31. DOWSON, D. and HIGGINSON, G.R., "Elastohydrodynamic Lubrication. The Fundamentals of Roller and Gear Lubrication", Pergamon Press, 1966.

32. DOWSON, D., HIGGINSON, G.R. and WHITAKER, A.V., "Elastohydrodynamic lubrication: a survey of isothermal solutions", J. Mech. Engng. Sci. 1962, Vol.4 (No.2), p.121.

33. CHENG, H.S. and STERNLIGHT, B., "A numerical solution for the pressure, temperature, and film thickness between two infinitely long, lubricated rilling and sliding cylinders, under heavy loads", J. Mech. Engng. Sci. 1965, Vol.87, p.695 - 707.

34. CROOK, A.W., "The lubrication of rollers, II - film thickness with relation to viscosity and speed", Phil. Trans. Roy. Soc. 1961, Vol.254 (Series A), p.223 - 236.

35. CHENG, H.S., "A refined solution to the thermal-elastohydrodynamic lubrication of rolling and sliding cylinders", Trans. ASLE 1965, Vol.8, p.397.

36. CHENG, H.S., "Isothermal Elastohydrodynamic Theory for the Full Range of Pressure Viscosity Coefficient", Trans. ASME J. Lub. Tech. 1972, Vol.94 (No.1).

37. DOWSON, D. and WHITAKER, A.V., "A numerical procedure for the solution of the elastohydrodynamic problem of rolling and sliding ocntacts lubricated by a Newtonian fluid", proc. Instn. Mech. Engrs. 1965-6, Vol.180 (Part 3B), p.57 - 71.

38. DOWSON, D. and WHITAKER, A.V., "The isothermal lubrication of cylinders", Trans. ASLE 1965, Vol.8 (No.3), p.224.

39. GREENWOOD, J.A., "Presentation of Elastohydrodynamic Results", J. Mech. Eng. Sci. April 1969, Vol.II (No.2), p.128 - 132.

40. JOHNSON,K.L., "Regimes of Elastohydrodynamic Lubrication", J. Mech. Eng. Sci. 1970, Vol.12 (No.1) p.9 - 16.

41. HOWLETT, J., "Film-lubrication between spherical surfaces: with an application to the theory of the four-ball lubricant testing instrument", J. Appl. Phys. 1946, Vol.17 (No.3), p.137 - 149.

42. KAPITZA, P.L., "Hydrodyamnic theory of lubrication during rolling", Zhurn. Tekh. Fiz. 1955, Vol.25 (No.4), p.747 - 762.

43. KOROVCHINSKII, M.V., "On the possible limit to the regime of hydrodynamic friction in the four ball machine", Trenie i Iznos v machinax., Akad. Nauk, Moscow 1958, Vol.12, p.242 - 285, (translated in "Friction and Wear in Machinery", ASME, New York 1960, p.233 - 273).

44. ARCHARD, J.F. and KIRK, M.T., "Lubrication at point contacts", Proc. Roy. Soc. 1961, Vol.261 (Series A), p.532 - 550.

45. ARCHARD, J.F. and COWKING, E.W., "Elastohydrodynamic lubrication at point contacts", Proc. Instn. Mech. Engrs. 1965-6, Vol.180 (Part 3B), p.47 - 56.

46. CHENG, H.S., "A numerical solution of the elastohydrodynamic film thickness in an elliptical contact", J. Lub. Tech., Trans. ASME 1970 Vol.92 (series F, No.1), p.155 - 162.

47. WEDEVEN, L.D., EVANS, D, and CAMERON, A., "Optical analysis of ball bearing starvation", ASME -ASLE Lubrication Conference, Cincinnati, Ohio, October 1970. ASME paper No.70-Lub-19.

48. RANGER, A.P., "Numerical Solutions to the Elastohydrodynamic Equations", Ph.D. Thesis, University of London.

49. PETROUSEVICH, A.I., KADNIR, D.S., SALUKIADZE, R.G. BAKASHUILI, D.K., and SCHWARZMAN, S.H., "The Investigation of Oil Film Thickness in Lubricated Ball Race Rolling Contact", Wear 1972, Vol.19, p.369 - 389.

50. SIBLEY, L.B., BELL, J.C., ORCUTT, K.J., ALLEN, C.N. and GOLDTHWAITE, W.H., "A Study of the Influence of Lubricant Properties on the Performance of Aircraft Gas Turbine Engine Rolling Contact Bearings", W.A.D.C. Tech. Rep. 1958, No.58 - 565.

51. SIRIPONGSE, C., ROGERS, P.R., and CAMERON, A., "Thin Film Lubrication: 1 - Discharge through Thin Oil Films", Engineering 1958, Vol.186, p.146 - 147.

52. MAcCONOCHIE, I.O., and CAMERON, A., "The Measurement of Oil Film Thickness on Gear Teeth", J. Basic Engng., Trans. ASME 1960, Vol.82 (Series D), p.29.

53. CROOK, A.W., "The lubrication of rollers", Phil. Trans. Roy. Soc. 1957-8, Vol.250 (Series A), p.387 - 409.

54. CROOK, A.W., "The Lubrication of Rollers, II - Film Thickness with Relation to Viscosity and Speed", Phil. Trans. Roy. Soc. 1961, Vol.254 (Series A), p.223 - 236.

55. CROOK, A.W., "Elastodydrodynamic lubrication of rollers", Nature 1961, Vol.190, p.1182.

56. SIBLEY, L.B. and ORCUTT, F.K., "Elastohydrodynamic lubrication of rolling contact surfaces", Trans. ASLE 1961, Vol.4 (No.2), p.234 - 249.

57. KIRK, M.T., "Hydrodynamic lubrication of perspex", Nature 1962, Vol.194, p.965.

58. ARCHARD, J.F. and KIRK, M.T., "Influence of elastic modulus on the lubrication of point contacts", Proc. Lubrication and Wear Convention (Bournemouth) 1963 Paper 15, p.181 - 189, (Instn. Mech. Engrs., London).

59. GOHAR, R. and CAMERON, A., "Optical measurement of oil film thickness under elastohydrodynamic lubrication", Nature 1963, Vol.200 p.458 - 459.

60. GOHAR, R., "Oil films under elastohydrodynamic conditions", Ph.D. Thesis, University of London, 1965.

61. CAMERON, A. and GOHAR, R., "Theoretical and experimental studies of the oil film in lubricated point contact", Proc. Roy. Soc. 1966, Vol.291 (Series A), p.520.

62. GOHAR, R. and CAMERON, A., "The mapping of elastohydrodynamic contacts", Trans. ASLE 1967, Vol.10, p.215 - 225.

63. GOHAR, R., "A ball-and-plate machine for measuring elastohydrodynamic oil films", Proc. Instn. Mech. Engrs. 1967-8 Vol.182 (Part 3G), p.43 - 45.

64. DYSON, A., NAYLOR, H. and WILSON, A.R., "The measurement of oil film thickness in elastohydrodynamic contacts", Proc. Instn. Mech. Engrs. 1965-6, Vol.180 (Part 3B), p.119.

65. FOORD, C.A., "Pitting and film thickness in rolling contact", Ph.D. Thesis, University of London, 1967.

66. FOORD, C.A., HAMANN, W.C. and CAMERON, A., "Evaluation of lubricants using optical elastohydrodynamic lubrication", Trans. ASLE 1968, Vol.11 (No.1), p.31 - 43.

67. FOORD, C.A., WEDEVEN, L.D., WESTLAKE, F.J. and CAMERON, A., "Optical elastohydrodynamics", Proc. Instn. Mech. Engrs. 1969-70, Vol.184 (Part 1), p.487 - 503.

68. WEDEVEN, L.D. and CAMERON, A., "The observation of elasto-hydrodynamic lubrication in a rolling element bearing using optical interferometry", Tenth International Symposium on Lubrication of Rolling Bearings 1968, Halle, Germany (published in Schmierungstechnik).

69. WEDEVEN, L.D., "Optical measurements in elastohydrodynamic rolling contact bearings", Ph.D. Thesis, University of London, 1970.

70. DOWSON, D. and JONES, D.A., "Lubricant entrapment between approaching elastic solids", Nature 1967, Vol.214, p.947.

71. DOWSON, D. and JONES, D.A., "An optical-interference method of measurement of time-dependent elastohydrodynamic film profiles", Proc. Instn. Mech. Engrs. 1967-8, Vol.182 (Part 3G), p.49 - 52.

72. WESTLAKE, F.J. and CAMERON, A., "Fluid film interferometry in lubrication studies", Nature 1967, Vol.214, p.633 - 634.

73. WESTLAKE, F.J. and CAMERON, A., "A study of ultra-thin lubricant films using an optical technique", Prcc. Instn. Mech. Engrs. 1967-8, Vol.182 (Part 3G), p.75 - 78.

74. WESTLAKE, F.J. and CAMERON, A., "High speed photographic study of lubricated contacts using optical interferometry", J. Phot. Sci. 1969, Vol.17 (No.4), p.137 - 140.

75. WESTLAKE, F.J., "A study of ultra-thin films", Ph.D. Thesis University of London, 1970.

76. WESTLAKE, F.J. and CAMERON, A., "Optical elastohydrodynamic fluid testing", ASLE/ASME Lubrication Conference, Pittsbury, Pa., October 1971, ASLE paper No.71-LC-12.

77. WESTLAKE, F.J. and CAMERON, A., "Interferometric Study of Point Contact Lubrication", Elastohydrodynamic Lubrication Symposium, Leeds 1972, Paper No. C39/72.

78. PAUL, G.R. and CAMERON, A.,"An absolute high-pressure micro-viscometer based on refractive indes", Proc. Roy. Soc., 1972, Vol,331, Series A, p.171 - 84.

79. THORP, N. and GOHAR, R., "Oil film thickness and shape for a ball sliding in a grooved raceway", ASLE/ASME Lubrication Conference, Pittsburgh, Pa., October 1971, ASME paper No. 71-Lub-18.

80. WYMER, D.G., "Elastohydrodynamic Lubrication of a Rolling Line Contact", Ph.D. Thesis, 1972. University of London.

81. WYMER, D.G., and CAMERON, A., Elastohydrodynamic Lubrication of a Line Contact. "Optical Analysis of a Roller Bearing", Proc. Instn. Mech. Engrs. 1974, Vol.188 (19/74) p.221 - 237.

82. JACKSON, A.J., "Optical Elastohydrodynamics of Rough Surfaces", Ph.D. Thesis 1973, University of London.

83. JACKSON, A.J. and CAMERON, A., "An Interferometric Study of the E.H.L. of Rough Surfaces", Presented at the ASLE/ ASME Lubrication Conference, Montreal, October 1974.

84. DOWSON, D. and LONGFIELD, M.D., "An elastohydrodynamic lubrication experiment", Nature 1963, Vol.197, p.586.

85. DOWSON, D. and LONGFIELD, M.D., "The distribution of pressure and temperature in a highly loaded lubricated contact", Proc. Lubrication and Wear Convention (Bournemouth) 1963, paper No.3, p.27 - 33 (Instn. Mech. Engrs., Lond.).

86. DOWSON, D. and LONGFIELD, M.D., "The lubrication of rolls of finite width: an investigation of oil-film characteristics", Third Annual Meeting of the Lubrication and Wear Group (Cardiff) 1964, paper No.7, (Instn. Mech. Engrs., Lond.).

87. LONGFIELD, M.D., "Pressure distributions in a highly loaded lubricated contact", Proc. Instn. Mech. Engrs. 1965-6, Vol.180 (Part 3B), p.113 - 118.

88. NIEMANN, G. and GARTNER, F., "Distribution of hydrodynamic pressure on counterformal line contacts", Trans. ASLE 1965, Vol.9 (No.3), p.235 - 249.

89. KANNEL, J.W., BELL, J.C. and ALLEN, C.M., "Methods for determining pressure distributions in lubricated rolling contact", Trans. ASLE 1965, Vol.8, p.250 - 270.

90. ORCUTT, F.K., "Experimental study of elastohydrodynamic lubrication", Trans. ASLE 1965, Vol.8, p.381 - 396.

91. CHENG, H.S., and ORCUTT, F.K., "A Correlation between Theoretical and Experimental Results on the Elastodydrodynamics Lubrication of Rolling and Sliding Contacts", Proc. Instn. Mech. Engrs. 1965-6, Vol.180 (Part 3B), p. p.158 - 168

92. KANNEL, J.W., "Measurements of pressures in rolling contact", Proc. Instn. Mech. Engrs. 1965-6, Vol.180 (Part 3B), p.135 - 142.

93. KANNEL, J.W., WALOWIT, J.A., BELL, J.C. and ALLEN, C.M., "The determination of stresses in rolling-contact elements", ASME/ASLE Lubrication Conference, Minneapolis, Minn., October 1966, ASME Paper No.66-Lub-16.

94. HAMILTON, G.M. and MOORE, S.L., "A modified gauge for investigating an elastohydrodynamic contact", Proc. Instn. Mech. Engrs. 1967-8, Vol.182 (Part 3A), p.251.

95. KLEMZ, B.L., GOHAR, R. and CAMERON, A., "Photoelastic studies of lubricated line contacts", Tribology Group 9th Annual Convention, Douglas, Isle of Man, May 1971, (Instn. Mech. Engrs., Lond.).

96. COPE, D.L. and HAINS, D.J., "Interferometric determination of elastohydrodynamic lubrication contact pressures", Proc. Instn. Mech. Engrs. 1969-70, Vol.184 (Part 1), p.633 - 643.

97. TURCHINA, V., SANBORN, D.M. and WINER, W.D., "Temperature Measurements in Sliding Elastohydrodynamic Point Contacts", Trans. ASME J. Lub. Tech. Paper No.73-Lub-23.

98. WYMER, D.G. and MACPHERSON, P.B., "An Infra-red Technique for the Measurement of Gear Tooth Surface Temperature", Presented at ASLE/ASME Lubrication Conference Montreal, October 1974.

99. CROOK, A.W., "The lubrication of rollers. IV. Measurements of friction and effective viscosity", Phil. Trans. Roy. Soc., 1963, Vol.255 (Series A), p.281.

100. JOHNSON, K.L., and CAMERON, R., "Shear Behaviour of Elasto-hydrodynamic Oil Films at High Rolling Contact Pressures", Proc. Instn. Mech. Engrs. London, 1967, Vol.182 (Part 1) p.307.

101. FORD, R.J. and FOORD, C.A., "Effect of a High Traction Fluid on Skidding in a High Speed Roller Bearing", Trans. ASME J. Lub. Tech., July 1974, Vol.96 (No. 3).

102. CROOK, A.W., "The Lubrication of Rollers, III - A Theoretical Discussion of Friction and the Temperature in the Oil Film", Phil. Trans. Roy. Soc. (A) 1969, Vol.254, p.237.

103. FEIN, R.S., J. Lub. Tech. Trans. ASME 1967, Vol.89, p.127 - 131.

104. HARRISON, G. and TRACHMAN, E.G., "The Role of Compressional Viscoelasticity on the Lubrication of Rolling Contacts", Trans. ASME J. Lub. Tech. 1972, Vol.94 (Series F) p.306.

105. CROOK, A.W., "The lubrication of rollers. IV. Measurements of friction and effective viscosity", Phil. Trans. Roy. Soc. 1963, Vol.255 (Series A), p.281.

106. DYSON, A., "Frictional Traction and Lubricant Rheology in Elastohydrodynamic Lubrication", Phil. Trans. Roy. Soc. A. 1970, p.266.

107. JOHNSON, K.L. and ROBERTS, A.D., "Observations of Viscoelastic Behaviour of an Elastohydrodynamic Lubricant Film", Proc. Roy. Soc. Lond. 1974, Vol.337, p.217 - 242.

108. SMITH, F.W., "Rolling Contact Lubrication - The Application of Elastohydrodynamic Theory", Trans. ASME J. Bas. Engng. 1965 (Series D), Vol.87, p.170.

109. TRACHMAN, E.G., and CHENG, H.S., "Thermal and non-Newtonion Effects on Traction in Elastohydrodynamic Contacts", Symposium on Elastohydrodynamic Lubrication, Leeds 1972, Paper C37/72.

110. BOOSER, E.R. and WILCOCK, D.F., "Minimum Oil Requirements of Ball Bearings", Lub. Engng. 1953, Vol.9 (No.3), p.140 - 3.

111. HORSCH, J.D., "Correlation of Gyro Spin-Axis Ball Bearing Performance with the Dynamic Lubricating Film", Trans ASLE 1963, Vol.6, p.112 - 124.

112. FLOBERG, L., "Lubrication of a rotating cylinder on a plane surface considering cavitation", Trans. Chalmers Univ. Tech., Sweden. 1959, Vol.216. Also, "Lubrication of two cylindrical surfaces....", Ibid., 1961, Vol.234.

113. BONESS, R.J., "Isoviscous lubrication of rigid cylinders - a modification to classical theory", J. Mech. Engng. Sci. 1966, Vol.8 (No.3), p.276.

114. DOWSON, D. and WHOMES, T.L., "Side-leakage factors for a rigid cylinder lubricated by an isoviscous fluid", Proc. Instn. Mech. Engrs. 1966-7, Vol.181 (Part 3B), p.165.

115. FEIN, R.S. and KREUTZ, K.L., "Interdisciplinery Approach to Friction and Wear", Nasa SP- 181 Symposium held at Southwest Research Institute, San Antonio, Texas, Nov. 1967. p.364 - 366.

116. ORCUTT, F.K. and CHENG, H.S., "Lubrication of rolling contact instrument bearings", Proc. Symp. on Gyro Spin-axis Hydrodynamic Bearings, December 1966, Vol.2, p.1 - 25. (The Instrumentation Laboratory, M.I.T., Cambridge, Mass.).

117. LAUDER, W., "Hydrodynamic Lubrication of Proximate Cylindrical Surfaces of Large Relative Curvature", Proc. Instn. Mech. Engrs. 1965, Vol.180 (Part 3B), p.101.

118. TIPEI, N., "Boundary Conditions of a Viscous Flow between surfaces with Rolling and Sliding Motion", ASME Trans. Series F. Jan. 1968, Vol.90 (No.1), p.254 - 261.

119. WOLVERIDGE, P.E., BAGLIN, K.P. and ARCHARD, J.F., "The starved lubrication of cylinders in line contact", Proc. Instn. Mech. Engrs. 1970-71, Vol.185 (No.81), p.1159 - 1169.

120. CASTLE, P. and DOWSON, D., "A theoretical analysis of the Starved Elastohydrodynamic Lubrication Problem for Cylinders in Line Contact", Instn. Mech. Engrs. Symposium on Elastohydrodynamic Lubrication, Leeds 1972, Paper 35/72, p.131 - 137.

121. ARCHARD, J.F., and BAGLIN, K.P., "Non dimensional Presentation of Frictional Tractions in Elastohydrodynamic Lubrication - Part II: Starved Conditions", Trans. ASME J. Lub. Tech. Paper No.74-Lub-32.

122. KINGSBURY, E., "Cross Flow in a Starved Elastohydrodynamic Contact", ASLE Trans. 1973, Vol.16 (A) p.276 - 280.

123. CHIU, Y.P., "An Analysis and Prediction of Lubricant Film Starvation in Rolling Contact Systems", Trans. ASLE Jan. 1974, Vol.17 (No.1), p.22 - 35.

124. KINGSBURY, E., Discussion, reference 123.

125. ZIEGLER, E., "Hydrodynamic Lubrication Improvement in Ball Bearings", Contract NAS 9-12133 Rep. No. PPD-72-E-10326. MAR. 1972 NORTHROP CORP. Electronics Div. Precision Products Dept. Norwood, Mass.

126. SMART, A.E. and TORD, R.J., "Measurement of Thin Liquid Films by a Fluorescence Technique", WEAR 1974, Vol.29, p.41 - 47.

127. DOWSON, D., "The Inlet Boundary Condition", Ist Leeds Lyon Research Symposium on Tribology, Leeds University, Sept.1974.

128. WEDEVEN, L.D., "Traction and Film Thickness Measurements Under Starved Elastohydrodynamic Conditions", Trans. ASME J. Lub. Tech. April 1975, Vol.97, (Series F) No.2, p.321 - 339.

129. GARNELL, P. and HIGGINSON, G.R., "Mechanics of Roller Bearings", Proc. Instn. Mech. Engrs. 1965-66, Vol.180 (Part 3B). p.128 - 156.

130. GARNELL, P., "Lubrication and Wear in Rolling Contact", First Paper: Further Investigations of the Mechanics of Roller Bearings. Proc. Instn. Mech. Engrs. 1966-67, Vol.181 (Part 1, No.16), p.339 -348.

131. KANNEL, S., BELL, S.C., WALOWIT, S.A. and ALLEN, C.M., "A Study of the Influence of Lubricants on High Speed Rolling Contact Bearing Performance", Part VIII Research on Elastohydrodynamic Lubrication of High Speed Rolling Contacts. June 1968. ASD-TDR-61-643.

132. GRAFTON, M., "Measurement of oil film thickness in a tapered roller thrust bearing", M.Sc. Thesis, University of Leeds, 1968.

133. JONES, D.A. and CREASE, A.B., "Measurement of film thickness in a taper roller bearing", Proc. Instn. Mech. Engrs. 1969-70, Vol.184 (Part 3L), p.103.

134. MEYER, D.R. and WILSON, C.C., "Measurement of Elastohydrodynamic Oil Film Thickness and Wear in a Ball Bearing by the Strain Gauge Method", Trans ASME J. Lub. Tech. 1971, Series V, Vol.93 (2), p.224 - 30.

135. O'BRIEN, K.T. and TAYLOR, C.M., "Cage Slip in Roller Bearings", J. Mech. Eng. Sci 1973, Vol.15 (No.5), P.370 - 378.

136. BAHADORAN, H., Ph.D. Thesis, 1974 University of London.

137. BAHADORAN, H. and GOHAR, R., "Oil Film Thickness in lightly Loaded Roller Bearings", J. Mech. Eng. Sc. 1974, Vol.16 (No.6), p.386 - 390.

138. DAWSON, P.H., "Effect of Metallic Contact on the Pitting of Lubricated Rolling Surfaces", J. Mech. Eng. Sc. 1962 Vol.4 (1), p.16 - 21.

139. LAWRENCE, J.C. and SCHMIDT, W.E., "Radio-isotope Techniques Applied to the Investigation of Surface Contact in Rolling Element Bearings", Trans. ASLE 1962, Vol.5, p.327 - 334.

140. TALLIAN, T.E., CHIU, Y.P., HUTTENLOCKER, J.A., KAMENSHINE, J.A., SIBLEY, L.B. and SINDLINGER, N.E., "Lubricant Films in Rolling contact of Rough Surfaces", Trans. ASLE 1964, Vol.7 (2), p.109 - 126.

141. TALLIAN, T.E., BRADY, E.F., McROD, J.I. and SIBLEY, L.B., "Lubricant Film Thickness and Wear in Rolling Point Contact", Trans. ASLE 1965, Vol.8, p.441 - 424.

142. TALLIAN, T.E. McCOOL, J.I. and SIBLEY, L.B., "Partial Elastohydrodynamic Lubrication in Rolling Contact", Proc. Instn. Mech. Engrs. 1965-66, Vol.180 (Part 3B).

143. TALLIAN, T.E., "Rolling Contact Failure Control through Lubrication", Proc. Instn. Mech. Engrs. (Fundamentals and Application to Design) 1967-68, Vol.182 (3A), p.205 - 236.

144. TALLIAN, T.E., "On Competing Failure Modes in Rolling Contact", Trans. ASLE Oct. 1967, Vol.10 (No.4) p.418 - 439.

145. HARRIS, T.A., "Rolling Bearing Analysis", John Witney & Sons Inc. 1966.

146. GIVEN, P.S., "Lubricant Film Effects on Rolling Contact Fatigue", Presentated at Dartmouth Bearing Conference 1966.

147. DANNER, C.H., "Fatigue Life of Tapered Roller Bearings Under Minimal Lubricant Films", Trans. ASLE 197C, Vol.13 (4), p.244 - 251.

148. SKURKA, J.C., "Elastohydrodynamic Lubrication of Roller Bearings", Trans. ASME J. Lub. Tech. April 1970, p.281 - 291.

149. POPINCEANU, N.G., GAFITANU, M.D., NASTASE, H., DIACONESCU, E.N. and CRETU, S.S., "A Study of Roller Bearings Fatigue Life with Mineral Oil Lubrication", Wear 1972, Vol.22, p.21 - 37.

150. APPELDOORN, J.K. and ROYLE, R.C., "Lubricant Fatigue Testing with Ceramic Balls", ASLE Paper No.64-AMIBI.

151. Discussion by McCOOL, J.I. on Paper Entitled "Some Considerations in Rolling Fatigue Evaluation", by KU, P.M., ANDERSON, E.L.,and CARPER, H.J., Trans. ASLE Vol.15 (2), p.128.

152. BELL, J.C., and KANNEL, J.W., "Aspects of Lubrication Affecting Life of Rolling Bearings", Metals Engineering Quaterly, American Society for Metals. Feb. 1967, p.28 - 35.

153. DIACONESCU, E.N., Ph.D. Thesis. University of London 1975.

154. TALLIAN, T.E., "The Theory of Partial Elastohydrodynamic Contacts", Wear 1972, Vol.21, p.99 - 101.

155. ARCHARD, J.F., "Elastohydrodynamic Lubrication of Real Surfaces", Tribology, 1973, Vol.6 (1), p.8 - 14.

156. FOGG, A., and WEBBER, J.S., "The Lubrication of Ball and Roller Bearings at High Speed", J. Instn. Pet. 1953, Vol.39 (359), p.744 - 764.

157. MACKS, E.F., NEMETH, Z.M., and ANDERSON, W.J., "Operating Characteristics of Cylindrical Roller Bearings at High Speeds", Trans. ASME, 1952, Vol.74 (5), p.705 - 713.

158. NAIK, V.V., KEIM, E.L., and NEIFERT, A.R., "High Speed Performance of Tapered Roller Thrust Bearings with Various Lubricating Systems", Trans. ASME J. Lub. Tech. 1970, Vol.92 Series F(1), p.97 - 104.

159. MURTEZA, R.E., "Optimium Methods for Oil-Jet Lubricating Jet Engine Main-Shaft Ball Bearings", Trans. ASME 58-A-258.

160. DOWSON, D., and HIGGINSON, G.R., "Theory of Roller Bearing Lubrication and Deformation", Lubrication and Wear Convention Instn. Mech. Engrs. 1963.

161. IIDA, K., and IGARASHI, A., "On the Behaviour of Rollers in a Cylindrical Roller Bearing", Bulletin of J.S.M.E. 1959, Vol.2 (No.8), p.538 - 545.

162. SMITH, C.F., "Some Aspects of Performance of High Speed Lightly Loaded Cylindrical Roller Bearings", Instn. Mech. Engrs. 1962, Vol.179 (No.22), p.566 - 601.

163. BONESS, R.J., "Cape and Roller Slip in High Speed Roller Bearings", J. Mech. Eng. Sc. 1969, Vol.II (No.2), p.181 - 188.

164. BONESS, R.J., "Effect of Oil Supply on Cage and Roller Motion in a Lubricated Roller Bearing", Trans. ASME J. Lub. Tech. 1970, Vol.92 (No.1), p.39 - 53.

165. HARGREAVES, R.A., and HIGGINSON, G.R., "Some Effects of Lubricant Starvation in Cylindrical Roller Bearings", Trans. ASME J. Lub. Tech. Paper No.75-LUBS-3.

166. DERJAGUIN, B., "Die Formelastrizität der dünner Wassenschichlen", Zeit für Physik 1933, Vol.84, p.657 - 670.

167. TOLANSKY, S., "Multiple-Beam Interferometry of Surfaces and Films", Oxford Clarendon Press 1948.

168. ALLAN, R.K., "Rolling Bearings", Sir Isaac Pitman & Sons Ltd., p.147.

169. HEDLEY, C.J., Ph.D. Thesis, University of London. To be Submitted.

170. LONGHURST, R.S., "Geometrical and Physical Optics", 2nd edition Longmans, Green & Co. Ltd., p.186.

171. GREENWOOD, S.A., and KAUZLARICH, J.T., "Inlet Shear Heating in Elastohydrodynamic Lubrication", Trans. ASME J. Lub. Tech. 1973, Vol.95 Series F(No.4), p.417 - 426.

172. MURCH, L.E., and WILSON, W.R.D., "A Thermal Elastohydrodynamic Inlet Zone Analysis", Trans. ASME J. Lub. Tech. April 1975, p.212 - 216.

173. WILSON, W.R.D., and WONG, C.J., "Analysis of the Film Formation Process in Plain Strain Forging", Trans. ASME J. Lub. Tech. Oct. 1974, Vol.96 Series F(No.4), p.605 - 610.

174. GLASSTONE, S., "Textbook of Physical Chemistry", Macmillan & Co. Ltd., London 1948.

175. BUTTER, T.C., RITCHEY, C and BENZS, C.A., "The Effect of Pressure on the Index of Refraction of Paraffin Oil and Glycerine", Phys. Rev. 1932, Vol.41, p.366 - 367.

176. CHU, P.S.Y., and CAMERON, A., "Compressibility and Thermal Expansion of Oils", J. Instn. Pet. 1963, Vol.49 (No.473), p.140 - 145.

177. "Viscosity and Density of over Forty Lubricants", Report of ASME Research Committee on Lubrication. ASME New York 1953.

178. CAMERON, A., "Principles of Lubrication", Longmans, London, 1966, p.49.

179. GREENWOOD, J.A. and TRIPP, J.H., "The elastic contact of rough spheres", J. Appl. Mech., Trans. ASME 1967, Vol.89 (Series E), p.153 - 159.

180. DYSON, A. and WILSON, A.R., "Film Thickness Elastohydrodynamic Lubrication at High Slide/Roll Ratios", Proc. Instn. Mech. Engrs. 1968-69, Vol.183 (Part 3P), p.81 - 97.

181. TIPEI, N., "Discussion on Lubrication of Two Rotating Cylinders at Variable Lubricant Supply, with Reference to the Tensile Strength of the Liquid Lubricant", Floberg L. Trans. ASME J. Lub. Tech. April 1973, Vol.95, p.164.

182. GOHAR, R., "Oil film thickness and rolling friction in elastohydrodynamic point contact", Trans. ASLE 1970, Paper No.70-Lub-2.